GEMS & GEMOLOGY

SUMMER 2015
VOLUME LI

THE QUARTERLY JOURNAL OF THE GEMOLOGICAL INSTITUTE OF AMERICA

Dual-Color Double Asterism in Corundum and Quartz

Photomicrography Techniques and Equipment

Ruby and Sapphire from Tajikistan

The Micro-World of Gem Inclusions

GEMS & GEMOLOGY

Summer 2015
VOLUME 51, No. 2


pg. 135

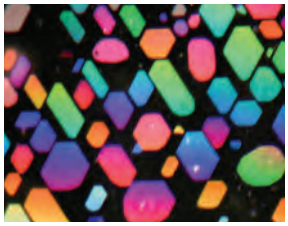
pg. 150

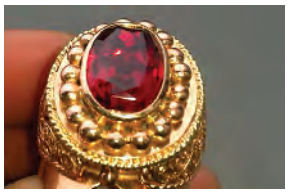
pg. 160

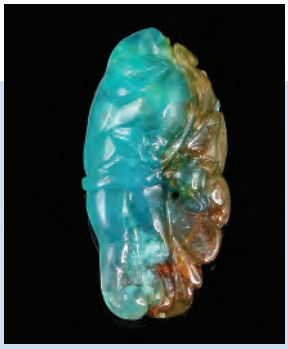
pg. 205

## Editorial



## Feature Articles



## Regular Features

GEMS & GEMOLOGY

gia.edu/gems-gemology

**Subscriptions**
Copies of the current issue may be purchased for $29.95 plus shipping. Subscriptions are $79.99 for one year (4 issues) in the U.S. and $99.99 elsewhere. Canadian subscribers should add GST. Discounts are available for group subscriptions, GIA alumni, and current GIA students. To purchase print subscriptions, visit store.gia.edu or contact Customer Service. For institutional rates, contact Customer Service.

**Database Coverage**
*Gems & Gemology*'s impact factor is 0.778, according to the 2013 Thomson Reuters Journal Citation Reports (issued July 2014). *G&G* is abstracted in Thomson Reuters products (Current Contents: Physical, Chemical & Earth Sciences and Science Citation Index—Expanded, including the Web of Knowledge) and other databases. For a complete list of sources abstracting *G&G*, go to gia.edu/gems-gemology, and click on "Publication Information."

**Manuscript Submissions**
*Gems & Gemology*, a peer-reviewed journal, welcomes the submission of articles on all aspects of the field. Please see the Author Guidelines at gia.edu/gems-gemology or contact the Managing Editor. Letters on articles published in *G&G* are also welcome. Please note that Field Reports, Lab Notes, Gem News International, and Micro-World entries are not peer-reviewed sections but do undergo technical and editorial review.





*Gems & Gemology* is published quarterly by the Gemological Institute of America, a nonprofit educational organization for the gem and jewelry industry.

Postmaster: Return undeliverable copies of *Gems & Gemology* to GIA, The Robert Mouawad Campus, 5345 Armada Drive, Carlsbad, CA 92008.

Our Canadian goods and service registration number is 126142892RT.




## About the Cover

*Nathan Renfro's article in this issue explores the role of image-processing software and lighting techniques in modern digital photomicrography. The cover image shows modified trigons on the surface of a diamond crystal from the Kelsey Lake mine on the Colorado-Wyoming border. This Nomarski differential interference contrast image was taken using a Nikon Eclipse LV100 microscope equipped with a 20× objective and a Canon 6D camera. Helicon Focus stacking software was used for extended depth-of-field image processing of 70 photomicrographs into a single image. Vertical field of view: 0.49 mm. Image by Nathan Renfro.*


Printing is by L+L Printers, Carlsbad, CA.
GIA World Headquarters The Robert Mouawad Campus 5345 Armada Drive Carlsbad, CA 92008 USA



ISSN 0016-626X

# **The Beauty and Value of Inclusions,** Plus Double Stars and Corundum from Tajikistan

We hope you enjoy this edition's unusual and distinctive cover image. It's especially fitting, as a number of contributions in this issue deal with aspects of gem inclusions: their documentation using modern digital photography and image-processing software, how some interact with light inside a fashioned gem to produce asterism, and the straightforward instructional value that might be gained through their study.

Our cover article, by Nathan Renfro, analytical manager of the gem identification department at GIA's Carlsbad laboratory, focuses on digital photomicrography for gemologists. Renfro's article builds on the landmark 2003 paper by his longtime mentor and master of gem-inclusion photography John Koivula, to offer a highly practical and relevant guide covering equipment and current techniques for the gemologist.

In the lead article, we present a paper by a team of researchers headed by Dr. Karl Schmetzer, a frequent contributor to *Gems & Gemology* during the 1980s and 1990s. We are delighted to welcome Dr. Schmetzer back to our journal. He and his coauthors offer a comprehensive description of a largely unappreciated form of asterism: the dual-color "double stars" observed in some natural sapphire, ruby, and quartz, as well as synthetic corundum, including diffusion-treated examples. The authors discuss the mechanism by which double stars are formed and present a historical summary of the manufacture and improvement of synthetic star corundum by diffusion treatment.

*"We invite gemologists to take a closer look at the astounding beauty and variety of the micro-world of gems."*

Our third article, by Russian researcher Dr. Elena Sorokina and her coauthors, provides an update on the geology, mining, and internal and external features of ruby and sapphire from Snezhnoe, Tajikistan. This is a welcome summary of a marble-hosted deposit with significant potential, one that has seen little study or previous coverage in the gemological literature.

After these three feature articles, you'll find our regular Lab Notes and Gem News International sections, which include further entries from the 2015 Tucson shows and a report of the recent Maine pegmatite workshop.

In addition, we present a new quarterly column on inclusions entitled "Micro-World." With this new regular feature, section editors Nathan Renfro, Elise Skalwold, and John Koivula aim to foster the wider appreciation of inclusions and to bolster practicing gemologists' observational skills by providing concise reports accompanied by stunning photomicrographs of specially chosen specimens. The authors invite gemologists to take a closer look at the astounding beauty and variety of inclusions in gems.

Finally, I'd like to thank Stuart and the entire *G&G* editorial and production staff. Due to the unexpected death of a close family member, I have been out of the United States for a period of weeks. As a result, I have come to appreciate the hard work and dedication of the entire *G&G* team even more.

All of us at *G&G* hope you enjoy the Summer issue!

Duncan Pay | Editor-in-Chief | dpay@gia.edu

# Dual-Color Double Stars in Ruby, Sapphire, and Quartz: Cause and Historical Account

Karl Schmetzer, Martin P. Steinbach, H. Albert Gilg, and Andrea R. Blake

A largely overlooked form of asterism consisting of dual-color double stars is found in natural sapphire, in diffusion-treated and non-diffusion-treated synthetic rubies and sapphires, and in natural quartz. To characterize and explain this phenomenon, examples of these materials were examined. In transparent or translucent samples, an optical pattern of a white six-rayed star and a bodycolored (e.g., red, orange, yellow, green, blue) six-rayed star was frequently observed. Grinding and repolishing experiments showed that the asterism of part of the synthetic samples was produced or enhanced by diffusion treatment. The mechanism responsible for the formation of the dual-color double stars is discussed. To produce the pattern, acicular inclusions must either be present in relatively thin layers confined to the dome and the base of diffusion-treated ruby or sapphire cabochons, or be distributed throughout the complete corundum (natural or synthetic) or quartz samples. The white star is caused by interaction of light with the upper layer of the cabochon's dome. The bodycolored star, in contrast, is generated by light that enters the cabochon, is reflected and scattered at the base layer of the cabochon, and then travels a second time back through the body of the sample. As further prerequisites for observation of the phenomenon, the gemstones must be transparent or translucent, with polished base and dome.

A historical summary of the manufacture and improvement of synthetic asteriated corundum by diffusion treatment offers additional insight into dual-color double-star stones. According to firsthand accounts and patent documents, diffusion has been used to produce or enhance asterism in synthetic and natural corundum since the 1950s. The treated material has been released commercially since at least the 1970s, and it is still produced and found on the international market.

Asterism in corundum and quartz is observed in various forms. Single six-rayed asterism is the most common form, found in natural ruby and sapphire from different sources around the world. This optical phenomenon is due to the presence of three series of acicular inclusions, in corundum mostly identified as rutile or hematite-ilmenite needles (Moon and Phillips, 1984). If both types of inclusion are present, twelve-rayed asterism is seen (Hughes, 1997; Schmetzer and Glas, 2001). In such samples, two six-rayed concentric stars consisting of three light bands each are rotated such that the twelve rays are evenly spaced and 30° apart (and alternate between the two acicular inclusion types).

See end of article for About the Authors and Acknowledgments.
Gems & Gemology, Vol. 51, No. 2, pp. 112–143,
http://dx.doi.org/10.5741/GEMS.51.2.112.


Asteriated natural sapphires and rubies with two slightly displaced six-rayed stars of identical white color have been mentioned on different occasions. This optical phenomenon results from lamellar twinning, with three series of rutile needles in each individual part of the twin (Koivula et al., 1993; McClure, 1998; Kondo, 2007).

Additionally, a natural star sapphire with two stars of different coloration was described by Koivula and Tannous (2001). The two stars were observed singly but on opposite sides of the double cabochon—i.e., the color of the star visible depended upon whether the stone was viewed from the "top" dome or the "bottom" dome. One star was an "ordinary" white star of the type commonly seen in sapphires and rubies, caused by reflection from inclusions near the surface toward the viewer. The other was a yellow-brown star, caused by reflection from inclusions

farther from the surface and thereby showing superimposition of the bodycolor of the host sapphire.

Phenomenal quartz has been known from various localities for more than a century, and asteriated material is seen occasionally in the trade, with most samples originating from Brazil or Madagascar (Cassedanne and Roditi, 1991; Pezzotta, 2001). The literature further demonstrates that asterism and related phenomena in quartz constitute a relatively complex topic and may take a plurality of forms. Most common are asteriated stones presenting six-rayed stars, with three groups of needle-like inclusions oriented in a plane perpendicular to the c-axis. Rarely, twelve-rayed stars are observed, which show six groups of needles (two sets of three) in the same plane. Even multi-star quartz samples revealing numerous stars on the surface of cabochons or complete spheres have been described in detail from a locality near Galle in Sri Lanka (Schmetzer and Glas, 2003). Rose quartz spheres also may show isolated light spots in addition to the typical six-rayed asterism (Schmetzer and Krzemnicki, 2006).

With respect to identification of the needles producing the phenomena, asterism in colorless quartz and rose quartz has frequently been associated with the presence of a network of oriented rutile needles (see, e.g., Eppler, 1958; Fryer et al., 1981, 1982b, 1985; Kiefert, 2003). Rutile needles are found in quartz in a multiplicity of crystallographic orientations, as established by von Vultée (1955, 1956). By use of five of these established orientations for rutile needles in quartz, a model was developed to explain all observed multi-star networks in quartz from Sri Lanka (Schmetzer and Glas, 2003). A sagenitic network of acicular rutile crystals has also been mentioned recently as causing the asterism seen in quartz samples from Myanmar (Schmetzer and Steinbach, 2014).

## In Brief

- Corundum (natural and synthetic) and quartz may exhibit asterism in the form of dual-color double stars.
- Reflection and scattering of light by acicular inclusions near the dome of cabochons create a white star, while such reflection and scattering of light by inclusions near the base create another star with the bodycolor of the host.
- Diffusion processes may contribute to the phenomenon and have been used to create or improve asterism in ruby and sapphire since the 1950s.

In addition, examinations of six-rayed star quartz from Niriella, Sri Lanka, showed the presence of three series of oriented sillimanite needles (Woensdregt et al., 1980). Oriented needle-like inclusions of ilmenite, on the other hand, were responsible for the six light bands in quartz from the state of Texas (Zolensky et al., 1988). In a yellow-green quartz from Tamil Nadu, India, showing a combination of asterism and chatoyancy, several series of unidentified fine to coarse needles were described (Choudhary and Vyas, 2009). These publications show that although rutile needles seem to be a well-established cause for asterism in some quartz varieties, other acicular inclusions should not be neglected.

To summarize, table 1 offers a short overview of the different star phenomena.

## PRODUCTION OF ASTERIATED SYNTHETIC RUBY AND SAPPHIRE

In synthetic ruby and sapphire, asterism is produced in a two-step process:

1. Growth of a non-asteriated crystal that contains distinct amounts of titanium in the corundum lattice
2. Heat treatment of the homogeneous titanium-bearing sample to form needle-like precipitates of a titanium-bearing phase

Two variants are known for the first step of this process. In one variant, titanium oxide is added to the aluminum oxide powder used for the production of synthetic ruby and sapphire boules by the Verneuil method (Burdick and Glenn, 1949; Burdick and Jones, 1954a) or by the Czochralski technique (Keig et al., 1972). In another variant, titanium is diffused into whole and half boules as well as pre-cut cabochons of synthetic Verneuil-grown corundum (Eversole and Burdick, 1954c; see also Carr and Nisevich, 1975a, 1976a, 1977).

After either variant of the first production step, heat treatment is performed for the formation of needle-like precipitates in the corundum matrix. This step exsolves three differently oriented series of needles, composed either of rutile or of another titanium-bearing phase. Reflection and scattering of light from these needles are then responsible for the three intersecting light bands of asteriated rubies and sapphires. The exsolution step is necessary regardless of which variant of the first production step is employed.

**TABLE 1.** Overview of various star phenomena.

| | Ruby and sapphire | | Quartz and rose quartz | |
|---|---|---|---|---|
| Single six-rayed star | Three series of needles in planes parallel to the basal face |  | Three series of needles in planes parallel to the basal face |  |
| Single twelve-rayed star | Six series of needles (two sets of three) in planes parallel to the basal face |  | Six series of needles (two sets of three) in planes parallel to the basal face |  |
| Single-color double stars consisting of two displaced stars with identical color | Twinned individual, each part of the twin with a single six-rayed star | 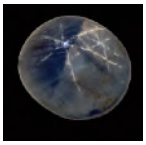 | | |
| Multiple stars with identical color[a] (or additional light spots) | | | Several series of needles parallel and inclined to the basal face (or additional flat inclusions) |  |
| Dual-color double stars with a white star and a bodycolored second star | To be described in this paper | 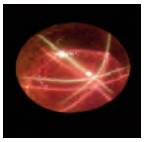 | To be described in this paper |  |

[a]*Also observed in garnets and spinels due to the cubic symmetry of the host (see, e.g., Schmetzer et al., 2002)*

Numerous papers have dealt with the examination and identification of the needle-like precipitates formed in Ti-doped corundum after annealing at temperatures in the range of 1500° to 1100°C (see references below and patent documents in table A-1). The different phases present as acicular inclusions have been characterized in the transmission electron microscope using electron diffraction and/or other microanalytical techniques. It has often been noted that twinned rutile needles are formed, but the exsolution of rhombic or monoclinic $TiO_2$ phases and even the formation of $Al_2TiO_5$ have been reported as well (Phillips et al., 1980; Langensiepen et al., 1983; Moon and Phillips, 1991; Xiao et al., 1997; Viti and Ferrari, 2006; He et al., 2011). For simplicity, we shall only mention "rutile" needles or precipitates, aware of the fact that other Ti-bearing phases might also be present.

Patents related to the different variants of production mentioned above were assigned to the Linde Air Products Company (New York) and later to Union Carbide and Carbon Corporation or to Union Carbide Corporation (of which Linde had become a division). Linde started manufacturing synthetic ruby and sapphire in the United States in the 1940s, when America was cut off from European supply of synthetic corundum ("U.S. develops synthetic sapphire industry," 1943; Alexander, 1946; Seemann, 1949; Pough, 1966). The method to produce asteriated corundum was discovered by J.N. Burdick and his colleagues at Linde in 1947 (see "The story of Linde stars," n.d.), and the first samples were available for gemological examination in the same year (Holmes, 1947). Linde's only competitor for the international market in the early decades of production was Wiede's Carbidwerk in Freyung, Germany (Breebaart, 1957; Ep-

*Figure 1. Synthetic star rubies and sapphires were manufactured by the Linde Air Products Company beginning in the late 1940s. The first commercially produced type of asteriated stones was opaque with a white, six-rayed star. The large ruby cabochon measures 9.9 × 8.0 mm and weighs 3.39 ct. Photo by K. Schmetzer; samples courtesy of C. Cavey.*

pler, 1957/1958). This company has been growing synthetic corundum since 1913. The existence of a competing manufacturer was possible because the basic patent (Burdick and Glenn, 1949) was granted only in the United States (see box A), and Wiede's developed and patented a slightly different process in Germany (Ancot and Eppler, 1957 a,b).

The asteriated synthetic rubies and sapphires produced by Linde (figure 1) were distributed and sold under various trade names, including the widely used "Linde stars." In the 1960s, asteriated corundum was commercially available in four different colors (white, red, blue, and black), and limited quantities of asteriated sapphires in other colors (green, yellow, and pink) were also produced (Meyer-Browne, 1962; Thurm, 1962; Taylor, 1964; Pough, 1966). Due to the concentration of needle-like precipitates primarily in a thin layer close to the surface of the Verneuil boules, the first stones manufactured showed higher transparency and somewhat incomplete stars compared to the material released from 1952 onward (Holmes, 1947; Liddicoat, 1963; Crowningshield, 1965). Production of synthetic star rubies and sapphires in the United States ceased in 1974 (Nassau, 1979). Conversely, production of non-asteriated, titanium-bearing sapphires continued. At Union Carbide, these titanium-bearing synthetics were grown using the Czochralski method and were primarily used as laser crystals, although such material with pink coloration has occasionally been faceted for gem use (Johnson et al., 1995).

It has been mentioned in the literature that synthetic star stones produced by diffusion have a higher transparency than normal star corundum but have not been marketed on a wide scale (Elwell, 1979). It was also noted that the diffusion process has not normally been used for producing synthetic stars (Nassau, 1980). However, no information as to the source of these statements is provided in the cited texts.

Asterism in natural corundum can be created or improved by the same diffusion process with subsequent heat treatment as described above. The related patent applications were assigned to Union Carbide Corporation (Carr and Nisevich, 1975a) or later to Astrid Corporation (Carr and Nisevich, 1976a, 1977).

## RECOGNITION OF DUAL-COLOR DOUBLE-STAR PHENOMENA IN CORUNDUM AND QUARTZ

Corundum and quartz samples showing a type of star phenomenon not accounted for among the more widely recognized forms of asterism described earlier and consisting of two differently colored six-rayed stars have occasionally been noted or depicted as well. For example, a double-star pattern was pictured by Arem (1987) for some synthetic "Heller Hope" star rubies and sapphires (a trade name used for Linde synthetics). The accompanying caption does not explicitly refer to these dual-color double stars, and in the text no comment related to this phenomenon is given. The material portrayed was a lot of mixed-color asteriated rubies and sapphires from the trade,

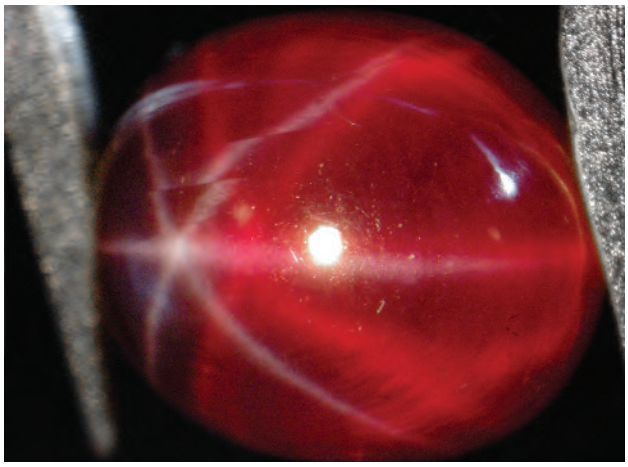

*Figure 2. This synthetic star ruby was described by Schmetzer and Hainschwang (2012); the sample shows a six-rayed white star, reflected from the surface of the cabochon, and a six-rayed orange-red star. The sample measures 10.3 × 8.7 mm and weighs 5.98 ct. Photo by K. Schmetzer.*

without any additional specification (J.E. Arem, pers. comm., 2013). A similar photo showing differently colored sapphires with dual-color double stars was also published without further comment by Gübelin and Koivula (2008).

Another instance of a double star in a synthetic ruby was recently described by Schmetzer and Hainschwang (2012). When examined in reflected light, the ruby cabochon showed the ordinary whitish six-rayed star of corundum and an orange-red star that seemed to emanate from the back of the sample (figure 2). This transparent cabochon consisted of a Verneuil-grown synthetic corundum core with tiny needle-like precipitates in the upper layer (in the curved dome) as well as within the slightly curved base of the stone. It was concluded that the formation of the orange-red star was caused by a complex interaction of the light reflected and scattered by needles (most likely rutile needles) in one or both surface layers and absorption of light reflected from the base of the cabochon, traveling twice through the body of the stone.

An analogous double-star pattern consisting of two differently colored stars (white and pink) was observed in reflected light in a rose quartz sphere (Killingback, 2006, 2011). It was assumed that the light forming the pinkish star was "reflected from the rear surface of the sphere and formed into the star as it comes up through the ball, to be refracted at the top surface on leaving" the rose quartz sphere (Killingback, 2006).

Subsequent to the 2012 publication of the Schmetzer and Hainschwang paper, one of the authors (KS) discussed the mode of formation of the double-star pattern in the synthetic ruby with several colleagues. Although asterism is commonly observed in gem materials in reflected light, designated as *epiasterism*, transparent gemstones such as quartz or rose quartz also show asterism in transmitted light, termed *diasterism* (Schmetzer and Glas, 2003; Killingback, 2009). Taking these facts into consideration, it was argued that the phenomenon is probably a "simple" reflection of an ordinary white star (light bands produced by forward scattering) at the base of the cabochon, without further interaction of light with needle-like inclusions confined to that base and without further interaction with needles in the upper surface layer.

Thus, the opportunity to examine several additional samples of synthetic corundum purchased recently by one of the authors in Bangkok, which showed light bands forming a dual-color double star in reflected light (figure 3), was valuable. Furthermore, several lots of "Linde" synthetics loaned from various collections and samples bought in the trade, mainly in the United States in 2013, were examined and compared with the material obtained in the Bangkok trade. Synthetics produced by Wiede's Carbidwerk and Hrand Djevahirdjian SA were likewise made available for study. Finally, a similar-appearing double-star pattern was examined in a natural sapphire, in rose quartz from Brazil, and in brownish pink quartz from India. The focus in examining all of these samples was to elucidate the almost completely overlooked optical phenomenon of dual-color double stars observed in reflected light.

*Figure 3. This pink synthetic sapphire showing a white six-rayed star and a pink star was purchased by one of the authors in Bangkok in 2010. The cabochon measures 14.4 × 11.2 mm and weighs 12.37 ct. Photo courtesy of M.P. Steinbach.*

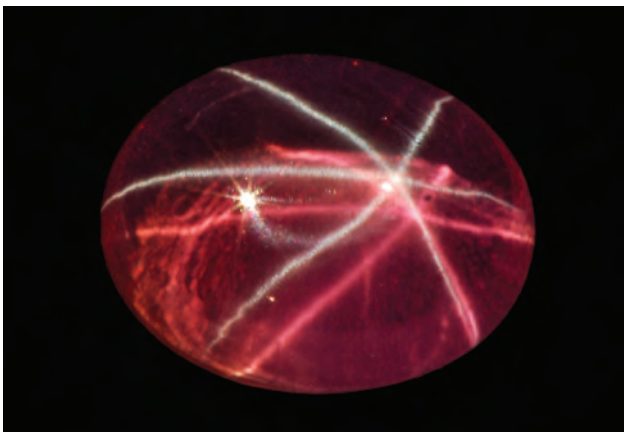

## BOX A: TECHNICAL INFORMATION IN PATENT DOCUMENTS

Various processes to create or enhance asterism in corundum are described in patent documents that were filed by Linde or by the Linde division of Union Carbide, before the production and related patents were transferred to Astrid Corporation, a company based in Hong Kong (table A-1). The first patent application was filed in August 1947 (published as U.S. patent 2,488,507 in November 1949). In principle, and as already summarized in the text, the production of asteriated corundum is based on a two-step process comprising (1) the growth of titanium-bearing corundum crystals, and (2) the formation of rutile precipitates by low-temperature annealing between 1500° and 1100°C. These precipitates are responsible for the reflection and scattering of incident light and the formation of three intersecting light bands of a six-rayed star. According to the patent documents available, the two steps described are performed under various conditions. However, from interviews with people involved in the production (see box B), it appears that additional "secret" steps or specific details not disclosed in patents may exist to optimize the processes for obtaining asterism. The first synthetic asteriated rubies and sapphires were grown by the Verneuil technique, with the addition of a titanium-bearing compound as a component of the nutrient powder (Burdick and Glenn, 1949). Without further dopants, colorless star sapphires are obtained; with the addition of chromium oxide or iron oxide, respectively, rubies or blue sapphires can be produced.

The disadvantage of this basic process is that the resultant needle-like precipitates are confined to the skin of the Verneuil boules, thus restricting the size and number of the cabochons that may be cut. Cabochons cut from the interior of the boules may not exhibit asterism, and blue synthetic sapphires may also show colorless zones in the growth sectors without titanium (figure A-1). Furthermore, cabochons cut with the titanium-bearing skin in the center may not show asterism on the sides toward the base (Burdick and Jones, 1954a).

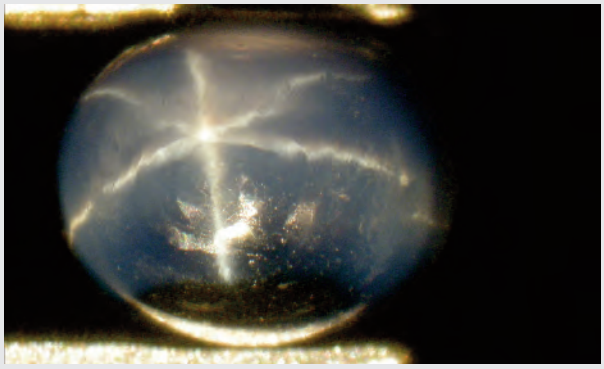

*Figure A-1. Blue synthetic sapphire with a large colorless zone, which probably represents the core of the original boule; the star is restricted to the blue zones of the cabochon. The sample, from an unknown producer, measures 5.8 × 4.8 mm and weighs 1.01 ct. Photo by K. Schmetzer.*

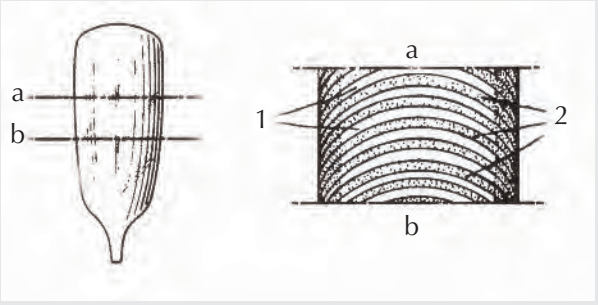


*Figure A-2. Left: A boule of synthetic Verneuil-grown sapphire produced under fluctuating temperature conditions. Right: An enlarged section through the boule between lines a and b showing the distribution of titanium in various growth zones. 1 indicates layers containing titanium-bearing precipitates only at the rim; 2 represents layers containing titanium-bearing precipitates in all zones, from the center to the rim. After German patent DE 897 844. Inventors: J.N. Burdick and R.A. Jones (1954b); applicant: Union Carbide and Carbon Corporation.*

To overcome these disadvantages and to grow rubies and sapphires with more complete stars, and without colorless zones in blue sapphires, it was necessary to have a more homogeneous distribution of titanium in the crystals. The more homogeneous distribution was accomplished by growing the Verneuil boules under fluctuating thermal conditions. In practice, this fluctuation was achieved by alternately increasing and decreasing the rate of oxygen fed to the oxygen-hydrogen flame of the Verneuil burner. It is described in the Burdick and Jones (1954a) U.S. patent that the synthetic sapphire and ruby boules grown under such conditions show—in the direction of crystal growth—layers with high titanium contents in all zones, alternating with layers where titanium contents are restricted to the rim of the boule (figure A-2).

Larger crystals with an even more homogeneous titanium distribution are grown by the Czochralski technique (Keig et al., 1972, 1973a). Crystals produced by this method show a uniform distribution of both color and titanium-bearing precipitates. Asteriated cabochons can be cut from any section of the synthetic crystals without size or shape restriction. In practice, ruby or sapphire crystals are pulled vertically by means of a seed crystal (figure A-3), which is dipped into an aluminum oxide melt doped with titanium oxide and further oxides of color-causing transition elements (e.g., chromium and iron).

An example of a large asteriated ruby that almost certainly was grown by Union Carbide using the Czochralski method, measuring 5 cm in diameter, was shown at a special exhibition at the Smithsonian Institution's National Museum of Natural History in the summer of 1973 (J.E.

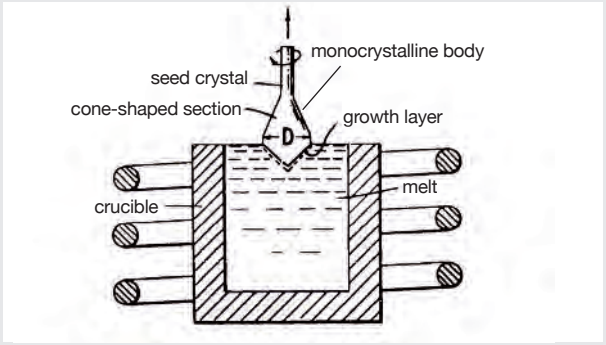


*Figure A-3. Growth of a large sapphire crystal from the melt by the Czochralski technique. D represents the diameter of the growing crystal. After German published patent application DE 2 208 150A. Inventors: G.A. Keig et al. (1973c); applicant: Union Carbide Corporation.*

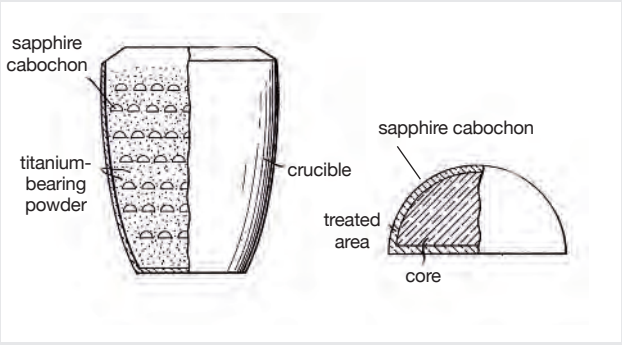


*Figure A-5. Left: Diffusion treatment of sapphires in titanium-bearing powder. Right: A treated cabochon with a diffusion layer. After German published patent application DE 2 262 104A. Inventors: R.R. Carr and S.D. Nisevich (1973c); applicant: Astrid Corporation.*

Arem, pers. comm., 2014; see figure A-4). However, this material was not available commercially, and further details of the production methods, especially for obtaining asterism, are unknown.

As an alternative to the methods described by Burdick and Jones (1954a) and Keig et al. (1972, 1973a), in which a titanium-bearing compound is added to the

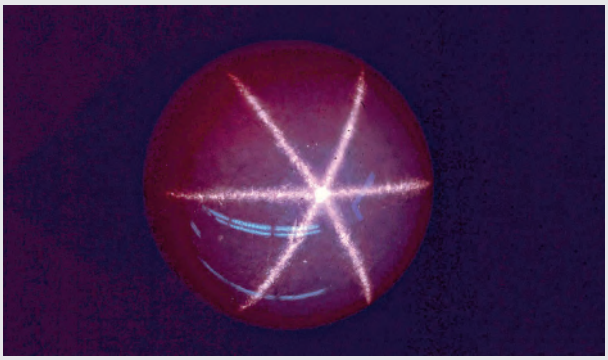

*Figure A-4. This large sphere of asteriated synthetic ruby, about 5 cm in diameter, was exhibited at the Smithsonian Institution's National Museum of Natural History in the summer of 1973. It is an example of the large ruby and sapphire crystals manufactured at Union Carbide in the early 1970s, though details of its production are unknown. Photo courtesy of J.E. Arem.*

powder used for crystal growth by the Verneuil or Czochralski technique, titanium can be induced into the corundum lattice by diffusion treatment of the already-grown, final crystal. This technique can also be applied to cabochon-cut materials. For the diffusion of titanium into the corundum, titanium oxide or a mixture of titanium oxide and aluminum oxide is placed in contact with a crystal, a boule, or a cabochon and annealed at temperatures in the range of 1950° to 1700°C (Eversole and Burdick, 1954c).

As one example, the Eversole and Burdick (1954c) patent describes spraying a slurry containing titanium oxide onto the surface of sapphire or ruby cabochons. To develop asterism, the cabochons are then annealed in a furnace at temperatures between 1875° and 1800°C. Another example involves embedding rubies or sapphires of various colors in a mixture of titanium oxide and aluminum oxide powder and then heating in crucibles at 1800°C for a period of 24 to 30 hours. Asterism is subsequently formed by the precipitation of titanium-bearing needles by low-temperature annealing as described above. The diffusion of titanium is restricted to a thin layer at the surface of the treated corundum boules or cabochons. This layer, however, is sufficient to produce the desired six-rayed asterism. It is worth noting that, although not worked out in detail,

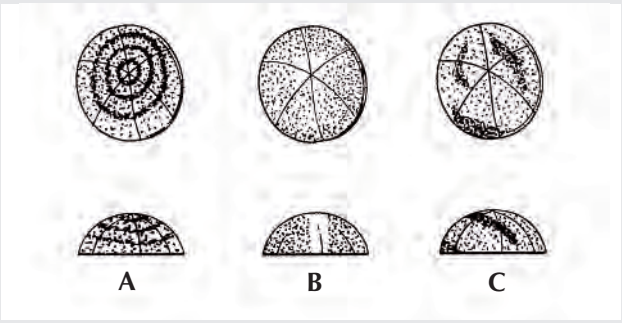


*Figure A-6. Examples of sapphires with undesirable color and color zoning that can be altered by diffusion treatment: (A) color banding, (B) a clear center, and (C) off-color, irregularly distributed color banding. After German published patent application DE 2 262 104A. Inventors: R.R. Carr and S.D. Nisevich (1973c); applicant: Astrid Corporation.*

Eversole and Burdick's patent (1954c) stated that even non-asteriated natural cabochons could be treated to produce asterism by the diffusion technique so invented. In one example, the treatment of "pale blue-green unasteriated nat-

**TABLE A-1.** Patent documents related to production or enhancement of asterism in corundum.

| Author(s)/applicant | U.S. patent documents/ publication year | Related patents (patent family)/publication year | Purpose | Technical details |
|---|---|---|---|---|
| J.N. Burdick and J.W. Glenn (Linde Air Products Company) | US 2,488,507 (1949) | | Manufacture of asteriated ruby and sapphire | Growth of titanium-doped corundum and subsequent annealing of the synthetic boule at temperatures between 1500° and 1100°C to form precipitates of a titanium compound |
| J.N. Burdick and R.A. Jones (Union Carbide and Carbon Corporation) | US 2,690,062 (1954a) | DE 897 844 (1954b)<br>DE 948 403 (1956)<br>GB 697,804 (1953b)<br>FR 1.029.418 (1953a)<br>CH 289 320 (1953c) | Manufacture of asteriated ruby and sapphire with homogeneous color distribution and complete six-rayed stars | Increasing the homogeneity of titanium distribution within the Verneuil boule, crystal growth under fluctuating thermal conditions |
| W.G. Eversole and J.N. Burdick (Union Carbide and Carbon Corporation) | US 2,690,630 (1954c) | DE 922 584 (1955a)<br>GB 712,735 (1954a)<br>FR 1.067.037 (1954b)<br>CH 307 914 (1955b) | Production of asterism in natural or synthetic corundum | Diffusion of titanium into a thin surface layer of a ruby or sapphire crystal at temperatures between 1950° and 1700°C and subsequent annealing of the corundum crystal at temperatures between 1500° and 1100°C to form precipitates of a titanium compound |
| G.A. Keig, J.C. Smith, and J.M.J. Watts (Union Carbide Corporation) | US 3,655,415 (1972)<br>US 3,725,092 (1973a) | DE 2 208 150A (1973c)<br>GB 1 377 428 (1974)<br>FR 2.172.913 (1973d)<br>CH 539 581 (1973b)<br>AT 327 863 (1976) | Manufacture of asteriated ruby and sapphire with homogeneous color distribution and complete six-rayed stars in any desired size | Growth of titanium-doped corundum by the Czochralski technique and subsequent annealing of the synthetic crystal at temperatures between 1500° and 1100°C to form precipitates of a titanium compound |
| R.R. Carr and S.D. Nisevich (Union Carbide Corporation)<br>R.R. Carr and S.D. Nisevich (Astrid Corporation, Ltd.)<br>R.R. Carr and S.D. Nisevich (Astrid Corporation, Ltd.) | US 3,897,529 (1975a)<br>US 3,950,596 (1976a)<br>US 4,039,726 (1977) | DE 2 262 104A (1973c)<br>GB 1 408 648 (1975b)<br>FR 2.164.690 (1973a)<br>CH 554 811 (1974)<br>AT 330 722 (1976b)<br>BE 793.007 (1973b) | Production of homogeneous color distribution or altering the appearance of color in asteriated and non-asteriated natural or synthetic corundum | Diffusion of titanium, diffusion of another transition metal, or diffusion of titanium together with another transition metal into a thin surface layer of a ruby or sapphire crystal at temperatures between 1850° and 1600°C; to produce asteriated corundum, subsequent annealing of the synthetic crystal at temperatures between 1500° and 1100°C to form precipitates of a titanium compound |

*US—United States; DE—Germany; GB—United Kingdom; FR—France; CH—Switzerland; AT—Austria; BE—Belgium*

ural sapphire" is mentioned, which indicates that diffusion treatment of natural sapphire to produce asterism has been known since 1954.

The diffusion process of Eversole and Burdick (1954c) was extended by Carr and Nisevich (1975a, 1976a, 1977) for altering the color appearance of natural and synthetic corundum. Through the use of diffusion processes as described in the patent documents (figure A-5), various uneven or undesired color distributions (figure A-6) of natural or synthetic, asteriated or non-asteriated ruby and sapphire crystals can be enhanced. Based on the intended final coloration, oxides of transition metals such as titanium, vanadium, chromium, iron, or nickel, alone or in combination, are diffused into the corundum sample. If asterism is to be developed or enhanced, in addition to the desired color improvement, a second low-temperature annealing step is always required to produce the necessary oriented titanium-bearing precipitates.

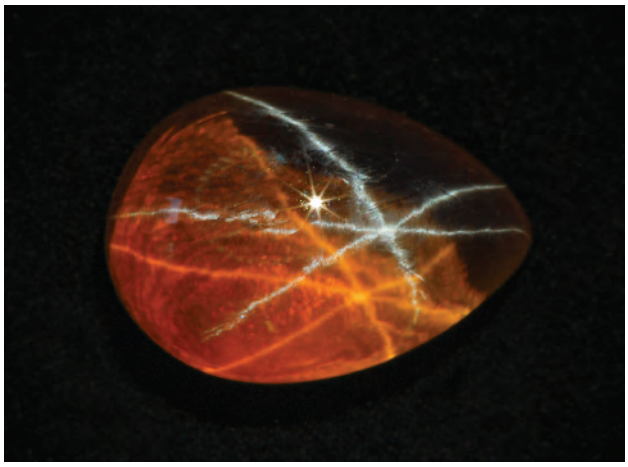

*Figure 4. This brownish yellow synthetic sapphire showing a white six-rayed star and a brownish yellow star was purchased by one of the authors in Bangkok in 2010. The cabochon measures 14.2 × 9.8 mm and weighs 9.76 ct. Photo courtesy of M.P. Steinbach.*

## SAMPLE TYPES AND EXAMINATION METHODS

The present study started with the examination of 15 asteriated synthetic rubies and sapphires of different colors that were purchased by one of the authors (MPS) in Bangkok in 2010 for his personal collection (figure 4). Neither the producer nor any details of the production technique were disclosed. An Internet search revealed that the company Thai Star Sapphire, based in Ladprao, Bangkok, is producing and offering synthetic stones of the complete color series so acquired and available for the present study (see "Thai star sapphire," n.d.). An additional extraordinarily large sample of that material, weighing 91 ct, was purchased in Bangkok in December 2014.

Similar transparent, diffusion-treated samples were made available from Wiede's Carbidwerk in Freyung, Germany, both from their production in the 1970s and from recent production. The authors were also able to examine two synthetic asteriated rubies cut in Idar-Oberstein, Germany, from the recent production of Hrand Djevahirdjian SA, one of the largest manufacturers of synthetic corundum and located since 1914 in Monthey, Switzerland.

To compare the foregoing types of samples with materials produced by Linde, the latter of which have been discussed in the literature, we collected and examined several series of asteriated Linde rubies and sapphires from different collections and the trade in the UK and Germany. Most of these 26 samples had been kept in private collections since the 1970s or before (see also box C). One of the Linde sapphire cabochons had been removed from vintage jewelry.

An Internet search further revealed that samples presently available in the gem and jewelry market under the trade name "Linde" include: (1) samples removed from vintage jewelry that had contained stones originally produced by Linde or the Linde division of Union Carbide; (2) "old stock" samples, without previous jewelry use, likewise manufactured by Linde before the production stopped and crystal growth and/or marketing was transferred to Astrid Corporation of Hong Kong in the 1970s; and (3) asteriated synthetic rubies and sapphires of various colors produced recently in Asia or elsewhere but marketed as "Linde." The "Linde" trademark has been owned by Charles and Brenda Cook of the United States since they acquired rights to the name in 2007 (C. Cook, pers. comm., 2014).

For the present investigation, we were able to purchase some Linde "old stock" material produced originally in the 1970s or before in the United States. These 66 samples can be traced back to a former employee of Union Carbide (D.L. Snyder, pers. comm., 2014).

The material currently marketed in the United States under the Linde name but obtained from Asian sources by the American distributor is represented by 13 samples. The majority of these synthetic rubies and sapphires were purchased by the distributor in Hong Kong as ready-made cabochons. The remaining cabochons offered a sampling of the distributor's acquisitions of similar material from other Asian markets such as India, Thailand, and mainland China (C. Cook, pers. comm., 2014).

The synthetic corundum samples from this study are summarized in table 2.

In addition to the foregoing synthetic corundum samples, we were able to examine a natural sapphire with a dual-color double-star pattern from the collection of one of the authors (MPS).

To augment the work with synthetic and natural corundum, we examined two almost colorless, slightly pink rose quartz cabochons from Brazil and two similar asteriated slightly brownish pink quartz stones from India, each of which showed the phenomenon of dual-color double stars. These samples came from the same author's collection.

All corundum and quartz samples were examined in a Schneider immersion microscope with Zeiss optics (up to 100× magnification). To better resolve acicular inclusions, the natural sapphire and four of the synthetic corundum cabochons were examined at higher magnification (up to 1000×) in reflected and transmitted light using a Leitz Ortholux II Pol-BK polarization

**TABLE 2.** Synthetic corundum samples studied.

| Number of samples | Source | Producer | Opaque samples without double stars | Transparent or translucent samples with double stars |
|---|---|---|---|---|
| 15 | Gem trade in Bangkok, Thailand, 2010 | Unknown | | ✓ |
| 1 | Gem trade in Bangkok, Thailand, 2014 | Unknown | | ✓ |
| 13 | C. and B. Cook, Silk Purse Jewelry (Palmetto, Florida), 2013 | Sold under the trade name "Linde" in the United States, but purchased on various Asian markets from unknown producers | ✓ | ✓ |
| 4 | H. Schulz, Wiede's Carbidwerk (Freyung, Germany), 2014 | Wiede's Carbidwerk (Freyung, Germany) | | ✓ |
| 2 | M. Kämmerling (Idar-Oberstein, Germany), 2014 | Hrand Djevahirdjian SA (Monthey, Switzerland) | ✓ | ✓ |
| 8 | C. Cavey (London, UK) | Linde/Union Carbide, (New York) | ✓ | |
| 3 | M.P. Steinbach (Idar-Oberstein) | Linde/Union Carbide | ✓ | |
| 13 | A. Hodgkinson (Portencross, Scotland) | Linde/Union Carbide | ✓ | ✓ |
| 2 | L. Gleave, Gem-A (London, UK) | Linde/Union Carbide | | ✓ |
| 6 + 60 | D.L. Snyder, The Brazilian Connection (Benton, Pennsylvania), 2013 | Linde/Union Carbide | ✓ | ✓ |

microscope. The investigation at high magnification was also performed for the four quartz cabochons.

To evaluate the possible influence of diffusion-treated layers on the formation of asterism, we removed thin layers of corundum material from the flat or slightly curved base of several synthetic cabochons and investigated for any change in the appearance of the samples. This grinding and repolishing process was performed up to three times. Similar procedures were applied to the curved dome of other samples.

The "old stock" Linde material included six finished and polished cabochons and a lot of 60 partially finished synthetic ruby and sapphire cabochons of varied quality and appearance. Among the partially finished cabochons without a detailed history of the production processes applied was a subgroup having what appeared to be inhomogeneous crusts on the surface. Seven samples from this subgroup were selected for chemical analysis by X-ray fluorescence spectroscopy using a Bruker Tracer III-SD handheld unit. A further analysis of the distribution of trace elements for five samples of this subgroup was performed by X-ray fluorescence mapping using a Bruker M4 Tornado scanning micron-scale X-ray fluorescence (μ-XRF) system. The diameter of the incident beam applied for the mapping process was 25 μm.

To characterize needle-like inclusions and the cause of asterism in the brownish pink and rose quartz samples, we employed micro-Raman spectroscopy using an XploRA confocal Raman microscope facility from Horiba with a 532 nm laser.

## RESULTS

**Natural Purplish Pink Sapphire from Myanmar.** Most natural asteriated rubies and sapphires are opaque or only slightly translucent and do not reveal the dual-color double stars that are the focus of this study. However, a transparent purplish pink sapphire, said to originate from Mogok, Myanmar, proved more relevant for the present research.

The gemstone showed two clearly separated six-rayed stars: one white star reflected from the dome of the cabochon and one purplish pink star confined to the curved base of the sample (figure 5). In reflected light, the white and the bodycolored star were each visible regardless of the direction of view—i.e., when viewed toward the dome of the sample and when viewed toward the curved base (figure 6). Moreover, in each viewing geometry, the bodycolored star was focused within the cabochon, and the white star was focused slightly outside the cabochon, between the sample and the observer.

Rutile needles in three orientations were discerned within all parts of the stone, but the rutile framework showed an irregular, patchy zoning with a variable concentration of needles in different parts of the sapphire. Specifically, certain growth planes parallel to the hexagonal prism *a* {11$\bar{2}$0} and parallel to the hexagonal dipyramid *n* {22$\bar{4}$3} exhibited a denser concentration of rutile needles (figure 7). These planes were identified in the immersion microscope by determining the angle formed by the growth planes with the optic axis of the sapphire.

At higher magnification, it was observed that the sapphire contained two types of needle-like inclusions. The first type (figures 8A–8C) consisted of needles up to 100 µm in length with a thickness of 0.3 to 2 µm. The second type of needles consisted of crystals that were mostly twinned, with a length between 50 and 200 µm and a thickness in the range of 5 to 10 µm. The twins were primarily V-shaped (figures 8 A, B, D, and E) and rarely knee-shaped (figure 8C). Occasionally, the needles were twinned along the needle axis, showing a distinct re-entrant angle

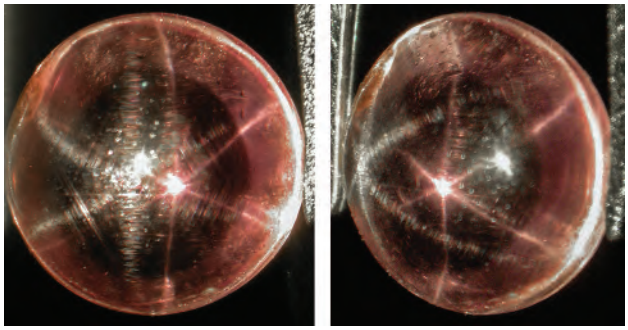

*Figure 5. This purplish pink sapphire from Myanmar shows a white star reflected from the dome of the cabochon and a bodycolored star reflected from the curved base of the sample; views to the center of the dome (left) and oblique to the center of the dome (right). The sample measures 7.0 mm in diameter and weighs 1.62 ct. Photos by K. Schmetzer.*

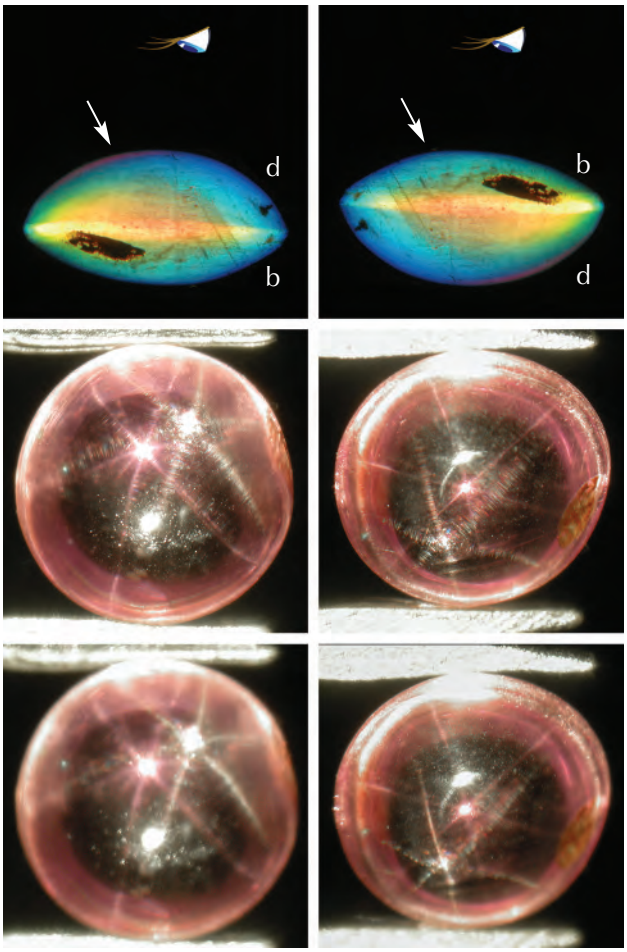


*Figure 6. Purplish pink sapphire from Myanmar in a view to the curved dome (d) (left column) and the curved base (b) of the cabochon (right column). In the top row, the white arrow indicates the direction of light, and the eye symbolizes the observer receiving the reflected light. In both orientations, the bodycolored six-rayed star is focused within the cabochon (middle row), and the white star is focused slightly outside the stone, between surface and observer (bottom row). The sample measures 7.0 mm in diameter, with a thickness of 3.5 mm, and weighs 1.62 ct. Photos by K. Schmetzer.*

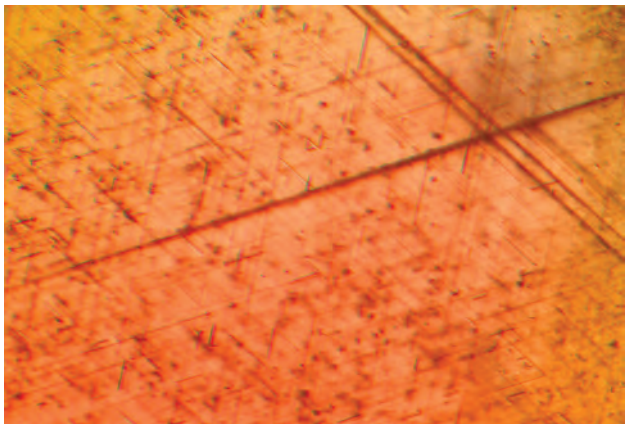

*Figure 7. A framework of rutile needles in a purplish pink sapphire from Myanmar. In a view exactly parallel to the c-axis, several intersecting planes parallel to the hexagonal prism a with a high concentration of needles are visible. Immersion, field of view 2.8 × 2.1 mm. Photo by K. Schmetzer.*

at the end of the needle (figure 8F). This latter type of twinning has been characterized in several papers by electron microscopic examination combined with electron diffraction, generally in synthetic ruby or sapphire (Phillips et al., 1980; Moon and Phillips, 1991; Xiao et al., 1997; He et al., 2011). The twin plane of these rutile needles is (101), and the same twin plane is assumed for the V-shaped twins. This indicates, with a twin plane parallel to the needle axis, that the axis of these elongated twinned needles is not the c-axis of the rutile crystals.

**Opaque Synthetic Corundum Samples with Single Stars.** The different groups and lots of Linde rubies and sapphires examined (samples produced by Linde in the United States up to 1974 and those distributed presently under the Linde trade name) contained samples of the "normal" material without double stars, showing only one white six-rayed star confined to the dome of the cabochons. The samples of this group of mostly larger synthetic rubies and sapphires were principally opaque, with minimal if any translucency (again, see figure 1). Opaque synthetic rubies and sapphires originating from Asian markets and sold under the Linde name, but with unknown producer(s), were similar in appearance, as was one ruby from Hrand Djevahirdjian SA.

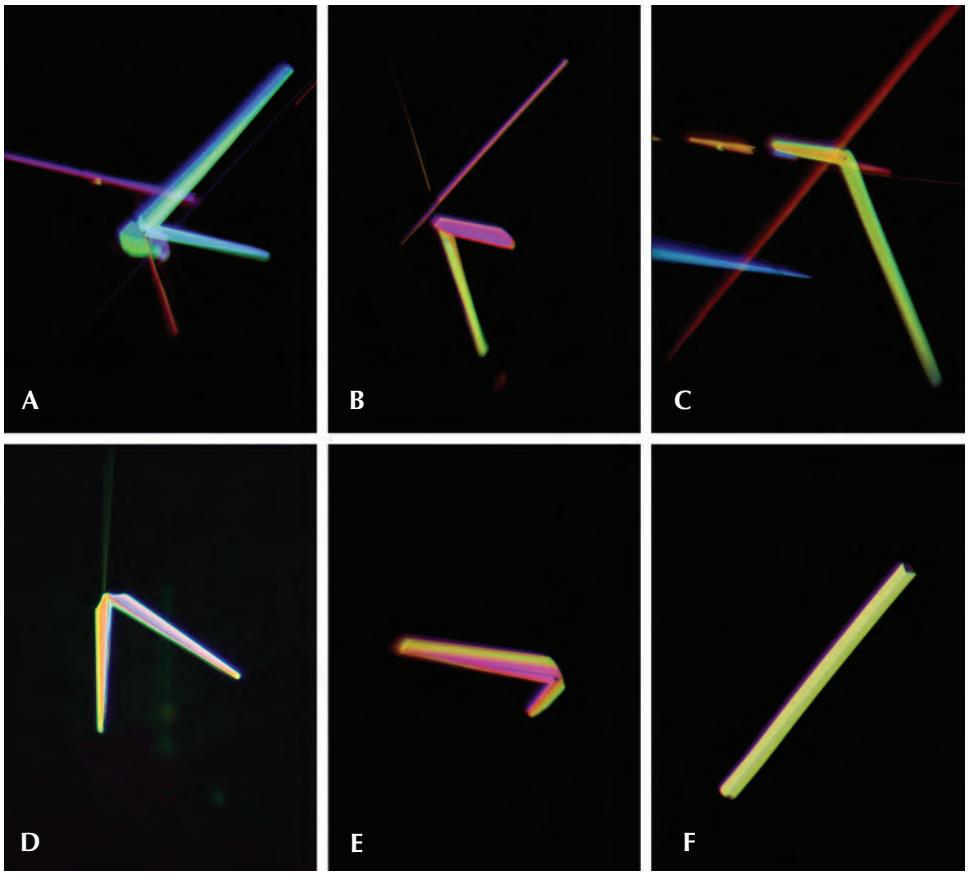


*Figure 8. Rutile needles in the purplish pink sapphire from Myanmar. The sapphire contains one type of needles with a smaller diameter (A, B, C) and a second type of somewhat thicker needles that are mostly twinned. This second type forms V-shaped twins (A, B, D, E), knee-shaped twins (C), or needles that are twinned along the needle axis (F). Reflected light, oil immersion; field of view 112 × 168 µm. Photos by H.-J. Bernhardt.*

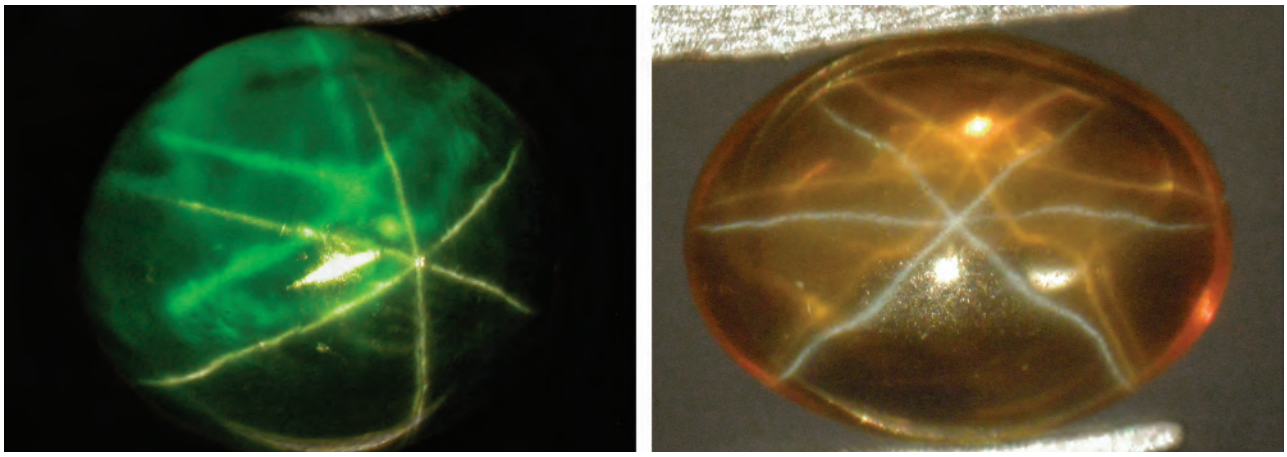

*Figure 9. These two synthetic sapphires show a white six-rayed star and a bodycolored star; the arms of the two stars seem to intersect with each other and meet again at the transition between dome and base of the cabochon. The green cabochon measures 15.6 × 14.1 mm and weighs 26.80 ct; the orange cabochon measures 10.0 × 8.0 mm and weighs 3.85 ct. Photos by K. Schmetzer.*

Upon microscopic examination with intense illumination, especially in immersion, a dense concentration of gas bubbles was observed, which frequently showed a distinct curved zoning consisting of layers with different concentrations of bubbles. Furthermore, irregularly curved boundaries, sometimes designated as "grain boundaries" or "subgrain boundaries" in the literature, were seen in most samples. Such boundaries may be explained by the fact that different parts of the crystals have slightly different orientations. Intersecting glide planes, commonly referred to by gemologists as Plato lines, were likewise evident in many samples. No needle-like inclusions were resolved with the magnification of the gemological microscope. Properties that would be uncommon for Verneuil-grown samples were absent.

The remainder of this section describes properties of various groups of transparent to translucent synthetic rubies and sapphires with dual-color double stars.

**Synthetic Samples of Recent Production Originating from Asian Markets.** This part describes two groups of synthetic materials that were purchased by the authors, one in Bangkok in 2010 and 2014 and the other in the United States (sold under the Linde trademark) in 2013. Both groups consisted mostly of transparent samples that showed two stars of different colors.

*Synthetic Samples Purchased in Bangkok in 2010 and 2014.* The 16 transparent synthetic rubies and sapphires that had been purchased in Bangkok were subdivided into two groups. A smaller group of three samples consisted of mixed-cut corundum with a polished curved upper part (dome) and a faceted back. These samples exhibited only the three intersecting light bands of an ordinary white six-rayed star, as is commonly seen in asteriated rubies and sapphires from various producers. The larger group of 13 contained samples fashioned with a polished curved dome and an almost rough (i.e., only lightly polished) and slightly curved to nearly flat base. Under fiber-optic illumination, all 13 samples of this group revealed one white six-rayed star and, in addition, three intersecting light bands producing a second, variously colored six-rayed star (figure 9; see also figure 4).

The ordinary white star was confined to the dome of the cabochons. In all samples, the second six-rayed star showed the bodycolor of the host corundum crystals (e.g., red, orange, yellow, or green). When these cabochons were illuminated through the center of the dome in a direction nearly perpendicular to the base and viewed parallel to the incident light, both stars showed the same orientation and overlapped each other. In contrast, when illuminated and/or viewed obliquely, both stars were clearly separated, and the bodycolored star seemed to emanate from the curved or almost flat, slightly polished base of the cabochon. The arms of both stars appeared to meet at the transition between dome and base (figure 9, right).

Under the microscope, it could be observed that the white star was focused slightly above the curved dome of the cabochons. The bodycolored star was focused below the white star and dome, within the body of the cabochon (figure 10). This effect was particularly noticeable in samples with a relatively high dome or cut with a broad girdle.

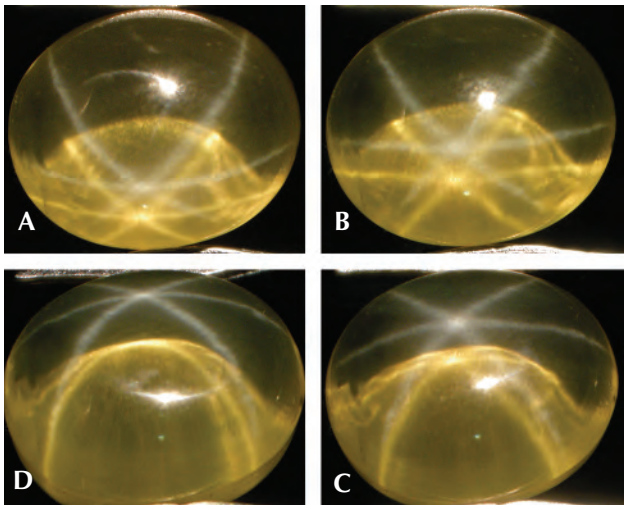


*Figure 10. This yellow synthetic sapphire shows a six-rayed white and a yellow star. Upon rotation using an east-west oriented rotation axis (sequence from A to D), it is observed that the yellow star reflected from the base is focused below the white star, within the cabochon. The sample measures 11.8 × 9.8 mm, with a thickness of 7.0 mm (girdle about 3.8 mm), and weighs 10.08 ct. Photos by K. Schmetzer.*

Microscopic examination also revealed internal characteristics, with most samples showing irregularly curved grain boundaries, best seen with crossed polarizers in immersion (figure 11, left and center). Some of these boundaries displayed interference colors, thereby establishing the slightly different orientations between different parts of the crystals. In addition, some of the corundum samples contained intersecting glide planes or Plato lines (figure 11, right). Sharp curved growth striations, characteristic of Verneuil-grown corundum, were observed in the rubies but not in the differently colored sapphires. Some of these synthetic sapphires showed only somewhat diffuse, curved growth lines, and a portion of the samples did not reveal any curved growth striations at all. Gas bubbles were seen only in two of the sapphires.

All microscopic features observed in the 16 rubies and sapphires typically characterize synthetic corundum crystals grown by the Verneuil method. Oriented needles were not discernible under the magnification of the gemological microscope.

In order to clarify which parts of the samples contained three series of small needles, the mechanism considered responsible for the production of six-rayed asterism and presumed to generate the white and the bodycolored stars examined here, we ground and repolished the slightly curved or almost plane base of four asteriated cabochons, as well as the dome of another synthetic sapphire.

After grinding and repolishing the base of the four cabochons, all samples showed only one remaining white six-rayed star (figure 12, left). The bodycolored star was no longer visible. Conversely, after grinding and repolishing the curved dome of the other cabochon, this sample showed only the second six-rayed star with the bodycolor of the sapphire, and the ordinary white star had disappeared (figure 12, right).

*Synthetic Samples Purchased in the United States in 2013, Originating from Various Asian Markets.* The visual appearance of the transparent synthetics produced recently in Asia but sold in the United States under the Linde trade name was consistent with that of the 13 (non-faceted) Bangkok samples described above. They revealed a white six-rayed star

*Figure 11. Microscopic features in Verneuil-grown diffusion-treated synthetic sapphires. Irregular grain boundaries are frequently observed under crossed polarizers (left and center); occasionally, glide planes (Plato lines) are also seen (right). Viewed in immersion; field of view: 8.1 × 6.1 mm (left), 9.5 × 7.2 mm (center), and 9.5 × 7.2 mm (right). Photos by K. Schmetzer.*

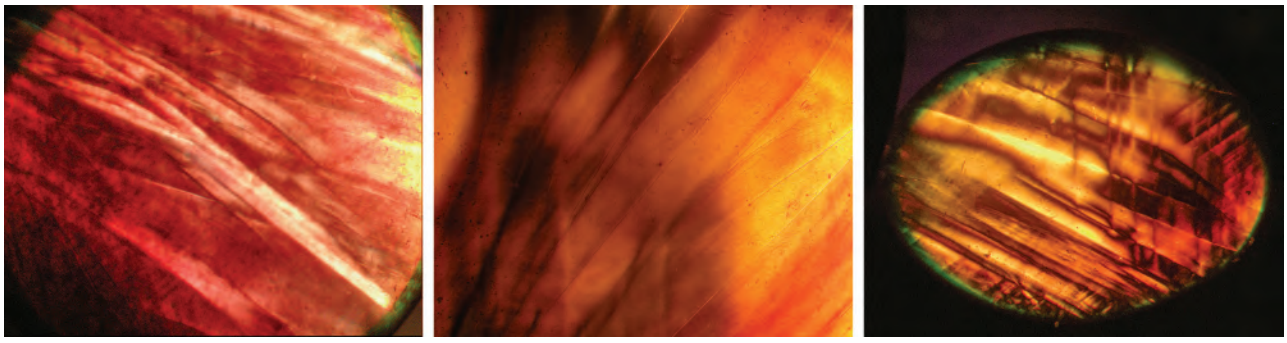

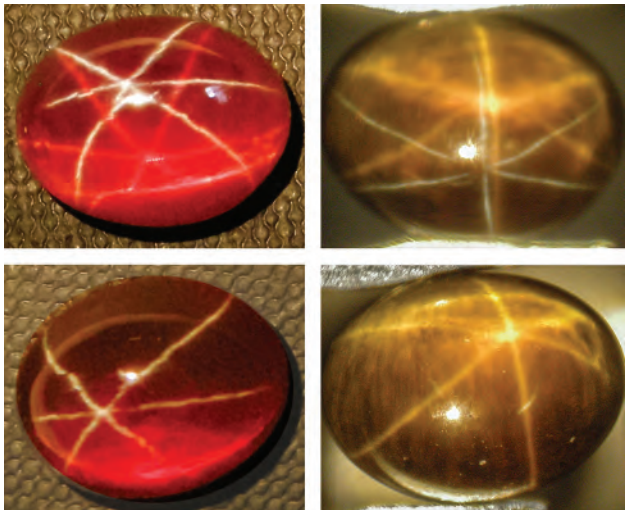

*Figure 12. Left: This red-orange synthetic sapphire shows a white star and a red-orange star (top); after grinding and repolishing of the base, the red-orange star is removed and only the white star is observed (bottom). The sample measures 13.2 × 10.4 mm and weighs 11.15 ct. Right: This light yellow-orange synthetic sapphire shows a white star and a yellow-orange star (top); after grinding and repolishing of the dome, the white star is removed and only the yellow-orange star remains (bottom). The sample measures 11.5 × 8.7 mm and weighs 6.94 ct. Photos by K. Schmetzer.*

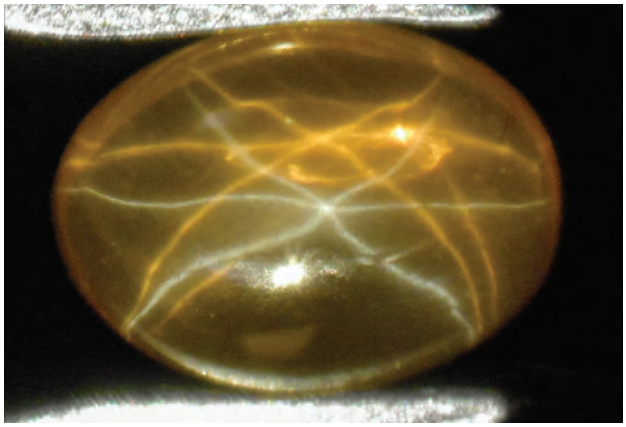

*Figure 13. This yellow-orange synthetic sapphire shows a white six-rayed star and a yellow-orange star; this material is currently distributed under the "Linde" trade name. The sample measures 8.2 × 6.2 mm and weighs 1.46 ct. Photo by K. Schmetzer.*

related to the curved dome of the cabochon and a second star reflecting the bodycolor of the sample (i.e., red, yellow-orange, or orange; figure 13).

The microscopic pattern was also analogous to that of the samples purchased in Bangkok. The synthetic rubies and orange sapphires showed curved growth striations, occasionally related to a zoning of gas bubbles (figure 14, left and center). Irregular grain boundaries and Plato lines were also seen in some instances (figure 14, right).

From the transparent samples of this group, we selected two synthetic rubies for grinding and repolishing, one sample at the base and one sample at the curved dome. The alterations were similar to those seen in the group of Bangkok samples described earlier. For the ruby ground and repolished at the base, the red star reflecting the bodycolor of the crystal was completely removed (figure 15, left). For the sample repolished at the dome, the white star confined to the upper surface was no longer present (figure 15, right).

To investigate the formation of stars in transmitted light (diasterism), we examined some samples in their as-received state, with upper and lower diffused

*Figure 14. Microscopic features in Verneuil-grown diffusion-treated synthetic rubies (left) and sapphires (center and right). Left: Synthetic ruby with curved growth lines and irregularly distributed gas bubbles. Center: Sapphire with curved zones showing different concentrations of gas bubbles. Right: Sapphire with irregularly shaped grain boundaries. Immersion, crossed polarizers; field of view: 4.5 × 3.4 mm (left), 4.5 × 3.4 mm (center), and 9.5 × 7.2 mm (right). Photos by K. Schmetzer.*

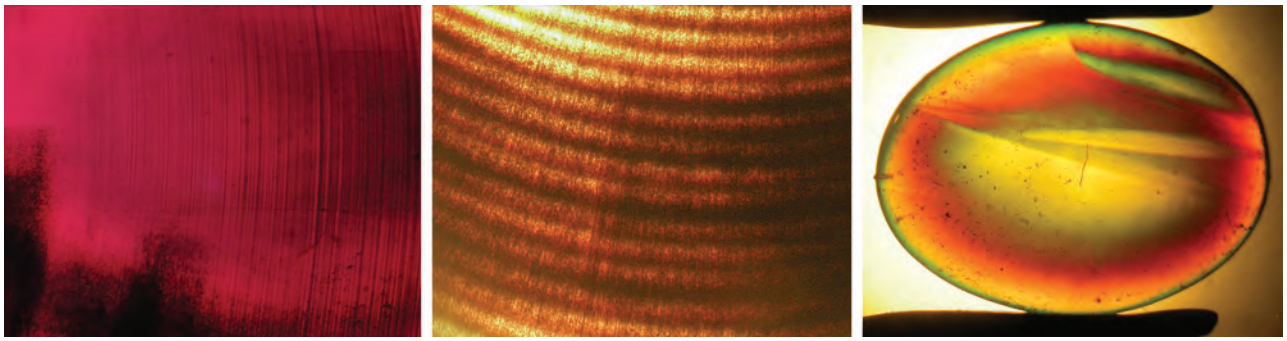

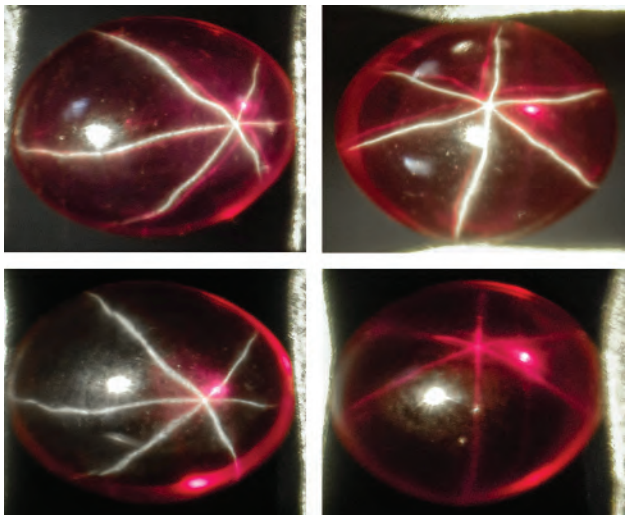

*Figure 15. Left: This synthetic ruby shows a white star and a red-purple star (top); after grinding and repolishing of the base, the red-purple star is removed and only the white star remains (bottom). The sample measures 8.1 × 6.3 mm and weighs 1.44 ct. Right: This synthetic ruby shows a white star and a red-purple star (top); after grinding and repolishing of the dome, the white star is removed and only the red-purple star remains (bottom). The sample measures 10.3 × 8.1 mm and weighs 3.51 ct. Photos by K. Schmetzer.*

layers intact, and other samples that had been ground and repolished as indicated above, either:

1. At the dome of the sample, leaving a diffusion-treated layer at the base, or
2. At the base of the cabochon, leaving a diffusion-treated layer at the dome

*Figure 16. In transmitted light, this yellow-orange synthetic sapphire shows a bodycolored six-rayed star; asterism in transmitted light is known as* diasterism. *The sample (see figure 13) measures 8.2 × 6.2 mm and weighs 1.46 ct. Photo by K. Schmetzer.*

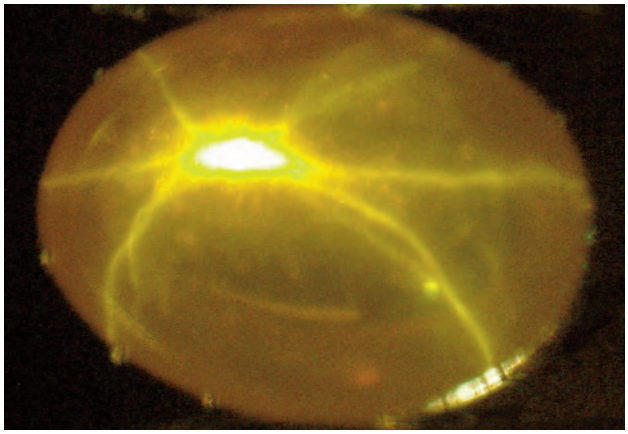

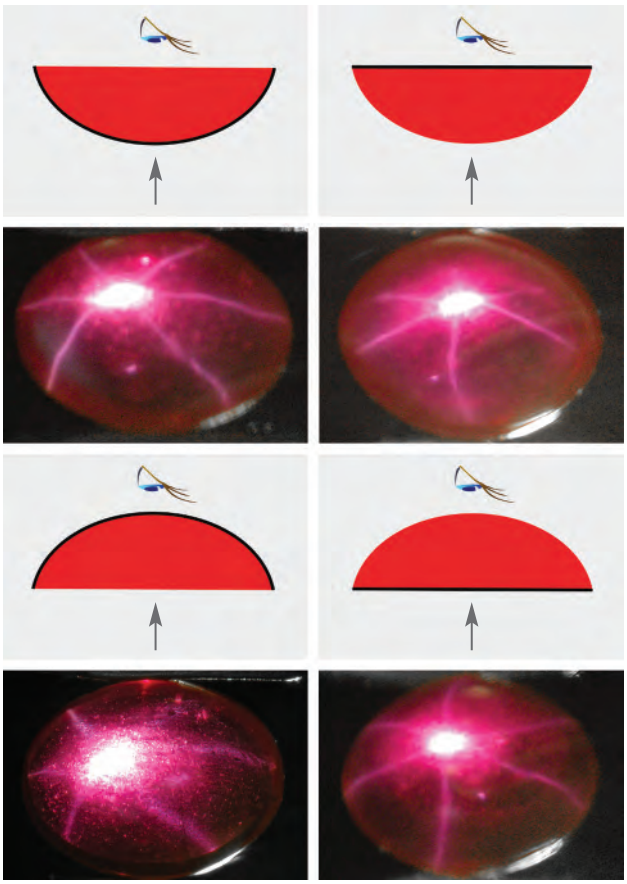

*Figure 17. Diasterism is observed in transmitted light in diffusion-treated synthetic rubies that have been ground and repolished at the base (left sample) or at the dome (right sample). The remaining diffusion-treated layer with rutile needles is schematically shown in black, with the arrow indicating the direction of light and the eye symbolizing the observer. In all four views, a bodycolored red-purple six-rayed star is observed. The sample on the left measures 8.1 × 6.3 mm and weighs 1.44 ct (see figure 15, left). The sample on the right measures 10.3 × 8.1 mm and weighs 3.51 ct (see figure 15, right). Photos by K. Schmetzer.*

For all types of samples, comparative observations were made with the light impinging either on the curved dome or on the flat base of the cabochons.

Samples in the as-received state showed a single bodycolored six-rayed star in transmitted light (figure 16). The observations for ground and repolished rubies are summarized in figure 17. In all four conditions of view depicted, a single star was seen in transmitted light. This demonstrated that regardless of the path of the incident transmitted beam of light, a star is formed, even in samples having only a small diffused layer with rutile needles on one side of the

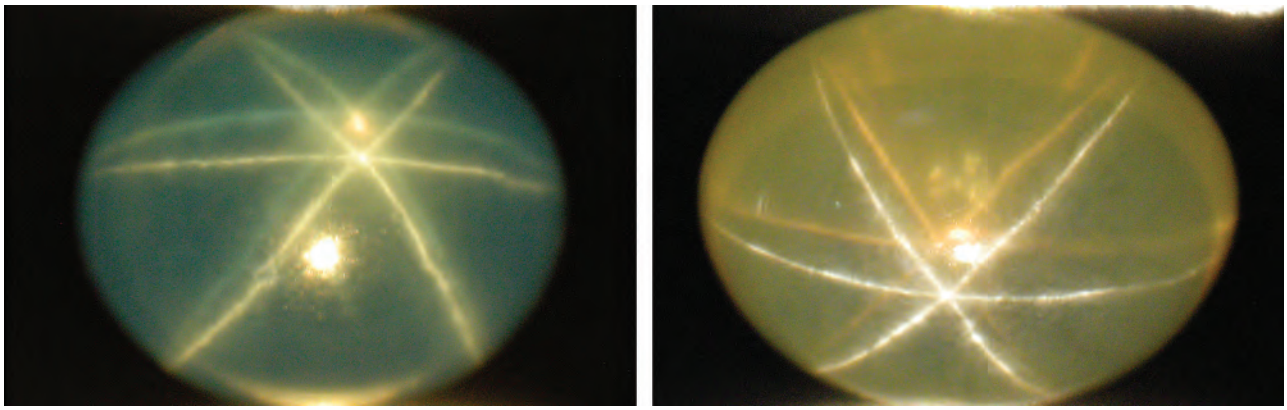

*Figure 18. A diffusion-treated blue synthetic sapphire from recent production (left) and a diffusion-treated synthetic yellow sapphire produced in the 1970s (right), both manufactured by Wiede's Carbidwerk. Both show a white star and a bodycolored blue or yellow star. The blue cabochon measures 12.2 × 10.2 mm and weighs 7.44 ct; the yellow cabochon measures 10.2 × 8.0 mm and weighs 3.91 ct. Photos by K. Schmetzer.*

cabochon, either at the flat or almost flat base or at the curved upper part.

**Samples Produced by Wiede's Carbidwerk.** Four diffusion-treated Verneuil synthetic sapphires were made available by Wiede's Carbidwerk: two samples (green and yellow) from the production of the 1970s, and two samples (blue and green) from recent production. All samples were transparent and showed dual-color double stars (figure 18). Microscopic examination revealed an intense curved growth zoning confined to areas with a variable concentration of gas bubbles (figure 19, left). All four sapphires showed irregular grain boundaries, which were best seen under crossed polarizers (figure 19, right).

**Samples Produced by Hrand Djevahirdjian SA.** Two samples from recent production of Hrand Djevahirdjian SA (Djeva) were examined for this study. One synthetic ruby, representing the majority of the company's production, was primarily opaque, with only slight translucence at the rim, and showed the normal six-rayed white star of corundum (figure 20, left). The other sample was transparent and revealed a dual-color double-star pattern consisting of a white star confined to the dome of the cabochon and a purplish red second star confined to the base (figure 20, right).

Both samples were grown and heat treated (to form needle-like precipitates) by Djeva in Switzerland and then cut from the rough by Viktor Kämmerling Company (Idar-Oberstein, Germany). In discussions with those involved in the production, it was mentioned that small transparent areas are found on rare occasions close to the tips of the Verneuil-grown ruby boules, near the seed used for crystal growth. The sample depicted in figure 20 (right) was cut from one such transparent area (M.

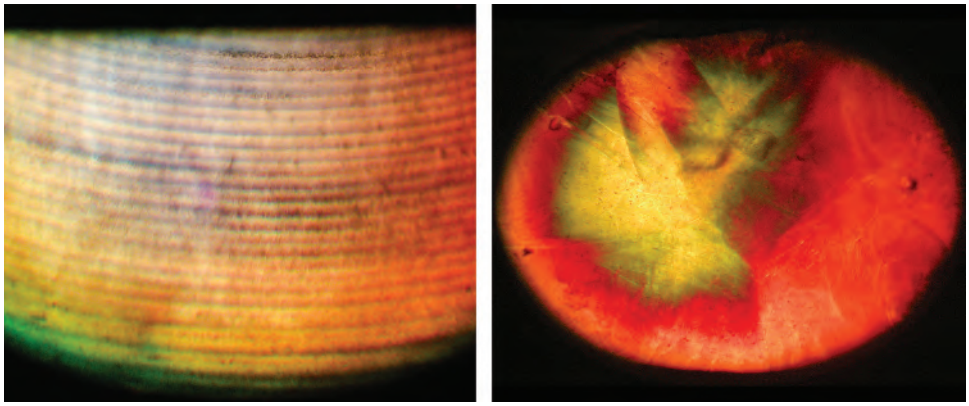

*Figure 19. Microscopic features in Verneuil-grown and diffusion-treated sapphires produced by Wiede's Carbidwerk. Left: Curved zones showing different concentrations of gas bubbles. Right: Irregularly shaped grain boundaries. Immersion, crossed polarizers; field of view: 7.6 × 5.7 mm (left) and 11.5 × 8.7 mm (right). Photos by K. Schmetzer.*

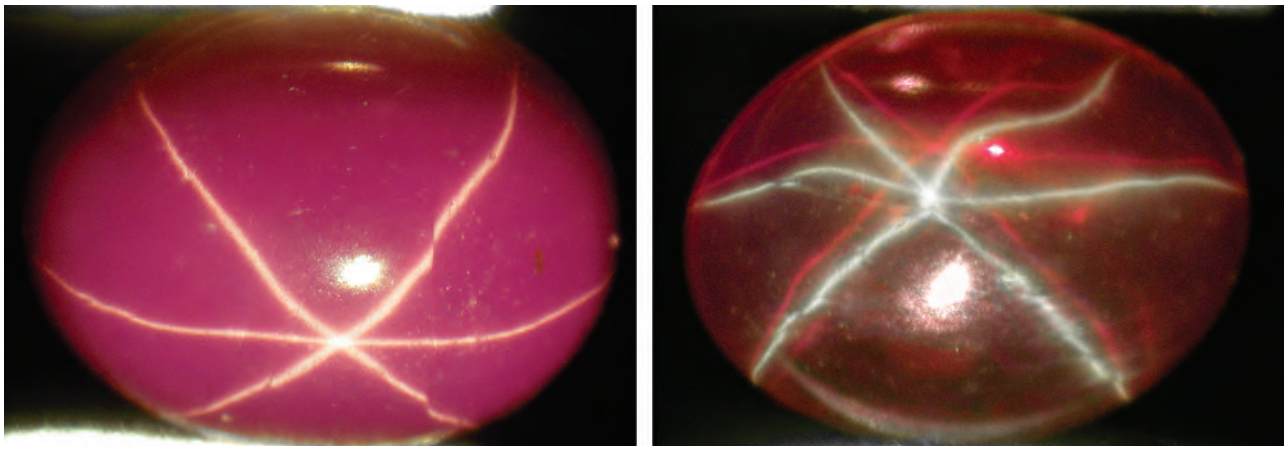

*Figure 20. Two synthetic Verneuil-grown rubies from the recent production of Hrand Djevahirdjian SA. The majority of the production consists of opaque material showing an ordinary six-rayed star (left). In a few of the Verneuil boules, a small transparent area is found; when cut as cabochons, these show a double-star pattern consisting of a white and a purplish red star (right). The opaque cabochon measures 9.0 × 7.0 mm and weighs 1.95 ct; the transparent sample measures 8.8 × 6.9 mm and weighs 2.70 ct. Photos by K. Schmetzer.*

Kämmerling, pers. comm., 2014). According to these discussions, neither the opaque to slightly translucent stone nor the transparent sample was diffusion treated.

Examined in the microscope, the transparent asteriated ruby showing the double-star pattern revealed only inclusions that are typical for Verneuil-grown synthetic rubies (e.g., curved growth striations, irregular grain boundaries, and Plato lines). The only difference seen in the opaque sample was an extremely high concentration of gas bubbles.

**Samples Produced by Linde.** As previously noted, until the mid-1970s Linde in the United States produced synthetic asteriated corundum in a wide range of colors, and dual-color double stars have been depicted in this material (Arem, 1987; Gübelin and Koivula, 2008). To evaluate the cause and possible mechanism of formation of these Linde double stars, we were able to examine several parcels of Linde synthetic rubies and sapphires kept in various collections in the UK and Germany. In addition, we were able to purchase some samples of "old stock" Linde material (see also box C).

*Samples of Linde Synthetics from a 1970s Collection.* A collection in the UK of 13 differently colored Linde synthetic sapphires and rubies purchased in the early 1970s was made available for examination (figure 21). The few opaque samples from this collection revealed only the ordinary white six-rayed star, but in translucent or transparent samples from this lot, another six-rayed star was apparent (figure 22). This star showed the bodycolor of the corundum host crystal.

Upon microscopic examination, the typical inclusions of Verneuil-grown synthetic rubies and sapphires were observed. The only difference between the opaque, translucent, and transparent samples from this series was a varying concentration of gas bubbles. In other words, samples with a high, layered concentration of gas bubbles were opaque, and samples with a smaller concentration of bubbles were translucent or transparent. These observations indicated that the samples were grown under similar conditions and simply reflected the variations that would be expected to occur during production in the different original boules and/or in different portions of the boules from which they were cut.

To determine if there were specific layers responsible for the formation of the different stars in this group of synthetic corundum cabochons, we were allowed by the owner to grind and repolish the almost plane base of two asteriated cabochons and the dome of a third sample. One or two grinding and repolishing steps were performed, and after each step the samples were reexamined to identify any changes.

After the first step, no distinct change in the appearance of the two differently colored stars was perceptible for any of the three samples. Neither the white star confined to the dome of the third cabochon mentioned above nor the bodycolored star confined to the base of the other two samples was

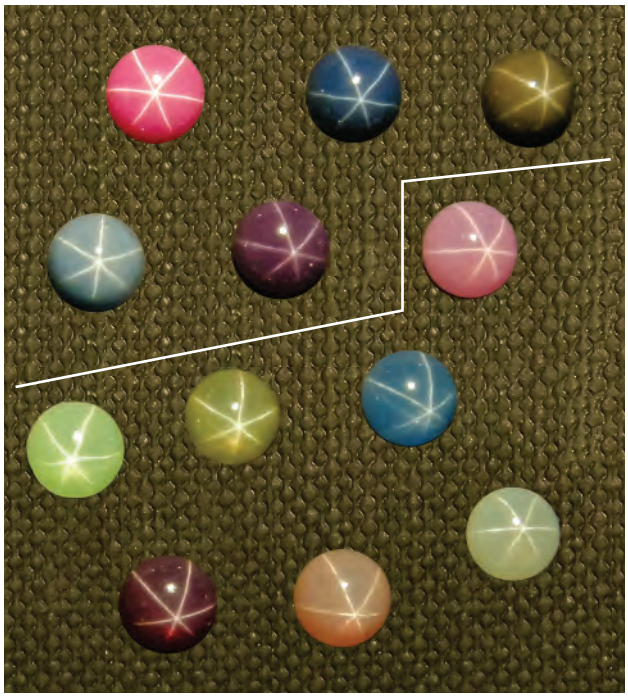

*Figure 21. A collection of Linde synthetic rubies and sapphires purchased in the 1970s, each showing a white six-rayed star. The seven cabochons below the line are transparent or translucent and also show a bodycolored star. The samples, which measure 5.0–5.2 mm in diameter, have a thickness of 2.5 to 2.7 mm and weigh 0.63–0.75 ct. Photo by K. Schmetzer; samples courtesy of A. Hodgkinson.*

removed or altered by the initial grinding and repolishing process (figure 22, left). After a second processing to remove additional thin layers from the bases of the latter two stones and the dome of the third cabochon, the bodycolored star of one pink sapphire became distinctly weaker and was almost removed (figure 22, right). In contrast, the white and bodycolored stars of the other two samples did not show a visible change.

*Samples of "Old Stock" Linde Material Purchased in the United States in 2013.* Further insight into the historic Linde production was obtained from examining the "old stock" material purchased in the United States in 2013. Two opaque synthetics within this group, one ruby and one blue sapphire, showed only the white star of ordinary asteriated samples and only the microscopic features that are common for such samples.

Two yellow and two light yellowish green synthetic sapphires within this group were transparent and revealed the dual-color double-star pattern, with a white star related to the dome of the cabochon and a bodycolored star confined to the base (figure 23).

Microscopic examination showed gas bubbles, irregular grain boundaries, and Plato lines (figure 24). In three samples, a very fine pattern of oriented needles was also observed. The sizes of these needles were at the resolution limit of a normal gemological microscope (up to 100× magnification).

One yellowish green and one yellow sample from this group were ground and repolished at their bases in two or three different steps. Neither revealed any change in the visual appearance of the stars after two rounds of grinding and repolishing. Finally, a third deeper grinding and repolishing was applied to the base of the yellowish green sample, but again no alteration of asterism was apparent (figure 23).

*Figure 22. Left: This light yellowish green sapphire shows a white star and a bodycolored star (top); after grinding and repolishing of the dome, the white star is not removed and both stars are still observed (bottom). The sample measures 5.0 mm in diameter, with a thickness of 2.4 mm, and weighs 0.58 ct (after grinding and repolishing). Right: This pink sapphire shows a white star and a bodycolored star (top); after grinding and repolishing of the base, the bodycolored star is almost completely removed and only the white star is still observed (bottom). The sample measures 5.1 mm in diameter, with a thickness of 2.4 mm, and weighs 0.61 ct (after grinding and repolishing). Photos by K. Schmetzer.*

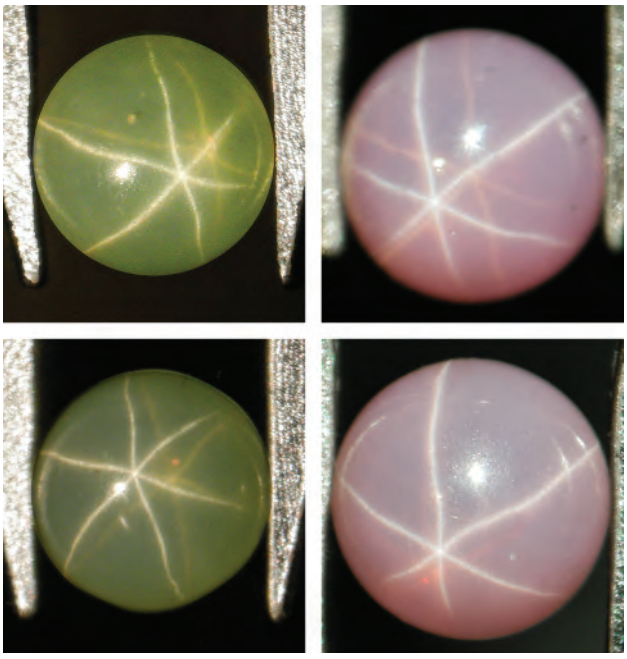

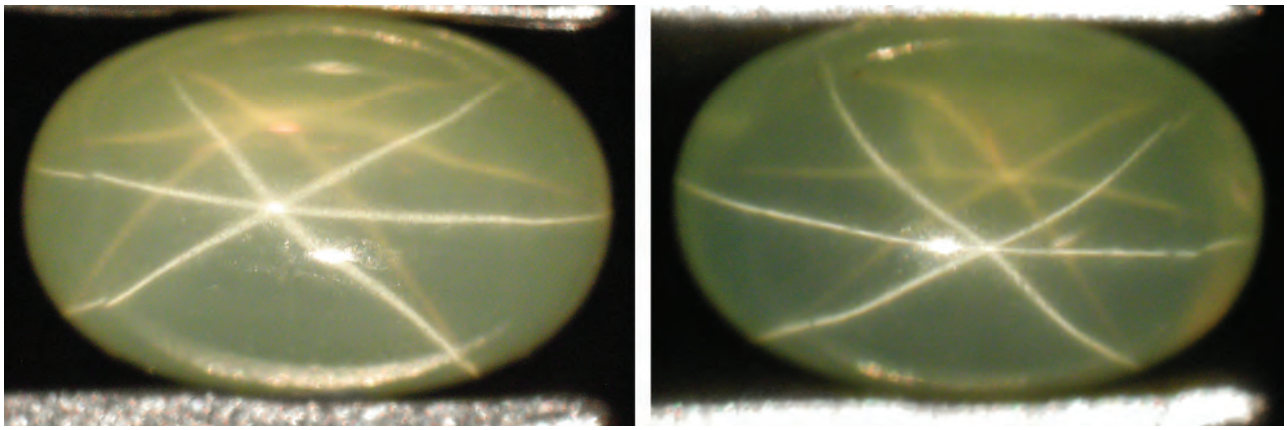

*Figure 23. This light yellowish green sapphire shows a white six-rayed star and a bodycolored star (left); after three grinding and repolishing steps at the base of the cabochon, the bodycolored star is not removed and both stars are still observed (right). The sample measures 6.0 × 4.1 mm, with a thickness of 2.6 mm, and weighs 0.54 ct (after grinding and repolishing). Photos by K. Schmetzer.*

As mentioned earlier, within a parcel of approximately 60 partially finished cabochons traced back to a former Union Carbide staff member was a group of samples having inhomogeneous crusts. We examined these crusts to better understand several steps of the production techniques applied by Linde in the late 1960s to the early 1970s, which have not previously been discussed in the gemological literature.

It is unknown if this lot of partially finished, preshaped stones consisted of rejected, in-process, or experimental samples. In general, the crusts covered only part of the surface of the cabochons (figure 25).

*Figure 24. Irregularly shaped grain boundaries within a Verneuil-grown synthetic sapphire produced by Union Carbide under the Linde trade name. Immersion, crossed polarizers, field of view 2.4 × 1.8 mm. Photo by K. Schmetzer.*

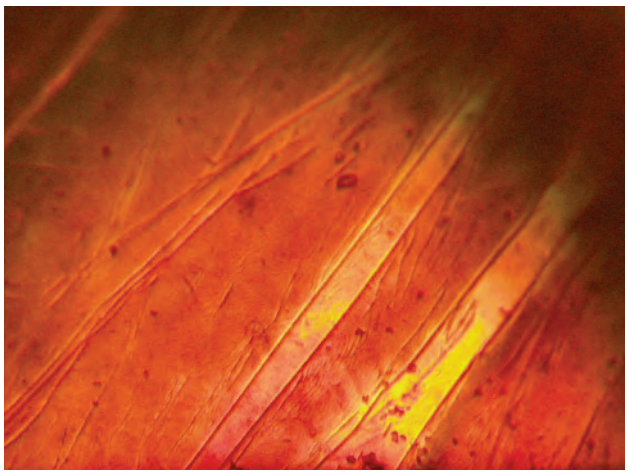

As previously detailed, the crusts on the surface of seven samples (red, purple, and green) were characterized by X-ray fluorescence, and five of these samples were also examined by micron-scale X-ray fluorescence mapping.

To recapitulate the results, it was found that the crusts, in most cases, consisted primarily of iron-bearing solids, occasionally associated with other trace elements, but no titanium was found as a major component. Thus, we concluded that the crustal elements were applied for diffusion to enhance the appearance, mainly color, of the samples, but not for improvement and/or creation of asterism. However, as already mentioned, it is unknown if these samples represented part of the commercial production or were simply test samples to investigate the possibility of color improvement.

**Needles in Synthetic Rubies and Sapphires at Higher Magnification.** Two cabochons of sample types proven to be diffusion-treated by the grinding and repolishing experiments and two cabochons that showed no alteration after such experiments were examined at higher magnification (up to 1000×) in reflected and transmitted light. In all four samples, elongated thin needles of similar visual appearance, most likely rutile needles, were observed (figure 26). Views toward the dome and toward the base of the cabochons revealed no perceptible difference in the appearance of the needles. The needles were up to 50 µm long, and their thickness ranged from 0.3 to 0.4 µm. Knee-shaped twins and V-shaped twins were seen occasionally.

*Figure 25. Inhomogeneous crusts of iron-bearing compounds on the base of a pre-shaped purple sapphire (left) and the base of a grayish green sapphire cabochon (right) from Linde. These samples may reflect diffusion treatment involving materials other than titanium, at least on an experimental basis, for enhancement of color in asteriated ruby and sapphire. The purple sample measures 8.3 × 6.4 mm, and the grayish green sample measures 7.1 × 5.1 mm. Photos by K. Schmetzer.*

**Quartz from Brazil and India.** During the course of this project, asteriated natural quartz samples from two sources were made available. (At present, synthetic asteriated quartz is unknown.) We were able to examine two almost colorless, very slightly pink rose quartz cabochons from Brazil, inspired in particular by the observations of Killingback (2006, 2011) on a transparent rose quartz sphere, and two slightly brownish pink quartz cabochons from India. Numerous localities in Brazil have been mentioned as sources for asteriated rose quartz (Cassedanne and Roditi, 1991), but the exact source for the samples

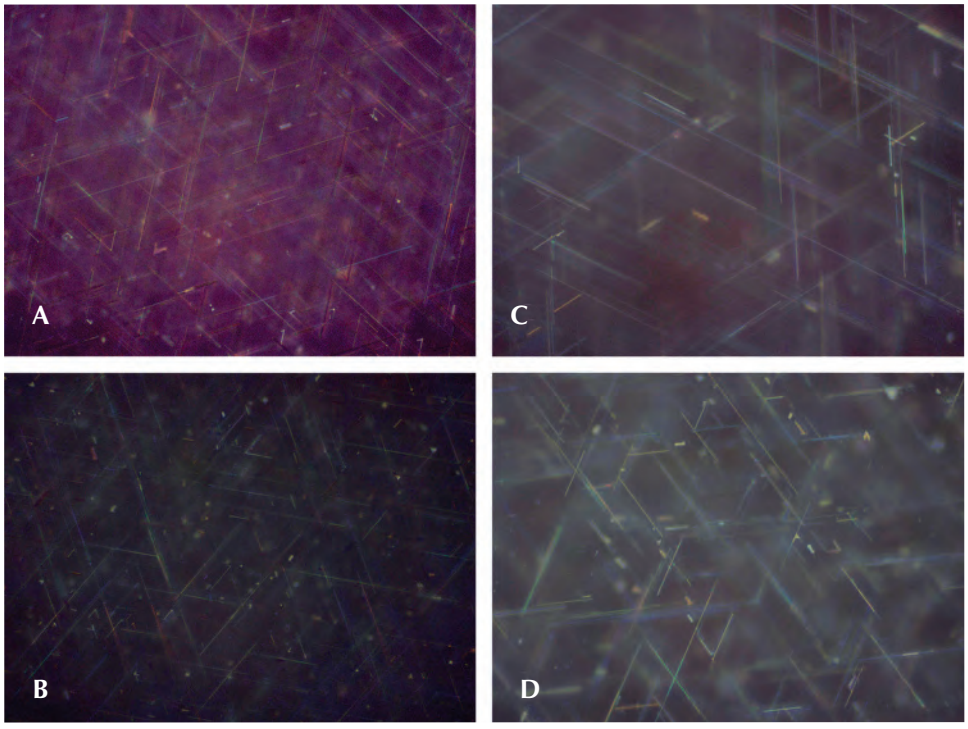


*Figure 26. Rutile needles in four corundum samples with double stars, as observed in a view toward the curved dome. A: Purplish ruby from a collection of Linde samples from the 1970s (see figure 21, lower left); B: Light yellowish green sapphire of "old stock" Linde material (see figure 23); C: Diffusion-treated ruby sold under the "Linde" trade name but traced back to the Asian market (see figure 15, left); D: Diffusion-treated yellow sapphire purchased in 2010 in Bangkok (see figure 10). Reflected light, oil immersion; field of view 92 × 69 µm. Photos by H.-J. Bernhardt.*

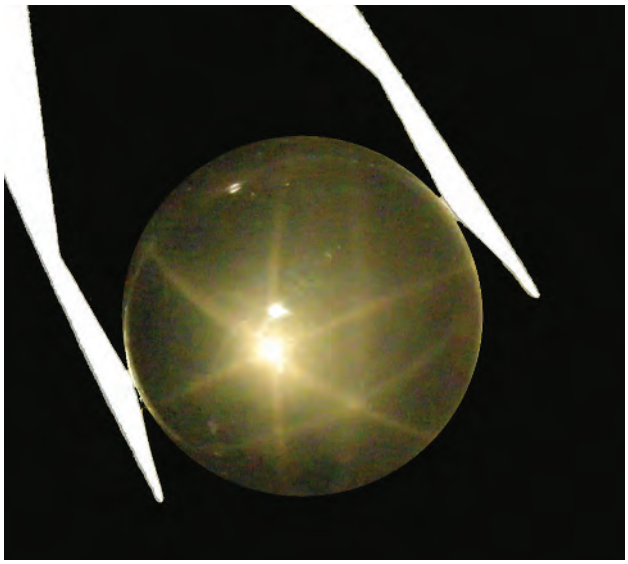

*Figure 27. Very light rose quartz cabochon from Brazil showing double stars in reflected light. The cabochon measures 21.0 mm in diameter and weighs 26.18 ct. Photo by K. Schmetzer.*

examined is unknown. In India, asteriated rose quartz is known from the Kekri region, in the Tonk district of Rajasthan (G. Choudhary, pers. comm., 2014). This might be the source for the two cabochons studied as part of the present research project.

*Rose Quartz from Brazil.* In reflected light, both Brazilian samples showed a six-rayed dual-color double-star pattern, closely resembling the pattern in very light-colored sapphires (figure 27). Again, the star related to the curved dome of the cabochons was white, but the color of the other star related to the plane base was slightly pink.

During the examination, it became apparent that asterism in transmitted light (diasterism), which produced a single star, was much stronger than asterism in reflected light (epiasterism), which produced the double-star pattern.

In the gemological microscope, no individual needles or elongated particles were resolved with the magnification permitted.

*Brownish Pink Quartz from India.* Compared to the color of the cabochons available from Brazil (see above), the Indian samples had a light "smoky" color component in addition to the ordinary pink that is typically seen in rose quartz.

When offered in the trade, such material is frequently sold with a rough (unpolished) base to enhance the visual appearance of the white six-rayed star. With this type of cabochon, a second star is generally not observed. After polishing the base of the two samples studied here, however, the presence of a second star confined to the base was clearly visible (figure 28). The light bands exhibited by the brownish pink material from India were less sharp than those seen in the rose quartz samples described above.

Examination with the gemological microscope again did not indicate any needle-like inclusions resolved with the magnification of the instrument.

**Needles in Quartz from Both Sources at Higher Magnification.** The Brazilian rose quartz and Indian quartz cabochons were examined at higher magnification (up to 1000×) in reflected and transmitted light. In all four samples, elongated thin needles were observed.

In the rose quartz cabochons from Brazil, some of these needles were oriented in three directions approximately perpendicular to the c-axis (i.e., in the basal plane), but other orientations inclined to this plane were also observed frequently (figure 29, A and B). An analysis of some of these needles by micro-Raman spectroscopy identified them as the mineral dumortierite (figure 29C). Previous studies involving dissolution of the host and examination of the residual fibers have established dumortierite as an inclusion in rose quartz from various localities (Applin and Hicks, 1987; Goreva et al., 2001; Ma et al., 2002). In the present case, we were able to identify some of the larger needles within the host by non-destructive means.

Notably, in both cabochons from Brazil, the network of needles oriented in the basal plane and visi-

*Figure 28. Slightly brownish pink quartz cabochon from India showing a double star in reflected light. The cabochon measures 24.2 × 18.8 mm and weighs 50.30 ct. Photo by K. Schmetzer.*

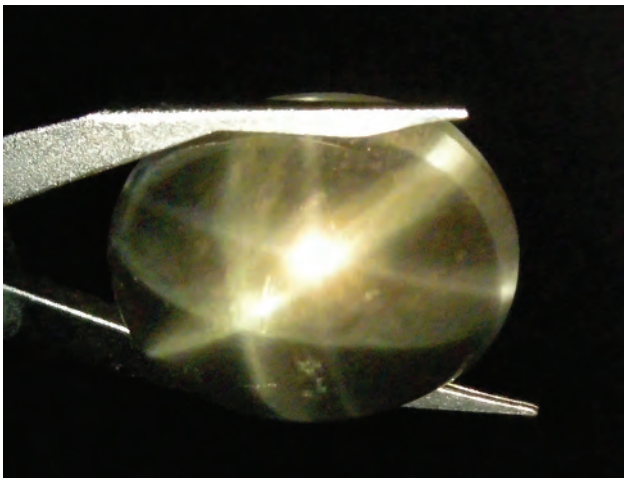

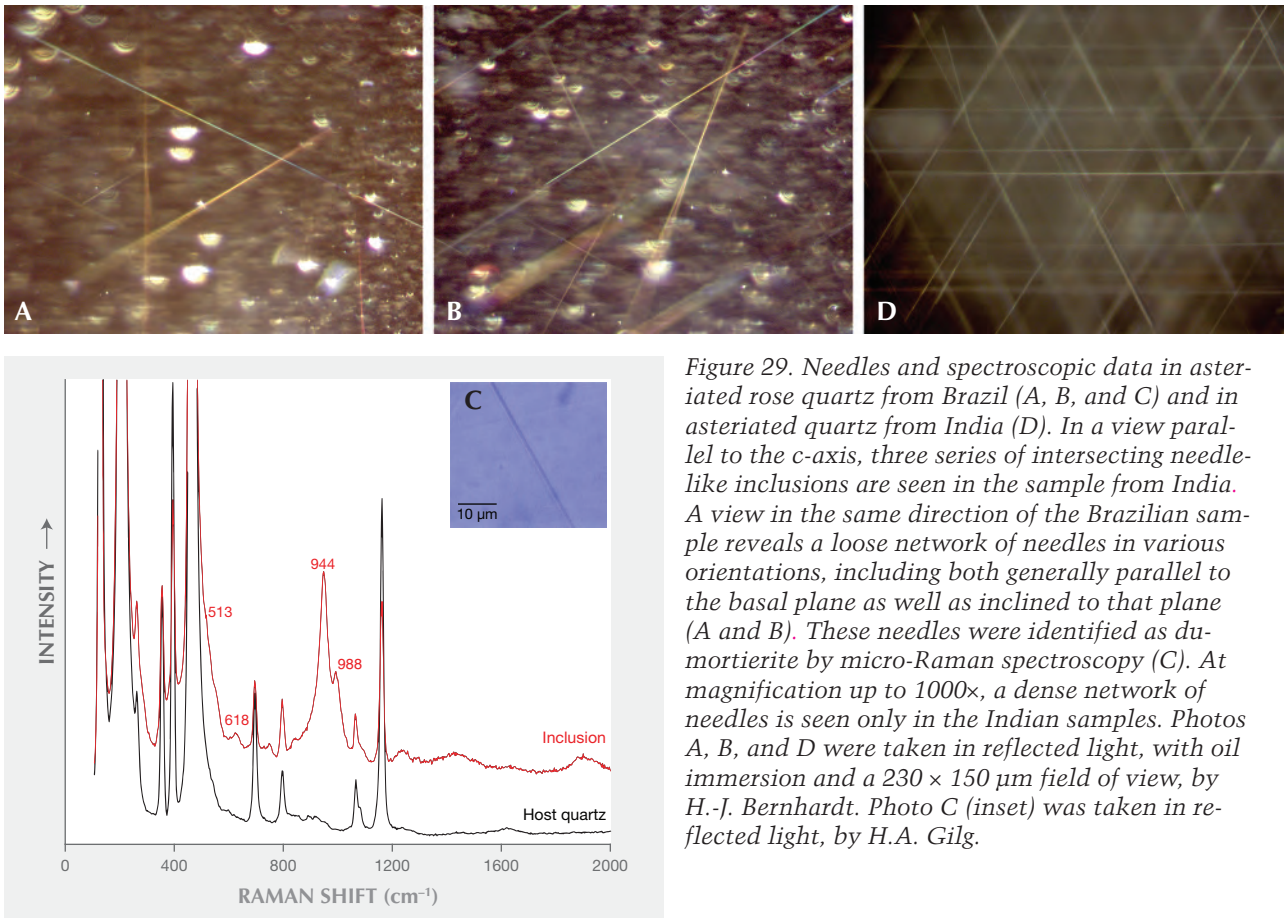


*Figure 29. Needles and spectroscopic data in asteriated rose quartz from Brazil (A, B, and C) and in asteriated quartz from India (D). In a view parallel to the c-axis, three series of intersecting needle-like inclusions are seen in the sample from India. A view in the same direction of the Brazilian sample reveals a loose network of needles in various orientations, including both generally parallel to the basal plane as well as inclined to that plane (A and B). These needles were identified as dumortierite by micro-Raman spectroscopy (C). At magnification up to 1000×, a dense network of needles is seen only in the Indian samples. Photos A, B, and D were taken in reflected light, with oil immersion and a 230 × 150 µm field of view, by H.-J. Bernhardt. Photo C (inset) was taken in reflected light, by H.A. Gilg.*

ble at higher magnification was not dense. This fact and the presence of similar needles inclined to the basal plane indicated that these needles were not responsible, at least not alone, for the asterism of the samples. Most likely, an additional denser network of smaller needles is also present.

In contrast to the Brazilian rose quartz just discussed, the samples from India featured a dense network of oriented needle-like inclusions in the basal plane, and only a few single needles were seen with an orientation oblique to that plane (figure 29D). An examination of some of these elongated inclusions by micro-Raman spectroscopy did not unequivocally identify the mineral or substance responsible. Nonetheless, it was evident that the appearance of needle-like inclusions differed in the samples from the two sources.

Although rutile needles are common inclusions in quartz, other needle-like inclusions (e.g., sillimanite or ilmenite) have also been identified in asteriated samples. Thus, without further examination, such as by electron microscopy and electron diffraction (given the small diameter of the needles), an attempt to offer a specific identification for the needles causing asterism in the rose quartz from Brazil and in the brownish pink quartz from India would be speculative.

## DISCUSSION

**Microscopic Features.** The Verneuil-grown synthetic rubies and sapphires did not exhibit any atypical microscopic features. Most samples revealed irregular grain boundaries, and several showed prismatic glide planes (Plato lines). Curved growth striations were typically seen in rubies, while the blue sapphires frequently showed curved layers with different concentrations of gas bubbles. Occasionally, gas bubbles were also seen in areas not related to growth features. The size of the rutile needles, in general, was near or below the resolution limit of the gemological microscope, but three series of needles could be clearly observed at higher magnification.

The main difference between the transparent or translucent samples showing the dual-color double-star pattern and the non-transparent samples without a double-star pattern was the concentration of gas bubbles.

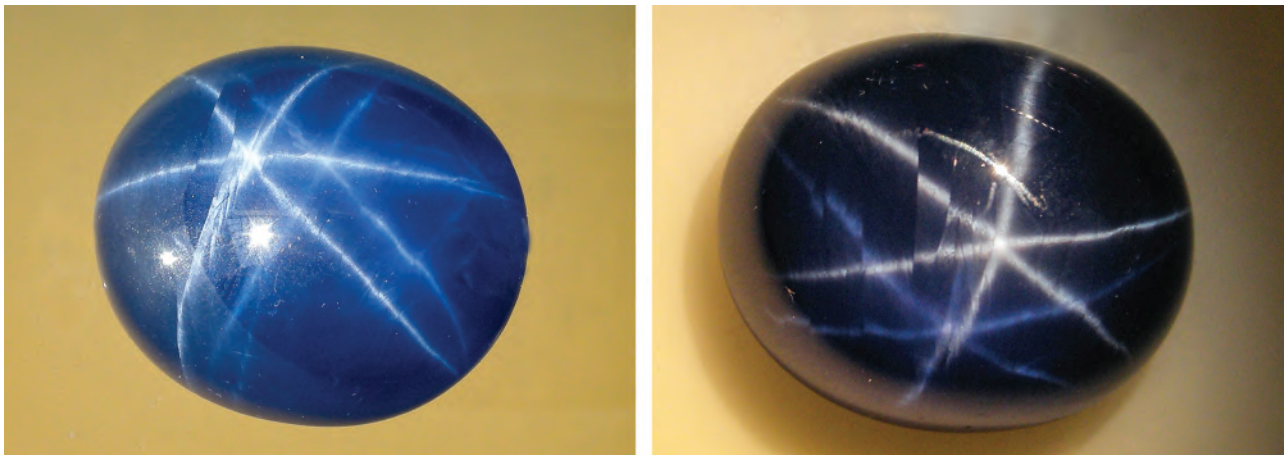

*Figure 30. Large diffusion-treated sapphire grown by the Verneuil method. The sample reveals, due its high transparency, a typical double-star pattern. The photos show the different visual appearance of the sample in direct sunlight (left) and under fiber-optic illumination (right). The arms of the stars are cut by grain boundaries, which indicates that parts of the crystal have slightly different orientation. The cabochon measures 27.7 × 23.5 mm and weighs 91.41 ct. Photos by K. Schmetzer.*

In the natural sapphire, the oriented needles were distinctly larger, especially in thickness. Their concentration varied in different parts of the stone and also tended to be higher along prismatic and dipyramidal growth planes. The sample was determined to be a single crystal, a property that caused the arms of the two six-rayed stars to be parallel. In twinned corundum crystals, the two stars are inclined to each other, and both stars show an identical white coloration. Dual-color double stars in natural rubies and sapphires are rare because most asteriated samples are neither transparent nor translucent, and therefore a reflection of light from the base cannot be seen.

In the asteriated brownish pink quartz samples from India, a dense network consisting of three series of oriented needle-like inclusions was observed. In the rose quartz from Brazil, only a very low density of needles, identified as dumortierite, was seen in an orientation parallel to the basal plane, and other needles inclined to this plane were also present. It could not be assumed that the relatively few needles visible in the basal plane were responsible for the observed asterism. Rather, there likely exists a denser network of smaller needles (not resolved with the magnification applied) generating the asterism in these rose quartz samples, but this topic needs further research.

**Formation of Dual-Color Double Stars in Rubies, Sapphires, and Quartz.** The dual-color double stars that are the subject of this study consist of a white six-rayed star and a bodycolored six-rayed star, a phenomenon different from the double stars of identical coloration that are sometimes observed in twinned rubies and sapphires. The two stars studied here are superimposed, overlapping each other, when the incident light is directed to the center of the cabochon and the observer looks parallel to this path of light. The two stars are clearly separated, however, if the observer and the incident beam of light are not parallel, which can be accomplished by shifting the observer, the incident light, or the cabochon.

For the observation of dual-color double stars, the surface at both the dome and the base of the cabochon needs some polish, but not necessarily a high-quality polish. Our experiments demonstrated this requirement. In certain samples (e.g., in some quartz cabochons), a bodycolored star was not seen when the base was completely rough. In these samples, the star became visible after polishing the surface. Similarly, some cabochons with extremely poor polish at the base showed only a very diffuse bodycolored star.

An analogous double-star pattern was also seen in reflected light for samples with two curved surfaces, irrespective of which curved surface layer the incident light was directed toward (again, see figure 6). Moreover, the size of the cabochon did not appear to be a factor in the ability to present a dual-color double-star pattern, provided the transparency was sufficient (figure 30).

The dual-color double stars described in this paper are observed in two basic groups of natural and synthetic corundum and natural quartz. One group consists of transparent to highly translucent natural or synthetic corundum and natural quartz with needle-like inclusions distributed throughout the entire body of the cabochon. A second group consists of dif-

## BOX B: INSIGHT INTO PRODUCTION TECHNIQUES APPLIED FOR THE FORMATION AND IMPROVEMENT OF ASTERIATED CORUNDUM SINCE THE LATE 1960S

During the course of this study, the authors communicated with individuals involved in the early production and marketing of asteriated synthetic corundum, shedding new light on its largely hidden past. The information summarized below comes from two main sources: the family that operates Wiede's Carbidwerk, and several former employees of Union Carbide (Linde). The summaries focus on aspects related to gemology and general production techniques for the materials released to the market. Details of production such as heating temperatures and times and the exact composition of nutrients and gases are outside the scope of the present paper.

### Insight from Wiede's Carbidwerk

One of the authors (KS) was able to speak with H. Schulz and his father C. Schulz, who have been directing Wiede's Carbidwerk in Freyung, Germany, since the late 1960s. Verneuil-grown and diffusion-treated star sapphires from recent production of the company and from the production of the 1970s were described earlier. From these interviews, we learned that diffusion treatment is applied to improve the intensity of weak stars, especially in transparent or translucent materials of certain colors. Furthermore, an uneven distribution of the star in various parts of the stone, sometimes associated with color zoning, can be improved by diffusion. Some trace elements used as dopants can cause complications if they are added in the nutrient for crystal growth together with titanium. This leads to the problem in which samples with asterism and specific colors such as bright green or bright yellow cannot be produced in one single step by the Verneuil technique. Instead, asteriated synthetic sapphires of such colors can be produced by adding the specific dopant for the desired color (e.g., cobalt for bright green or nickel for bright yellow) to the nutrient for Verneuil growth of the sapphires, then adding titanium by diffusion to the surface of the samples in a second step, and finally producing rutile precipitates by subsequent heat treatment.

The reverse process of adding titanium to the nutrient and then diffusing a color-causing trace element in a subsequent step is also a possible method for achieving asteriated sapphires of the desired coloration. Since the 1970s, however, Wiede's Carbidwerk has principally utilized the first variant described for commercial production, including for the samples supplied for this paper.

The existence of a bodycolored second star has been known to the producers at Wiede's for decades. Their experience has been that some clients want stones with this specific pattern, while others ask that the bodycolored second star be removed (e.g., by a slight grinding and repolishing of the cabochon's base).

### Insight from Former Linde Employees

Jennifer Stone-Sundberg, an employee of the former Union Carbide crystal growth facility from 2002 to 2008, and Milan Kokta, who worked at Union Carbide from 1977 to 2007 and devoted part of his research to improving the lasing properties of titanium-bearing synthetic sapphire (see the patents by Kokta in the references list), located some of the former staff members at Linde to obtain firsthand information. The following summary is based on interviews with Tony Keig, Milan Kokta, Larry Rothrock, Jim Smith, and one individual who wishes to remain anonymous:

From 1966 to 1968, the Linde subsidiary of Union Carbide produced red, white, blue, and black star material, with approximately 80% of the production blue,

fusion-treated rubies and sapphires in which precipitates of rutile needles are restricted to thin layers at the dome and base of the samples. The white star is formed by reflection and scattering of light at the needle-bearing surface layer confined to the dome of the cabochons; the bodycolored star is formed by reflection and scattering of light at the needle-bearing surface layer confined to the base. If either surface layer is free of needle-like inclusions, the related star is not seen.

Grinding and repolishing the first group of samples will not change the visual impression of the double stars, because the surface-related layers still contain acicular inclusions. Conversely, the white stars as well as the bodycolored stars of the second group can be removed by simple grinding and repolishing of the curved dome or the planar base. For some samples, especially synthetic rubies and sapphires purchased recently in Asia, the stars were removed completely after one or two grinding and repolishing steps. These results proved diffusion treatment of the samples to create asterism.

15% red, close to 5% black, and a very small fraction of 1% white. Linde expanded beyond blue, red, white, and black in the very late 1960s to produce the birthstone colors, the motivation behind all of the offerings outside of red and blue.

Verneuil raw materials did contain titanium, but many of the other metals for colors could not be successfully incorporated in the growth process and had to be added via post-growth diffusion. Specifically, attempts at incorporating an amount of dopant higher than that needed for some technical applications such as laser purposes, and necessary to produce satisfactory color in combination with asterism in gem materials, led to a rapid reduction in crystal quality. Therefore, Union Carbide experimented with diffusion to enhance or create a variety of colors in asteriated material.

These experiments proved effective, and post-growth diffusion was employed commercially for coloration purposes, either with or separate from the heat treatment needed to bring out the star. Some amount of titanium was always incorporated into the melt, and the crystal was then oxidized to bring out the star. If a different bodycolor was desired, the metals for that would be diffused in post-growth processing. Additionally, post-growth diffusion of titanium in flame-fusion material was utilized if the star obtained after growth and heat treatment was not sufficiently strong.

Later, the company changed the focus of its crystal growth efforts exclusively to the Czochralski technique. This method proved undesirable for the commercial production of asteriated synthetic gems, but it was used for some time in the 1980s to produce non-phenomenal ruby, blue sapphire, and green garnet synthetic gem material. However, Czochralski-grown materials for jewelry purposes did not reach the market in large quantities as had the Verneuil-grown Linde star material in the decades before. In the mid-1970s, with the shift toward Czochralski growth of corundum and a similar shift toward technical applications such as solid-state laser crystals, the company completely ceased production and marketing of Verneuil-grown star sapphire. The equipment (burners) was sold to third parties outside of the company, and the patents dealing with diffusion of various color-causing trace elements were transferred to Astrid Corporation (see table A-1).

The information from the directors of Wiede's Carbidwerk and from former employees of Union Carbide is thus consistent with the results presented in this paper. Their comments corroborate a variety of aspects regarding diffusion and asterism that were demonstrated empirically in the samples studied. These aspects include: (1) production of asteriated materials through the use of a titanium dopant in the growth process and through post-growth diffusion; (2) use of diffusion to create asterism and to enhance weak or incomplete stars; and (3) a need for technical reasons in certain color varieties to add titanium and the coloring element separately. On this latter point, it is also noteworthy that the patent documents by Carr and Nisevich (first application of this series filed in the United States on December 20, 1971, published 1973 to 1977; see table A-1) mention diffusion of the following elements or combinations of elements along with titanium into the corundum lattice: iron, chromium, vanadium, cobalt, nickel, and magnesium. However, the specific examples given of the colors produced by the diffusion process are limited (e.g., gray-green after diffusion of nickel, or pink after diffusion of chromium).

In transparent or translucent materials produced by the Linde subsidiary of Union Carbide and distributed as "Linde stars," testing was somewhat limited. Nonetheless, grinding and repolishing led to a distinct decrease in the intensity of the bodycolored star for a pink synthetic sapphire. This result established that the cabochon had undergone diffusion to create or improve its asterism. Other samples loaned from various collections could not be ground and repolished or handled destructively (e.g., cut in slices). Consequently, for part of the samples it was not possible by non-destructive analyses to decide whether tiny rutile needles were present within the entire sample or confined to the layers at the outer surfaces.

For the yellow or yellowish green "old stock" Linde samples we purchased, asterism was not changed after grinding and repolishing. Thus, experimentation did not offer any direct proof of diffusion treatment for these samples but did strongly suggest use of a titanium oxide raw material in the original crystal growth charge.

Microscopy of the yellow and yellowish green samples showed the presence of needle-like precipitates in the outermost layers of the cabochons. No changes were observed in these samples, even after deeper grinding and repolishing steps, which would have removed, at least partly, an existing diffusion layer. This fact indicates that rutile precipitates permeated the body of these synthetic sapphires. The distribution of rutile needles throughout the cabochons was also established for a transparent sample cut from a ruby boule grown by Djeva in Switzerland and a natural sapphire from Myanmar.

Accordingly, through comparison of commonalities between the treated and untreated corundum samples, the following mechanisms can be applied to explain the phenomenon in both groups:

1. The ordinary white star is formed by reflection and scattering of light at a layer confined to the curved dome of the cabochon and consisting of a matrix of corundum and minute needle-like precipitates of a titanium-bearing substance (rutile needles).
2. The bodycolored second star is formed by reflection and scattering of light at a layer confined to the plane or slightly curved base of the cabochon and consisting of a matrix of corundum and minute needle-like precipitates of a titanium-bearing substance (rutile needles).
3. The light forming the second star travels twice through the body of the cabochon and is absorbed by trace elements such as vanadium, chromium, iron, nickel, or cobalt, which are responsible for the bodycolor of the corundum crystals. Thus, the color of the second star is identical to the bodycolor of the host corundum.

The observations described for quartz cabochons clearly indicate the following mechanisms for the formation of the dual-color double-star pattern in transparent, very light-colored samples that is quite similar to the mechanism of such double star formation in transparent corundum. In particular:

1. The ordinary white star is formed by reflection and scattering of light at the curved dome of the cabochon.
2. The slightly pink, almost colorless second star is formed by reflection and scattering of light at the plane or slightly curved base of the cabochon.
3. The light forming the second star travels twice through the body of the cabochon and is absorbed by the color-causing substances that are responsible for the pink coloration of the quartz. In very light, almost colorless host crystals, the second six-rayed star is likewise only very slightly colored, almost colorless.

In both corundum and quartz, the formation of dual-color double stars depends on the presence of three series of acicular inclusions. These inclusions are inclined to each other but located on basal planes perpendicular to the optic axis of the samples.

**Implications Regarding the Production of Synthetic Asteriated Corundum and the Role of Diffusion.** The empirical results and interpretations described in the preceding sections led to conclusions regarding the production of asteriated synthetic corundum, particularly the prominent but largely unexplored role of diffusion. To date, diffusion treatment has been discussed in gemological contexts primarily for enhancement of natural colors in rubies and sapphires and for development or improvement of asterism in natural stones. Although there has been some knowledge of the different "Linde" patents (see table A-1), the same cannot be said for the broader commercial application of diffusion treatment processes to synthetic materials since the 1970s.

Rather, it would appear that those involved in the trade in the 1970s and 1980s were unaware of these applications or assumed that they were not used commercially on a large scale (Nassau, 1981; Crowningshield and Nassau, 1981; Hughes, 1991, 1997). Therefore, some insight into production techniques was sought directly from those involved, through interviews as detailed in box B. An application of this information combined with the results of the present study is given in box C.

The remarks of the producers and the empirical results of the present study intersected in establishing that many diffusion techniques were used historically and are still applied to produce the various types of dual-color double stars in synthetic rubies and sapphires seen on the market today. Moreover, the prevalence of the treated stones may depend in part on individual dealer preferences, which can dictate whether the synthetic rubies and sapphires are sold with the phenomenon or ground and repolished to remove the bodycolored stars. However, it should be noted that the particular technique of diffusing both

titanium and another color-causing dopant was not observed among the samples examined in this paper. An example of such material, with an enrichment of titanium and chromium by diffusion or overgrowth in the outermost layers of an orange-red ruby, was recently described by Schmetzer and Hainschwang (2012).

A detailed discussion of known and possible use of diffusion processes for the enhancement or creation of stars and for improvement of color in natural corundum samples, including through application of these techniques available since at least the early 1970s, is likewise beyond the scope of the present paper. Moreover, the results of this study suggest that detecting the diffusion of titanium (with or without an additional colorant) into natural stones to intensify their stars, regardless of any additional change to the stone's bodycolor, may constitute one of the greater challenges for the gemological community.

## CONCLUSIONS

The examination of various types of natural and synthetic rubies, sapphires, and quartz showing dual-color double stars as an optical phenomenon sheds light on understanding this pattern as well as on the production techniques for asteriated corundum from the 1950s to the present day. In order to produce synthetic asteriated rubies and sapphires of desired color and with intense stars, Verneuil-grown samples were often diffusion treated to create or enhance the cabochon's bodycolor, its asterism, or both. The formation of dual-color double stars is related to needle-like inclusions or rutile precipitates in the outermost layers of synthetic corundum cabochons or to similar acicular inclusions distributed throughout the entire body of natural or synthetic corundum or natural quartz. Reflection and scattering involving the inclusions near the dome creates the white star commonly seen, while reflection and scattering involving the inclusions at or near the base produces the bodycolored second star.

## BOX C: APPLICATION OF RESULTS TO TWO HISTORICAL SAMPLES

Two synthetic sapphire samples produced by Linde and exhibiting interesting features are kept in the reference and teaching collection of the Gemmological Association of Great Britain (Gem-A) in London. An opportunity to examine these samples afforded a chance to apply the results of our investigations as detailed above to propose an explanation for the stones' genesis.

### Visual Appearance and Microscopic Examination

One sample was a transparent synthetic sapphire cabochon that showed an extremely uneven color distribution, with a primarily colorless core and a blue rim. A six-rayed star was confined only to the blue areas of the sample (figure C-1). A similar blue synthetic sapphire with an incomplete star has already been described in the literature (Koivula and Kammerling, 1991), and a ruby showing this phenomenon was mentioned in Fryer et al. (1982a).

Upon microscopic examination, it was observed that gas bubbles were present only within the blue layers of the sample and that the concentration of the bubbles differed between these layers. In detail, the observed pattern was a mixture of the three basic patterns depicted in figure A-6. Similar blue Linde non-asteriated synthetic sapphire cabochons with uneven color distribution have been encountered by one of the authors (KS) in various collections, and one such example is shown in figure A-1.

The second Linde sample was a completely transparent, color-zoned blue synthetic sapphire. The blue coloration was concentrated toward the rim of the sample, but a six-rayed star extended over the entire cabochon. The stone showed a high concentration of gas bubbles only in some of the outermost parts of the sample (figure C-2). This synthetic sapphire also exhibited a six-rayed second star confined to the base of the cabochon.

### Possible Growth Conditions

Unfortunately, it is not documented when these two synthetic sapphires became part of the Gem-A teaching and reference collection (L. Gleave, pers. comm., 2013). Nonetheless, the descriptions of the manufacturing processes in patent documents (see box A) and the results of the present study indicated that both Linde samples were grown at an early stage of production.

As described by Burdick and Jones (1954a) in the patent assigned to Union Carbide (Linde), complete stars extending over the entire curved domes of the cabochons were created by growing the synthetic corundum boules

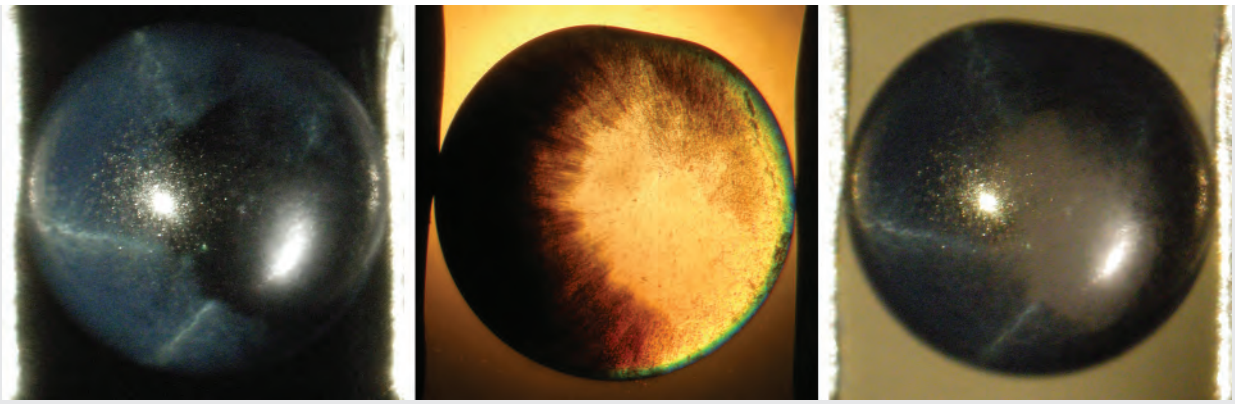

*Figure C-1. Linde synthetic blue sapphire with pronounced color zoning and asterism. Left and right: The sample in the same orientation but with a different background. Center: The sample in the same orientation, viewed in immersion. The areas of the cabochon with a high concentration of gas bubbles are blue in daylight and show asterism; those without gas bubbles are colorless and do not show asterism. The sample measures 6.4 mm in diameter and weighs 1.34 ct. Photos by K. Schmetzer; sample courtesy of Gem-A.*

under fluctuating thermal conditions. This fluctuation was achieved by alternately increasing and decreasing the rate of oxygen fed to the oxygen-hydrogen flame used for crystal growth in the Verneuil process. This operating protocol caused the formation of alternating convex layers with different titanium distributions (see figure A-2) and led to a homogeneous distribution of the blue coloration as well as the formation of stars with six rays extending equally down the sides of cabochons. This process would probably result in a layered pattern in the concentration of gas bubbles.

Before this technique was applied, most blue synthetic sapphires showed an uneven color distribution and an incomplete star reflected from the surface. Only those samples cut with the dome of the cabochon being formed by the outermost layer of the original corundum boule did not show this undesired zoning. It is assumed that after crystal growth and subsequent annealing to develop rutile precipitates, both samples from the Gem-A collection revealed such an incomplete star associated with an inhomogeneous color distribution. The second sapphire now showing a complete double-star pattern in all differently colored areas most likely was later diffusion treated to improve its visual appearance, especially to produce a complete six-rayed star. Thus, it is proposed that the second sample may be described as a blue synthetic star sapphire with an originally incomplete star that was improved by diffusion treatment. Within that step the second star, reflected and scattered from the base, might also have been formed.

Consequently, the properties of both Gem-A samples would appear to be consistent with the techniques applied by Linde in the early years of production. The appearance of the first sample suggests an absence of post-growth diffusion, while the features of the second sample correspond with what would be expected for one of the early blue Linde sapphires that had been subjected to the diffusion process patented in the 1950s for correction of the incomplete star.

*Figure C-2. Linde synthetic blue sapphire with pronounced color zoning and asterism. Left and right: The sample in the same orientation but with a different background. Center: The sample in the same orientation, viewed in immersion. The areas of the cabochon with a high concentration of gas bubbles are intense blue in daylight; those without gas bubbles are lighter blue or colorless. A double-star pattern is observed in all parts of the cabochon. The sample measures 7.0 × 5.0 mm and weighs 1.14 ct. Photos by K. Schmetzer; sample courtesy of Gem-A.*

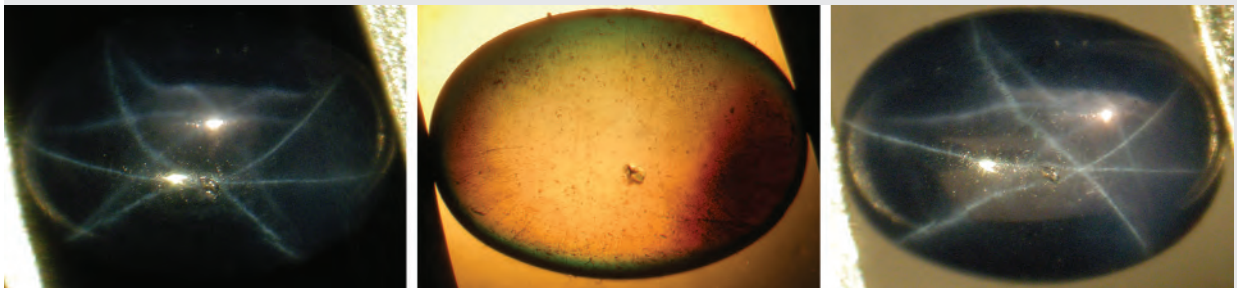

ABOUT THE AUTHORS

*Dr. Schmetzer is an independent researcher living in Petershausen, near Munich, Germany. Mr. Steinbach is a gem merchant and collector residing in Idar-Oberstein, Germany. Prof. Gilg is professor at the Chair of Engineering Geology, Technical University of Munich. Miss Blake is a gemologist residing in Chevy Chase, Maryland.*

ACKNOWLEDGMENTS

*This study is based on numerous samples from the collection of one of the authors and on rubies and sapphires kindly submitted from the stock of various companies as well as from different collections: C. Cavey (London); C. Cook and B. Cook (Silk Purse Jewelry, Palmetto, Florida); L. Gleave (Gem-A, London); A. Hodgkinson (Portencross, Scotland); H. Schulz (Wiede's Carbidwerk, Freyung, Germany); and D.L. Snyder (The Brazilian Connection, Benton, Pennsylvania).*

*Technical information about production and diffusion treatment of Verneuil-grown synthetic corundum was submitted by H. Schulz and C. Schulz (Wiede's Carbidwerk, Freyung, Germany), as well as by Jennifer Stone-Sundberg (Crystal Solutions, Portland, Oregon) and Milan Kokta (Washougal, Washington). H.-J. Bernhardt (Ruhr-University, Bochum, Germany) examined some ruby, sapphire, and quartz samples optically at high magnification. Roald Tagle (Bruker Nano GmbH, Berlin) is acknowledged for help performing the scanning µ-XRF analyses.*

*Grinding and repolishing of various samples was performed by Wild and Petsch Company (Kirschweiler, Germany), and by A. Franzmann Company (Hettenrodt, Germany), which are also acknowledged.*

## REFERENCES

Alexander A.E. (1946) Genuine and synthetic rubies and sapphires. *Journal of Chemical Education*, Vol. 23, No. 9, pp. 418–422, 459.

Ancot E., Eppler W.F. (1957a) Verfahren zur Herstellung von synthetischer, Asterismus aufweisender Korunde. DE 1 002 300, issued August 14.

Ancot E., Eppler W.F. (1957b) Verfahren zur Herstellung synthetischer Sternkorunde. DE 1 007 753, issued October 24.

Applin K.R., Hicks B.D. (1987) Fibers of dumortierite in quartz. *American Mineralogist*, Vol. 72, No. 1–2, pp. 170–172.

Arem J.E. (1987) *Color Encyclopedia of Gemstones*, 2nd ed. New York, Van Nostrand Reinhold Company, 248 pp.

Breebaart A.J. (1957) Structure & inclusions of synthetic starstones. *Journal of Gemmology*, Vol. 6, No. 2, pp. 72–74.

Burdick J.N., Glenn J.W. Jr. (1949) Synthetic star rubies and star sapphires, and process for producing same. US 2,488,507, issued November 15.

Burdick J.N., Jones R.A. (1953a) Cristaux de corindon synthétique. FR 1.029.418, issued June 2.

Burdick J.N., Jones R.A. (1953b) Improvements in and relating to the manufacture of synthetic corundum containing titanium. GB 697,804, issued September 30

(Burdick J.N., Jones R.A.) The Linde Air Products Company (1953c) Procédé de fabrication d'un corps monocristallin de corindon synthétique. CH 289 320, issued July 1.

Burdick J.N., Jones R.A. (1954a) Synthetic corundum crystals and process for making same. US 2,690,062, issued November 28.

Burdick J.N., Jones R.A. (1954b) Verfahren zur Herstellung von eine Titanverbindung enthaltenden synthetischen Korundkristallen. DE 897 844, issued February 1.

Burdick J.N., Jones R.A. (1956) Verfahren zum Ausscheiden Sternmuster aufweisender Cabochons aus synthetischen Korundeinkristallen. DE 948 403, issued September 20.

Carr R.R., Nisevich S.D. (1973a) Procédé de modification des caratéristiques d'aspect d'un cristal de corindon. FR 2.164.690, issued August 3.

Carr R.R., Nisevich S.D. (1973b) Procédé pour modifier l'aspect de cristaux de corindon et cristaux ainsi obtenus. BE 793.007, issued June 19.

Carr R.R., Nisevich S.D. (1973c) Veränderung des Aussehens von Korundkristallen. DE 2 262 104A, issued July 19.

Carr R.R., Nisevich S.D. (1974) Procédé de préparation de cristaux de corindon présentant une coloration sans défaut. CH 554 811, issued October 15.

Carr R.R., Nisevich S.D. (1975a) Altering the appearance of corundum crystals. US 3,897,529, issued July 29.

Carr R.R., Nisevich S.D. (1975b) Treatment of corundum crystals. GB 1 408 648, issued October 1.

Carr R.R., Nisevich S.D. (1976a) Altering the appearance of corundum crystals. US 3,950,596, issued April 13.

(Carr R.R., Nisevich S.D.) Union Carbide Corporation (1976b) Verfahren zur Veränderung des Aussehens von Korundkristallen. AT 330 722, issued July 12.

Carr R.R., Nisevich S.D. (1977) Altering the appearance of corundum crystals. US 4,039,726, issued August 2.

Cassedanne J.P., Roditi M. (1991) Crystallized and massive rose quartz deposits in Brazil. *Journal of Gemmology*, Vol. 22, No. 5, pp. 273–286.

Choudhary G., Vyas M.B. (2009) 'Multiphenomenal' quartz from India. *Gems & Jewellery*, Vol. 18, No. 1, pp. 10–12.

Crowningshield R. (1965) Pre-1952 synthetic star rubies. *G&G*, Vol. 11, No. 11, pp. 331–333.

Crowningshield R., Nassau K. (1981) The heat and diffusion treatment of natural and synthetic sapphires. *Journal of Gemmology*, Vol. 17, No. 8, pp. 528–541.

Elwell D. (1979) *Man-Made Gemstones*. Ellis Horwood Ltd., Chichester, 191 pp.

Eppler Fr. (1957/1958) Synthetischer Sternsaphir und synthetischer Sternrubin. *Zeitschrift der Deutschen Gesellschaft für Edelsteinkunde*, No. 22, pp. 4–7.

Eppler W.F. (1958) Notes on asterism in corundum, rose quartz and almandine garnet and chatoyancy in beryl. *Journal of Gemmology*, Vol. 6, No. 5, pp. 195–212.

Eversole W.G., Burdick J.N. (1954a) Improvement in producing asteriated corundum crystals. GB 712,735, issued July 28.

Eversole W.G., Burdick J.N. (1954b) Procédé de fabrication de cristaux de corindon à structure en étoile. FR 1.067.037, issued June 11.

Eversole W.G., Burdick J.N. (1954c) Producing asteriated corundum crystals. US 2,690,630, issued October 5.
Eversole W.G., Burdick J.N. (1955a) Verfahren zur Herstellung von strahl- oder sternbildenden (asterisierenden) Korundkristallen. DE 922 584, issued January 20.
(Eversole W.G., Burdick J.N.) Union Carbide and Carbon Corporation (1955b) Procédé de traitement de cristaux de corindon pour les render susceptibles d'astérisation par la chaleur. CH 307 914, issued July 1.
Fryer C., Crowningshield R., Hurwit K.N., Kane R.E., Eds. (1981) Gem Trade Lab Notes: Star quartz. *G&G*, Vol. 17, No. 4, p. 230.
——— (1982a) Gem Trade Lab Notes: Ruby, synthetic star. *G&G*, Vol. 18, No. 2, pp. 105–106.
——— (1982b) Gem Trade Lab Notes: Star quartz. *G&G*, Vol. 18, No. 4, p. 231.
——— (1985) Gem Trade Lab Notes: Quartz, multi- star. *G&G*, Vol. 21, No. 1, pp. 45–46.
Goreva J.S., Ma C., Rossman G.R. (2001) Fibrous nanoinclusions in massive rose quartz: The origin of rose coloration. *American Mineralogist*, Vol. 86, No. 4, pp. 466–472.
Gübelin E.J., Koivula, J.I. (2008) *Photoatlas of Inclusions in Gemstones, Volume 3*. Basel, Opinio Publishers, 672 pp.
Holmes R.J. (1947) The new "Linde stars." *G&G*, Vol. 5, No. 11, pp. 452–454, 478–479.
He J., Lagerlof K.P.D., Heuer A.H. (2011) Structural evolution of $TiO_2$ precipitates in Ti-doped sapphire ($\alpha$-$Al_2O_3$). *Journal of the American Ceramic Society*, Vol. 94, No. 4, pp. 1272–1280.
Hughes R.W. (1991) There's a rumble in the jungle: the sapphire face-lift face-off saga. *Gemological Digest*, Vol. 3, No. 2, pp. 17–31. Available at http://www.ruby-sapphire.com/blue_surface_diffusion.htm
——— (1997) *Ruby & Sapphire*. RWH Publishing Boulder, CO, 511 pp.
Johnson M.L., Mercer M.E., Fritsch E., Maddison P., Shigley J.E. (1995) "Ti-sapphire": Czochralski-pulled synthetic pink sapphire from Union Carbide. *G&G*, Vol. 31, No. 3, pp. 188–195, http://dx.doi.org/10.5741/GEMS.31.3.188.
Keig G.A., Smith J.C., Watts J.M.J. (1972) Asteriated synthetic corundum gem stones and method and apparatus for their production. US 3,655,415, issued April 11.
Keig G.A., Smith J.C., Watts J.M.J. (1973a) Asteriated synthetic corundum gem stones. US 3,725,092, issued April 3.
Keig G.A., Smith J.C., Watts J.M.J. (1973b) Procédé de preparation d'un cristal en corindon astérié synthétique. CH 539 581, issued September 14.
Keig G.A., Smith J.C., Watts J.M.J. (1973c) Synthetischer Korund und Verfahren und Vorrichtung zu seiner Herstellung. DE 2 208 150A, issued September 6.
(Keig G.A., Smith J.C., Watts J.M.J.) Union Carbide Corporation (1973d) Procédé et dispositif de realization de cristaux de corindon à astérisme. FR 2.172.913, issued October 5.
Keig G.A., Smith J.C., Watts J.M.J. (1974) Synthetic corundum. GB 1 377 428, issued December 18.
(Keig G.A., Smith J.C., Watts J.M.J.) Union Carbide Corporation (1976) Synthetischer, monokristalliner Korund. AT 327 863, issued February 25.
Kiefert L. (2003) Gem News International: An unusual star quartz. *G&G*, Vol. 39, No. 3, pp. 234–235.
Killingback H. (2006) Diasterism in rose quartz. *Gems & Jewellery*, Vol. 16, No. 2, p. 64.
——— (2009) A twelve-ray star rose quartz from Madagascar. *Gems & Jewellery*, Vol. 18, No. 2, pp. 18–20.
——— (2011) Diasterism in rose quartz. *Midlands Focus*, No. 19, pp. 16–25.
Koivula J.I., Kammerling R.C., Eds. (1991) Gem News: Novel synthetic star sapphire. *G&G*, Vol. 27, No. 4, pp. 263–264.
Koivula J.I., Kammerling R.C., Fritsch E., Eds. (1993) Gem News: Unusual double star sapphire. *G&G*, Vol. 29, No. 3, pp. 212–213.
Koivula, J.I., Tannous M. (2001) Gem Trade Lab Notes: Star sapphire with two stars of two different colors. *G&G*, Vol. 37, No. 3, pp. 218–219.
Kokta M.R. (1986) Process for enhancing Ti:$Al_2O_3$ tunable laser crystal fluorescence by annealing. US 4,587,035, issued May 6.
Kokta M.R. (1987) Process for enhancing Ti:$Al_2O_3$ tunable laser crystal fluorescence by controlling crystal growth atmosphere. US 4,711,696, issued December 8.
Kokta M.R. (1989) Process for enhancing fluorescence of Ti:$Al_2O_3$ tunable laser crystals. US 4,836,953, issued June 6.
Kokta M.R. (1991) Process for enhancing fluorescence of tunable titanium-doped oxide laser crystals. US 4,988,402, issued January 29.
Kondo D.M. (2007) Lab Notes: Sapphire with a double star. *G&G*, Vol. 43, No. 4, p. 365.
Langensiepen R.A., Tressler R.E., Howell P.R. (1983) A preliminary study of precipitation in $Ti^{4+}$-doped polycrystalline alumina. *Journal of Materials Science*, Vol. 18, No. 9, pp. 2771–2776.
Liddicoat R.T. Jr. (1963) Early star sapphire. *G&G*, Vol. 11, No. 4, pp. 116–117.
Ma C., Goreva J.S., Rossman G.R. (2002) Fibrous nanoinclusions in massive rose quartz: HRTEM and AEM investigations. *American Mineralogist*, Vol. 87, No. 2–3, pp. 269–276.
McClure S.F. (1998) Ruby, with a true double star. *G&G*, Vol. 34, No. 3, p. 217.
Meyer-Browne G. (1962) Synthetic star stones. *The Gemmologist*, Vol. 31, No. 376, pp. 201–203,
Moon A.R., Phillips M.R. (1984) An electron microscopy study of exsolved phases in natural black Australian sapphire. *Micron and Microscopica Acta*, Vol. 15, No. 3, pp. 143–146, http://dx.doi.org/10.1016/0739-6260(84)90044-3.
——— (1991) Titania precipitation in sapphire containing iron and titanium. *Physics and Chemistry of Minerals*, Vol. 18, No. 4, pp. 251–258, http://dx.doi.org/10.1007/BF00202577.
Nassau K. (1979) Synthetic gemstone developments in the nineteen seventies. *G&G*, Vol. 16, No. 8, pp. 226–239.
——— (1980) *Gems Made by Man*. Chilton Book Company, Radnor, PA, 364 pp.
——— (1981) Heat treating ruby and sapphire: technical aspects. *G&G*, Vol. 17, No. 3, pp. 121–131, http://dx.doi.org/10.5741/GEMS.17.3.121.
Pezzotta F. (2001) Madagascar. A mineral and gemstone paradise. *extraLapis English*, No. 1, p. 51.
Phillips D.S., Heuer A.H., Mitchell T.E. (1980) Precipitation in star sapphire. I. Identification of the precipitate. *Philosophical Magazine A*, Vol. 42, No. 3, pp. 385–404.
Pough F.H. (1966) Linde's science re-creates gems in a few hours. *Lapidary Journal*, Vol. 20, No. 1, pp. 56–64.
Schmetzer K., Bernhardt H.-J., Kiefert L. (2002) Star garnets and star garnet cat's-eyes from Ambatondrazaka, Madagascar. *Journal of Gemmology*, Vol. 28, No. 1, pp. 13–23.
Schmetzer K., Glas M. (2001) Zwölfstrahliger Sternsaphir aus Bang-kha-cha, Thailand. *Lapis*, Vol. 26, No. 11, pp. 40–42, 54.
——— (2003) Multi-star quartzes from Sri Lanka. *Journal of Gemmology*, Vol. 28, No. 6, pp. 321–332.
Schmetzer K., Krzemnicki M. (2006) The orientation and symmetry of light spots and asterism in rose quartz spheres from Madagascar. *Journal of Gemmology*, Vol. 30, No. 3/4, pp. 183–191.
Schmetzer K., Steinbach M.P (2014) Quartz with sagenitic rutile inclusions from Myanmar. *Australian Gemmologist*, Vol. 25, No. 5, pp. 175–177.
Schmetzer K., Hainschwang T. (2012) Star ruby. *Gems & Jewellery*, Vol. 20, No. 4, pp. 14–17.
Seemann A.K. (1949) American synthetic crystals. *G&G*, Vol. 6, No. 5, pp. 151–159.
The story of Linde stars (n.d.) www.thebrazilianconnection.com/Linde_info.html.

Taylor A.M. (1964) Growth of chrysoberyl crystals and development therein of chatoyancy for cat's-eye gemstones. Technical Memorandum B-390, Status Report, Union Carbide Corporation, Linde Division, 29 pp. (unpublished).
Thai star sapphire (n.d.) http://www.tradeindia.com/fp458250/Star-Sapphire-Gemstone.html.
Thurm R. (1962) Ein neuer synthetischer Sternsaphir. *Zeitschrift der Deutschen Gesellschaft für Edelsteinkunde*, No. 39, pp. 27–30.
U.S. develops synthetic sapphire industry (1943) *G&G*, Vol. 4, No. 6, pp. 88–90.
Viti C., Ferrari M. (2006) The nature of Ti-rich inclusions responsible for asterism in Verneuil-grown corundums. *European Journal of Mineralogy*, Vol. 18, No. 6, pp. 823–834, http://dx.doi.org/10.1127/0935-1221/2006/0018-0823.
von Vultée J. (1955) Über die orientierten Verwachsungen von Rutil in Quarz. *Neues Jahrbuch für Mineralogie Abhandlungen*, Vol. 87, No. 3, pp. 389–415.
——— (1956) Die Verwachsungsgesetze der orientierten Einlagerungen von Rutil in Quarz. *Zeitschrift für Kristallographie*, Vol. 107, No. 1–2, pp. 1–17.
Woensdregt C.F., Weibel M., Wessicken R. (1980) Star quartz asterism caused by sillimanite. *Schweizerische Mineralogische und Petrographische Mitteilungen*, Vol. 60, pp. 129–132.
Xiao S.Q., Dahmen U., Heuer A.H. (1997) Phase transformation of $TiO_2$ precipitates in sapphire ($\alpha$-$Al_2O_3$) induced by the loss of coherency. *Philosophical Magazine A*, Vol. 75, No. 1, pp. 221–238, http://dx.doi.org/10.1080/01418619708210292.
Zolensky M.E., Sylvester P.J., Paces J.B. (1988) Origin and significance of the blue coloration in quartz from Llano rhyolite (llanite), north-central Llano County, Texas. *American Mineralogist*, Vol. 73, No. 3–4, pp. 313–323.

# DIGITAL PHOTOMICROGRAPHY FOR GEMOLOGISTS

Nathan Renfro

Until recently, film was the preferred medium used for capturing images through the microscope, primarily due to resolution limitations of digital-format cameras. The image quality that can now be achieved by digital cameras is equal, and in many ways superior, to the quality offered by film. Digital photomicrography allows gemologists the opportunity to instantly see the resultant images, which can then be adjusted with image-refining software so that they represent their subject as realistically as possible. This article offers examples of some basic techniques and tips on the application of digital processing to get the most out of photomicrographs.

The inclusion scenes observed in the micro-world of gems often reveal a tremendous amount about the identity and origin of an unknown gemstone. By capturing these microcosms in a recorded image, the information is preserved for easy reference. This information can sometimes be limited due to the photomicrographer's own knowledge of the subject, but resources such as the three-volume *Photoatlas of Inclusions in Gemstones* (Gübelin and Koivula 1986, 2005, 2008) aid in understanding the subjects the gemologist may encounter through the microscope.

Photomicrography is the method by which images, magnified through a microscope, are collected by a camera. These images often represent subjects ranging in size from less than 1 mm to 1–2 cm. Photomicrographs do not only serve as educational and research references; many are aesthetically pleasing and can be viewed as examples of natural art, and have even been used as a marketing tool for gem materials (Koivula et al., 1994). All one has to do is attach a camera in the optical path of a microscope to take advantage of the beautiful micro-world of gems. This was previously accomplished using film, often with tremendous results due to the superb color rendition and high resolution that film could offer. The downside to this method is the expense of developing and the delay in seeing the resultant image. As predicted by Koivula (2003), the limitations of film have essentially been eliminated by the digital age. Digital camera technology has developed to the point that image quality rivals that of film, and the photomicrographer no longer incurs the cost of developing film just to see the resultant image. Digital photography also allows for instantly viewing captured images and in making post-processing adjustments that gives the photographer the ability to compensate for sub-par lighting conditions and make post-capture corrections. This article covers the basics of gemological photomicrography, from equipment configurations to lighting conditions and image processing software, which will assist aspiring photomicrographers in merging science and art (figure 1).

## THE MICROSCOPE

The most practical photomicrography system begins with a trinocular microscope to allow traditional observation and image capture simultaneously. However, a binocular microscope with a live display to a video monitor may also provide sufficient results, even if it is not as easy to use. There are many limiting factors in photomicrography, one of which is the quality of the optics between the subject and the camera. For the best results, photomicrographers should acquire the best optics possible within their budget. It is usually better to purchase a used high-quality microscope with excellent optics than a new microscope with merely adequate optics. As Internet commerce has evolved, it has become quite easy to

See end of article for About the Authors and Acknowledgments.
GEMS & GEMOLOGY, Vol. 51, No. 2, pp. 144–159,
http://dx.doi.org/10.5741/GEMS.51.2.144.

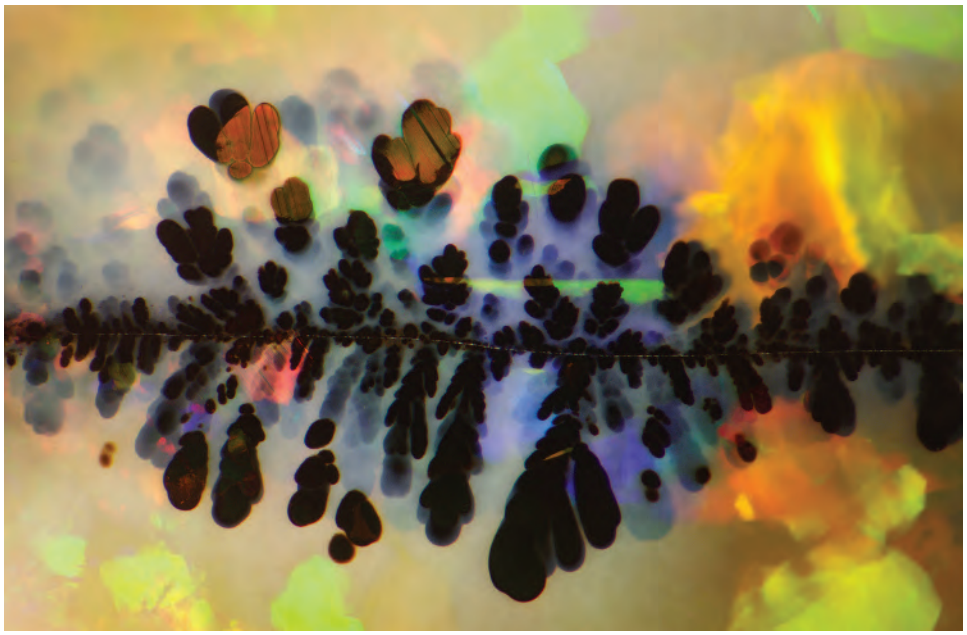

*Figure 1. The black manganese oxide "plumes" in this Australian opal serve as a good example of art and science merging in gemology. Photomicrograph by Nathan Renfro, field of view 5.85 mm. Note: Field of view is horizontal throughout this paper unless otherwise specified.*

purchase a high-quality used microscope for a reasonable price; however, this cost will still be in the range of a few thousand dollars for a good used microscope in working order. New microscopes with high-quality optics will cost several times that. Two recommended models no longer in production, but often available from online resellers, are the Wild Heerbrugg M400 series photomacroscopes and the Nikon SMZ10 trinocular head microscope (figure 2). Both instruments have excellent optics but offer

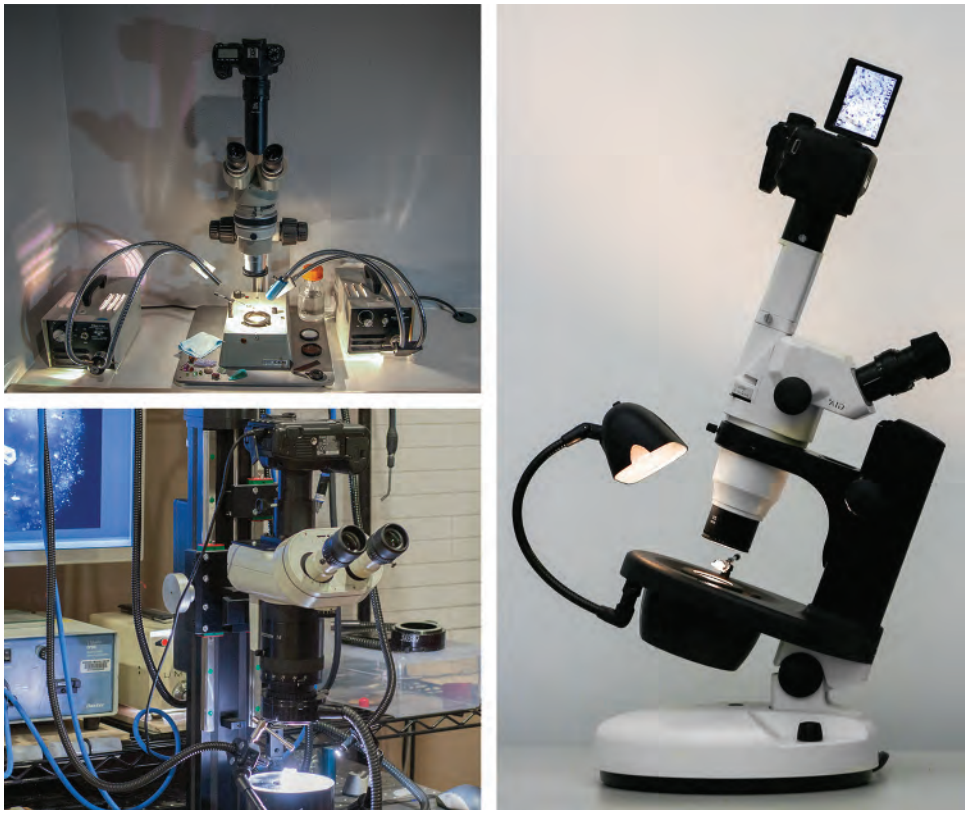

*Figure 2. Top left: The author's photomicrography equipment consists of a Nikon SMZ-10 microscope with custom darkfield base mated to a Canon 6D DSLR camera with two bifurcated fiber-optic illuminators. Bottom left: This Wild Heerbrugg M450 photomacroscope with Apozoom lens is mounted to a Macrorail stepping mast bolted to a Thorlabs optical table with a Canon 5D Mark II camera. Right: The GIA DLScope trinocular microscope is easily equipped for photomicrography, as shown with a Canon 70D DSLR camera, bifurcated fiber-optic illuminator, and auxiliary doubling lens. Photos by Nathan Renfro (top left), Darren Bates (bottom left), and Ziyin Sun (right).*

## Box A: The Evolution of the Gemological Microscope

Gemological microscopy has evolved from the late 19th century drawtube brass microscopes (figure 3, top left) into using much more advanced stereomicroscopes that primarily used darkfield illumination. The application of this lighting to gemology was first patented by Robert Shipley Jr. in 1939 (figure 3, top right) (U.S. Patent no. 2,157,437); darkfield has essentially been the standard lighting environment for gemology ever since. Though there have been some advancement in optical trains and ergonomics, the gemological microscope has remained largely unchanged for several decades. In 2011, GIA's Carlsbad laboratory acquired a custom-outfitted compound microscope for research applications. This Nikon Eclipse LV100 (figure 3, bottom left) can provide a viewing magnification of up to 1000×, whereas standard gemological microscopes usually have a maximum viewing magnification of approximately 120× with the use of an auxiliary doubling lens. This microscope system is outfitted with extra-long working distance objectives, differential interference contrast components, an assortment of filters, fluorescence imaging capabilities, and Nikon's NIS-Elements software, which can control the stage height for automated extended depth-of-field imaging. This microscope will allow researchers to reexamine specimens with a new perspective and could enable the observation of previously unseen features in gem materials. While not necessarily a practical microscope for routine gemological examination, this type of system could represent the future in gemological discovery. In April 2015, the inclusion research department at the Carlsbad lab acquired a well-equipped Nikon SMZ25 microscope system with a 25:1 zoom ratio, a Nikon DS-Ri2 high-resolution digital camera and Super High Resolution (SHR) objectives (figure 3, bottom right). This microscope system demonstrates the latest developments in optical microscopy and digital photomicrography.

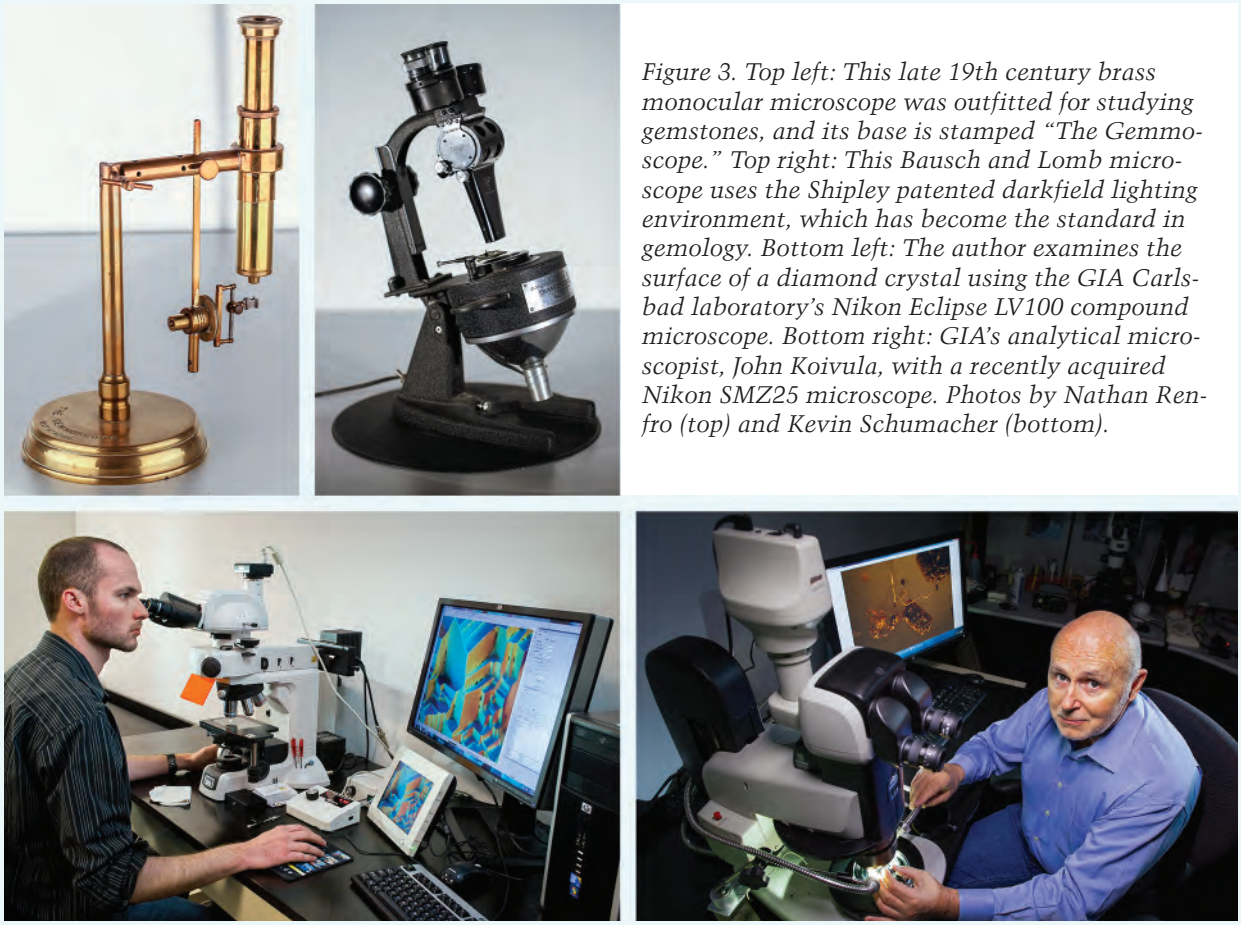

*Figure 3. Top left: This late 19th century brass monocular microscope was outfitted for studying gemstones, and its base is stamped "The Gemmoscope." Top right: This Bausch and Lomb microscope uses the Shipley patented darkfield lighting environment, which has become the standard in gemology. Bottom left: The author examines the surface of a diamond crystal using the GIA Carlsbad laboratory's Nikon Eclipse LV100 compound microscope. Bottom right: GIA's analytical microscopist, John Koivula, with a recently acquired Nikon SMZ25 microscope. Photos by Nathan Renfro (top) and Kevin Schumacher (bottom).*

their own unique features. The Nikon SMZ10 has the ability to capture stereo pairs for three-dimensional (3D) viewing by moving a selector switch that changes the optical path projected to the trinocular port. The Wild M400 has a single optical path that is perpendicular to the stage. This eliminates the lateral shift problems encountered as one adjusts the microscope stage in systems with angled optical paths. The downside to both of these microscopes is their age. Even though they are built to last several lifetimes, their scarcity can make it difficult to source desirable accessories such camera adapters, 2× objectives, and model-specific polarizing filters.

## DIGITAL CAMERAS

Since the inception of the digital camera concept in 1972 (Trenholm, 2007), it has been a long road to develop the technology that would surpass the quality of film. This development in digital imaging has essentially been the death of film photography; the only practical option for photomicrographers today is to adapt their microscope to a digital camera. One of the most significant benefits of the digital age is that photography has become much more cost effective, allowing many more people to enjoy this rewarding hobby. Previously, the cost of purchasing and developing high-quality film could be as much as $2–$3 per final bracketed image (J. Koivula, pers. comm., 2014). Now, the photomicrographer can capture as many images as desired at no additional expense. This facilitates repeated practice, as one does not have to be concerned with the cost of film "waste."

Modern digital cameras with complementary metal oxide semiconductor (CMOS) sensors offer excellent color rendition, very high resolution capability, and a tremendous amount of control over many parameters, including shutter speed, white balance, International Organization for Standardization (ISO) settings, and exposure compensation. While budget is important when choosing a camera for photomicrography, other factors to consider are resolution, weight, vibration control, and remote control capability. Camera choices can be as simple as the digital camera on your smartphone (Boehm, 2014) all the way to a professional-grade digital single-lens reflex (DSLR) camera. The author currently uses a Canon 6D DSLR. Several notable features are the high-resolution, full-frame (36 mm × 24 mm) sensor and Wi-Fi capability for wireless remote shooting, which helps to eliminate potential image-blurring vibrations. This particular camera is also appealing because of the lightweight composite body, compared to other DSLR full-frame cameras with heavier alloy bodies, helps to prevent the focusing rack from becoming overloaded, making it easier to maintain image focus. Many of these features can be found on other DSLR cameras as well; this model serves as an example of criteria to consider when selecting a camera for photomicrography.

## ADAPTING A DIGITAL CAMERA TO A MICROSCOPE

One of the biggest challenges in adapting almost any microscope for image capture is mating the camera to the microscope so that it is parfocal. This is when the image at the camera sensor is in focus at the same time as the image viewed in the microscope oculars. Parfocality makes image composition much easier and saves significant time. Certain manufacturers of specialty adapters offer ready-made solutions for camera adaptation, but some microscopes may require additional components to achieve parfocality. The author's Nikon SMZ10 was mated to a DSLR camera by using a Diagnostic Instruments PA1-12A adapter tube with a helicoid-style extension tube for parfocality adjustment; this was then connected to a Canon adapter for the camera (figure 4).

Once the camera is selected and attached to the microscope, there are additional considerations regarding the relay lens in the trinocular port. The primary factor that should influence your choice of magnification of this optical element is the sensor size of your camera. The best choice of relay optic is one that completely fills the sensor (to avoid vi-

### In Brief

- The development of digital camera technology has made photomicrography more accessible and affordable than in the past.
- High-quality used microscopes are better suited for photomicrography than inexpensive newer models.
- DSLR cameras can produce images that rival the quality of film and are well suited for capturing photomicrographic images.
- Software such as Helicon Focus and Adobe Photoshop are powerful tools that can be used to get the best results from digital photomicrography.

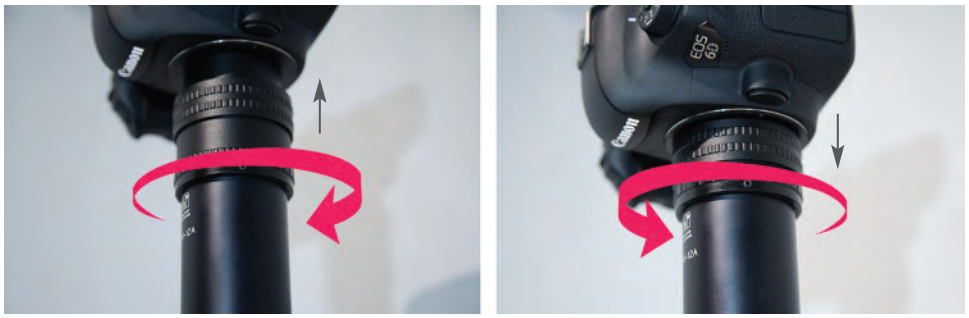

*Figure 4. A helicoid-style extension tube easily allows for up and down movement of the camera in order achieve parfocality with the microscope oculars. Photos by Nathan Renfro.*

gnetting, or fuzzy dark edges) and does not waste too much light through over-magnification as the image is projected on the camera sensor.

For microscopes without a trinocular port, adapters that mount the camera onto an ocular present a very reasonable solution (figure 5, left). Since traditional observation is not possible in this configuration, the photomicrographer must rely on a live view displayed on a monitor to set up the specimen (figure 5, right). With the significant advances in smartphone cameras, it is possible for the hobbyist to take decent-quality photomicrographs with these devices (Boehm, 2014). Inexpensive products to facilitate smartphone photomicrography also exist (Overton, 2010). The most obvious advantage to smartphone photomicrography is portability, a simple matter of carrying a smartphone and a loupe in the field (Boehm, 2014).

## GETTING STARTED: CLEANING AND VIBRATION CONTROL

Two important considerations for photography through the microscope in achieving satisfactory results are sample cleaning and vibration control (Koivula, 1981). A clean sample simply makes a much more striking image. If one is investing the time required to take a high-quality photomicrograph, the results are dramatically improved if some time is spent properly cleaning a sample prior to setting up the image. Typically, this can be accomplished with a stone cloth and a damp sponge to remove as much dust and finger oil as possible. This will save significant time in post-capture image processing and dust spot removal, which will be discussed later in the article.

Vibrations can cause loss of detail by blurring an image. This happens when subject movement occurs

*Figure 5. Left: A camera adapter that slips over the microscope's ocular can turn a binocular microscope into a photomicroscope, as seen on the author's GIA Gemolite Mark V. Right: A live view shown on a computer monitor is used for focusing and composition because the oculars are blocked by the camera. The camera is remotely controlled by the software, which helps prevent vibration-induced blurring that would occur by manually pressing the shutter button. Photos by Nathan Renfro.*

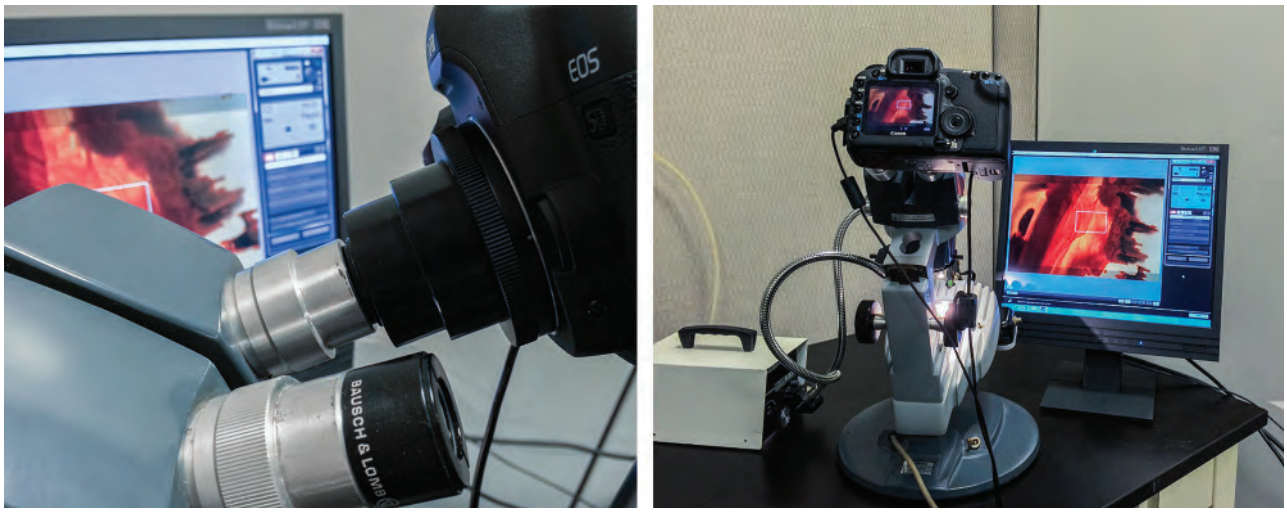

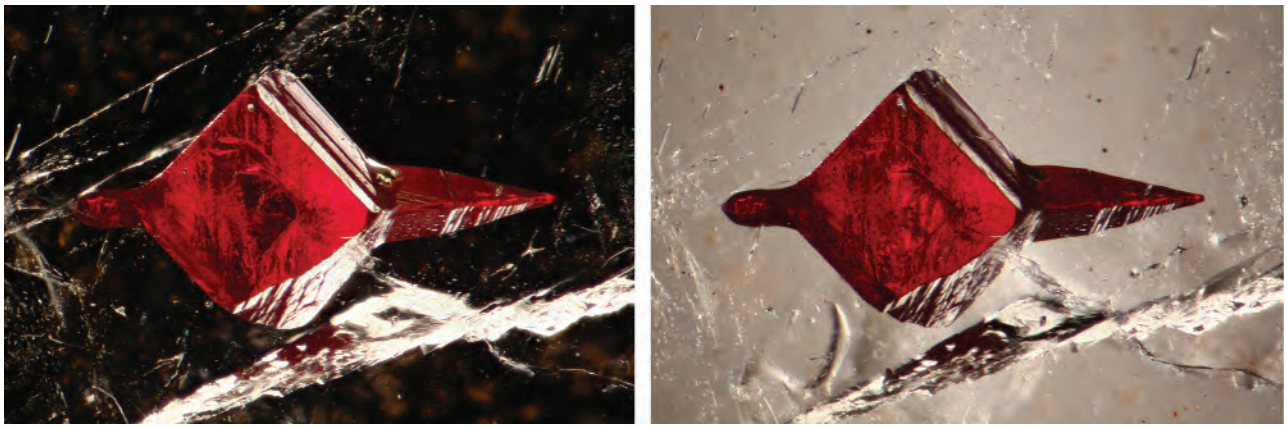

*Figure 6. This cinnabar inclusion in barite is shown using darkfield (left) and brightfield (right) illumination. Photomicrographs by Nathan Renfro, field of view 2.88 mm.*

over the exposure time. Two solutions for this problem are eliminating causes of movement or decreasing exposure time. By making the microscope more rigid or isolated from the environment, the photomicrographer minimizes vibration-induced problems. A floating optical table is best, but this is generally too expensive for hobbyists. To help eliminate vibrational movement, one can add shock-absorbing antivibration mounts or rubber pads underneath the microscope to help prevent vibrations from reaching the subject.

Another solution to help eliminate vibration-induced blurring is to decrease the exposure time so there is less chance for the subject to move. With digital photomicrography, you can increase the light sensitivity of your camera by adjusting the ISO setting, the modern equivalent to the American Standards Association's (ASA) "film speed." If your camera is more sensitive to light, then the required exposure time decreases; however, if the ISO is adjusted too high, image quality may suffer from what is known as "noise" or a grainy salt-and-pepper type appearance.

For users of DSLR cameras in particular, the mirror and shutter movements may cause some additional vibrations. If selecting a DSLR digital camera for photomicrography, it may be worthwhile to choose one with a "silent shutter" mode, which will greatly reduce camera-induced vibrations.

## LIGHTING TECHNIQUES

Lighting is the single most important factor in taking a high-quality photomicrograph. Without proper illumination, satisfactory results will never be achieved. Most gemologists are familiar with several types of broadly suitable lighting. Brightfield, darkfield, and reflected light are the types of illumination typically used in gemology. There are several other types of environments or modifications to these types of light that will greatly enhance the appearance of almost any photomicrograph. The difficulty is in knowing which type of lighting or combination of lighting to use for a given inclusion scene. This valuable insight, which must be learned through reading literature on photomicrography and significant practice, has been extensively covered (Koivula 1981, 1982a, 1982b, 1984, 2003).

Darkfield illumination is probably the most familiar type of lighting for general observation, because most gemological microscopes are equipped with a darkfield base. This type of lighting allows light-scattering inclusions to stand out in high relief against a dark background and can be useful for highlighting small inclusions (figure 6, left). While this lighting environment is useful for general observation, the high degree of contrast produced between the inclusions and background is not always desirable or aesthetically pleasing. One important consideration in darkfield photomicrography is that undesirable dust particles and surface scratches will be conspicuous, which may limit this lighting environment in all but the most pristine of specimens.

Brightfield illumination, or transmitted light, is a technique in which the specimen is placed between the objective and a bright direct illumination source (figure 6, right). This type of lighting is particularly useful for examining color-zoned specimens and masking the appearance of fine dust particles; how-

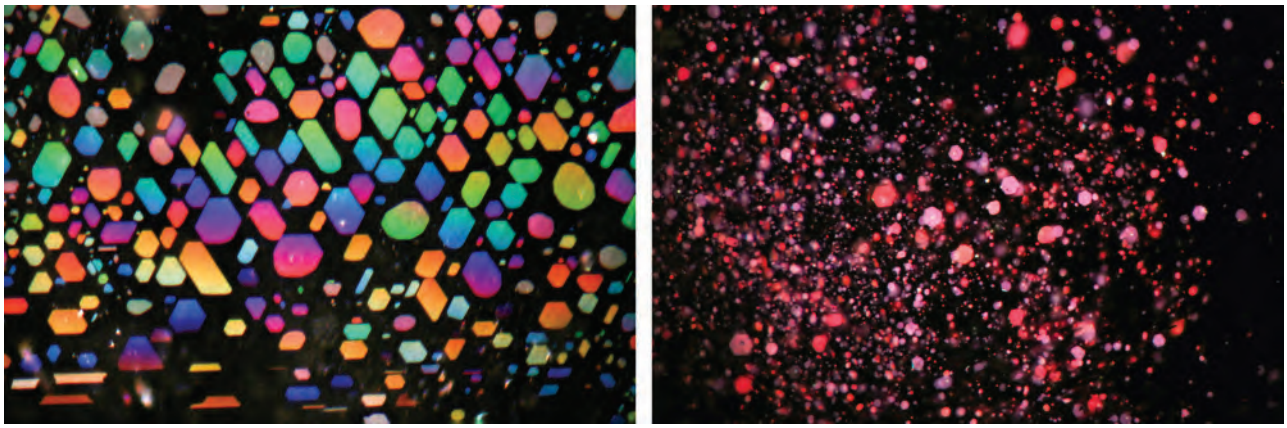

*Figure 7. Thin, reflective, oriented fluid inclusions, as seen in this aquamarine (left, vertical field of view 2.54 mm) and covellite in this pink fire quartz (right, 6.13 mm vertical field of view), often reveal vibrant displays of color under oblique fiber-optic illumination. Photomicrographs by Nathan Renfro.*

ever, detail may be lost when examining overly dark or opaque inclusions. Brightfield illumination can be further enhanced by using a diffuser plate to control the light intensity if direct transmitted light sacrifices too much detail by creating bright reflective areas, sometimes called "hot spots" (Koivula, 2003).

Diffuse reflected light is useful for examining surface features and revealing differences in luster between two dissimilar materials. This lighting is also suitable for detecting coatings, as they often display a higher luster than the substrate material.

Fiber-optic illumination may be the most underused and single most useful form of illumination in gemology. Quite often, crystallographically-oriented inclusions can be well hidden unless an illumination direction can be achieved to facilitate light scatter from these particles. Because of the widely adjustable position of the fiber-optic illuminator, hidden inclusions are often easily revealed (figure 7). When using a fiber-optic illuminator, controlled light can be guided to the subject at an oblique angle to highlight any unseen iridescent components (figure 8; Koivula, 1982a). Crystallographically-oriented thin film inclusions are often particularly responsive to oblique fiber-optic illumination (Koivula, 1980), revealing vivid colors when this method is used (figure 9).

While the use of polarized light is quite familiar to most gemologists by way of the polariscope, using polarized light in conjunction with the microscope may be foreign. The most significant use of a polarizer in gemological photomicrography is the elimination of doubling in birefringent materials by placing a polarizing filter, called an analyzer, between the objective and the subject (figure 10). This polarizing filter will eliminate one of the refraction directions, thereby making the image appear singly refractive. Crossed-polarized light, created by adding another polarizing filter between the subject and light source oriented 90 degrees to the plane of polarization of the analyzer, can also reveal low-relief, nearly invisible inclusions in high contrast due to strain and optical misalignment. Also, the vibrant colors occasionally observed from birefringent inclusions in polarized light are a welcome sight to almost any photomicrographer (figure 11). Polarized light can be further enhanced by the use of a first-order red compensator. Also known as a full-wave plate, this

*Figure 8. Oblique fiber-optic illumination can be used to reveal iridescent colors in reflective inclusions that might go otherwise unseen. Photo by Nathan Renfro.*

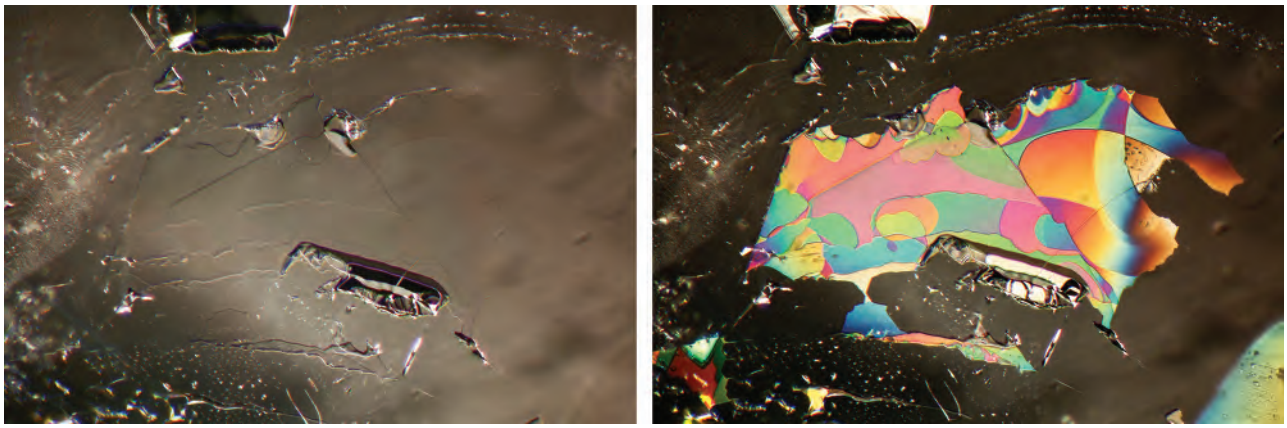

*Figure 9. Viewed only with shadowed brightfield lighting, this partially healed cleavage crack looks rather ordinary. With the addition of oblique fiber-optic illumination, unexpected interference colors caused by thin film iridescence are revealed. Photomicrographs by Nathan Renfro; field of view 2.96 mm.*

type of filter significantly decreases the exposure time required to capture an image in polarized light and can dramatically enhance strain color (figure 12) (Koivula, 1984).

Ultraviolet (UV) light has limited but occasional use in photomicrography. UV illumination can induce a fluorescent reaction in certain subjects, producing visually striking results that can be photographed (figure 13); however, exposure times greatly increase, as the lumination intensity is typically far less than any other lighting environment mentioned. This increased exposure time may lead to vibration-induced blurring of images. Also, it should be noted that UV light may be harmful to the photomicrographer's eyes, so exposure should be kept to a minimum and proper protective equipment should always be used.

The photomicrographer will quickly realize that sometimes no single type of lighting is adequate to produce a high-quality photomicrograph for a particular specimen. Significantly more impressive results may be produced using combinations and/or modifications of the lighting previously mentioned. Learning which combinations to use and when to use them is an important skill developed with practice. Once the correct illumination sources are selected,

*Figure 10. Left: Because of birefringence in anisotropic materials such as tourmaline, image doubling is often a problem, as revealed by these apatite crystals. Right: A polarizing filter placed between the objective lens and the subject, rotated to the appropriate position, does away with image doubling by eliminating one of the birefringent light paths. Photomicrographs by Nathan Renfro; field of view 1.50 mm.*

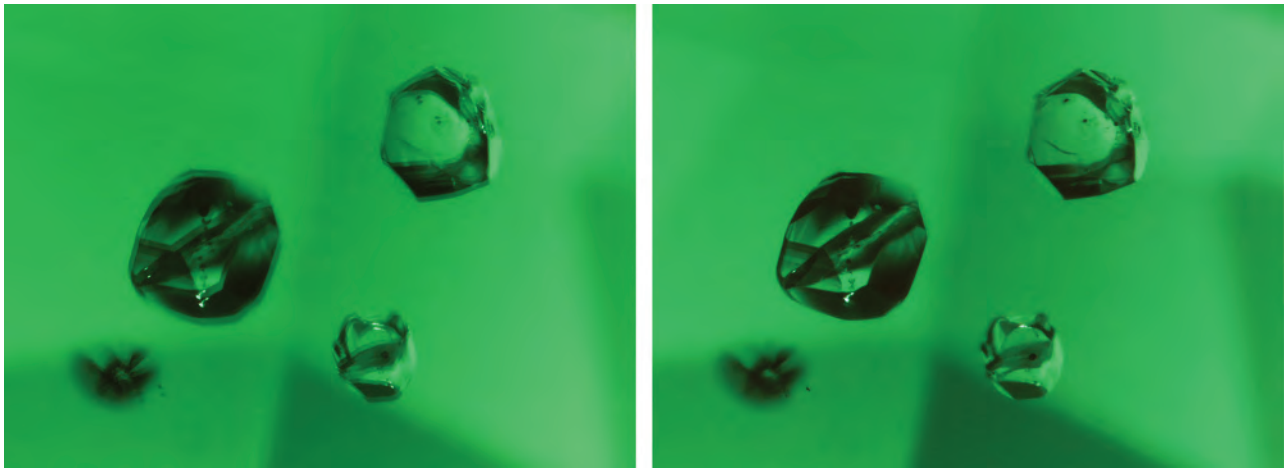

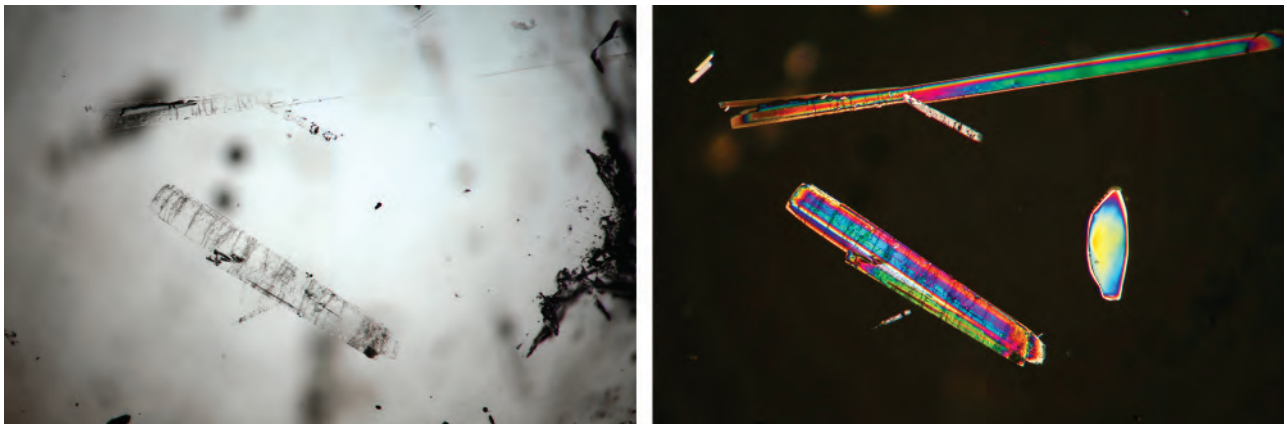

*Figure 11. Left: This rock crystal quartz host, as seen in transmitted light, shows low-relief, colorless, needle-like amphibole inclusions. Right: When the same field is observed with polarized light, the amphibole inclusions stand out in a vivid display of interference colors. Also, a nearly invisible inclusion of quartz reveals its crystallographic misalignment in polarized light. Photomicrographs by Nathan Renfro; field of view 5.10 mm.*

the next challenge is controlling the light in order to balance the contrast in an image and resolve the most detail. One of the biggest problems in lighting is controlling hot spots. A useful technique utilizes a piece of opaque black paper (or similar material) carefully inserted to block the precise source of light causing the hot spot without blocking the desirable light that is illuminating the subject (Koivula, 2003). Another lighting modification is a similar, carefully controlled approach of contrast enhancement called "shadowing" (Koivula, 1982b). Shadowing effects provide a tremendous amount of contrast in inherently low-contrast specimens by adding dark areas to otherwise light subjects (figure 14). To create shadowed illumination, an opaque black paper or similar material is slowly moved in between the illumination source and the specimen until contrast and detail are at a maximum (see again figure 14). This shadowing technique can be applied to darkfield, brightfield, and even reflected light environments.

## DIFFERENTIAL INTERFERENCE CONTRAST

A remarkable lighting technique that has only occasionally been applied to gemology is episcopic differential interference contrast (DIC). This reflected light, contrast-enhancing technique (Koivula, 2000) has produced some of the most vibrant displays of color and geometric patterns ever observed in gemology. A specialized microscope equipped with a Nomarski-modified Wollaston prism and polarizing filters is required for this type of microscopy (figure 15). Sheared wave fronts created by the prism are focused on the speci-

*Figure 12. This spinel hosting a carbonate crystal, as seen in brightfield (left), shows significant anomalous double refraction, or strain, under crossed polarized light (center). This strain is further enhanced by using a first-order red compensator in the optical path, which adds a blue color component to the strain and also decreases the exposure time required to capture the image (right). Photomicrographs by Nathan Renfro; field of view 2.20 mm.*

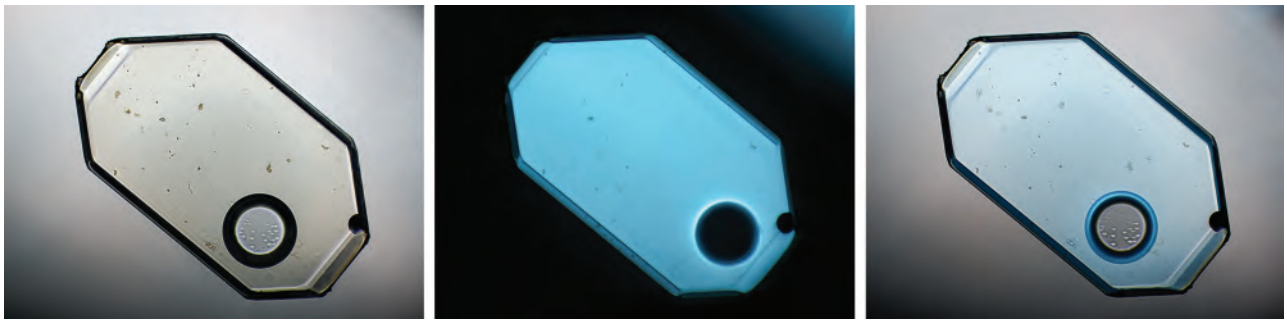

*Figure 13. This tabular negative crystal in quartz was photographed with diffuse transmitted light (left), long-wave ultraviolet light (center), and a combination of visible and LWUV light (right). Each image produces a strikingly different result, demonstrating the interesting results attained through combination lighting. Photomicrographs by Nathan Renfro; field of view 1.24 mm.*

men by the objective and travel slightly different path lengths due to the surface topography of the specimen. These variations in topography are transformed into amplitude or intensity variations, revealing the topographic profile of the specimen (Brandmaier et al., 2013). DIC microscopy is capable of yielding both grayscale images and "optically stained" full-color images by simply adjusting the position of the prism in

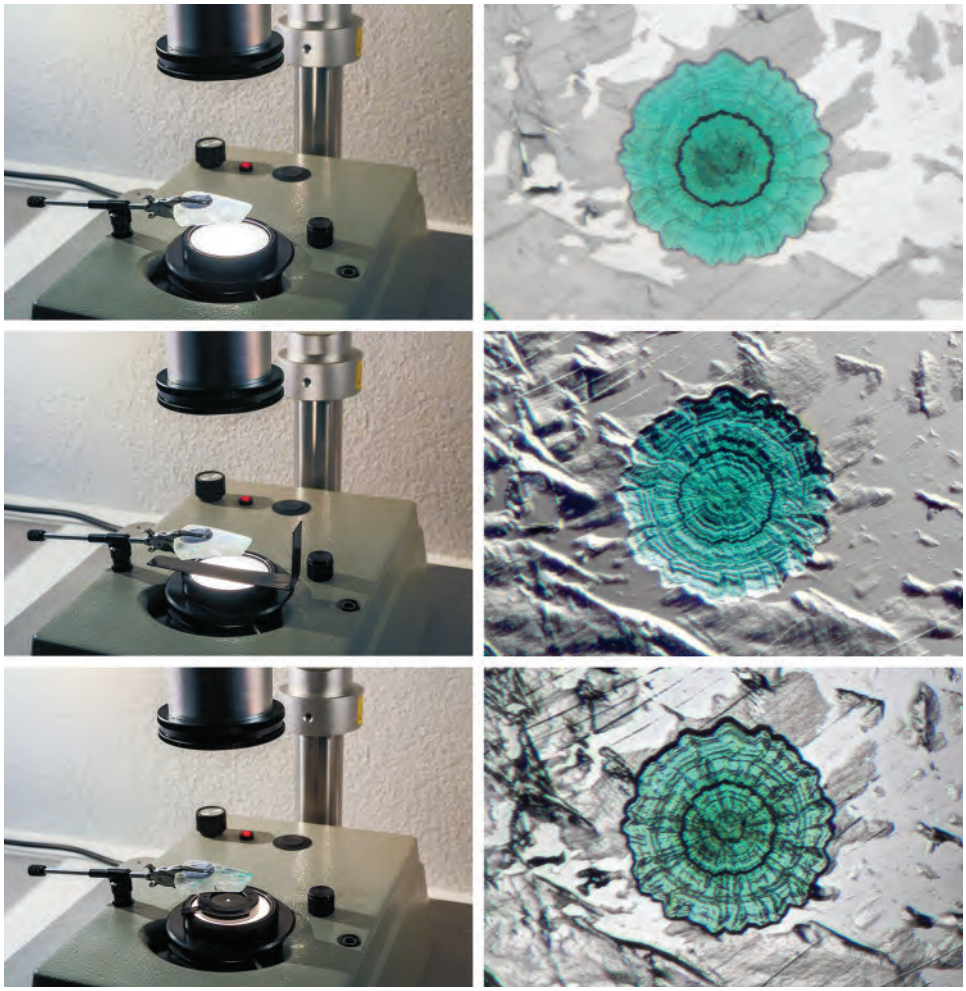

*Figure 14. Transmitted, diffuse lighting (top left) is used to photograph an epigenetic malachite disc (Renfro, 2013), approximately 0.58 mm in diameter (top right). This lighting is ideal when photographing colored inclusions, but contrast is significantly diminished. Placing a black strip of opaque material between the light source and the subject (center left) can create a shadowing environment, significantly enhancing contrast in the subject and giving rise to previously unseen detail (center right). Differently shaped tools can be used to create various shadow effects, as seen when a small iris diaphragm (bottom left) is used to create a circular shadowing environment (bottom right). Photos and photomicrographs by Nathan Renfro.*

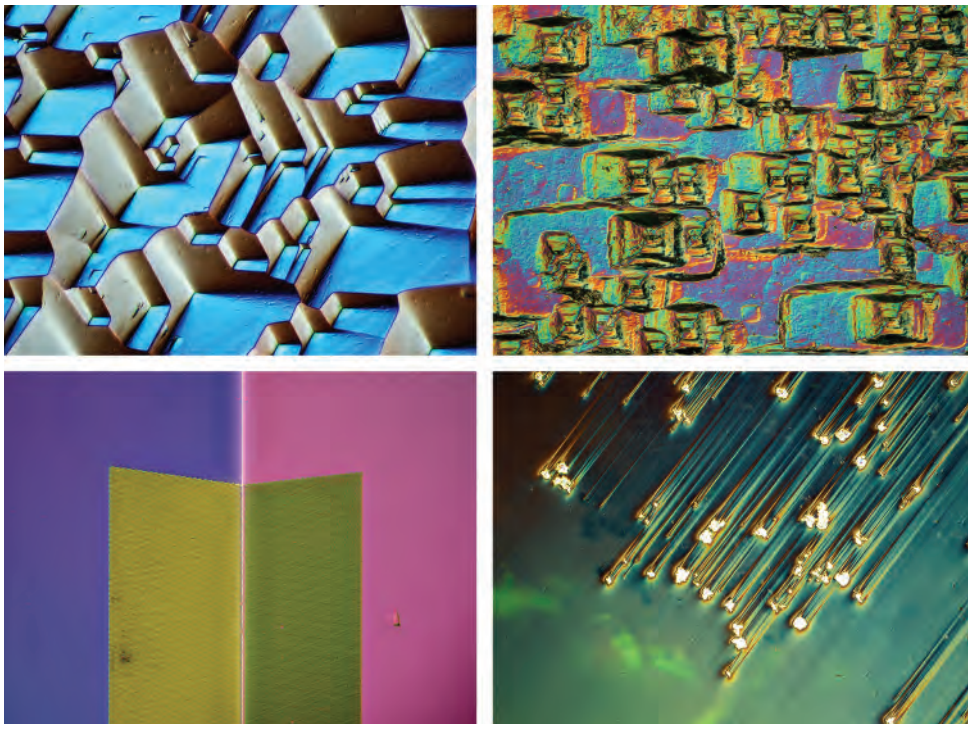

*Figure 15. These differential interference contrast images show a variety of interesting surface structures, including (clockwise from top left): the etched surface of a diamond crystal from Wyoming (field of view 0.25 mm); the etched prism face of an emerald from North Carolina (field of view 0.62 mm); the surface of an Australian opal with pyrite inclusions that break the surface, leaving drag lines from the polishing process trailing behind (field of view 1.24 mm); and plasma etching on two pavilion facets of a "fire polish" diamond (field of view 0.62 mm). Photomicrographs by Nathan Renfro.*

the optical path (figure 15). The surfaces of highly-reflective mineral inclusions can also be carefully examined through their host mineral using DIC (figure 16); however, this technique is not always possible for subsurface inclusions if they are located too deep in the host material, or if the host is too reflective.

## DIGITAL IMAGE PROCESSING

In addition to the previously mentioned advantages, digital photography also allows for a wide range of post-processing tools that can improve image appearance. While software makes it possible to modify images to the point that the image does not accurately represent the subject, the goal of gemological photomicrography is to document inclusions as realistically as possible. Therefore, it is not useful to digitally modify images beyond their natural observed appearance. Software enhancement that makes images appear as close to the actual subject as possible is a tremendously useful tool that, when applied appropriately, is very welcome in the digital photography world. Two particularly important image-processing tools are extended depth-of-field, also called "extended depth of focus" or "focus stacking" and high dynamic range (HDR) imaging.

In an extended depth-of-field, is when a series of images are captured at regularly spaced focal planes and digitally combined to extend the depth-of-field beyond what is possible in a single image (figures 17 and 18). This is particularly important for photomicrography at high magnification, since depth-of-field decreases at higher magnification. This digital processing technique allows the photomicrographer to capture inclusion scenes with tremendous detail at high magnification that would otherwise be impos-

*Figure 16. Even subsurface inclusions, such as this platy hexagonal metal sulfide crystal in a rock crystal quartz host, can be examined using DIC. Photomicrograph by Nathan Renfro; field of view 0.25 mm.*

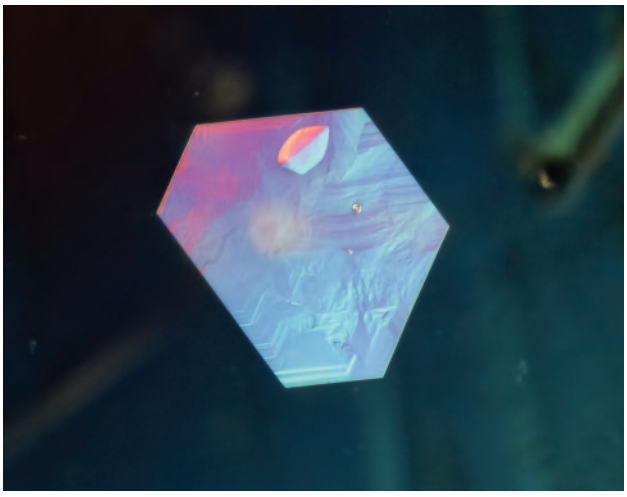

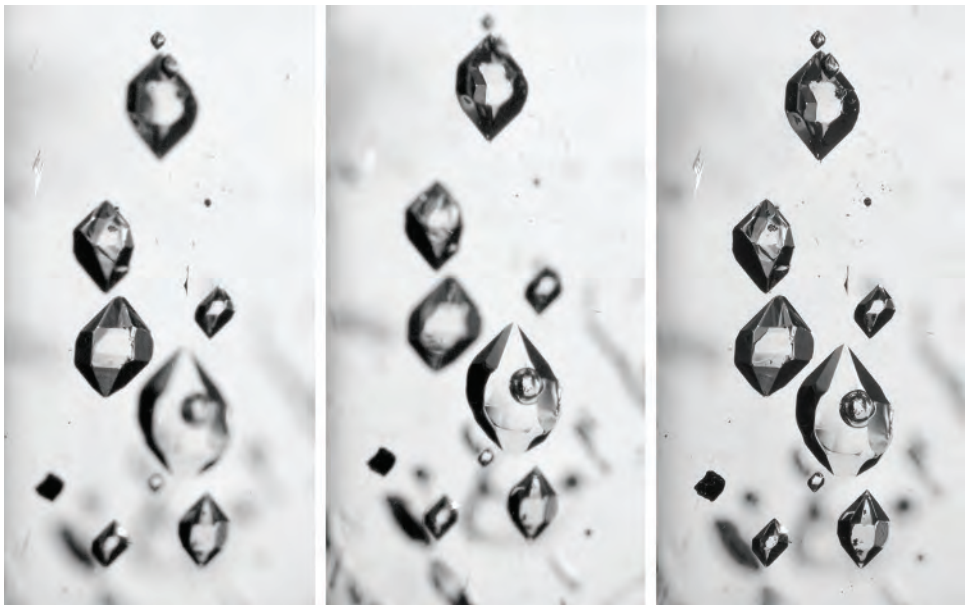

*Figure 17. These fluid-filled negative crystals in rock crystal quartz were photographed using an extended depth-of-field to achieve an image with sharp focus. The left-hand image shows the foreground in focus while the background inclusions are blurry. The center image shows the background in focus while the foreground is blurry. Approximately 30 images stacked together produced an entirely in-focus image of the cluster, as seen on the right. Photomicrographs by Nathan Renfro, field of view 6.55 mm.*

sible in a single frame image. There are several programs to facilitate focus stacking, including Zerene Stacker (Prince, 2014), Helicon Focus, and NIS Elements. One requirement is that the image set must be stepped at fairly regular intervals. While it is possible to slowly turn the focus knob on a microscope by hand, it is impractical to do so in regular increments without some way to measure each step. The addition of a dial indicator or similar measurement device on the microscope focusing rack may be a cost-effective solution, allowing regular focus intervals to facilitate extended depth-of-field imaging (figure 19, left). A focus mount with a fine adjustment will also help the user precisely index the focus height. More sophisticated solutions may involve a focus rail with a stepper motor, which can be digitally controlled through a compatible software program to index the microscope focus at very precise, regular intervals (figure 19, right). This equipment is particularly useful for very large depth ranges, which would require many images.

HDR is another useful processing technique. In digital photomicrography, reflections from facets and other inclusions can create scenarios where some areas of the image are beyond the dynamic range of the camera sensor. In other words, the difference between the lightest and darkest areas in the inclusion scene is beyond what the camera sensor can measure in a single image. The most effective approach is to effectively control the illumination source so that all lighting that falls in the image frame is within the camera's ability to capture. Another consideration is adjusting the camera's ISO setting to the lowest possible value. This typically allows the camera to op-

*Figure 18. This chalcedony contains bands of hematite and goethite clusters scattered throughout a very large depth-of-field. To get the entire image in focus, extended depth-of-field imaging was used, composing 40 images at different depths (left and center) and stacking them together with software to produce and entirely in focus image (right). Photomicrographs by Nathan Renfro; field of view 8.70 mm.*

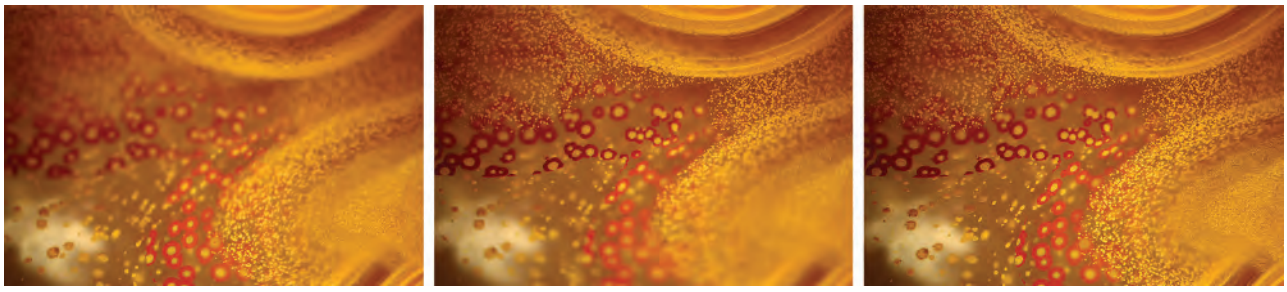

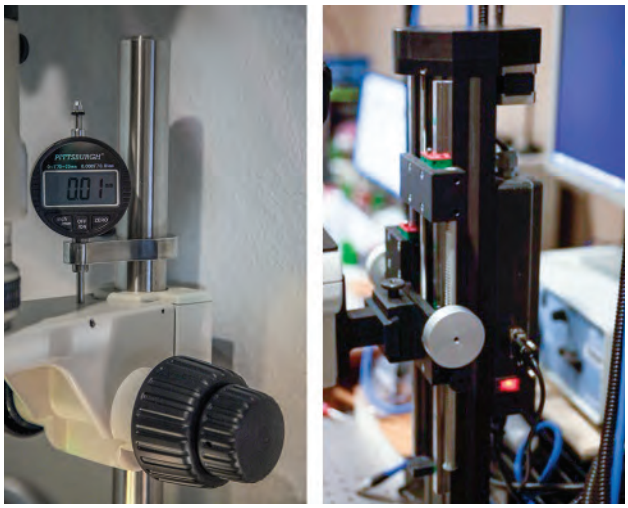

*Figure 19. A digital indicator was attached to the author's microscope stand to accurately measure the step intervals for extended depth-of-field imaging. Left: The fine focus adjustment allows the microscope height to be precisely controlled to step intervals as small as 2.5 microns. Right: Sophisticated equipment such as this "Macrorail" can be used for automated image stacking when combined with the appropriate software. Photos by Nathan Renfro (left) and Darren Bates (right).*

erate at the largest possible dynamic range. HDR imaging can help combat the appearance of overly bright or dark areas in an image when lighting cannot be controlled to eliminate loss of detail. Similar to focus stacking, the photomicrographer must capture several images that are combined into one final image. Instead of changing the focus, as with image stacking, the exposure time is changed. Details resolvable at several different exposures are combined into a single image that is beyond the detail possible from any single exposure. Sometimes this effectively reproduces what the gemologist actually sees when observing the specimen in the microscope. The human brain and eye do not suffer from the relatively narrow dynamic range of a digital camera sensor, so in some cases, a high dynamic range image may approximate the actual subject than any single exposure alone (figure 20). HDR imaging can be accomplished using software designed for this task, often available on the Internet, such as Nikon NIS Elements, Canon Digital Professional, Oloneo HDR, and Photomatix Pro. Some cameras have built-in HDR processing capabilities, including many smartphones and some Canon and Nikon DSLR cameras. This convenient built-in feature helps automate HDR imaging without the need for secondary image-processing software.

Other types of post-processing digital image software help the photographer make fine adjustments to the captured image. Sometimes the settings used to capture an image can be improved. Unlike film-based photography, the digital world offers tools to modify brightness, contrast, and color without having to retake a photograph or take several exposures at different settings to see which one looks best. Some digital software also offers enhancement tools that clean up images and remove artifacts such as minute spots of dust on the sample or spot artifacts from dust on the camera sensor (figure 21). These tools help photographers adjust images to more accurately

*Figure 20. These radial manganese oxide "flowers" in Ethiopian opal provide too much contrast for the camera sensor to resolve all of the detail in the inclusion. The image at the left was underexposed, so detail is lost in the dark center of the MgO flower. The center image was overexposed to resolve detail in the dark areas, but all detail is lost in the bright areas. These varying exposure images were combined using HDR software (Nikon's NIS Elements) to produce the image on the right, which shows more detail than any single image. Photomicrographs by Nathan Renfro; field of view 2.47 mm.*

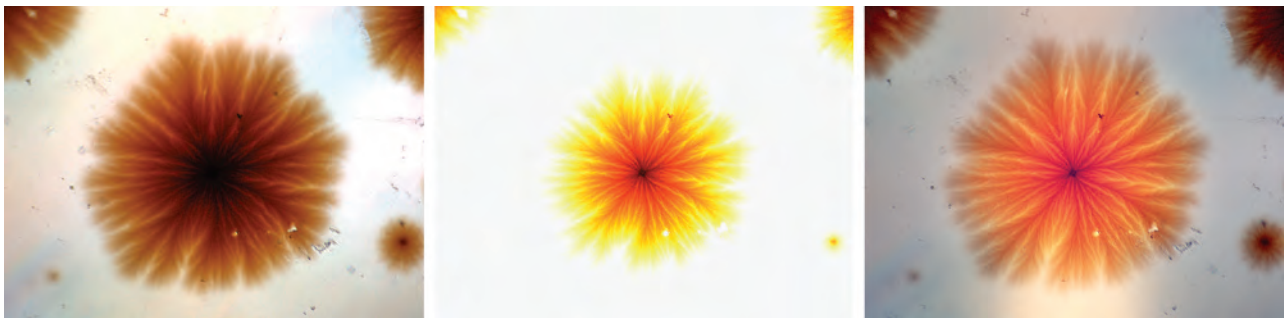

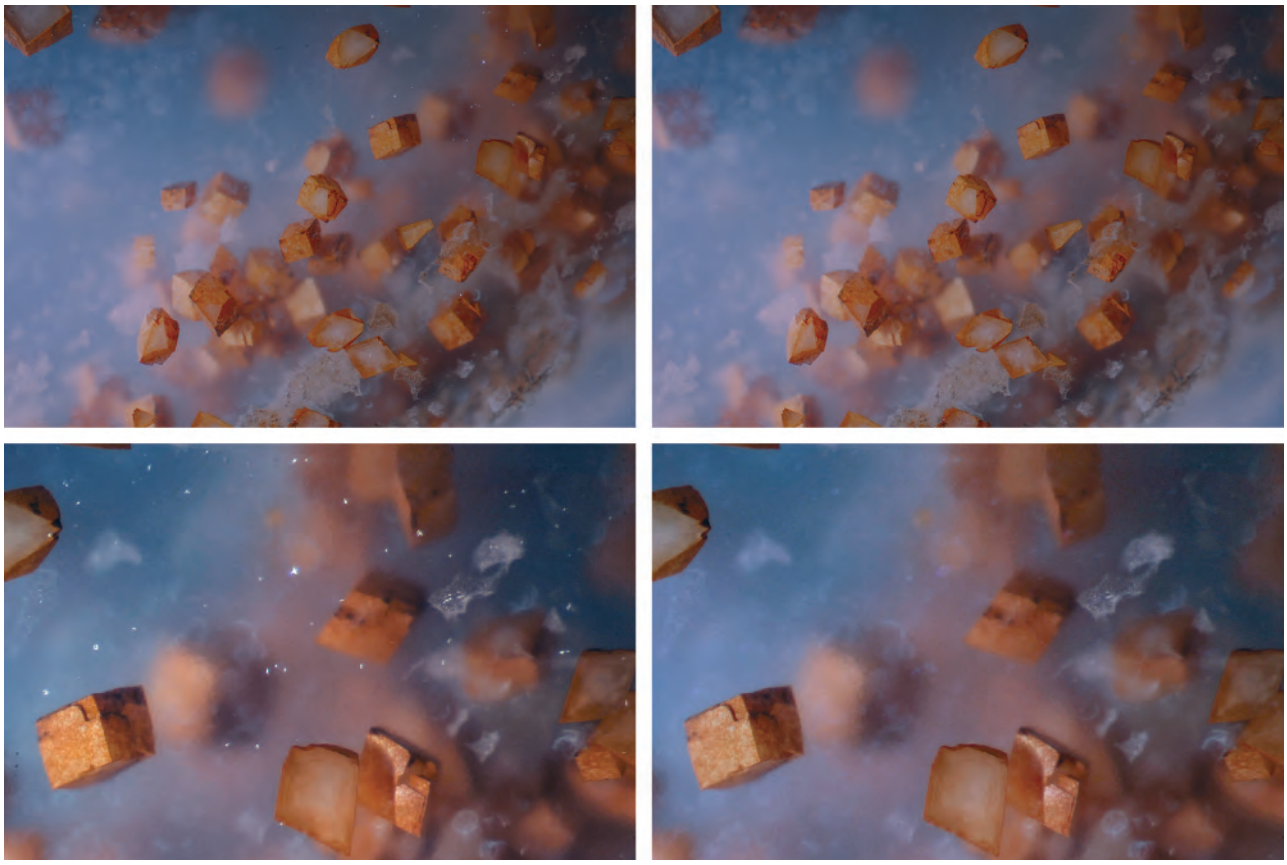

*Figure 21. Fine dust spots (top left, field of view 6.95 mm) on the surface of this chalcedony with carbonate inclusions from Turkey detract from the interesting inclusion scene. Image editing software such as Adobe Photoshop has touch-up tools that allow digital removal of dust spots and unwanted minute artifacts, as shown in the edited image (top right, field of view 6.95 mm). Zooming in on the top right portion of the image with significant dust (bottom left, field of view 3.10 mm), the difference before and after dust removal with Adobe Photoshop is much more apparent (bottom right, field of view 3.10 mm). Photomicrographs by Nathan Renfro.*

represent their subjects. The most popular of these programs is almost certainly Adobe Photoshop, but many photography-specific post-processing programs have been developed with the onset of digital photography. Photoshop Lightroom is also a popular option for image post processing and organization, but other programs such as Pixelmator (for Macs and iPads) and GIMP (GNU Image Manipulating Program) offer easy-to-use digital image correction tools. Photomicrographers will also want to consider the file type. Raw files are much larger than JPEG files, but also better for post-image processing adjustments.

## SUBJECT SIZE

One of the most important attributes conveyed by a photomicrograph is the size of the subject. There are a few ways to present this information: indicating the magnification used to capture the image for a particular format (size of the camera sensor), overlaying a scale bar onto the image itself, or indicating the field of view as a numerical measurement. Gemological texts have historically indicated the magnification that was used to observe a subject to convey the relative size of the inclusion scene and how it would look in the reader's own microscope. The rationale here is that most gemologists are familiar with the magnification range used during routine gemological microscopy, which may not be true of a numerical value presented in a possibly unfamiliar unit, such as microns. The biggest problem with using magnification in the digital age is maintaining accuracy during the post-processing phase, as images are often formatted and cropped in ways that render the original magnification meaningless.

The magnification factor of an optical microscope is determined by multiplying the magnification factors of all optical components between the specimen and the observer's eye. While this represents the observed magnification, the actual magnification of the recorded image can vary depending on the size of the camera sensor, and will likely be very different from the observed magnification factor. The easiest method to determine the magnification at the camera sensor is to use a microscope calibration slide (figure 22) to determine the actual field of view the camera captures. If the field of view and the physical size of the camera sensor are known, then the magnification factor at the camera sensor can be calculated by dividing the sensor width by the horizontal field of view of the subject as measured by the calibration slide. This recorded magnification becomes meaningless as soon as the image is cropped or enlarged from the original footprint of the camera sensor, which will almost certainly occur. This is why a more precise way to communicate the actual size the photomicrograph represents is needed. This can be accomplished by the use of a scale bar or a field of view measurement.

In most scientific publications, scale bars are used to indicate subject size by overlaying a line of known length on some portion of the photomicrograph (Hord, 2004). This is an accurate way to convey subject size in a photomicrograph. Some software, such as Helicon Focus, provides a tool that lets the user quickly add a scale bar to their images. Despite the benefit of the information they contain, scale bars do obscure a portion of the image. Gemology is an observational science, and gemologists are privileged to view beautiful scenes that are preserved in photomicrographs. The artificial addition of a scale bar may be perceived as an unnecessary blemish on an otherwise artistic scene, which is reason enough for this author to exclude scale bars. Fortunately, there is a compromise that overcomes the problems with using magnification and scale bars to convey subject size: expressing a field of view measurement for the final image in the caption. This offers an accurate account of subject size without marring an otherwise pristine inclusion scene with an unsightly scale bar.

## CONCLUSION

Photomicrography is a tremendously rewarding aspect of gemology. It appeals to all types of practitioners, from scientists to artists and everyone in between. With technological developments in the last decade, digital-format photography has spurred the development of a wide range of tools to enhance images in ways never before possible. Digital photography has also helped to offset cost-related issues, since there are almost no consumable items that the photomicrographer must purchase after an initial investment in equipment, allowing many more people to participate in this branch of gemology.


*Figure 22. A microscope calibration slide, such as the one manufactured by Bausch and Lomb Optical Co., can be used to determine the actual field of view of an image taken through the microscope. Photo by Robison McMurtry.*

Because of the spectacular level that digital technology has already achieved in the last decade alone, it is hard to imagine how photomicrography might evolve in the next 10 years. One area with significant room for improvement is lighting options. Light-emitting diode technology is improving at a rapid rate, and the implementation of LED lighting in photomicrography will be a welcome improvement, as it comes closer to "natural-looking" full spectrum lighting. Camera technology will likely continue to improve as higher-resolution and higher-sensitivity sensors are developed. Canon recently announced the release of a full-frame DSLR with more than 50 megapixels of resolution, the highest of any 35mm format camera to date (Canon, 2015). Two models, the 5DS and 5DSR may prove to be well suited for photomicrography. Vibration may also be curtailed as mirrorless digital cameras become more refined. Hopefully, the overall cost of digital camera equipment will be lower, allowing more users to acquire better equipment and capture better images.

With practice and patience, anyone can enjoy this branch of gemology and share their observations and discoveries within the micro-world of gems.

ABOUT THE AUTHOR

*Mr. Renfro is the analytical manager of the gem identification department, and analytical microscopist of the inclusion research department, at GIA in Carlsbad, California.*

ACKNOWLEDGMENTS

*The author would like to thank Gene Goldsand, Danny J. Sanchez, Kevin Schumacher, and Eric Welch for their helpful discussions regarding equipment and software. The author also thanks Shane McClure for several helpful recommendations on the composition of gemological photomicrographs. Lastly, the author thanks John Koivula for the continued mentorship, friendship, and overwhelming support that made this article possible.*

## REFERENCES

Boehm E. (2014) Photomicrography using a smartphone camera. *The Journal of Gemmology*, Vol. 34, No. 1, pp. 6–7.

Brandmaier C., Spring K., Davidson M. (2013) Reflected light DIC microscopy, http://www.microscopyu.com/articles/dic/reflecteddic.html

Canon (2015) Canon U.S.A. introduces the world's highest resolution full-frame DSLR cameras: EOS 5DS and EOS 5DS R. Press release, Feb. 5.

Gübelin E., Koivula J. (1986) *Photoatlas of Inclusions in Gemstones*, Volume 1. ABC Edition, Zurich.

——— (2005) *Photoatlas of Inclusions in Gemstones*, Volume 2. Opinio Verlag, Basel, Switzerland.

——— (2008) *Photoatlas of Inclusions in Gemstones*, Volume 3. Opinio Verlag, Basel, Switzerland.

Hord B. (2004) Letters: Expressing magnification in photomicrographs. *G&G*, Vol. 40, No. 3, p. 199.

Koivula J.I. (1980) "Thin films"—Elusive beauty in the world of inclusions. *G&G*, Vol. 16, No. 9, pp. 326–330.

——— (1981) Photographing inclusions. *G&G*, Vol. 17, No. 3, pp. 132–142.

——— (1982a) Pinpoint illumination: A controllable system of lighting for gem microscopy. *G&G*, Vol. 18, No. 2, pp. 83–86.

——— (1982b) Shadowing: A new method of image enhancement for gemological microscopy. *G&G*, Vol. 18, No. 3, pp. 160–164.

——— (1984) The first order red compensator: An effective gemological tool. *G&G*, Vol. 20, No. 2, pp. 101–105.

——— (2000) *The Microworld of Diamonds*. Gemworld International. Northbrook, Illinois.

——— (2003) Photomicrography for gemologists. *G&G*, Vol. 39, No. 1, pp. 4–23.

Koivula J.I., Kammerling R., Fritsch E., Eds. (1994) Gem News International: Amber marketed with photomicrography. *G&G*, Vol. 30, No. 2, p. 124.

Overton T.W. (2010) Gem News International: Smartphone photomicrography. *G&G*, Vol. 46, No. 4, pp. 325–326.

Prince N. (2014) Use of stacking software for expanding depth-of-field in inclusion photomicrography. *The Journal of Gemmology*, Vol. 34 No. 3, pp. 188–189.

Renfro N.D. (2013) Gem News International: Unusual epigenetic malachite discs in quartz. *G&G*, Vol. 49, No. 3, pp. 178–179.

Shipley Jr. R.M. (1939) United States Patent Office, Dark Field Illuminator, Patent number 2,157,437.

Trenholm R. (2007) Photos: The history of the digital camera, Nov. 2, http://www.cnet.com/news/photos-the-history-of-the-digital-camera.

# Rubies and Sapphires from Snezhnoe, Tajikistan

Elena S. Sorokina, Andrey K. Litvinenko, Wolfgang Hofmeister, Tobias Häger, Dorrit E. Jacob, and Zamoniddin Z. Nasriddinov

Discovered during the late 1970s, the Snezhnoe ruby and sapphire deposit in Tajikistan was active until the collapse of the former Soviet Union in the early 1990s and the outbreak of regional conflicts. This marble-hosted occurrence has seen renewed interest, as it is a large and potentially productive deposit that has not been sufficiently studied. Testing of samples identified solid inclusions of margarite enriched with Na and Li (calcic ephesite or soda margarite). These are believed to be previously unreported for gem corundum. Allanite, muscovite, and fuchsite (chromium-bearing muscovite) were identified for the first time in ruby and sapphire from Snezhnoe. These and other inclusions such as zircon, rutile, K-feldspar, and Ca-Na-plagioclase could serve to distinguish them from stones mined elsewhere. Concentrations of trace elements were typical for ruby and sapphire of the same formation type. The highest Cr concentrations were observed within the bright red marble-hosted rubies, and these values were very similar to those of the famous Burmese rubies from Mogok.

Corundum—$\alpha$-$Al_2O_3$—is a common, though minor, component of many metamorphic rocks. Gem-quality varieties of ruby and sapphire occur in only a few primary metamorphic and magmatic rock types depleted in silica and enriched in alumina (Giuliani et al., 2007) and in the secondary placers formed by the erosion of these rocks (e.g., Hughes, 1997; Kievlenko, 2003).

The traditional supplier of ruby and sapphire to the world markets is Southeast Asia. Burmese rubies from the Mogok deposit have historically held the highest value, stemming from their "pigeon's blood" color, a bright red with a slightly purple hue (Hughes, 1997; Smith, 1998). The supply situation has changed dramatically in recent years, with the discovery of new deposits in East Africa and the continued mining of the Central and Southeast Asian occurrences.

Situated within the Pamir Mountains, Tajikistan produces a variety of gemstones, including ruby (figures 1 and 2), sapphire, spinel, aquamarine, chrysoberyl, tourmaline, topaz, clinohumite, garnet, scapolite, lazurite, and variscite (Litvinenko and Barnov, 2010). The occurrence of ruby in the Pamirs was first suggested by the Soviet mineralo-

*Figure 1. The bright red faceted ruby in this gold ring is from the large and potentially productive Snezhnoe deposit in Tajikistan. Photo by Zamoniddin Z. Nasriddinov.*

See end of article for About the Authors and Acknowledgments.
Gems & Gemology, Vol. 51, No. 2, pp. 160–175,
http://dx.doi.org/10.5741/GEMS.51.2.160.

*Figure 2. These rough ruby crystals are from the Snezhnoe deposit. Photo by Zamoniddin Z. Nasriddinov.*

gist and geochemist A.E. Fersman in the early 1930s (Popov, 1936). Fersman predicted the location of ruby deposits in the Precambrian metamorphic rocks of the southwestern Pamirs, where the geological conditions are similar to those in Myanmar and Sri Lanka. This hypothesis was confirmed by Ya. A. Gurevich, I.M. Derzhavets, and colleagues during a prospecting expedition to the Pamirs in 1965, when they found a group of ruby and sapphire deposits on the western slope of the Ishkashim ridge (Litvinenko and Barnov, 2010).

## In Brief

- The Snezhnoe ruby occurrence in Tajikistan is a large and potentially productive source of gem corundum.
- The highest Cr concentrations were observed in the bright red marble-hosted ruby, which had a value close to those of similar genetic type, including the famous Burmese rubies from Mogok.
- The study identified previously undocumented solid inclusions that are useful for the origin determination of this gemstone.

Marble-hosted ruby deposits were first detected in the Shakhdarin series (Archean age) in 1979 (Konovalenko and Rossovsky, 1980). The subsequent discovery of a new gem deposit structure—a ruby belt on the eastern part of the Central Pamirs—became something of a sensation in the 1980s (Litvinenko and Barnov, 2010). More than 50 marble-hosted ruby occurrences confined to the gneiss-marble suite of the Muzkol metamorphic complex (Paleoproterozoic) have been found within this zone. The largest of these are Snezhnoe and Trika, discovered in 1980, and Nadezhda, which followed a decade later (Litvinenko and Barnov, 2010). After the collapse of the Soviet Union, all mining and prospecting activity at these deposits was suspended for more than 15 years. Today, production figures are kept confidential by the Tajik government. Regional conflicts, combined with difficult access and climate conditions, have complicated further study of these gem deposits, though a period of stability allowed foreign researchers to visit them in the early 21st century (Bowersox, 2005; Hughes et al., 2006).

Petrographic, mineralogical, and gemological research has been conducted at various times, both by Soviet and then Russian scientists (Dmitriev, 1983; Dmitriev and Ishan-Sho, 1987; Dufour et al., 2007) and their foreign counterparts (Henn and Bank, 1990; Smith, 1998). For this article, we have updated knowledge about the geology of the Snezhnoe deposit and separated various types of ruby and sapphire crystals according to their morphology, gemological properties (including reflectance and luminescence spectra), trace-element composition, and previously unreported solid inclusions.

## REGIONAL GEOLOGY

The Snezhnoe deposit is confined to the Kukurt anticlinal fold belonging to the south wing of the Shatput anticline (Kievlenko, 2003) within the eastern

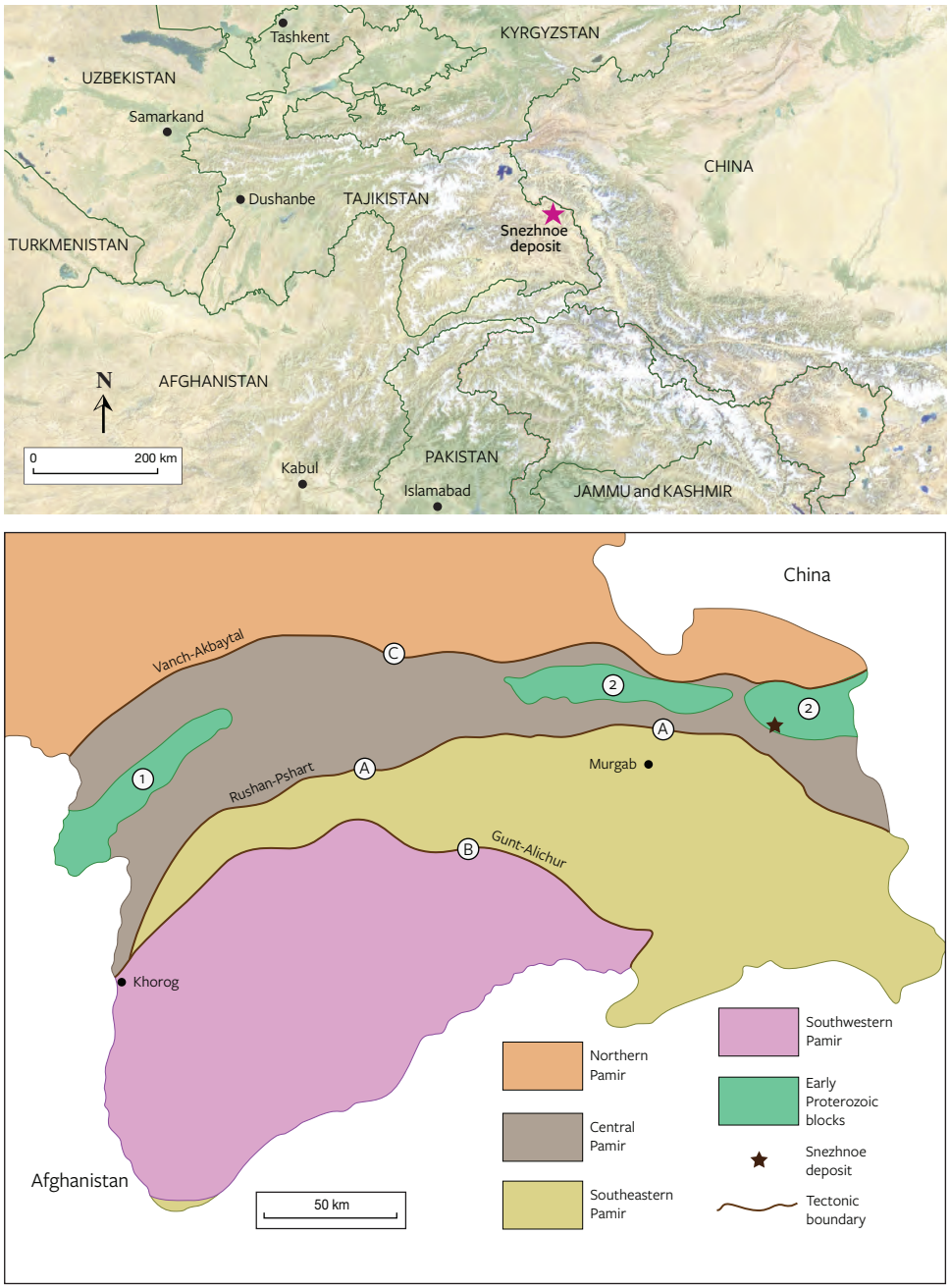


*Figure 3. Top: A map of the Snezhnoe marble-hosted ruby deposit within Central Asia. Bottom: A regional geological map of the Pamir Mountains of Tajikistan and the location of the Snezhnoe deposit. The northern, central, southeastern, and southwestern Pamirs are folded regions around early Proterozoic blocks, one of which includes the Snezhnoe deposit. The northern Pamir is related to the Hercynides, whereas the central, southeastern, and southwestern Pamir represent Cimmerian Plate remnants. There are deep faults or tectonic boundaries between these regions. The circled A represents the Rushan-Pshart deep fault, while the circled B indicates the Gunt-Alichur deep fault. The circled C represents the Vanch-Akbaytal deep fault. The circled 1 indicates the Vanch-Yazgulem anticlinorium (an anticlinal structure of regional extent), the circled 2 the Muzkol-Rangkul anticlinorium. The distance between Khorog and Murgab is 255 km. Modified from Barkhatov (1963).*

part of the Muzkol–Rangkul anticlinorium (outcrop of the Precambrian crystalline basement by Rossovsky, 1987; figure 3). The core of the Kukurt fold is characterized by the development of granite-gneiss in the Zarbuluk complex (possibly Proterozoic, age not determined) surrounded by gneisses and schist (Belautin suite), calcite and dolomite marbles (Sarydzhilgin suite), and quartzites and quartz sandstones (Buruluk suite) of the Muzkol metamorphic complex (Paleoproterozoic). A massif composed of leucocratic granites from the Shatpur intrusive complex (Cretaceous-Paleogene) is adjacent to the eastern part of the fold. The southern part of the fold is cut by the Muzkol regional fault, separating the Precambrian formations from Paleozoic–Mesozoic sedimentary rocks (figure 4).

The ruby-hosted Sarydzhilgin suite, along with other suites of the Muzkol metamorphic complex (total thickness exceeding 6 km), underwent at least two tectonic metamorphic cycles. The first took place 1.8–1.6 billion years ago (Budanova, 1991) at amphibolite facies (temperature and pressure approx-

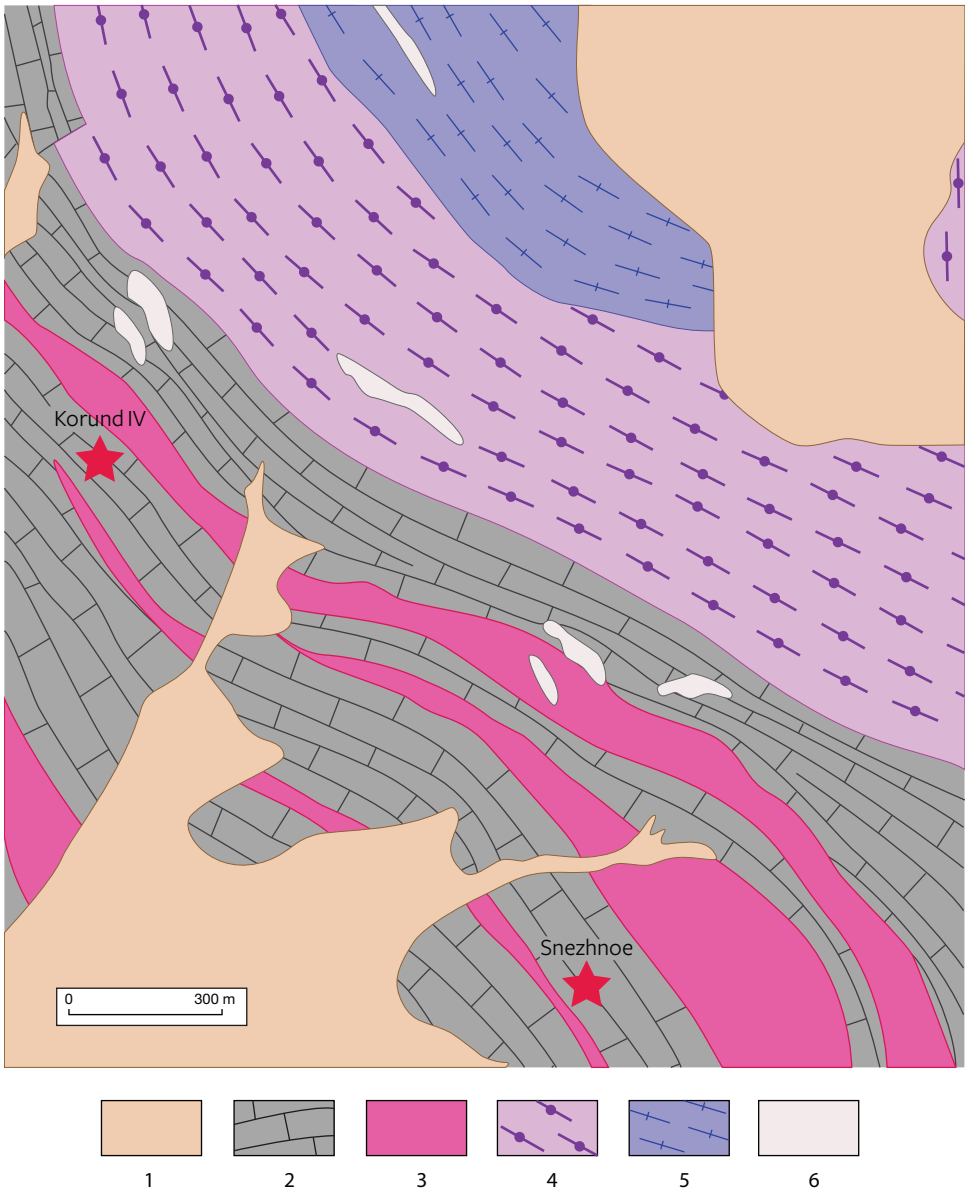


*Figure 4. This map illustrates the regional geology of the Snezhnoe deposit. 1—sedimentary rocks; Sarydzhilgin suite: 2—marbles; 3—kyanite-garnet-biotite, feldspar-biotite, and biotite schists; Belautin suite: 4—garnet gneisses and 5—garnet-biotite gneisses; 6—leucocratic granites of the Shatput intrusive complex. Stars indicate the location of gem corundum deposits. Modified from Kievlenko (2003).*

imately 700°C and 8 kbar), and the second cycle occurred 100–20 million years ago (Budanova, 1993). This is a zonal metamorphism migrating from greenschist facies at 350ºC and 4 kbar through epidote-amphibolite facies up to 800ºC and 9 kbar (complete melting zone) (Sorokina et al., 2014). There are several theories concerning the geological age of ruby and sapphire crystals in marble, and some researchers believe that formation took place during modern alpine regional metamorphism (Dmitriev and Ishan-Sho, 1987; Dufour et al., 2007).

## LOCAL GEOLOGY AND MINERAL ASSEMBLAGE

The Snezhnoe deposit is located in the eastern part of the Pamir Mountains in Tajikistan. The occurrence is situated 30 km northeast of Murgab and about 20 km south of Rangkul, a pair of villages near the Chinese border. It is on the eastern bank of the Aksu River, at an altitude more than 4,000 meters above sea level. The region containing the corundum deposits lies along the Kukurt pegmatite belt, which is enriched with gem scapolite. Ruby and pink sapphire have been found in the formation of coarse-

*Figure 5. An outcrop of white marbles and dumps at the Snezhnoe deposit. Photo by Andrey K. Litvinenko.*

grained calcite marbles from the Sarydzhilgin suite of the Muzkol metamorphic series (Paleoproterozoic), with a total thickness of about 20 m (figure 5). This formation lies between layers of kyanite-garnet-biotite schist and marbles.

Two ruby-mineralized zones are arranged *en echelon* (in closely spaced, parallel, or subparallel step-like planes) in coarse-grained calcite marble parallel to their bedding planes. They can be traced along the strike for 150 to 200 m. The mineralized zones are represented by micaceous lenses (2–15 m in length, with maximum thickness of 1 m) and ruby-bearing marbles contacting with these lenses (figure 6).

Minerals found in micaceous lenses in Snezhnoe include various types of mica (fuchsite and phlogopite), plagioclase (from albite to anorthite), and scapolite (40–

*Figure 6. A cross-section of the Snezhnoe marble-hosted ruby deposit illustrates: (1) white marble, (2) graphite, (3) mica, (4) scapolite and plagioclase, (5) ruby, and (6) the main bedding surface controlling ruby mineralization. Modified from Nasriddinov (2013).*

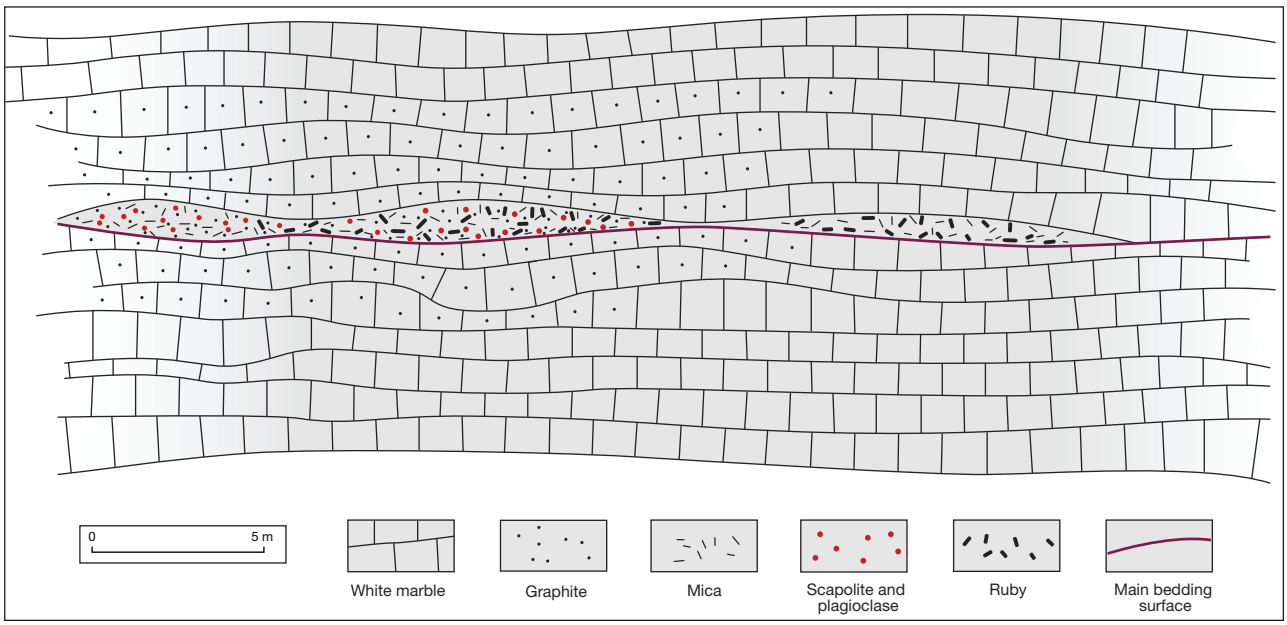

*Figure 7. This outcrop of ruby-bearing micaceous lenses within marble has a total thickness of 15 cm. Red ruby crystal can be seen in the center of the photo, surrounded by green fuchsite. Photo by Zamoniddin Z. Nasriddinov.*

60% meionite), as well as ruby and sapphire, rutile, goethite, carbonates (calcite and dolomite), minerals of the chlorite group, graphite, K-feldspar, and kaolinite (Sorokina, 2011; Sorokina et al., 2012; figure 7). Furthermore, there are marbles that consist mainly of calcite (up to 90%), ruby, mica (phlogopite and fuchsite), goethite, scapolite (about 60% meionite), plagioclase (albite to oligoclase), and graphite. Other researchers have reported amphibole (Rossovsky, 1987), pyrite, and dravite (Kievlenko, 2003).

Soviet-era estimates of the Snezhnoe deposit indicated possible reserves of many hundred thousand carats of gem corundum. The authors of the present article visited the occurrence in 1982, 1986, 2008, 2009, 2012, and 2013. It is currently being worked to a depth of 30 m by the state-run Chamast enterprise, which is conducting underground mining with drilling tools and large trucks.

## MATERIALS AND METHODS

The authors borrowed 41 ruby-bearing rock samples from Snezhnoe from the collection of the Fedorovsky All-Russian Research Institute of Mineral Resources (FGUP VIMS), which obtained them in the early 1980s. Two additional samples of ruby in marble from this deposit were loaned by the Vernadsky Geological Museum of Russian Academy of Science, courtesy of former chief curator Dr. Mikhail N. Kandinov.

To prepare the sample wafers, the authors cut a section of rock containing ruby and sapphire crystals. The surrounding matrix was either dissolved by 10% HCl acid or mechanically removed, or a combination of the two. Standard gemological properties were recorded, including hydrostatic SG, color, and refractive index. We performed long-wave (365 nm) and short-wave (254 nm) photoluminescence spectroscopy and observed microscopic features using an MBS-10 binocular microscope. To obtain reflectance spectra in the visible range (380–800 nm), we used a Leica-Leitz MPV-SP spectrometer with a reflection probe and a resolution of 1 nm and an integration time of 500 ms. Photoluminescence spectroscopy was performed at FGUP VIMS using a MSFU-K (LOMO) microspectrophotometer with an LGI-505 nitrogen laser (337.1 nm wavelength emission), a CAMAC registration system, an IRIS-3m generator, and an MDR-23 monochromator connected to a computer.

Laser ablation–inductively coupled plasma–mass spectrometry (LA-ICP-MS) was carried out at Johannes Gutenberg University in Mainz, Germany, with an ESI/NWR-193 laser system (193 nm) coupled to an Agilent 7500ce quadrupole ICP-MS with helium as the carrier gas. The laser spots had a diameter of 50 µm on the samples and 100 µm on the reference standards. Analyses were carried out at an energy density of 2.02 J/cm$^{-2}$ with a 10 Hz repetition rate, using NIST SRM 612 glass as an external standard and NIST SRM 610 as an unknown for quality control. $^{27}$Al, measured as $Al_2O_3$ by electron microprobe, was used as the internal standard for rubies. $^{29}$Si, based on $SiO_2$ from electron microprobe data, was used for micas. Data reduction was carried out with Glitter commercial software. Detection limits were typically in the lower parts-per-billion range, and analytical uncertainties were generally between 5% and 15%, based on the external reproducibility of the reference materials (Jacob, 2006). Microprobe analysis was carried out at the Fersman Mineralogical Museum of the Russian Academy of Sciences. For these analyses, we used a Link ISIS energy-dispersive spectrometer (EDS) electronic probe microanalyzer attached to a CamScan D4 scanning electron microscope.

## DESCRIPTION OF THE ROUGH

Rough ruby and sapphire samples from the Snezhnoe deposit were found in different parts of mineralized zones and had a distinct appearance. Ruby and sapphire crystals within micaceous lenses were normally translucent—the intergrowth of transparent and translucent areas could be observed in some crystals—and displayed visible morphological defects, such as polysynthetic twinning and parting

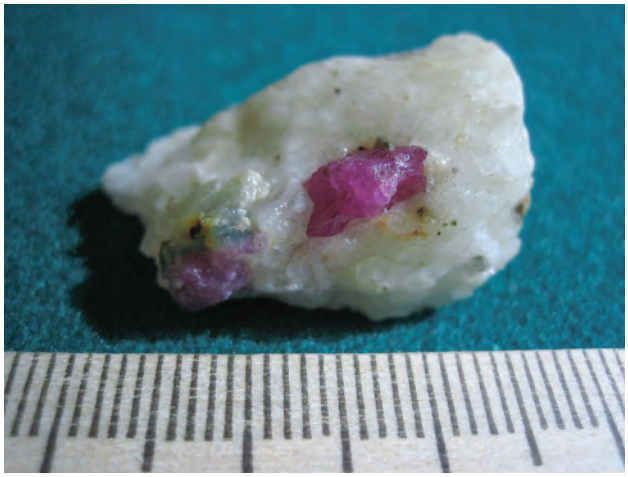

*Figure 8. Ruby crystals within a 2 cm calcitic marble. Photo by Elena S. Sorokina.*

parallel to the *c*, *a*, and *r* corundum faces. As a result, they were usually unsuitable for faceting or even cabochons. Their morphology and color varied from purple elongated prisms to slightly pink prismatic rhombohedra and deep red pinacoid crystals. Dipyramids were also found in the samples. The average crystal size varied from 20 to 30 mm, in rare instances reaching 50–60 mm in length.

At the Snezhnoe deposit, bright red gem-quality ruby crystals with a slightly purple hue are found in marble (figure 8). These samples were characterized by a prismatic habit with *c*, *r*, and *z* faces, as well as irregular morphology with normally rounded faces (figure 9). Most of these samples were transparent and much shorter in length than the type found within micaceous lenses, often no longer than 8–10 mm. The ruby crystals were free of visible morphological defects except for occasional parting, typically parallel to the *c* and *r* crystal faces.

## RESULTS AND DISCUSSION

**Gemological Characteristics.** The gemological properties of rubies and sapphires from the Snezhnoe deposit were similar to those previously observed by other researchers (Henn and Bank, 1990; Smith, 1998) and quite typical for corundum overall (table 1).

The results of this study showed a refractive index of $n_o$ = 1.762–1.764 and $n_e$ = 1.772–1.774. Birefringence was 0.008–0.009. Specific gravity ranged from 3.99 to 4.01. Pleochroism was usually weak to medium for crystals from the micaceous lenses but strong in marble-hosted samples; dichroism was orange-red parallel to the c-axis and reddish violet perpendicular to the c-axis. The samples luminesced strong red under long-wave UV and weak red under short-wave UV.

**Internal Growth Structure.** Ruby and sapphire from micaceous lenses contained abundant defects. Purple and dark red specimens showed parting along the *r*

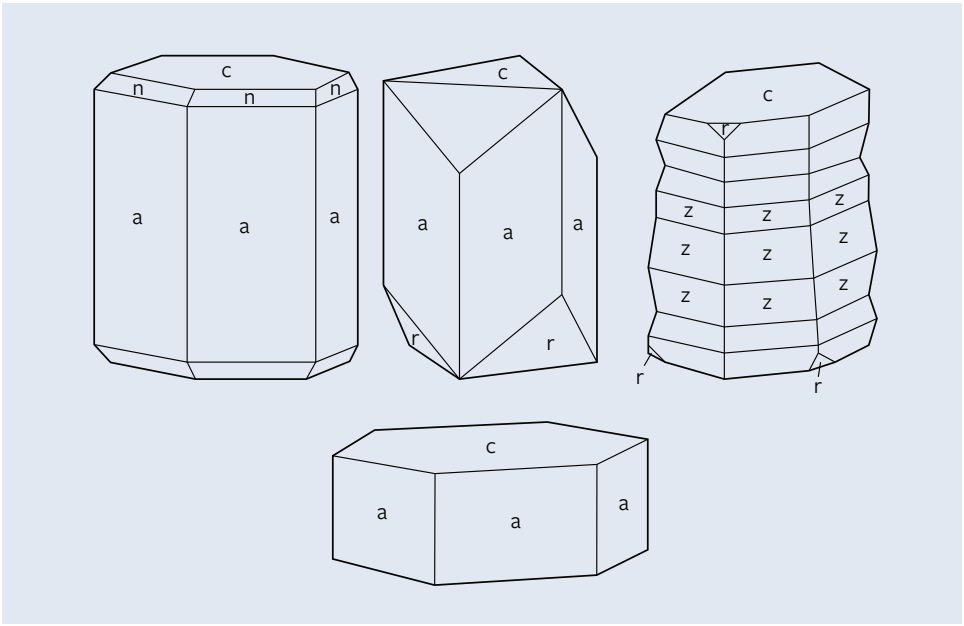


*Figure 9. Crystal morphology of gem corundum from Snezhnoe. Top, left to right: an elongated prismatic habit with* a, n, *and* c *faces; a rhombohedral-prismatic habit with* a, r, *and* c *faces; and a prismatic habit with* z, c, *and* r *faces. Bottom: a pinacoid habit with* c *and* a *faces. Modified from Goldschmidt (1918).*

**TABLE 1.** Gemological properties of corundum from the Snezhnoe deposit compared with previous studies.

| Property | Ruby and sapphire from micaceous lenses | Marble-hosted ruby | Ruby (Henn and Bank, 1990) | Ruby and sapphire (Smith, 1998) |
|---|---|---|---|---|
| Color | Purple, light pink, and dark red | Bright red with a slightly purple hue | Reddish, red, and violet-red | Purplish pink to purplish red |
| Transparency | Often translucent, rarely transparent | Often transparent | Transparent | Highly transparent |
| Quality | Cabochon-quality, rarely suitable for cutting | Gem-quality | Gem-quality | Gem-quality |
| Pleochroism | Weak to moderate dichroism<br>Parallel to c-axis: orange-red<br>Perpendicular to c-axis: reddish violet | Strong dichroism | Weak dichroism; e—reddish to light red and o—red to violet red | Moderate to strong dichroism<br>Parallel to c-axis: pinkish/reddish-orange to red-orange<br>Perpendicular to c-axis: purple-pink to purple-red |
| Refractive index | $n_e$ = 1.762–1.764, $n_o$ = 1.772–1.774 | | $n_e$ = 1.761–1.762, $n_o$ = 1.769–1.770 | $n_e$ = 1.761–1.762, $n_o$ = 1.770 |
| Birefringence | 0.008–0.009 | | 0.008 | 0.008–0.009 |
| Density (g/cm$^3$) | 3.99–4.01 | | 3.98 | 3.99–4.02 |
| Reaction to long- and short-wave ultraviolet radiation | LW—strongly red; SW—red, weak | | LW—strongly red; SW—red | LW—strong to very strong, slightly orange-red to red; SW—very weak to medium red |
| Photoluminescence spectra | Doublet R-lines at 692 and 694 nm from single $Cr^{3+}$ and N lines from $Cr^{3+}$ pairs in long-wave part of spectra | | | |
| Absorption (reflectance) spectra | Wide bands at about 410 and 555 nm from $Cr^{3+}$; luminescence line at 694 nm from $Cr^{3+}$ | | Perpendicular to c-axis: 555 and 404 nm<br>Parallel to c-axis: 547 and 400 nm of $Cr^{3+}$, lines at 693 nm from $Cr^{3+}$ | Wide bands at about 405 and 550 nm from $Cr^{3+}$; weak bands at about 468, 475, 476, 659, 692, and 694 nm |
| Internal features | Parting and twinning. Solid inclusions of allanite, rutile, zircon, soda margarite (calcic ephesite), muscovite, fuchsite, K-feldspar, and Ca-Na-plagioclase. | | Twinning, healing cracks, fluid inclusions, rutile, and growth striae | Growth structures, color zoning, twinning, negative crystals, and solid inclusions of calcite, titanite, zircon, rutile, and plagioclase |
| Trace elements (wt.%) | See table 5 | | $Cr_2O_3$ (0.20), FeO (0.08), and $TiO_2$ (0.01) | $Cr_2O_3$ (0.185–0.516), $TiO_2$ (0.017–0.156), $Fe_2O_3$ (0.004–0.018), $V_2O_5$ (0.015–0.025), $Ga_2O_3$ (0.010–0.014) |

and *a* faces, respectively. Pink sapphires exhibited polysynthetic twinning along the *r* face. Marble-hosted ruby did not show any visible defects, probably due to the recrystallization process, which may also explain their rounded faces.

**Inclusions.** *Ruby and Sapphire from Micaceous Lenses*. One of the most interesting findings of this

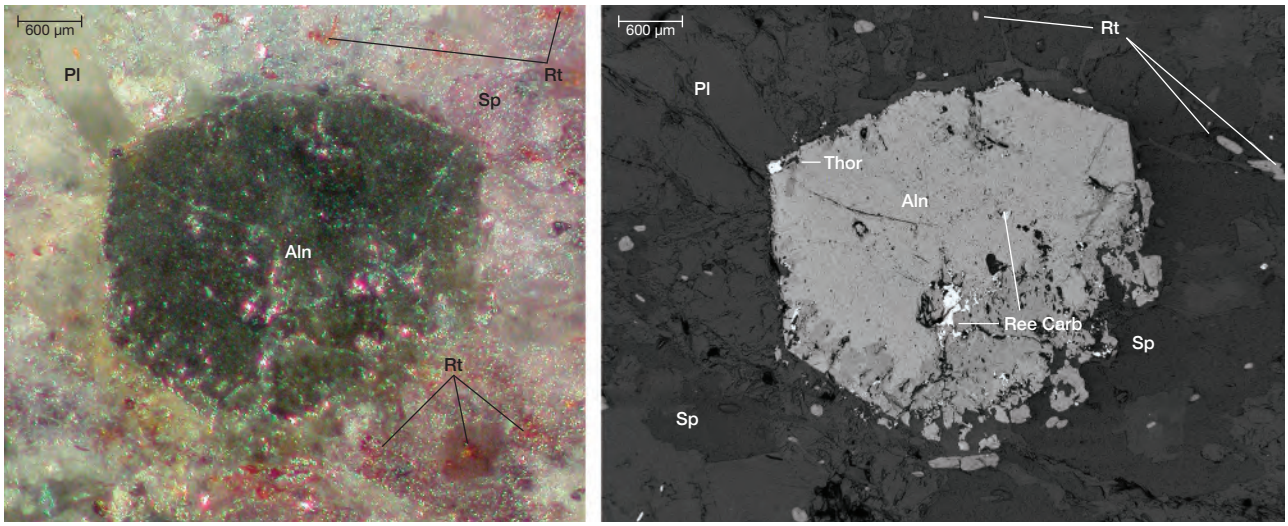


*Figure 10. The photomicrograph on the left and the backscattered electron image on the right show a large allanite (Aln) crystal in contact with plagioclase (Pl) and sapphire (Sp), small allanite (right bottom corner of the large allanite crystal), and rutile (Rt) in pink sapphire from Snezhnoe. REE carbonates (Ree Carb) and thorianite (Thor) are included in the allanite. Also seen are plagioclase (Pl) and muscovite (Ms). Photomicrograph by Elena S. Sorokina. The BSE image is from Sorokina et al. (2012).*

study was that protogenetic inclusions of allanite were recognized in about 10% of the samples. Hexagonal allanite crystals with relicts of U-bearing thorianite and REE carbonates were also detected next to plagioclase and sapphire (Sorokina et al., 2012; figure 10). Inclusions and hexagonal crystals of allanite contained rare earth elements (table 2).

Another notable finding involved syngenetic particles and flakes of light blue mica (figure 11) with sizes varying from approximately 200 to 300 µm. Samples from Snezhnoe have previously been examined by X-ray powder diffraction, which identified diffraction lines close to margarite mica.

Using data from microprobe analyses, we found that the main mica cations were Ca and Na. The ratio of their ions was approximately 1:1. In a few samples, Na ions outnumbered Ca, reaching the ionic number of 0.59 in structural formula (table 3).

To identify the chemical elements that compensated the charge of the Na ions replacing Ca within the mica structure, we turned to LA-ICP-MS (table 4). These analyses showed an additional Li component, a finding that would have been impossible to determine by electron microprobe (see Schaller et al., 1967, and references therein). The maximum concentration of Li within mica is about 2020 ppm. Moreover, we detected Cr and Sr up to 2186 ppm and 1518 ppm, respectively. Therefore, the blue mineral inclusions are mica of the margarite-ephesite series—calcic ephesite or soda margarite, enriched with Cr and Sr.

We also observed rounded, transparent inclusions (probably protogenetic) that were previously identified as zircon (Smith, 1998). The zircon inclusions, ranging from approximately 50 to 70 µm in size, showed high relief and strong interference colors. $HfO_2$, up to 2.05 wt.%, was detected in the composition of this solid inclusion (see again table 2).

High-relief particles of dark brown rutile were observed as syngenetic inclusions (previously detected by Henn and Bank, 1990), ranging from approximately 150 to 300 µm (figure 12). They showed twinning with an angle of about 115°. The rutile inclusions were nor-

*Figure 11. This backscattered electron image shows particles of blue mica and rutile (Rt) inclusions in ruby (Rb) from Snezhnoe. From Sorokina (2011).*

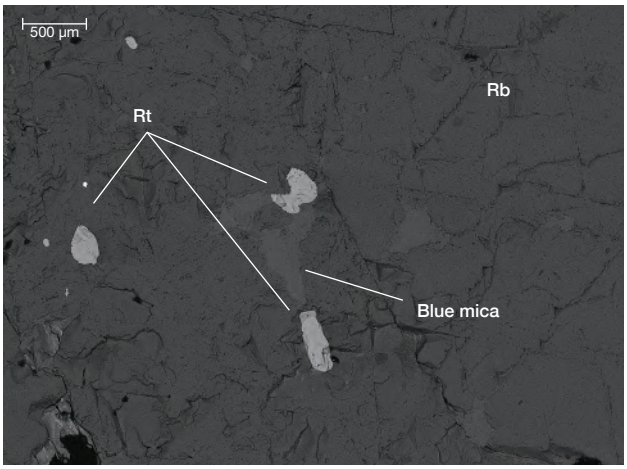

**TABLE 2.** Composition of solid inclusions within corundum from Snezhnoe by electron microprobe analysis.[a,b,c]

| Oxides (wt.%) | Allanite (n=6)[a] | Thorianite (n=3) | REE carbonate (n=1) | Zircon (n=2) | Rutile (n=2) | Fuchsite (n=1) |
|---|---|---|---|---|---|---|
| $H_2O$ (calculated) | 1.47 | – | 13.55 | – | – | – |
| $CO_2$ (calculated) | – | – | 24.83 | – | – | – |
| $Na_2O$ | – | – | – | – | – | 3.88 |
| MgO | 0.56–1.29 (0.87)[b] | 0.12 | – | – | – | 1.01 |
| $Al_2O_3$ | 20.45–23.81 (33.07) | 0.17 | 1.06 | – | – | 35.51 |
| $SiO_2$ | 32.42–34.58 (33.07) | 0.27 | 1.5 | 30.13–31.50 (30.82) | – | 45.28 |
| $K_2O$ | – | – | – | – | – | 6.04 |
| CaO | 12.19–15.13 (12.82) | 0.15 | 0.73 | – | – | 0.82 |
| $TiO_2$ | bdl–0.5 (0.23) | – | – | – | 98.33–98.94 (98.64) | – |
| MnO | bdl–0.39 (0.16) | – | – | – | – | – |
| $Cr_2O_3$ | – | – | – | – | 0.49–0.81 (0.65) | 0.93 |
| FeO | – | – | 0.21 | – | – | – |
| $Fe_2O_3$ | 5.32–9.2 (8.0) | – | – | – | – | – |
| $ZrO_2$ | – | – | – | 63.98–66.46 (65.22) | – | – |
| $Y_2O_3$ | bdl–0.39 (0.24) | – | 0.48 | – | – | – |
| $La_2O_3$ | 3.7–6.14 (4.84) | – | 11.36 | – | – | – |
| $Hf_2O$ | – | – | – | bdl–2.06 (1.03) | – | – |
| $Ce_2O_3$ | 7.93–11.08 (9.99) | 0.21 | 29.32 | – | – | – |
| $Pr_2O_3$ | 0.34–1.31 (0.86) | – | 3.2 | – | – | – |
| $Nd_2O_3$ | 3.03–4.19 (3.55) | – | 12.45 | – | – | – |
| $Sm_2O_3$ | 0.19–0.85 (0.48) | – | 1.15 | – | – | – |
| $Gd_2O_3$ | 0.19–0.82 (0.48) | 0.30 | 1.15 | – | – | – |
| $ThO_2$ | 0.55–1.0 (0.81) | 80.36 | 0.86 | – | – | – |
| $UO_2$ | bdl–0.15 (0.03) | 17.52 | – | – | – | – |
| Total | 99.32–100.34 (99.57) | 99.1 | 102.37 | 94.12–100.0 (97.06) | 98.95–99.75 (99.35) | 93.86 |

[a] *n = number of measurements.*
[b] *Minimum and maximum values are given, along with average (in parentheses); bdl = below detection limit.*
[c] *Thorianite and REE carbonate are within the allanite crystal.*

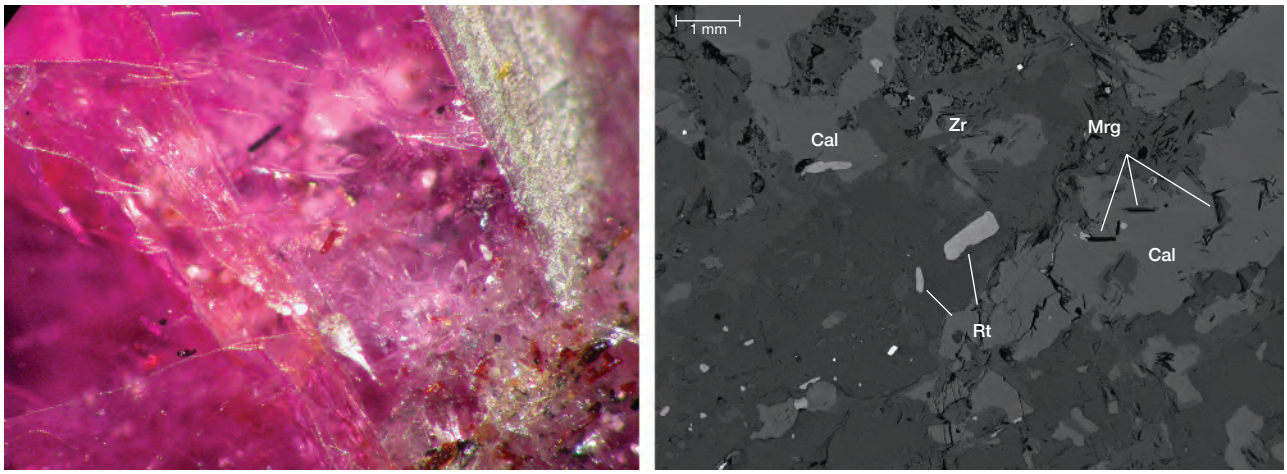


*Figure 12. Left: Brown prismatic rutile inclusions within ruby from Snezhnoe. Photomicrograph by Elena S. Sorokina, magnified 35×. Right: A backscattered electron image of zircon (Zr) and rutile (Rt) inclusions in pink sapphire from the deposit (Cal = calcite, Mrg = margarite). From Sorokina (2011).*

mally enriched with Cr (up to 0.81 wt.%; table 2).

Similar to previous studies (e.g., Smith, 1998), we also detected the transparent irregular form of feldspar inclusions within ruby crystals. Two types

**TABLE 3.** Chemical composition of mica inclusions of the margarite-ephesite series by electron microprobe analysis.[a,b]

| Oxides (wt.%) | Sample 1 | Sample 2 | Sample 3 | Sample 4 | Sample 5 | Sample 6 | Sample 7 | Sample 8 | Sample 9 | Sample 10 |
|---|---|---|---|---|---|---|---|---|---|---|
| $Na_2O$ | 3.95 | 3.74 | 3.44 | 3.97 | 4.67 | 3.97 | 3.92 | 3.23 | 4.72 | 3.29 |
| MgO | 0.53 | 0.36 | 0.52 | 0.54 | 0.67 | 0.56 | 0.65 | 0.54 | 0.35 | 0.51 |
| $Al_2O_3$ | 47.35 | 45.21 | 48.19 | 46.29 | 45.69 | 47.39 | 45.94 | 45.60 | 37.13 | 47.15 |
| $SiO_2$ | 35.91 | 37.04 | 35.62 | 36.34 | 38.75 | 35.61 | 38.80 | 36.72 | 48.57 | 36.19 |
| $K_2O$ | 0.40 | 0.73 | 0.66 | 0.42 | 0.64 | 0.26 | 0.94 | 1.20 | 2.32 | 0.55 |
| CaO | 7.09 | 5.89 | 7.52 | 6.55 | 5.48 | 7.10 | 6.21 | 6.64 | 0.27 | 7.17 |
| $Fe_2O_3$ | bdl | 0.23 | 0.27 | 0.32 | 0.38 | 0.33 | 0.44 | 0.42 | 0.38 | bdl |
| Total | 95.41 | 93.19 | 96.21 | 94.43 | 96.28 | 95.23 | 96.90 | 94.34 | 93.73 | 95.00 |
| Cations | Sample 1 | Sample 2 | Sample 3 | Sample 4 | Sample 5 | Sample 6 | Sample 7 | Sample 8 | Sample 9 | Sample 10 |
| Na | 0.50 | 0.48 | 0.43 | 0.51 | 0.58 | 0.51 | 0.49 | 0.41 | 0.59 | 0.42 |
| Mg | 0.05 | 0.04 | 0.05 | 0.05 | 0.06 | 0.05 | 0.06 | 0.05 | 0.03 | 0.05 |
| Al | 3.65 | 3.55 | 3.69 | 3.60 | 3.47 | 3.66 | 3.48 | 3.55 | 2.83 | 3.64 |
| Si | 2.35 | 2.47 | 2.31 | 2.40 | 2.50 | 2.33 | 2.49 | 2.43 | 3.14 | 2.37 |
| K | 0.03 | 0.06 | 0.05 | 0.04 | 0.05 | 0.02 | 0.08 | 0.10 | 0.19 | 0.05 |
| Ca | 0.50 | 0.42 | 0.52 | 0.46 | 0.38 | 0.50 | 0.43 | 0.47 | 0.02 | 0.50 |
| $Fe^{3+}$ | - | 0.01 | 0.01 | 0.02 | 0.02 | 0.02 | 0.02 | 0.02 | 0.02 | - |
| Total | 7.08 | 7.03 | 7.08 | 7.07 | 7.07 | 7.09 | 7.04 | 7.04 | 6.83 | 7.04 |

[a] *The structural formula of mica of the margarite-ephesite series is based on 11 atoms of oxygen.*
[b] *bdl = below detection limit*

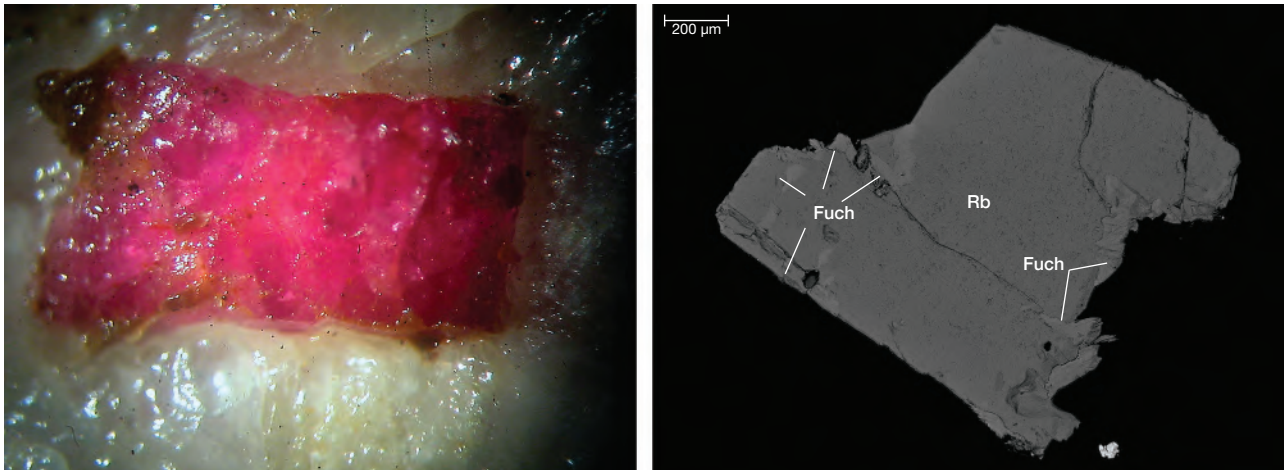


*Figure 13. Left: Intergrowth of a 0.2 cm ruby crystal and green fuchsite within a white calcitic matrix. Photomicrograph by Elena S. Sorokina. Right: A backscattered electron image showing solid inclusions of fuchsite (Fuch) within ruby (Rb). From Sorokina (2011).*

of feldspar were detected: K-feldspar (microcline) and Ca-Na plagioclase (labradorite-anorthite). Most of the feldspar inclusions were twinned, measuring approximately 300 to 400 µm. Their birefringence was 0.006–0.007; relief was low, with crystals showing cleavages in two directions.

*Ruby from Marbles.* Flakes of fuchsite with $Cr_2O_3$ concentration above 1 wt.% (Deer et al., 1962) and intergrowths of green muscovite and fuchsite were detected within this type of ruby sample (figure 13 and table 2). The birefringence in thin sections ranged up to 0.027. Flakes of these mica inclusions were replaced in part by a green mineral of the chlorite group, probably prochlorite.

Smith (1998) previously identified other solid inclusions in rubies and sapphires from the Snezhnoe deposit, such as calcite and titanite. Although margarite is a common inclusion for gem corundum, the discovery of mica of the margarite-ephesite series (calcic ephesite or soda margarite) has not been reported in ruby, to the best of our knowledge (Gübelin and Koivula, 1986, and references therein; Hughes, 1997). Moreover, allanite is rarely detected in corundum (Hänni, 1990; Sutherland et al., 2008), and along with muscovite and fuchsite it has not been reported within ruby and sapphire from Snezhnoe until now. Therefore, these features can be used together with zircon, rutile, and feldspar inclusions to distinguish these gemstones from Tajikistan.

**Chemical Composition.** To study the composition of ruby and sapphire from Snezhnoe, we performed LA-ICP-MS analysis on 22 elements and electron microprobe analysis for Fe (table 5). The results showed that quantities of chromophores such as Ti, V, Cr, and Fe were within the normal range for ruby of similar formation type (table 6). The samples from mica-

**TABLE 4.** Trace-element composition (ppmw) of mica of the margarite-ephesite series by LA-ICP-MS.

| Sample no. | Li | Be | B | Na | Mg | $SiO_2$* (wt.%) | K | Ca | Sc | Ti | V | Cr | Mn | Co | Ni | Zn | Ga | Rb | Sr | Ba |
|---|---|---|---|---|---|---|---|---|---|---|---|---|---|---|---|---|---|---|---|---|
| 1 | 1662 | 15 | 116 | 29,722 | 2157 | 36.74 | 7539 | 39,535 | 9.97 | 292 | 120 | 2186 | 2.50 | 1.40 | 11.5 | 21.0 | 74.8 | 16.7 | 1518 | 410 |
| 2 | 2020 | 18 | 127 | 30,049 | 2222 | 36.74 | 4163 | 45,066 | 8.94 | 306 | 126 | 909 | 4.80 | 1.50 | 10.4 | 29.8 | 60.3 | 10.9 | 1201 | 116 |
| 3 | 1956 | 13 | 107 | 31,870 | 2246 | 36.74 | 4706 | 40,585 | 8.45 | 317 | 123 | 605 | 4.80 | 1.20 | 10.1 | 23.4 | 54.6 | 13.1 | 1164 | 102 |
| Average | 1879 | 15 | 116 | 30,547 | 2208 | 36.74 | 5469 | 41,728 | 9.12 | 305 | 123 | 1233 | 4.00 | 1.30 | 10.7 | 24.7 | 63.2 | 13.6 | 1294 | 209 |

** $SiO_2$ composition was determined by electron microprobe analysis.*

**TABLE 5.** Trace-element composition (ppmw) of corundum from Snezhnoe, by LA-ICP-MS.[a,b,c]

| Chemical element | From micaceous lenses | | | From marble |
|---|---|---|---|---|
| | Purple sapphire (n=3) | Slightly pink sapphire (n = 8) | Dark red ruby (n = 3) | Bright red ruby with a slightly purple hue (n= 6) |
| Cr | 416–661 (530) | 687–1775 (1077) | 2012–2820 (2376) | 1696–4204 (3190) |
| Ti | 17.2–50.3 (28.5) | 52.5–165 (92) | 30.8–69.9 (49.3) | 5.7–75.4 (31.5) |
| V | 38.4–41.0 (39.7) | 37.5–49.2 (43.1) | 93.0– 95.1 (93.7) | 51.5–122 (95.3) |
| Ga | 52.5–56.9 (55.1) | 53.4–63.3 (59) | 67.2–87.6 (79.1) | 60.9–83.4 (71.3) |
| Fe[b] | bdl | bdl | bdl | bdl |
| Mg | 12.3–24.6 (17.97) | 17.7–898 (205) | 16. 6–35.9 (24.2) | 3.67–71.9 (27.9) |
| Mn | bdl–0.300 (0.1) | bdl–2.11 (0.61) | bdl–0.61 (0.34) | bdl–6.82 (1.75) |
| Ca | bdl–296 (115) | bdl–4363 (1066) | bdl–188 (85.8) | 39.5–926 (387) |
| Na | bdl–8.19 (4.76) | 39.9–4764 (1182) | 34.3–176 (85.3) | bdl–316 (59.8) |
| Si | 1001–1724 (1358) | 1217–28,407 (10,731) | 1044–1645 (1300) | 869–3225 (1674) |
| P | 23.5–27.7 (25.7) | 18.9–62.4 (33.6) | bdl–19.8 (10.6) | 15.4–34.7 (23.2) |
| K | bdl–13.6 (5.87) | 4.75–3833 (668) | bdl–49.0 (19.5) | bdl–31.7 (9.23) |
| Sc | bdl | bdl–0.441 (0.226) | bdl | bdl–0.531 (0.181) |
| Co | bdl–0.174 (0.08) | bdl–2.98 (0.87) | bdl–0.069 (0.02) | bdl–0.393 (0.13) |
| Ni | 0.490–4.04 (1.7) | bdl–109 (22.6) | bdl | bdl–6.51 (2.95) |
| Cu | 0.5–2.43 (1.2) | bdl–228 (54.8) | bdl | bdl–22.6 (4.21) |
| Zn | 1.14–6.21 (3.63) | 1.49–129 (26.8) | bdl–1.22 (0.4) | bdl–31.9 (11.4) |
| Ge | bdl | bdl–1.69 (0.21) | bdl | bdl |
| Mo | bdl | bdl–1.81 (0.42) | bdl | bdl |
| La | bdl | bdl–0.380 (0.15) | bdl–0.052 (0.02) | bdl–0.248 (0.17) |
| Nd | bdl | bdl–0.73 (0.14) | bdl | bdl–0.235 (0.04) |
| W | bdl–0.284 (0.095) | bdl–0.201 (0.03) | bdl–0.187 (0.12) | bdl |
| Bi | bdl–0.182 (0.08) | bdl–7.12 (1.97) | bdl | bdl–0.134 (0.02) |

[a] *Minimum and maximum values are given, along with average (in parentheses).*
[b] *Fe was analyzed by electron microprobe.*
[c] *Zr, Nb, Sm, Dy, and Ta were measured but found to be consistently below detection limits; bdl = below detection limits.*

ceous lenses contained the following concentrations of trace elements: 416–2820 ppm Cr, 17.2–165 ppm Ti, 37–95 ppm V, and 52–87 ppm Ga. For marble-hosted ruby, the ranges were: 1696–4204 ppm Cr, 5.7–75 ppm Ti, 51–122 ppm V, and 60–83 ppm Ga. The highest Cr concentrations were observed in the bright red marble-hosted ruby. These values were close to those of other rubies of similar formation type, including samples from Mogok, Myanmar (analyzed by Muhlmeister et al., 1998; table 6).

**Spectroscopy.** Corundum from Snezhnoe ranges from purple (416–661 ppm Cr) to slightly pink (687–1775 ppm Cr) to dark red (2012–2820 ppm Cr). The range of ruby color includes the bright red with slightly purple hue known as "pigeon's blood" (1696–4204 ppm Cr). Reflectance spectra were recorded from these four different types. The common features were wide bands at about 410 and 555 nm and a line at 694, related to $Cr^{3+}$ transitions (Marfunin, 1974; figure 14). Thus, we concluded that the main chromophore for these samples is $Cr^{3+}$. A higher chromium concentration enhances the depth of red color from slightly pink to dark red to bright red with a hint of purple. Another possible chromophore for the purple sapphires is $V^{3+}$; note the concentration of vanadium in table 5. Difficulty in detecting the $V^{3+}$ chromophore is caused by the low $V^{3+}$ to $Cr^{3+}$ ratio (table 5) and the superposition

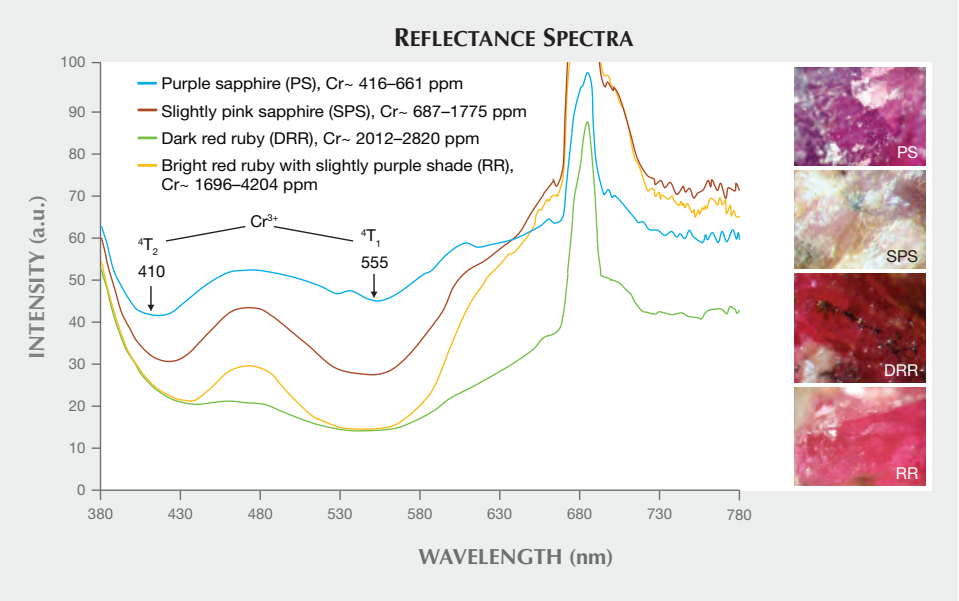


*Figure 14. Typical reflectance spectra for the different colors of corundum from Snezhnoe: purple sapphire (blue line, 416–661 ppm); slightly pink sapphire (red line, 687–1775 ppm); dark red ruby (green line, 2012–2820 ppm); and bright red ruby (orange line, 1696–4204 ppm). Modified from Sorokina (2011).*

of their absorption bands (Schmetzer and Bank, 1981; Platonov et al., 1984).

Luminescence spectra commonly show an R-line of single $Cr^{3+}$ at 692 nm and a few N-lines of $Cr^{3+}$ pairs at around the 699–710 nm (Taraschan, 1978; figure 15). The intensity of luminescence increased with Cr content in the samples. The highest intensity was observed in bright red ruby.

## CONCLUSIONS

Located high in the Pamir Mountains of Tajikistan, the Snezhnoe deposit is a unique source of corundum, including various colors of pink to purple sapphire and "pigeon's blood" ruby. Although its reserves of gem-quality corundum are estimated at many hundred thousand carats, the occurrence has seen only limited study. This article reviewed the geology of Snezhnoe and characterized the corundum from this source. We reported gemological features (RI, birefringence, densitvy, pleochroism, dichroism, and photoluminescence) very similar to those previously published by Henn and Bank (1990) and Smith (1998). $Cr^{3+}$ bands

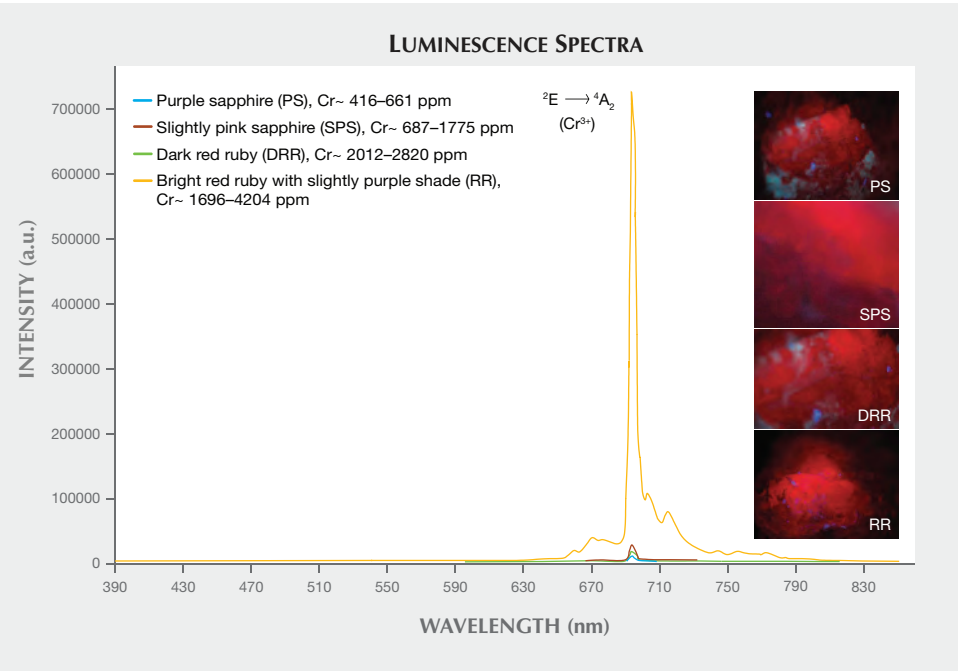


*Figure 15. Typical luminescence spectra of the different types of corundum samples from Snezhnoe: purple sapphire (blue line, 416–661 ppm Cr), slightly pink sapphire (red line, 687–1775 ppm Cr), dark red ruby (green line, 2012–2820 ppm Cr), and bright red ruby (orange line, 1696–4204 ppm Cr). Modified from Sorokina (2011).*

**TABLE 6.** Chemical composition of marble-hosted ruby from various deposits by LA-ICP-MS[a], EDXRF[b], and EDS[c] analyses.

| Oxide (wt.%) | Snezhnoe, Tajikistan (n = 6) | Luc Yen, Vietnam (n = 1) | Afghanistan (n = 15) | Mogok, Myanmar (n = 19) | Mong Hsu, Myanmar (n = 11) | Nepal (n = 3) | Southern Yunnan, China (n = 2) |
|---|---|---|---|---|---|---|---|
| $TiO_2$ | 0.0009–0.011 (0.0064) | 0.02 | 0.009–0.091 (0.045) | 0.015–0.047 (0.026) | 0.019–0.207 (0.078) | 0.059–0.096 (0.080) | 0.007–0.024 (0.016) |
| $V_2O_3$ | 0.0076–0.0179 (0.0166) | 0.01 | bdl–0.016 (0.009) | 0.028–0.171 (0.066) | 0.024–0.104 (0.048) | 0.014–0.024 (0.017) | 0.017–0.022 (0.020) |
| $Cr_2O_3$ | 0.2476–0.6138 (0.5545) | 0.37 | 0.205–0.575 (0.350) | 0.255–1.02 (0.562) | 0.576–1.16 (0.887) | 0.190–0.347 (0.260) | 0.608–1.29 (0.950) |
| FeO | bdl | – | 0.009–0.133 (0.070) | 0.006–0.080 (0.028) | bdl–0.022 (0.010) | 0.012–0.038 (0.029) | 0.012–0.072 (0.042) |
| $Fe_2O_3$ | bdl | 0.02 | – | – | – | – | – |
| $Ga_2O_3$ | 0.0082–0.0112 (0.0097) | 0.01 | bdl–0.011 (0.006) | bdl–0.026 (0.012) | bdl–0.014 (0.009) | 0.009–0.025 (0.018) | 0.008 |

[a] *Oxide values for Tajik rubies are recalculated from table 5; n = number of measurements; minimum and maximum values are given, along with average (in parentheses); bdl = below detection limit.*
[b] *Values for rubies from Afghanistan, Myanmar, Nepal, and southern Yunnan are from Muhlmeister et al. (1998).*
[c] *Values for Vietnamese rubies are from Pham et al. (2004).*

and lines were common features recorded in the luminescence and reflectance spectra for the ruby and sapphire. Previously undocumented solid inclusions of mica from the margarite-ephesite series were found in our samples. Inclusions such as allanite, muscovite, and fuchsite were discovered for the first time within corundum from Snezhnoe, to the best of our knowledge. These can be used along with other inclusions (zircon, rutile, K-feldspar, and Ca-Na-plagioclase) for possible origin identification of rubies and sapphires from Snezhnoe. LA-ICP-MS detected 22 trace elements, including the main chromophores (Cr, V, and Ti) and a common trace element in natural corundum (Ga). The concentration values were within acceptable range for isomorphic impurities in the mineral structure. The highest Cr concentrations were observed in the bright red marble-hosted ruby, which had a value close to those of similar genetic type, including the famous Burmese rubies from Mogok.

As we continue to learn more about marble-hosted ruby occurrences in Central Asia, further investigations remain necessary to better understand the genetic nature of the Snezhnoe deposit and the geological processes that took place there long ago.


## ABOUT THE AUTHORS

*Dr. Sorokina (elensorokina@mail.ru) is a research fellow at the Fedorovsky All-Russian Research Institute of Mineral Resources (FGUP VIMS) and the Fersman Mineralogical Museum of the Russian Academy of Sciences in Moscow. Dr. Litvinenko is the head of the department of gemology at the Institute of Geology of Mineral Resources at the Russian State Geological Prospecting University in Moscow. Dr. Hofmeister is professor and vice president of research at Johannes Gutenberg University in Mainz, Germany, director of the university's department of gem-materials sciences and gemology, and head of the Centre for Gemstone Research in Idar-Oberstein, Germany. Dr. Häger is a senior scientist at the Centre for Gemstone Research at Johannes Gutenberg University, lecturer in the gemstone and jewellery design department at the University for Applied Sciences and managing director at the Centre for Gemstones Research in Idar-Oberstein. Dr. Jacob is an associate professor in the department of earth and planetary sciences at Macquarie University in North Ryde, Australia. Dr. Nasriddinov is dean of the department of geosciences at the Mining and Metallurgy Institute in Chkalovsk of Tajikistan.*



## ACKNOWLEDGMENTS

*The authors thank our colleagues Prof. Dr. Elena G. Ozhogina, Drs. Vadim V. Moroshkin and Victor A. Rassulov, Mrs. Anastasia V. Iospa from FGUP VIMS, Dr. Mikhail N. Kandinov from Vernadsky Geological Museum, and Mr. Leonid A. Pautov, Drs. Atali A. Agakhanov and Vladimir Yu. Karpenko from Fersman Mineralogical Museum for their assistance in sample collection, collaborations on analytical studies, and discussion of the manuscript. We also thank the anonymous reviewers for their helpful suggestions.*

## REFERENCES


Barkhatov B.P. (1963) *Tectonics of the Pamirs*. Leningrad University, USSR [in Russian].

Bowersox G. (2005) July–August, 2005 Hindu Kush/Pamir Mountains Expedition. http://www.gems-afghan.com/cgi-bin/aslides.pl?12&1.

Budanova K.T. (1991) *Metamorphic Formations of Tajikistan*. Donish Publishers, Dushanbe, Tajikistan (in Russian).

Budanova K.T. (1993) Mineralogical petrochemical characterization of high-alumina rocks in eastern part of central Pamirs. *Izvestiya of Tajikistan AS (Proceedings of the Tajikistan Academy of Sciences)*, No. 1, pp. 26–33 [in Russian].

Deer W.A., Howie R.A., Zussman J. (1962) *Rock-Forming Minerals, Volume 3: Sheet Silicates*. Wiley, New York.

Dmitriev E.A. (1983) Types of corundum mineralization in the Precambrian marbles of the Muzkol-Rangkulsky anticlinorium. In A.V. Klimkin, *Proceedings on Geology and Prospecting of the Gemstone Deposits of Tajikistan*. Donish Publishers, Dushanbe, Tajikistan, pp. 34–36 [in Russian].

Dmitriev E.A., Ishan-Sho G.A. (1987) Chromium-bearing muscovites in metamorphic and hydrothermal formations of the Pamirs. *Zapiski VMO (Proceedings of the All-Union Mineralogical Society)*, Vol. 116, No. 6, pp. 690–697 [in Russian].

Dufour M.S., Kol'tsov A.B., Zolotarev A.A., Kuznetsov A.B. (2007) Corundum-bearing metasomatic rocks in the Central Pamirs. *Petrology*, Vol. 15, No. 2, pp. 151–167, http://dx.doi.org/10.1134/S0869591107020038.

Giuliani G., Ohnenstetter D., Garnier V., Rakotondrazafy M., Schwarz D. (2007) The geology and genesis of gem corundum deposits. In L.A. Groat, Ed., *Geology of Gem Deposits*. Mineralogical Association of Canada, Quebec, pp. 23–78.

Goldschmidt V. (1918) *Atlas der Krystallformen*. Band V., Heidelberg.

Gübelin E.J., Koivula J.I. (1986) *Photoatlas of Inclusions in Gemstones*. ABC, Zurich.

Hänni H. A. (1990) A contribution to the distinguishing of sapphire from Kashmir. *Journal of Gemmology*, Vol. 22, No. 2, pp. 67–75.

Henn U., Bank H. (1990) Rubine aus dem Pamir-Gebirge, USSR. *Zeitschrift der Deutschen Gemmologischen Gesellschaft*, Vol. 39, No. 4, pp. 201–205.

Hughes R.W. (1997) *Ruby & Sapphire*. RWH Publishing, Boulder, CO.

Hughes R.W., Pardieu V., Soubiraa G., Schorr D. (2006) Moon over the Pamirs: Chasing ruby and spinel in Tajikistan. http://www.ruby-sapphire.com/tajikistan_ruby_and_spinel.htm.

Jacob D.E. (2006) High sensitivity analysis of trace element-poor geological reference glasses by laser-ablation inductively coupled plasma-mass spectrometry (LA-ICP-MS). *Geostandards and Geoanalytical Research*, Vol. 30, No. 3, pp. 221–235, http://dx.doi.org/10.1111/j.1751-908X.2006.tb01064.x.

Kievlenko E.P. (2003) *Geology of Gems*. Ocean Pictures Ltd., Littleton, CO.

Konovalenko S.I., Rossovsky L.N. (1980) The first finding of ruby in marbles of Southwestern Pamirs. *Zapiski VMO (Proceedings of the All-Union Mineralogical Society)*, Vol. 109, No. 6, pp. 707–709 (in Russian).

Litvinenko A.K., Barnov N.G. (2010) The history of Pamirs gemstones. *Izvestiya Visshikh Uchebnykh Zavedeniy, Geologiya i Razvedka (Proceedings of Higher Educational Institutions, Geology and Prospecting)*, No. 4, pp. 70–74 [in Russian].

Marfunin A.S. (1974) *An Introduction to the Physics of Minerals*. Nedra, Moscow [in Russian].

Muhlmeister S., Fritsch E., Shigley J.E., Devouard B., Laurs B.M. (1998) Separating natural and synthetic rubies on the basis of trace-element chemistry. *G&G*, Vol. 34, No. 2, pp. 80–101, http://dx.doi.org/10.5741/GEMS.34.2.80.

Nasriddinov Z.Z. (2013) Geological and mineralogical features, determining quality of rough from Snezhnoe deposit. Unpublished Ph.D. thesis, Russian State Geological Prospecting University, Moscow, Russia, 96 pp.

Pham V. L., Hoáng Quang V., Garnier V., Giuliani G., Ohnenstetter D., Lhomme T., Schwarz D., Fallick A., Dubessy J., Phan Trong T. (2004) Gem corundum deposits in Vietnam. *Journal of Gemmology*, Vol. 29, No. 3, pp. 129–142.

Platonov A.N., Taran M.N., Balitsky V.S. (1984) *Nature of Colour of Gems*. Nedra, Moscow [in Russian].

Popov V.I. (1936) *Minerals of Southern Tajikistan. Pamir, Badakhshan, Darwaz, Karategin*. Vol. 28, Leningrad [in Russian].

Rossovsky L.N. (1987) Ruby and sapphire deposits of the Alpine-Himalayan fold belt and their formation conditions. In A.V. Klimkin, Ed., *Proceedings on Geology and Prospecting of Gemstone Deposits in Tajikistan*, Donish Publishers, Dushanbe, Tajikistan, pp. 36–38 [in Russian].

Schaller W.T., Carron M.K., Fleischer M. (1967) Ephesite, $Na(LiAl_2)(Al_2Si_2)O_{10}(OH)_2$, a trioctahedral member of the margarite group, and related brittle micas. *The American Mineralogist*, Vol. 52, Nos. 1–2, pp. 1689–1696.

Schmetzer K., Bank H. (1981) The color of natural corundum. *Neues Jahrbuch für Mineralogie Monatshefte*, Vol. 1981, No. 2, pp. 59–68.

Smith C.P. (1998) Rubies and pink sapphires from the Pamir Mountain Range in Tajikistan, former USSR. *Journal of Gemmology*, Vol. 26, No. 2, pp. 103–109.

Sorokina E.S. (2011) Ontogeny and quality of gem ruby from the deposits of Central and South-East Asia. Unpublished Ph.D. thesis, Fedorovsky All-Russian Research Institute of Mineral Resources, Moscow, Russia, 128 pp.

Sorokina E.S., Ozhogina E.G., Jacob D.E., Hofmeister W. (2012) Some features of corundum ontogeny and the quality of ruby from Snezhnoe deposit, Tajikistan (the Eastern Pamirs). *Zapiski RMO (Proceedings of the Russian Mineralogical Society)*, Vol. 141, No. 6, pp. 100–108 [in Russian].

Sorokina E.S., Hofmeister W., Litvinenko A., Häger T., Jacob D., Nasriddinov Z. (2014) Ruby and sapphire from Tajikistan, Central Asia: new geological and mineralogical data. *21st General Meeting of the International Mineralogical Association*, Johannesburg, South Africa, September 1–5.

Sutherland F.L., Duroc-Danner J.M., Meffre S. (2008) Age and origin of gem corundum and zircon megacrysts from the Mercaderes-Rio Mayo area, South-West Colombia, South America. *Ore Geology Reviews*, Vol. 34, pp. 155–168, http://dx.doi.org/10.1016/j.oregeorev.2008.01.004.

Taraschan A.N. (1978) *Luminescence of Minerals*. Naukova Dumka, Kiev [in Russian].


## DIAMOND

### Intense Blue, with Very High Boron Concentration

Natural blue diamonds are extremely rare in nature and highly desired within the gem industry. One of the world's most famous gemstones, the Hope diamond, is classified as a natural type IIb blue diamond. It contains the impurity boron within the diamond carbon lattice. The presence of boron as an impurity in natural diamond is rare, as the amount of uncompensated boron found is typically less than 0.5 ppm.

Housed in the Smithsonian Institute in Washington, DC, the Hope is part of a collection incorporating many boron-containing natural type IIb diamonds, and has been part of a study relating boron concentrations and the intensity of blue coloration in natural and synthetic diamond (E. Gaillou et al., "Boron in natural type IIb blue diamonds: Chemical and spectroscopic measurements," *American Mineralogist*, Vol. 97, 2012, pp. 1–18).

The East Coast laboratory recently received a 1.18 ct Fancy Intense blue diamond (figure 1) for a colored diamond grading report. The diamond's old European-style cut indicated that this was not a recently faceted gemstone. The clarity was very high, adding to the rarity of this blue diamond. When exposed to short-wave UV fluorescence (about 230 nm), the diamond displayed blue phosphorescence (figure 2). Phosphorescence is a diagnostic feature of natural type IIb diamonds; red phosphorescence is also frequently observed, the most notable example being the Hope diamond.

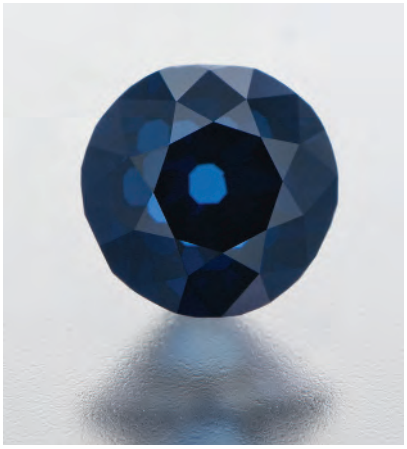

*Figure 1. This 1.18 ct Fancy Intense blue diamond was recently seen in the New York lab.*

Infrared absorption spectroscopy identified the diamond as type IIb, with a very high concentration of uncompensated boron for a natural diamond, even for a stone with synthetic boron doping (figure 3). Further analysis, including photoluminescence spectroscopy, proved it to be a natural diamond. From the mid-infrared absorption spectrum, we determined a boron concentration of 5.84 ppm atomic. By normalizing the mid-IR spectrum, we obtained the integrated intensity of an absorption peak centered at 1290 $cm^{-1}$ (A.T. Collins, "Determination of the boron concentration in diamond using optical spectroscopy," *Proceedings of the 61st Diamond Conference*, 2010, Warwick, UK). Most documented type IIb diamonds in this color range only have recorded uncompensated boron concentrations between approximately 0.24 and 0.36 ppm (E. Gaillou et al., "Study of the Blue Moon diamond," Spring 2015 *G&G*, pp. 280–286).

This is the highest boron concentration ever reported in a natural diamond. Compared to other docu-

*Figure 2. Blue phosphorescence was observed in the DiamondView after the stone's exposure to strong short-wave UV radiation.*

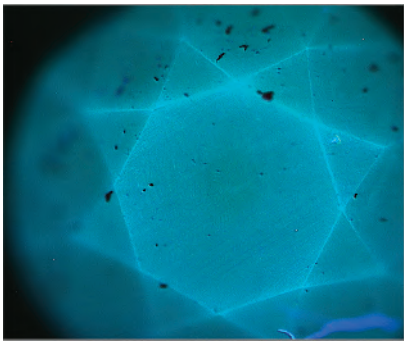

*Editors' note: All items were written by staff members of GIA laboratories.*

Gems & Gemology, Vol. 51, No. 2, pp. 176–188.

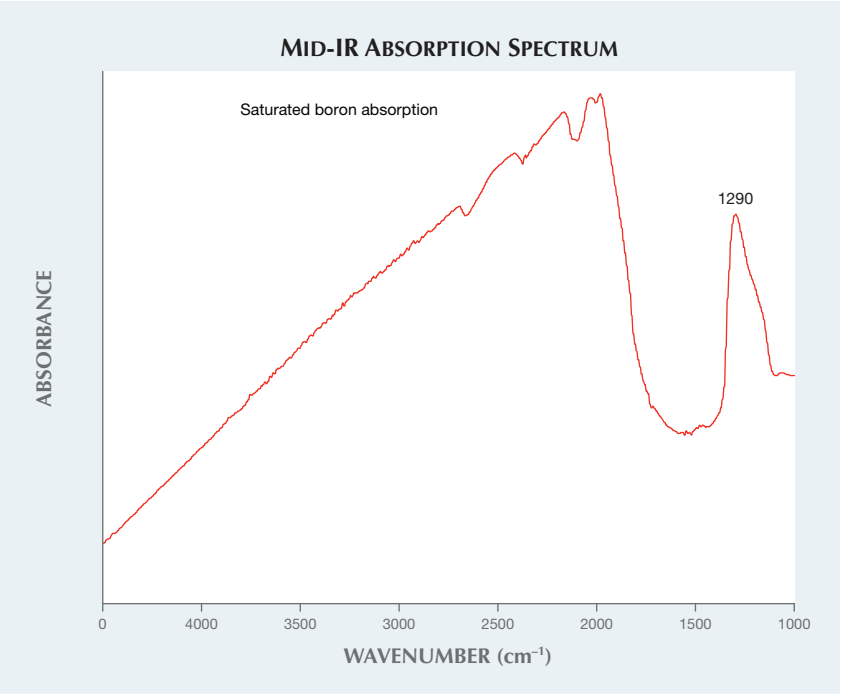


*Figure 3. Normalized mid-IR absorption spectrum of the 1.18 ct Fancy Intense blue type IIb diamond, with saturated boron–related absorption and a 1290 cm$^{-1}$ peak.*

mented type IIb diamonds, the concentration is staggeringly high. This diamond's intense blue color rivals that of the Hope, leading one to believe that boron contributes strongly to the color of natural blue type IIb diamonds. This has never been proven, however, and there is not a well-defined relationship between blue color and uncompensated boron concentration in diamond (Gaillou et al., 2012).

Further observation and analytical study may prove a correlation between optically active boron and the intensity of blue color in natural diamonds.

*Paul Johnson and Wuyi Wang*

## Rare Type IIb Gray-Purple

Photoluminescence (PL) spectroscopy using several laser excitations has become the most important method for determining diamond color origin. Part of PL analysis is observing peaks that correlate with a diamond's color, type, or other gemological properties, but for which the physical model is still unknown. One such center is the PL peak at 776.4 nm, which is commonly observed in type IIb diamonds with intensely colored (i.e., Fancy to Fancy Deep) blue to gray color and in combination with red phosphorescence (S. Eaton-Magaña and R. Lu, "Phosphorescence in type IIb diamonds," *Diamond and Related Materials*, Vol. 20, No. 7, 2011, pp. 983–989). Recently, the Carlsbad laboratory tested a 1.42 ct colored diamond that showed an extremely strong 776.4 nm emission. Infrared absorption spectroscopy confirmed the specimen as a type IIb natural diamond with a boron concentration of approximately 28 ppb. This stone was notable not only for this intense emission, but also for its Fancy gray-purple color (figure 4). This is an extremely rare combination in a type IIb diamond.

Type IIb diamonds sometimes have a violet color description, but they rarely exhibit hues that are outside the blue-gray-violet range. While the perceived difference between a violet and purple diamond may be quite subtle, it is an important distinction when determining color origin. An additional reddish component that distinguishes purple from violet diamonds is extremely rare among type IIb fancy color diamonds. Other type IIb hues include gray-green or yellowish green (e.g., Summer 2009 Lab Notes, p. 136; Spring 2012 Lab Notes, pp. 47–48). Purple diamonds are quite rare and almost exclusively type Ia, their color deriving from the 550 nm band observed in their visible absorption spectra (S. V. Titkov et al., "Natural-color purple diamonds from Siberia," Spring 2008 *G&G*, pp. 56–64). This absorption band is also the cause of color for many pink to red diamonds; however, the absorption spectrum for this diamond was featureless within the visible range, which is typical for type IIb diamonds. This stone is likely the first purple type IIb diamond examined at GIA.

*Figure 4. This 1.42 ct type IIb natural diamond was significant for its unusual Fancy gray-purple color and its strong emission at 776.4 nm under PL spectroscopy.*

The diamond had the strongest 776.4 nm PL emission yet observed by the author (figure 5). The configuration of the optical center is unknown but might include a boron-vacancy complex (T. Ardon and S. Eaton-Magaña, "Spatial distribution of boron and PL optical centers in type IIb diamond," 2013 GSA Annual Meeting). Red phosphorescence, centered at 660 nm, was observed using DiamondView and excited by both ultraviolet and visible-light wavelengths

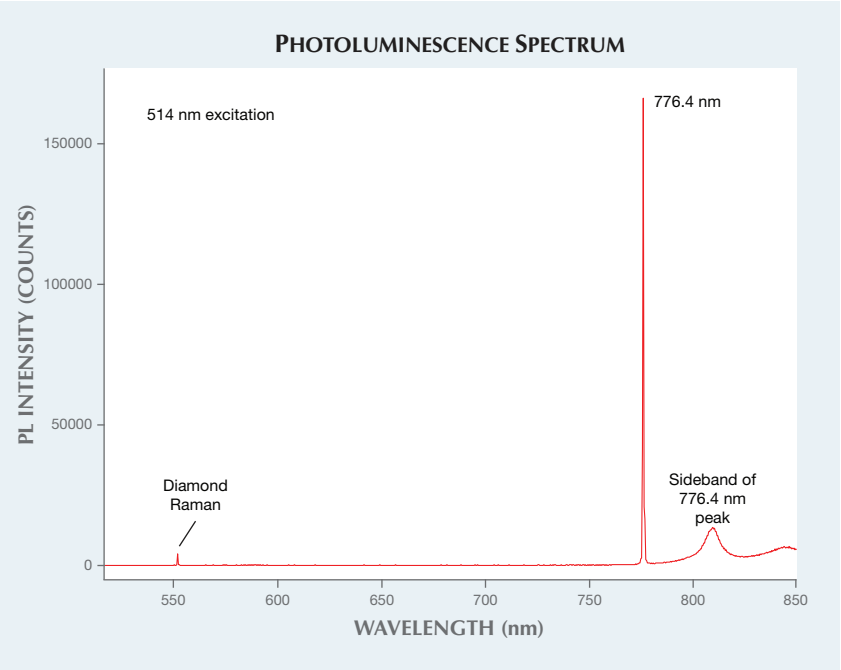


*Figure 5. With 514 nm excitation and liquid-nitrogen temperatures, the 776 nm PL peak dwarfs the diamond Raman peak at 552.4 nm and all other PL features in the spectrum. The intensity ratio between the 776 nm peak and the diamond Raman peak is about 42:1.*

using fluorescence spectroscopy. The 776.4 nm PL peak is observed when the diamond is at liquid-nitrogen temperatures, but it is outside the visible range and not excited at room temperature. Therefore, this near-infrared emission, while strong, does not contribute to the color of the diamond. The diamond's red phosphorescence, while subtle, may have been sufficient to introduce enough reddish component to render a purple color call (as opposed to the more common blue to violet). The singular occurrence of the very strong 776.4 nm PL peak and an unusual bodycolor for a type IIb diamond make this stone notable.

*Sally Eaton-Magaña*

## FLUORITE Sphere with Phosphorescent Coating

A large green 2,685 ct sphere measuring 120 mm (figure 6, left) was recently examined in the Carlsbad lab.

*Figure 6. This large fluorite sphere proved to be coated with a fine-grained phosphorescent powder and a colorless plastic.*

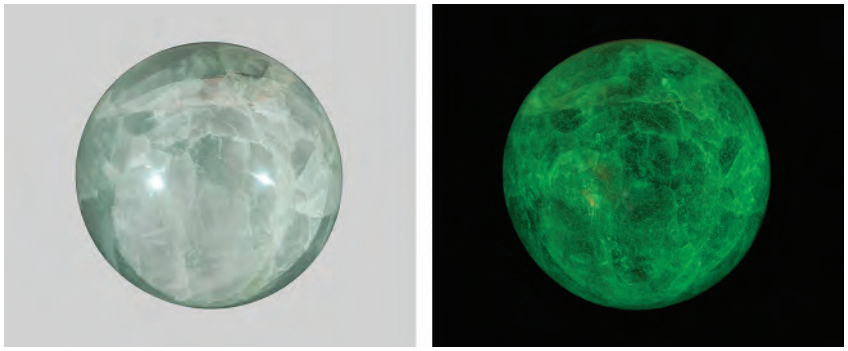

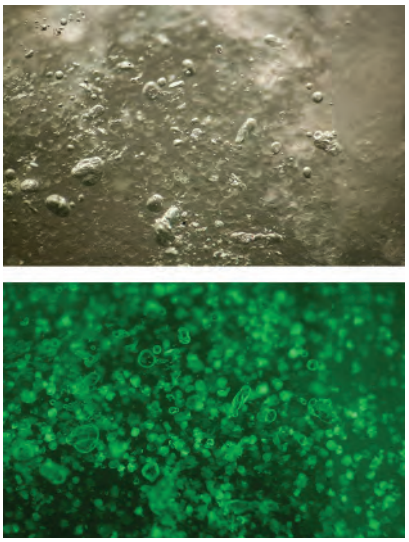

*Figure 7. Gas bubbles were trapped in the colorless plastic coating of this "night glowing pearl" (top), and a granular material underneath the colorless coating was the source of the phosphorescence (bottom). Field of view 3.55 mm.*

The sphere displayed an unusual phosphorescent reaction when exposed to a strong illumination source (figure 6, right). These phosphorescent stones are commonly referred to by the misnomer "night glowing pearl."

The sphere was warm to the touch. Microscopic examination revealed a colorless plastic coating, readily identifiable by the numerous gas bubbles trapped within (figure 7, top). Upon further inspection, a subsurface granular material that contributed a very subtle green component to the sphere's overall bodycolor was observed (figure 7, bottom). The granular material was also responsible for the material's phosphorescence. It was apparent from these observations that the colorless coating was used to adhere the fine-grained powder to the surface of the sphere. The coating acted as an enhancement, contributing a near-vitreous luster to the finished sphere. The stone also contained numerous cleavage cracks oriented in numerous unrelated directions, and fractures along grain boundaries indicative of a crys-

talline aggregate material. Because the fine-grained powder was coated with polymer, we were unable to analyze it for identification; however, the appearance was consistent with that of a strontium aluminate material that has been previously reported to coat "night glowing pearls" (Spring 2005 Lab Notes, pp. 46–47).

Due to the plastic coating, a refractive index measurement of the substrate material was not possible. Raman spectroscopy positively identified the substrate material as fluorite, which was consistent with the microscopic appearance.

While "night glowing pearls" have been characterized, this example was unique because of its large size and the fact that the phosphorescent reaction was easily induced by visible light. It was also unusual that the phosphorescent material was nearly invisible to the naked eye, creating the appearance of a normal, uncoated fluorite sphere.

*Nathan Renfro*

## PEARLS

### Assembled and Bead-Cultured

A cream and white baroque pearl weighing 10.27 ct (figure 8) was recently submitted with seven other pearls to the Bangkok laboratory for a GIA Quality Assurance Report, which provides rapid identification for sorting purposes. The pearl appeared to have been assembled, as it possessed an odd translucent ring at one end, indicating where separate components had been joined together.

Prior to examination with real-time microradiography, it seemed likely that a shell bead nucleus was hidden from view, as the banded structure of a shell was observed in the translucent area when viewed with transmitted light from a fiber-optic light source. The transparent bonding agent used to join the two parts also contained black impurities (figure 9, left). Obvious gas bubbles were visible with a loupe or gemological microscope. Out of scientific interest, the pearl was also examined with X-ray fluorescence and DiamondView imaging. X-ray fluorescence showed a strong reaction in the damaged and repaired area, as would be expected because of its thinner nacre coverage. DiamondView imaging revealed the banding within the bead, the dark inclusions in the bonding agent, and the bonding agent itself (figure 9, right).

*Figure 8. The 10.27 ct baroque cultured pearl exhibited a suspicious translucent ring at one end.*

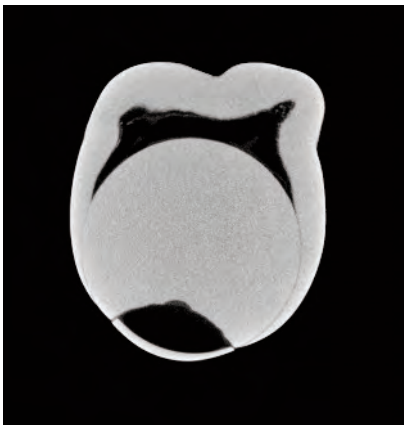

*Figure 10. The broken bead and the nacreous cap applied to conceal the damage are clearly visible in this X-ray computed microtomography (μ-CT) slice.*

Real-time microradiography revealed the bead nucleus as well as an extremely thin nacreous cap that had been used to cover the damaged bead. While X-ray computed microtomography (μ-CT) would not normally be needed to identify such an obviously bead-nucleated pearl, it was used to display the results with even greater clarity (figure 10). This analytical technique clearly showed the broken bead and an area where a new piece of nacre had been applied to repair the pearl. This would explain the mismatching translucent ring.

This study demonstrated how the internal secrets of pearls can be revealed by a variety of techniques.

*Areeya Manustrong*

### Strong Pinkish Purple Freshwater Bead-Cultured Pearls

Freshwater cultured pearls are known for their wide range of attractive colors, including different combinations of white, orange, pink, and purple hues (S. Akamatsu et al., "The cur-

*Figure 9. Left: Weak banding was faintly visible beneath the repaired and assembled area when viewed with a strong light source. Field of view 8 mm. Right: The banding was more noticeable in the DiamondView.*

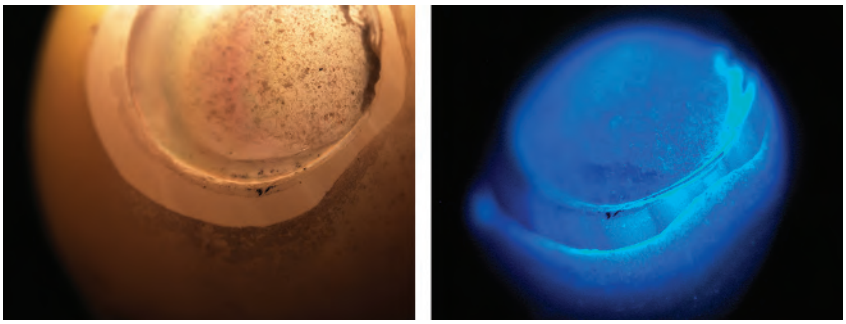

*Figure 11. This necklace of freshwater bead-cultured pearls from China displays strong pinkish purple hues with orient.*

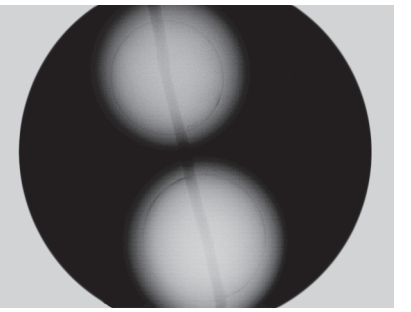

*Figure 12. Real-time X-ray microradiography analysis revealed the round shell bead nucleus used to culture each of the pearls.*

rent status of Chinese freshwater cultured pearls," Summer 2001 *G&G*, pp. 96–113). Jack Lynch of Sea Hunt Pearls (San Francisco) recently submitted a necklace consisting of 33 strong pinkish purple near-round pearls, ranging from 11.90 to 13.85 mm in diameter (figure 11), to GIA's New York laboratory. The unusually intense color and large size of the pearls immediately drew our attention. Mr. Lynch indicated that the pearls were farmed in both the Hunan and Hubei provinces of China, over a period of three and a half to four years.

Real-time X-ray microradiography (RTX) analysis revealed that all of the pearls in the necklace were bead cultured and had relatively thick nacre (figure 12). Energy-dispersive X-ray fluorescence (EDXRF) analysis detected a high concentration of manganese, confirming that these pearls were grown in a freshwater environment. Furthermore, Raman spectroscopy verified that their color was natural, with two strong peaks around 1130 and 1510 $cm^{-1}$ associated with natural polyenic pigments found under 514 nm laser excitation (figure 13), consistent with previous studies (S. Karampelas et al., "Role of polyenes in the coloration of cultured freshwater pearls," *European Journal of Mineralogy*, Vol. 21, 2009, pp. 85–97).

Earlier Chinese production with large beads resulted in a high mortality rate. We continue to see larger bead-nucleated freshwater cultured pearls, so it appears that the process has greatly improved, either through better techniques or hybrid mollusks (D. Fiske et al., "Continuity and change in Chinese freshwater pearl culture." Summer 2007 *G&G*, pp. 138–145). Pearls with larger size, a near-round shape, and intense coloration are highly sought after and more valuable than traditional prod-

*Figure 13. Raman spectroscopic analysis on the pearl's surface showed two natural polyenic pigment peaks at 1130 and 1510 $cm^{-1}$.*

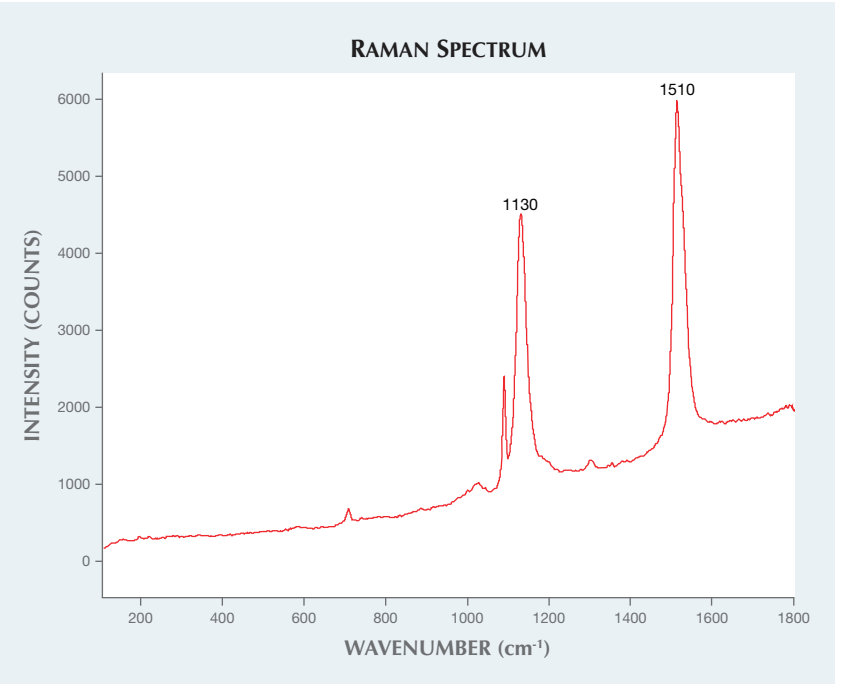

ucts. The owner's inquiries revealed that the pearls were formed under an extremely controlled environment and culturing procedures in mussels that produce the material marketed as "Edison pearls." This necklace proves that current culturing techniques can achieve a wide range of vibrant hues, providing interesting and unique products for the market.

*Yixin (Jessie) Zhou and Chunhui Zhou*

### Beryllium-Diffused and Lead Glass–Filled Orange SAPPHIRE

The Carlsbad laboratory recently received a 4.25 ct transparent orange oval mixed-cut stone (figure 14) for a colored stone identification report. Standard gemological testing established the following properties: RI—1.762 to 1.770; birefringence—0.008; optic sign—uniaxial negative; pleochroism—strong orange and very light yellow; and SG—3.98. All of these properties are consistent with both natural and synthetic sapphire.

Under magnification, the most distinctive internal characteristic was the presence of numerous fractures partially healed by glassy flux-like droplets. Some had a wispy veil and fingerprint-like appearance. One fracture with large healed areas showed a strong flash effect, which appeared greenish blue under brightfield illumination (figure 15, left) and orange-red under darkfield illumination (figure 15, center) when rotating the stone to another direction. Under diffused lighting, the outline of the large partially healed areas stood out clearly (figure 15, right). The flash effect indicates that the fracture was healed using a material with a high refractive index, possibly lead glass (S. F. McClure et al., "Identification and durability of lead glass–filled rubies," Spring 2006 *G&G*, pp. 22–34).

*Figure 14. This 4.25 ct orange sapphire was submitted for a colored stone identification report.*

Heat-treated sapphires submitted to GIA are routinely checked using advanced analytical tools. Energy-dispersive X-ray fluorescence (EDXRF) analysis was performed on the table facet where the large healed fracture with flash effect was located. The presence of Pb was clearly detected, indicating the filler was lead glass. Laser ablation–inductively coupled plasma–mass spectrometry (LA-ICP-MS) was used to confirm the stone's natural trace-element chemistry and detect the beryllium-diffusion treatment. Beryllium was present in all laser ablation spots, but analysis of the partially healed fractures revealed high Pb content in addition to Be. In one spot, both high Be (156 ppmw) and Pb (23,300 ppmw) were present, which provided some possible insight into the treatment process.

Corundum selected for lead-glass filling usually goes through a two-step process. The material is heated at temperatures from 900° to 1400°C to remove the impurities in fissures, followed by another heating at 900° to 1000°C in the presence of a lead-glass mixture to fill the fractures (V. Pardieu, "Lead glass filled/repaired rubies," Asian Institute of Gemological Sciences Gem Testing Laboratory, 2005, http://fieldgemology.org/Ruby_lead_glass_treatment). Beryllium diffusion requires a temperature range from 1800° to 1850°C, close to corundum's melting temperature of 2045°C, which requires a special resistance furnace (J. L. Emmett et al., "Beryllium diffusion of ruby and sapphire," Summer 2003 *G&G*, pp. 84–135). If the stone had been filled first, the lead-glass filler likely would have melted and flowed out of the fractures during the beryllium diffusion treatment (McClure et al., 2006). It is unlikely that the Be diffusion and lead

*Figure 15. Under brightfield illumination, the large healed fracture showed a greenish blue flash effect (left). Under darkfield illumination, the same fracture showed an orange-red flash effect (center). Under diffused lighting (right), the outline of the fracture became distinct. Field of view 3.45 mm.*

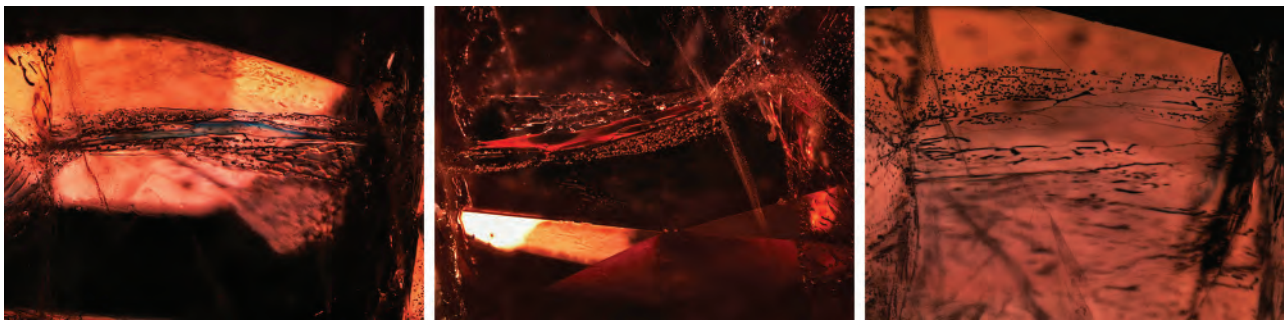

glass–filling treatments occurred simultaneously. Such a process has not been documented and would likely pose technical challenges, partly because the relatively high temperature required for the beryllium diffusion treatment would have outgassed much of the lead and caused serious toxic gas exposure.

The best possible explanation is that the stone was beryllium diffused at a high temperature to improve its color before being treated with lead glass at a lower temperature to improve its clarity. If some residue of the original Be treatment was left in a fracture that was later filled with lead glass, this could explain the correlation of high Be and high Pb in one of our LA-ICP-MS analyses.

GIA's laboratories have identified numerous beryllium-diffused or lead glass–filled stones. That the two treatments were applied in a single sapphire is very rare. It is the first time such a stone has been examined by the GIA laboratory.

*Ziyin Sun*

## LPHT-Annealed Pink CVD SYNTHETIC DIAMONDS

Due to nitrogen vacancy and hydrogen complexes, as-grown CVD synthetic diamonds are usually brown, which are less desirable than other colors. Post-growth treatments such as high-pressure, high-temperature (HPHT) treatment and/or irradiation and annealing, are applied to these synthetics to create attractive colors. In the past, we have reported HPHT-treated and multi-step treated pink CVD synthetics. Recently, the New York lab examined three pink CVD-grown diamonds that were treated with the technique known as low-pressure, high-temperature (LPHT) annealing.

The 0.37 ct rectangle, 0.31 ct rectangle, and 0.25 ct round brilliant were graded as Fancy Deep brownish orangy pink, Fancy Deep brown-pink, and Fancy brown-pink, respectively (figure 16). They were classified as type Ib diamond containing single substitutional nitrogen atoms ($N_s^0$) with absorption bands at 1130 and 1344 $cm^{-1}$ (figure 17). The 0.37 ct sample contained a $VS_2$-grade feather and a few burn marks on the main facets; otherwise, all three were very "clean." The DiamondView images showed typical orange fluorescence and linear growth striations, which are caused by uneven uptake of defects along the growth steps (again, see figure 16). The orange fluorescence is usually observed in N-doped CVD synthetics.

The mid-IR spectra revealed post-growth LPHT annealing treatment. In figure 17, the absorption bands of C-H stretching at 2810, 2870, 2900, 2937, 2948, and 3031 $cm^{-1}$ are created by LPHT annealing (see Y. Meng et al., "Enhanced optical properties of chemical vapor deposited single crystal diamond by low-pressure/high-temperature annealing," *PNAS*, Vol. 105, No. 46, 2008, pp. 17620–17625). They were modified and shifted from the peaks of unstable hydrogenated amorphous carbon complexes and $NVH^-$ defects during the annealing process. The 3123 $cm^{-1}$ ($NVH^0$) band,

*Figure 16. Three LPHT-annealed CVD synthetic diamonds: Fancy Deep brownish orangy pink 0.37 ct (top left), Fancy Deep brown-pink 0.31 ct (top middle), and Fancy brown-pink 0.25 ct (top right). Their DiamondView images (bottom row) show orange fluorescence with linear growth striations.*

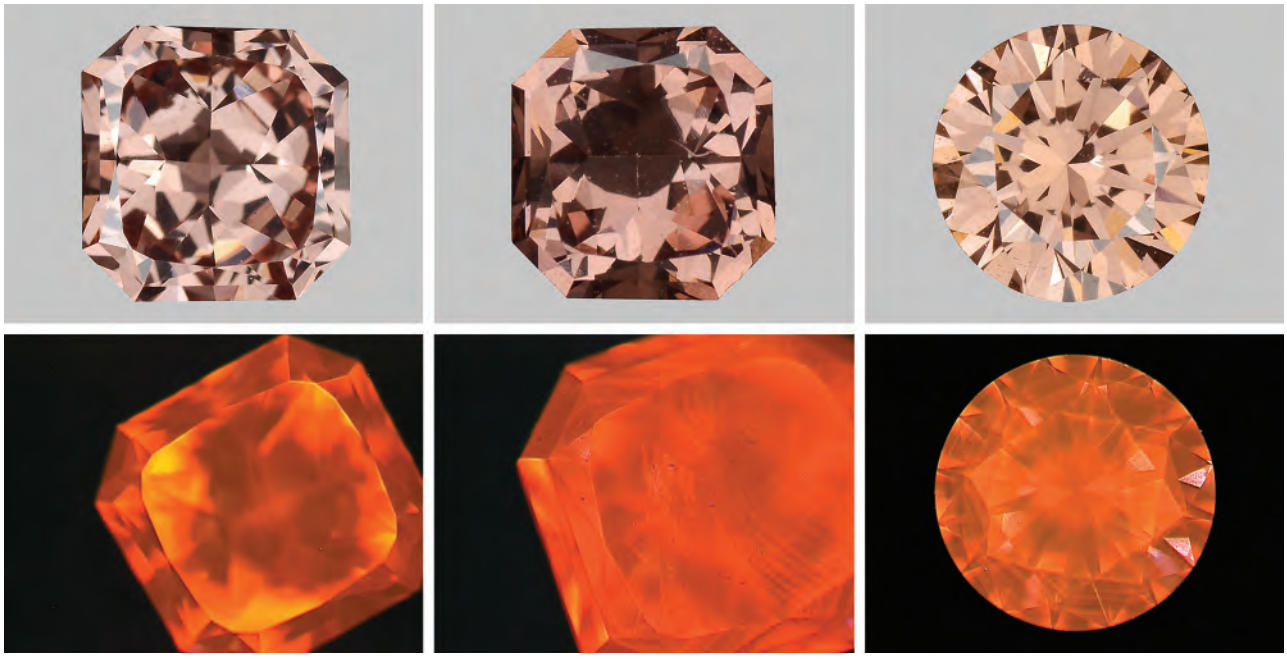

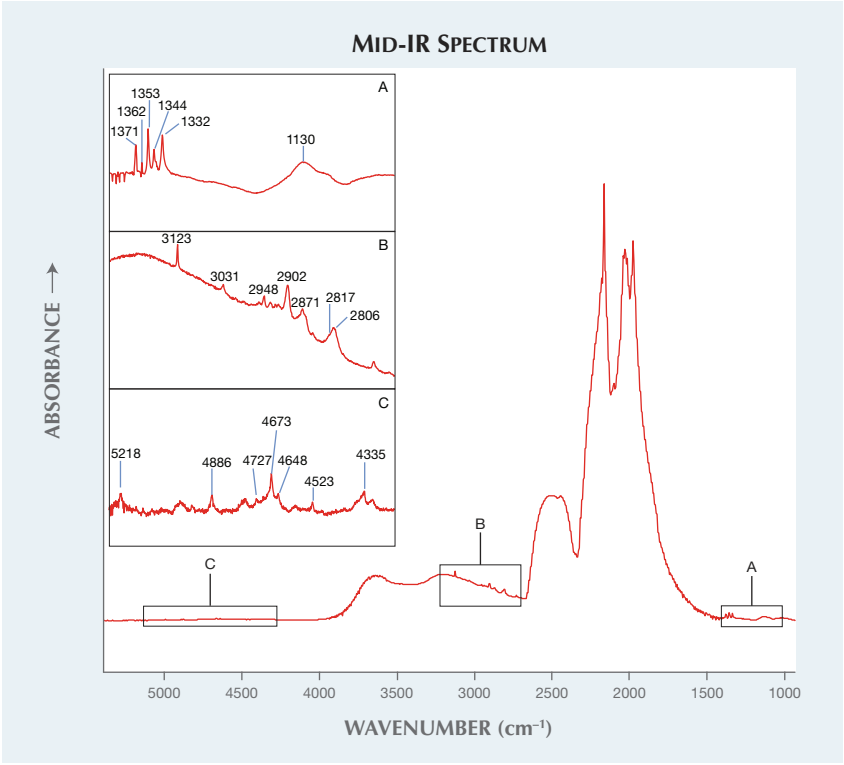


*Figure 17. These CVD synthetics are classified as type Ib with $N_s^0$ atoms at 1130 and 1344 cm$^{-1}$ (inset A). The LPHT annealing was revealed by C-H stretching bands, as seen in inset B. Additional unknown bands were also observed (inset C).*

which is a common defect in as-grown CVD synthetic diamonds and annealed out by HPHT treatment, is present. This defect was detected in LPHT-annealed CVD synthetics (again, see Meng et al., 2008). The 3107 cm$^{-1}$ (N3VH), which can be created by HPHT annealing in CVD synthetic diamonds, is absent. Positively charged single substitutional nitrogen atoms ($Ns^+$) were detected at 1332 cm$^{-1}$. Additionally, unknown bands were also detected at 1353, 1362, 1371, 4335, 4523, 4648, 4673, 4727, 4886, and 5218 cm$^{-1}$. A broad absorption band with absorption maxima at approximately 525 nm and sharp nitrogen-vacancy (N-V) centers at 575 nm ($NV^0$) and 637 nm ($NV^-$) in the visible-NIR spectrum are responsible for pink and orange color components in these samples (figure 18). The vivid orange fluorescence in DiamondView images are also attributed to N-V centers. The H3 center is observed at 503 nm. There are also unknown additional absorption bands at 419.5, 485.8, 495.1, 666.5, 685.4, 711.7, 753.1, 781.4, and 850.3 nm. Very strong N-V centers can be observed in the 514 nm PL spectra.

HPHT annealing can be achieved at temperatures ranging from 1800°–2500°C and pressures greater than 5 GPa. High pressure is required in order to prevent graphitization, especially in natural diamond. In contrast, LPHT annealing is performed at temperatures 1400–2200°C and pressures below 300 torr (<3.99 × 10$^{-5}$ GPa, below atmospheric pressure) (again see Meng et al., 2008). Graphitization became significant above 2200°C. At temperatures above 700°C, vacancies started to move and were trapped at single substitutional nitrogen atoms, creating N-V centers; however, nitrogen atoms become mobile at temperatures above 1700°C, causing the N-V centers to anneal out. Therefore, strong N-V centers (which are much greater than the diamond Raman peak) in the 514 nm PL spectra of these samples suggested that they were annealed at temperatures below 1700°C. Lack of a peak at 3107 cm$^{-1}$ is also suggestive of an annealing temperature below 1700°C. This upper temperature limit is further supported by presence of a band at 3123 cm$^{-1}$, which can be annealed out at above 1800°C. Incorporation of H3 center occurs above 1500°C; thus, annealing temperatures for these samples can be proposed as 1500°C < $T$ < 1700°C. According to Meng's experiment, this temperature range can be correlated with pressure from 150 to 200 torr, with annealing time from 10 to 720 minutes.

Brown as-grown CVD synthetics have been changed to brownish pink by LPHT annealing for 15 minutes by Meng et al. (2008); they were also able to improve colorless CVD-grown diamonds by an average of three color grades. LPHT treatment may have created the attractive pink hue in these samples, although it could not completely eliminate the brown coloration. We expect to encounter more LPHT-treated diamonds in the future.

*Kyaw Soe Moe, Ulrika D'Haenens-Johansson, and Wuyi Wang*

## Near-Colorless Melee-Sized HPHT Synthetic Diamonds Identified in GIA Laboratory

With significant development in diamond treatments and synthesis over the last decade, the trade has serious concerns about treated and/or synthetic material mixed with natural melee-sized stones. The mixing of treated and synthetic diamonds with yellow natural melees was previously reported (Winter 2014 Lab Notes, pp. 293–294; Spring 2015 Lab Notes, pp. 64–65). In order to ensure consumer confidence, it is essential to screen melees so as to distinguish all treated and synthetic goods.

Recently, the Bangkok lab had the opportunity to examine six melee-sized specimens submitted for synthetics and treatment screening. The

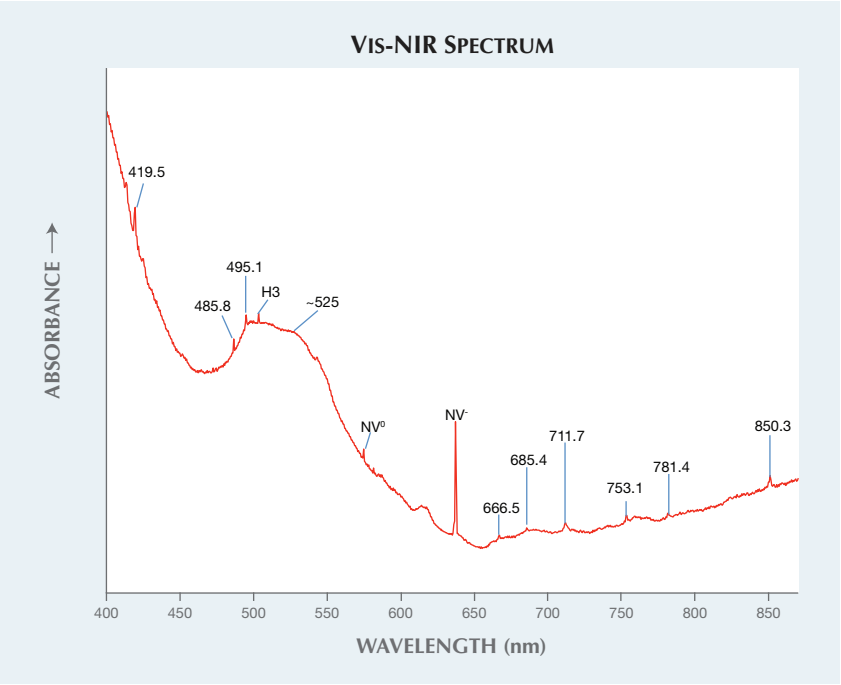


*Figure 18. Absorption maxima at approximately 525 nm and N-V centers are responsible for the pink color in these samples. The H3 center can be observed, along with many unknown bands.*

transparent, near-colorless round brilliants ranged in size from 0.005 to 0.01 ct (figure 19). Microscopic observation revealed no obvious inclusions. Between crossed polarizing filters, very little or no strain was observed. Infrared absorption spectra showed that four of the samples were type IIa diamonds with no detectable defect-related absorption, while the other two were type IIb diamonds accompanied by uncompensated boron showing moderately strong absorption at approximately 2800 $cm^{-1}$. Photoluminescence spectra obtained at liquid-nitrogen temperature with 514 and 633 nm laser excitations revealed an emission doublet of the negatively charged silicon split-vacancy defect $[Si\text{-}V]^-$ at 736.6/736.9 nm for five of the samples, while 830 nm laser excitation showed an emission doublet at 883.0/884.7 nm owing to a nickel-related defect for all six samples (figure 20). DiamondView imaging revealed either blue or green fluorescence, together with characteristic growth features of HPHT synthesis, as seen in figure 21. Strong blue phosphorescence was also observed for all six samples. These gemological and spectroscopic features confirmed that the specimens were grown by HPHT synthesis.

To the best of our knowledge, this is the first examination of near-colorless HPHT synthetics of these sizes by a gemological laboratory. Discovery of these HPHT synthetic diamond melee reaffirms the need to screen the huge volume of near-colorless melee currently in the trade.

*Wasura Soonthorntantikul and Piradee Siritheerakul*

## Phosphorescence of SYNTHETIC SAPPHIRE

Phosphorescent features in synthetic colorless sapphires have previously been reported in *G&G* (Fall 2013 GNI, pp. 182–183). A 1.14 ct colorless sample was recently submitted to the New York lab for identification (figure 22, left). The gemological properties determined the stone was corundum. The specimen was free of inclusions, with no detectable gas bubbles or curved striae. Quantitative chemical analysis, showing a lack of gallium as well as iron levels below the detection limit, indicated that the sample was synthetic. The material was also transpar-

*Figure 19. These six near-colorless round brilliant melee, ranging from 0.01 to 0.005 ct, proved to be HPHT synthetic diamonds.*

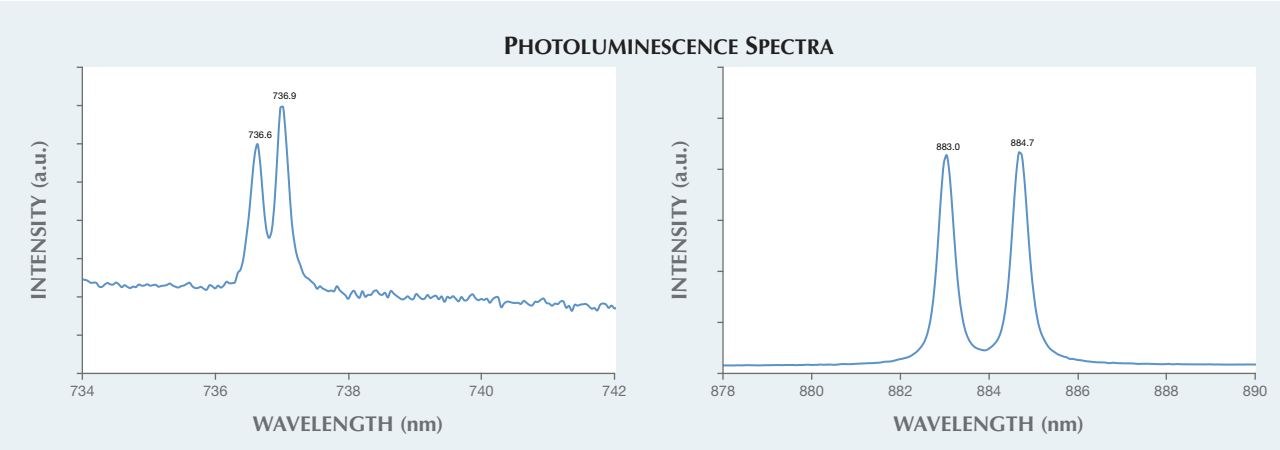


*Figure 20. Photoluminescence spectra at liquid-nitrogen temperature of a small near-colorless HPHT synthetic diamond. The spectra displayed emission peaks at 736.6 and 736.9 nm related to a [Si-V]⁻ defect (left, 514 nm laser excitation) and at 883.0 and 884.7 nm associated with a Ni-related defect (right, 830 nm laser excitation).*

ent to short-wave ultraviolet radiation, whereas natural colorless sapphires do not transmit short-wave UV light due to the quenching effect from trace impurities (S. Elen and E. Fritsch, "The separation of natural from synthetic colorless sapphire," Spring 1999 *G&G*, pp. 30–41). This is the same test used to effectively separate type I and II diamonds; nitrogen impurities in diamonds are strong absorbers of light in the short-wave UV range between 225–320 nm (C. M. Breeding, "The 'type' classification system of diamonds and its importance in gemology," Summer 2009 *G&G*, pp. 96–111). The UV-visible spectrum shown in figure 23 also illustrates the transparency with the absorption edge at approximately 216 nm, whereas natural near-colorless sapphires typically have an absorption edge around 300 nm.

Figure 24 illustrates the phosphorescence band centered at approximately 424 nm, along with other minor decay bands observed in the visible spectrum that mix together to produce the blue phosphorescence observed in figure 22 (right). The phosphorescence lasted about 25 seconds, until the excited electrons dissipated. The only trace elements detected with LA-ICP-MS were Ti (21 ppma average), and Cr, Mg, and Ca (below 5 ppma). Chalky blue fluorescence in sapphires is believed to be due to $Ti^{4+}$ charge-transfer transition of isolated $Ti^{4+}$ ions or Ti-Al vacancy pairs. The fluorescence peak is usually between 410 and 420 nm, but shifts to higher wavelengths as Ti concentrations increase (B. D. Evans, "Ubiquitous blue luminescence from undoped synthetic sapphire," *Journal of Lumines-*

*Figure 21. This DiamondView image of one sample (third from the left in figure 19) shows the characteristic growth features of HPHT-grown synthetic diamonds.*

*Figure 22. Left: The 1.14 ct synthetic sapphire under daylight-equivalent lighting. Right: The sample exhibited phosphorescence in this DiamondView image.*

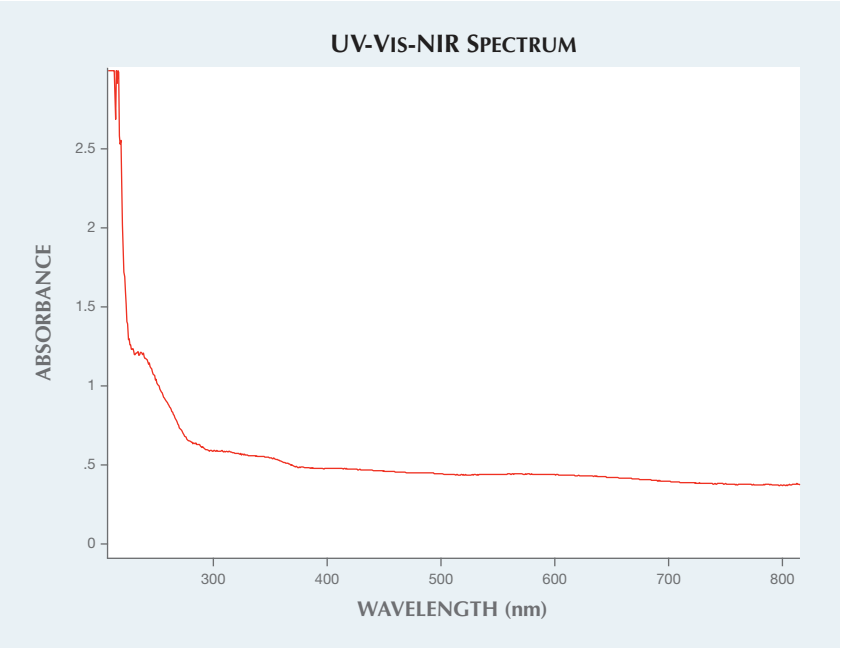


*Figure 23. Transparency was observed in the UV-Vis-NIR spectrum.*

*cence*, Vol. 60–61, 1994, pp. 620–626; W.C. Wong et al., "Charge-exchange processes in titanium-doped sapphire crystals. I. Charge-exchange energies and titanium-bound exitons," *Physical Review B*, Vol. 61, No. 9, 1995, pp. 5682–5698). The phosphorescence in synthetic colorless sapphires could be related to this property, with the addition of the decay route including forbidden energy transition states. Phosphorescence in synthetic colorless sapphires is still not well understood, and additional research is needed to verify the origin of this phenomenon.

*Figure 24. The phosphorescence spectrum of the synthetic sapphire shows the main band centered at approximately 426 nm, along with smaller bands in the visible-light region.*

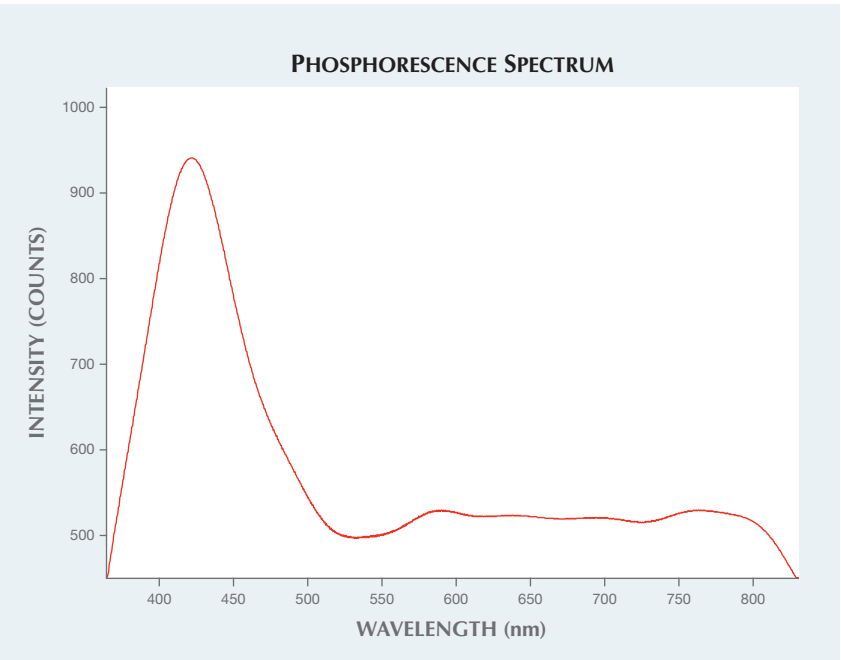


*Akhil Sehgal*

## Chemical Analysis of ZIRCON

Radioactive elements such as thorium and uranium existed at higher concentrations during earlier ages of the earth; crystal formations from these periods were therefore more susceptible to acquiring higher concentrations of these materials. Zircon has a particular affinity for attracting rare earth elements such as uranium and thorium into its crystal structure due to similarities in the three elements' cation sizes, which allows U and Th to substitute for Zr in the crystal lattice, and other bonding properties such as coordination, electronegativity, and cation change. The isotopes break down through radioactive decay, releasing harmful doses of radiation to the host crystal. This destroys the crystal structure of zircon until it is nearly amorphous, in a process called metamictization (J.A. Woodhead, "The metamictization of zircon: Radiation dose-dependent structural characteristics," *American Mineralogist*, Vol. 76, 1991, pp. 74–82).

In gemology, zircon is categorized by the degree of radioactive degradation that has taken place. Highly degraded material with little to no crystal structure remaining is termed "low" or "metamict" zircon. "High" zircon is crystalline and nearly unaffected by radiation, while "intermediate" zircon is semi-crystalline, between the amorphicity of low zircon and the ordered crystalline structure of high zircon.

Five zircon samples were analyzed in this study based on their apparent crystallinity (figure 25). Raman spectroscopy shows the degradation of the crystal structure from its original structure, which can be illustrated by comparing it to zircon that has not been affected by radiation (figure 26). Infrared spectra (figure 27) also show

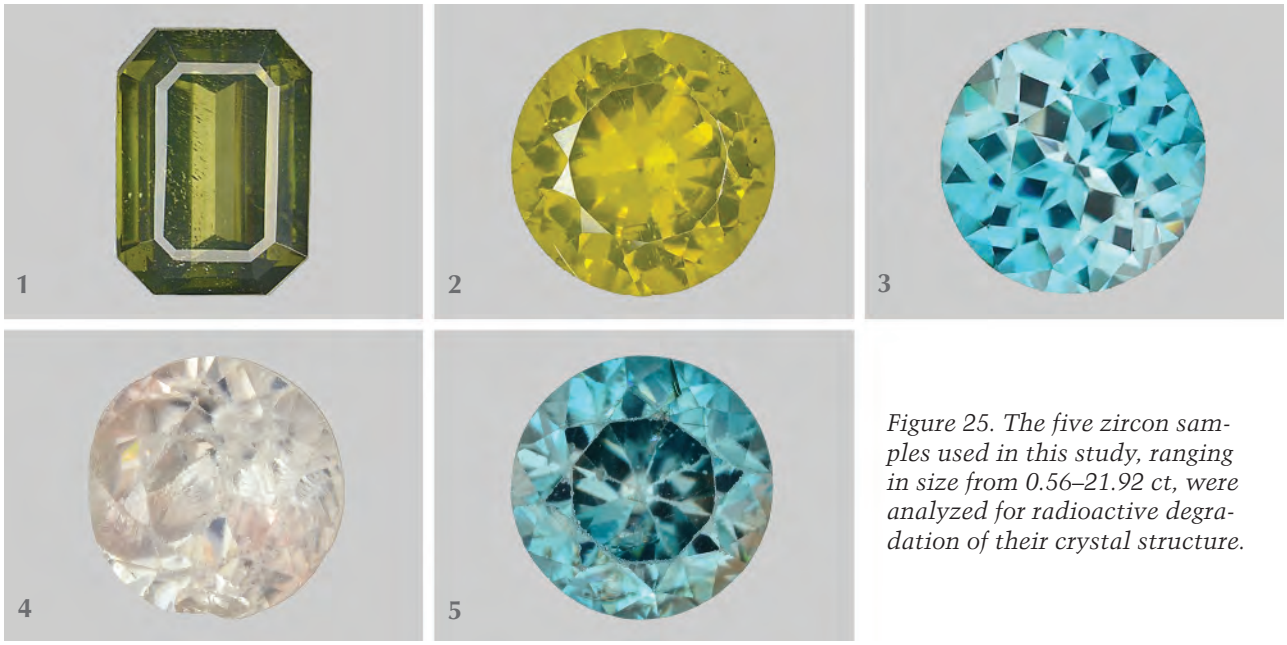


*Figure 25. The five zircon samples used in this study, ranging in size from 0.56–21.92 ct, were analyzed for radioactive degradation of their crystal structure.*

differences between the low and high zircons, as the former displays peak broadening and baseline irregularities.

Trace-element analysis of high and low/intermediate zircon using LA-ICP-MS illustrated variations in concentrations of several elements, including thorium, uranium, and lead. While uranium and thorium are easily incorporated into the crystal structure, the same is not true for lead, which can only appear in zircon as the byproduct of the radioactive decay chains of thorium and uranium. Due to this property, scientists have been able to accurately date zircons and Earth's age using isotope ratio analysis by comparing the lead to uranium ($^{238}U/^{206}Pb$) and lead to thorium ($^{232}Th/^{208}Pb$) ratios. These results showed the low zircon samples to be far older than the high zircon. Isotopic elemental analysis using LA-ICP-MS (table 1) determined that the low zircon was approximately a billion years old. This is far older than the high zircon samples, which were determined to be approximately 100 million years old. The higher content of radioactive elements earlier in Earth's formation, along with the longer period of time for metamictization to occur, contributed to the structures of the low zircons.

*Figure 26. Raman analysis of samples 2 and 4, illustrating the difference between "low" and "high" zircons. Low zircon displaying amorphicity by peak loss and broadening.*

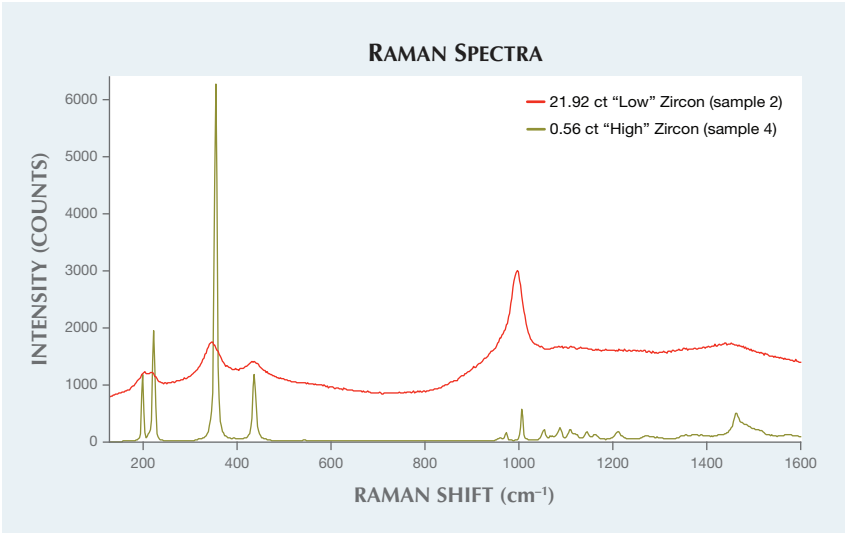


Trace-element analysis combined with spectroscopy can also detect treatments in zircon. Heat treatment, which is commonly performed on all types of zircon for color modification, can reestablish the crystal structure that was originally destroyed by natural processes. Zircon crystals with high lead content must have experienced a considerable amount of radiation exposure, leading to their lower crystalline order. High-lead zircon samples that show an ordered crystalline structure could have initially been low or intermediate and heat treated to restore the crystal structure. By correlating the trace-element chemistry with other analytical tools such as Raman spectroscopy, it may be possible to determine heat treatment of some types of zircons.

**TABLE 1.** Isotopic elemental analysis of zircon using LA-ICP-MS.

| Sample | Weight | $^{206}$Pb | $^{208}$Pb | $^{232}$Th | $^{238}$U |
|---|---|---|---|---|---|
| (1) Greenish yellow "low" zircon | 16.32 ct | 848.40 | 54.53 | 237.10 | 4529.00 |
| (2) Greenish yellow "low" zircon | 21.92 ct | 636.67 | 24.67 | 603.00 | 2083.33 |
| (3) Greenish blue "high" zircon | 10.14 ct | bdl* | bdl* | 51.83 | 73.17 |
| (4) Near-colorless "high" zircon | 0.56 ct | 0.81 | 0.63 | 200.00 | 210.17 |
| (5) Blue "high" zircon | 1.96 ct | 0.12 | 0.19 | 85.02 | 99.98 |

** Below detection limit.*

Nearly all blue and near-colorless zircons have undergone heat treatment, as these colors are rarely found in nature; the majority of zircon rough is brown. The blue color of zircon is theorized to come from the chromophore $U^{4+}$ cations, depending on how the uranium cations interact within the crystal structure. "Electric" blue zircon's color is typically produced by heating the stone to 1000°C in a reducing environment, while near-colorless material is produced at about the same temperature in an oxidizing environment. Heat treatment of zircons that have not had significant radiation damage can restore the crystallinity at the temperatures used for color modification treatments. Although very metamict zircons must undergo higher temperatures and longer duration of heating to restore a degree of crystallinity, these zircons will never achieve the electric blue color. It is difficult to even produce gem-quality material from this material. Zircon with poor crystallinity has more variation in polycrystalline grain orientation, bond length, element location, and bonding, as well as varying amorphicity. Knowledge of zircon's chemistry can facilitate the identification of treatments and growth conditions, and can be applied to determine various correlations pertaining to color and origin.

*Akhil Sehgal*

*Figure 27. FTIR spectra of the zircon samples. The metamict zircons, samples 1 and 2, display an undefined baseline and broader bands than the high zircons.*

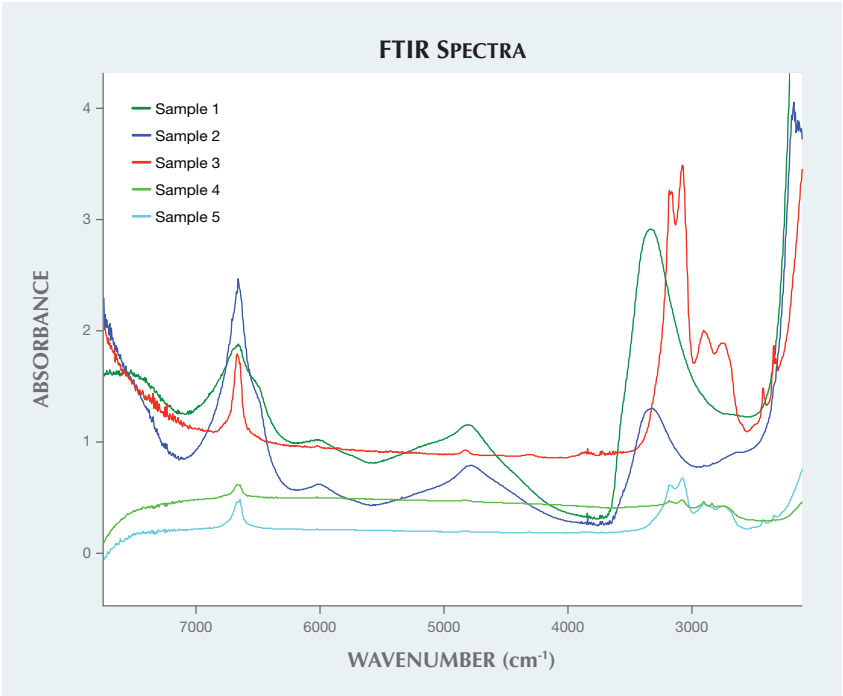


*PHOTO CREDITS:*
*Jian Xin (Jae) Liao—1, 11, 16 (top right), 25; Paul Johnson—2; Robison McMurtry—4, 14; Don Mengason—6; Nathan Renfro—7; Nuttapol Kitdee—8, 19; Areeya Manustrong—9; Yixin (Jessie) Zhou—12; Ziyin Sun—15; Sood Oil (Judy) Chia—16 (top left and middle), 22 (left); Kyaw Soe Moe—16 (bottom); Charuwan Khowpong—21; Akhil Sehgal—22 (right).*

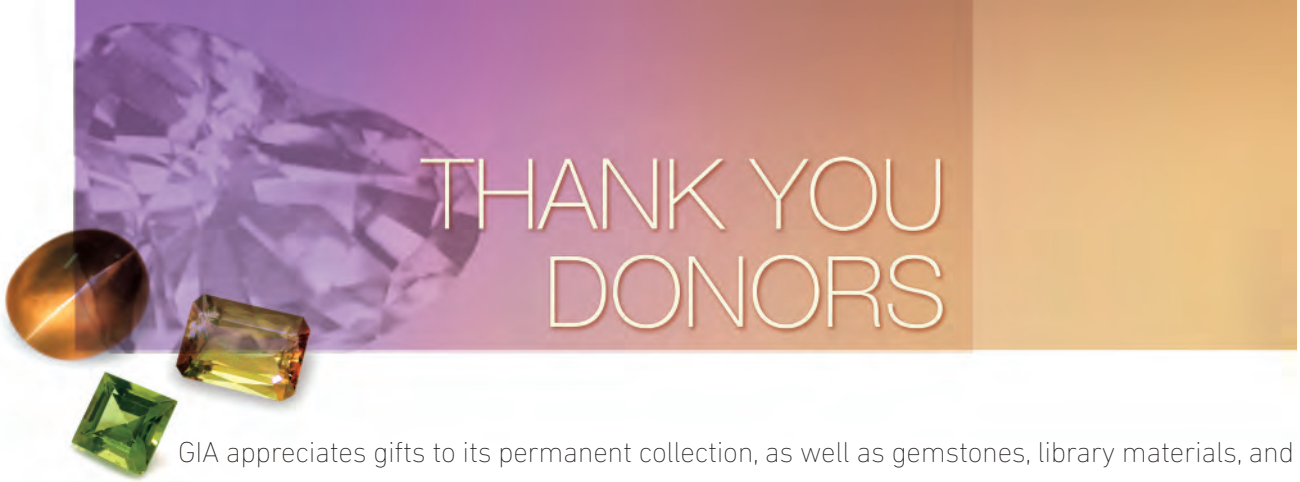

# THANK YOU DONORS

GIA appreciates gifts to its permanent collection, as well as gemstones, library materials, and other non-cash assets to be used in education and research activities. These contributions help GIA further its public service mission while offering donors philanthropic benefits. We extend sincere thanks to all 2014 contributors.

## CIRCLE OF HONOR*

*$100,000 and higher*

Dr. Suman Agrawal
Robert and Marlene Anderson
Thomas Cacek
Dr. James Y. Hung
Bill Larson

## 2014 DONORS

*$50,000 to $99,999*

Dr. Suman Agrawal
In Memory of Richard P. Helwig

*$10,000 to $49,999*

Robert L. & Marlene Anderson
Johnie Alan Henderson

*$5,000 to $9,999*

In Memory of R. Jed Smith

*$2,500 to $4,999*

Gina Dronet
Dr. James Y. Hung
In Memory of Eileen Irvin
James S. Rosenheim, G.G.
Victor Tuzlukov

*$1,000 to $2,499*

Bill Barker
Dr. Alexander Bulatov
Dayananda Kulathunga
Bill Larson

*$500 to $999*

Richard Brown
Mark Mauthner
Tara Pearls

*Under $500*

Cosmo Altobelli
René Brus
Craig Selimotic Danforth
Israel (Eli) Eliezri, Colgem Ltd.
Fallbrook Gem & Mineral Society
Family of William L. Carnow
Si & Ann Frazier
Don Hoover
House of Onyx, Inc.
A.J.A. (Bram) Janse
Amanda J. Luke
Martha McKee-Hayden
Linda MacNeil, Artist/Jeweler
In Memory of William "Bill" Junkin
In Memory of Mona Freeman Ellis
In Memory of Curtis P. Shuh
Milenyum Mining Limited, Turkey
Tali Nay
Marcus Origlieri
Pala International
Malik Rehman
Hussain Rezayee
Nathan Rochester
Daniel Sauer
W. Constantin Wild & Co.
Alan Zell

**If you are interested in making a donation and receiving tax benefits information, please contact:**

MCKENZIE SANTIMER
call: (760) 603-4150
fax: (760) 603-4056
email: mckenzie.santimer@gia.edu

* All are cumulative donations


The purpose of this new quarterly column in *Gems & Gemology* is to encourage the appreciation of inclusions in forensic gemology and to help build the observational skill set of the practicing gemologist. By providing concise information and vividly clear photomicrographs and photomacrographs of new or otherwise interesting inclusion specimens, the column aims to narrow the knowledge gap between advanced inclusionists and gemologists working in mainstream general practice.

The micro-world of gems lies at the very core of gemology. Sometimes its nature contributes to the allure of a gem, as is the case with such coveted gems as sunstones, star sapphires, and cat's-eye chrysoberyls. At other times that world may seem a dreadful distraction to an otherwise beautiful, marketable specimen. But even in what appears to be a perfectly clean gem, this micro-world waits for gemologists to dive into its depths and thoroughly explore its landscape. The visitor will be greeted with a beautiful and wondrous inner space, and the unexpected secrets revealed will come to enrich one's understanding of gem materials in innumerable ways.

While hints of the internal features may be glimpsed with the loupe or the unaided eye, true access is afforded by the microscope. This is unequivocally the most important instrument in the gemologist's arsenal once its proper use is mastered, particularly with the application of special lighting techniques and the use of various filters (see N. Renfro, "Digital photomicrography for gemologists" in the current issue, as well as J. I. Koivula, "Photomicrography for gemologists," Spring 2003 *G&G*, pp. 4–23).

For newcomers, an understanding of the micro-world may seem elusive, even daunting. Continual practice, careful observation, and patience will refine both technique and interpretive prowess for both new and experienced inclusionists. Observation through the microscope serves as the very foundation for many conclusions drawn on a specimen. This can include identification, treatment detection, separation of natural and synthetic materials, and geographic origin—even secrets of a gem's genesis and the secrets of the earth's depths may ultimately be revealed.

In building proficiency of the micro-world through this column, readers will also expand their personal knowledge base and ability with a microscope. Mastery of microscopy, combined with at least a basic grasp of mineralogy, is essential for understanding the nature of gems and the geologic processes that occur within the earth. This increased knowledge will eventually translate into a better comprehension of the inclusion scenes that may be encountered in one's own micro-world.

With this column, we hope to inspire gemologists to simply take the time for a closer look. We invite you to join us for an extended tour through the astounding beauty and variety that is the micro-world of gems and other related materials.

*Elise A. Skalwold, Nathan Renfro, and John I. Koivula*

*Editors' note: Interested contributors should contact Nathan Renfro at nrenfro@gia.edu and Jennifer-Lynn Archuleta at jennifer.archuleta@gia.edu for submission information.*

Gems & Gemology, Vol. 51, No. 2, pp. 190–197.


## Amber with Mite Inclusion

A most unusual mite (figure 1, left) was discovered as an inclusion in an approximately 30-million-year-old double-polished plate of amber from the Dominican Republic (figure 1, right). The specimen was acquired from the private collection of William W. Pinch of Pittsford, New York. The plate itself weighed 0.77 ct and measured 13.15 × 7.59 × 2.76 mm, while the mite's body was 0.34 mm in length.

What made this mite unusual was that the longest front leg measured approximately 2.10 mm, disproportionately long in relation to the rest of its body. This type of mite, of the genus *Podocinum*, might be awkward-looking, but its morphology has survived millions of years virtually un-

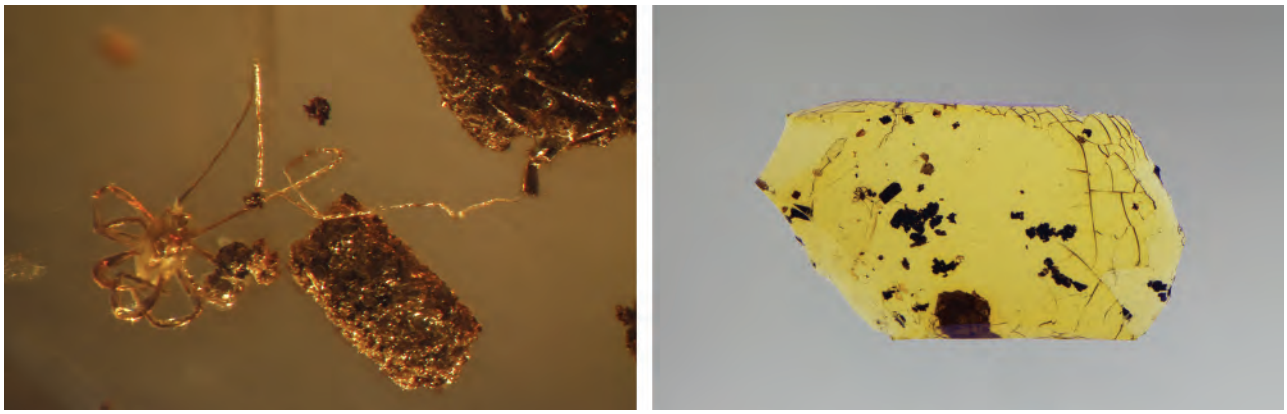

*Figure 1. A mite with exceptionally long front legs (2.1 mm), as seen using shadowed transmitted and fiber-optic illumination (left), was found in this small 13.15-mm-long fragment of amber (right). Images by Nathan Renfro.*

changed, an indication that it was just as efficient a predator then as its living counterpart today. *Podocinum* is a very slow-moving mite that lives in loose soil, feeding on springtails (*Collembola*). As it travels about, the mite uses its extremely long front legs to explore the soil around it and quickly snare any springtail that happens to come too close.

A literature search failed to turn up any other example of a *Podocinum* mite as an inclusion in amber, making this an even more interesting specimen. So while a small polished piece of amber itself might have virtually no commercial or scientific value, the addition of a well-preserved microscopic organism completely changes the value factor of the specimen.

*John I. Koivula*

## Apatite "Piñata"

While gemologists are accustomed to transparent and translucent materials with microscopically visible inclusions, semi-translucent to opaque gems are generally not considered potential hosts of interesting inclusions. Consequently, only the surfaces of these materials are really explored microscopically. This should not dissuade the avid inclusionist from taking the opportunity to look closely at them for unexpected surprises that may be revealed.

Apatite is appreciated for its range of beautiful colors and other optical properties, as well as its morphological characteristics. Most gem apatite is the fluorine end-member of the apatite group known as fluorapatite, or apatite-(CaF). Transparent gem-quality apatite often contains interesting inclusions such as tourtmaline, glass, biotite, goethite, hematite, manganese oxide, and pyrrhotite, so it seems logical that the semi-translucent to opaque form would also host inclusions, albeit obscure ones.

The Otter Lake locality in southern Quebec, Canada, is well known for producing aesthetic cabinet specimens featuring elongated prismatic fluorapatite crystals on orangy or pinkish marble matrix, sometimes with deep purple fluorite in the associated mineral assemblage as well. Damaged crystals of limited potential commercial value as faceted gems or mineral specimens may be fashioned into lapidary items such as carvings, cabochons, and spheres (figure 2), or simply find their way into study collections.

A fascinating dark green apatite crystal obtained from Luciana Barbosa of the Gemological Center in Asheville, North Carolina, recently captured our attention. This specimen, from the Yates uranium mine at Otter Lake, measured 31.16 mm in length and weighed 99.21 ct (figure 3).

What made this crystal interesting was that it had cracked in half along a plane more or less perpendicular to its length, exposing the otherwise unseen inclusions (figure

*Figure 2. A 42.92 mm polished sphere with an exposed orange calcite inclusion was fashioned by Dale Carson from fluorapatite recovered from the Yates uranium mine in Otter Lake, Pontiac County, Quebec, Canada. Photo by Elise A. Skalwold.*

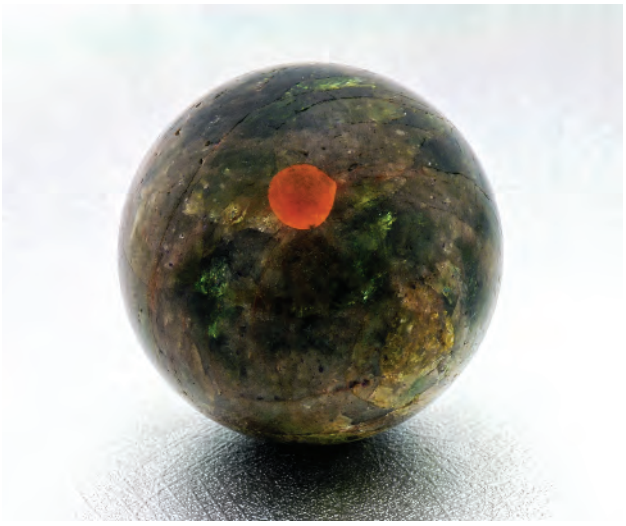

*Figure 3. This 31.16-mm-long fluorapatite crystal was also recovered from the Yates uranium mine. Photo by Elise A. Skalwold.*

4). The two spherical inclusions were identified by Raman analysis as brownish orange calcite, the larger of which measured 5.74 mm in diameter (figure 5). Because of its size, this inclusion was probably at least somewhat responsible for the host apatite cracking apart.

Upon closer inspection and Raman analysis, two tiny deep purple fluorite crystals could be seen perched on the surface of the largest included calcite sphere (again, see figure 5). The resulting bouquet of contrasting colors and the surprising spherical form of the calcite inclusions with purple fluorite "eyes" turned mishap into treasure, reminiscent of breaking open a piñata to find candy within. These calcite spheres are a mineralogical enigma, though current research suggests they formed at high temperature from entrapped carbonate melt (F. Sinaei-Esfahani, "Localized metasomatism of Grenvillian marble leading to its melting, Autoroute 5 near Old Chelsea, Quebec," master's the-

*Figure 4. Two orange spherical inclusions were exposed when the fluorapatite crystal fractured in half. Photo by Elise A. Skalwold.*

sis, Department of Earth and Planetary Sciences, McGill University, Montreal, 2013).

While providing valuable insights into geological processes, such inclusions in gems and minerals never fail to enrich the day-to-day experience of gemologists and mineralogists.

*Elise A. Skalwold and John I. Koivula*

*Figure 5. The larger inclusion in the apatite, a 5.74 mm sphere of orange calcite, featured a pair of purple "eyes" on its surface. Upon further analysis, these were revealed to be fluorite. Photomicrograph by John I. Koivula.*

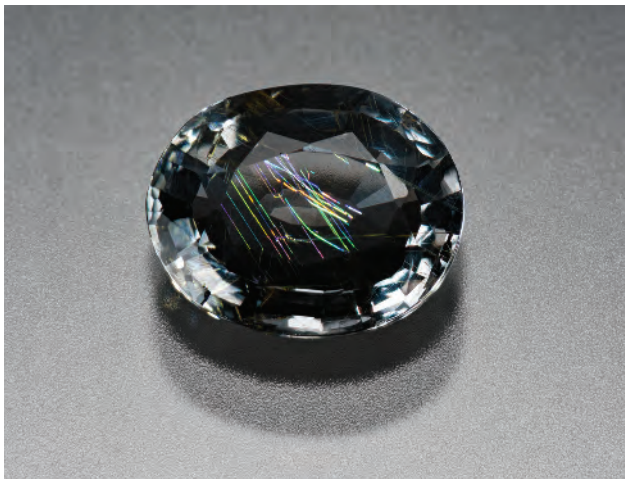

*Figure 6. This 0.86 ct gray musgravite displays an unusual iridescent phenomenon that is clearly visible in the table facet. Photo by Kevin Schumacher.*

### Iridescent Musgravite

Musgravite is a rare mineral closely related by composition to the mineral taaffeite. This magnesium-rich beryllium oxide crystallizes in the trigonal system, in contrast to the hexagonal system of taaffeite, and is highly sought after by rare stone collectors. A 0.86 ct musgravite, identified by Raman spectroscopy, contained a particularly interesting inclusion scene consisting of numerous etch tubes that broke the surface of the faceted stone (figure 6). With a direct source of light, these etch tubes displayed vibrant colors resulting from thin-film iridescence in the air-filled, crystallographically aligned tubes (figure 7). This is the first musgravite gemstone displaying any type of optical phenomenon that this author has examined to date.

*Nathan Renfro*

### Cat's-Eye Phenakite

While the beryllium silicate phenakite is known to gemologists both as a by-product inclusion in synthetic emeralds and in association with natural beryllium-containing gems such as emerald and chrysoberyl (see Fall 2003 Gem News International, pp. 226–227), it is rarely encountered in the laboratory as a fashioned gemstone. Although phenakite does occur in nature as transparent pegmatitic crystals from localities such as Brazil, and as alluvial stream-rounded Sri Lankan pebbles suitable for cutting, such gems are generally considered collector curiosities and are not often submitted to gemological laboratories for identification. Therefore, any occasion to document such a rare and unusual gem material is always of interest, especially if it also displays an optical phenomenon.

We recently had the opportunity to examine a large colorless cabochon represented as phenakite that was provided for examination by Elaine Rohrbach of GemFare in Pittstown, New Jersey. This gem measured approximately 18.19 × 17.77 × 14.81 mm, weighed 38.34 ct, and was transparent to the unaided eye. Although it appeared to be es-

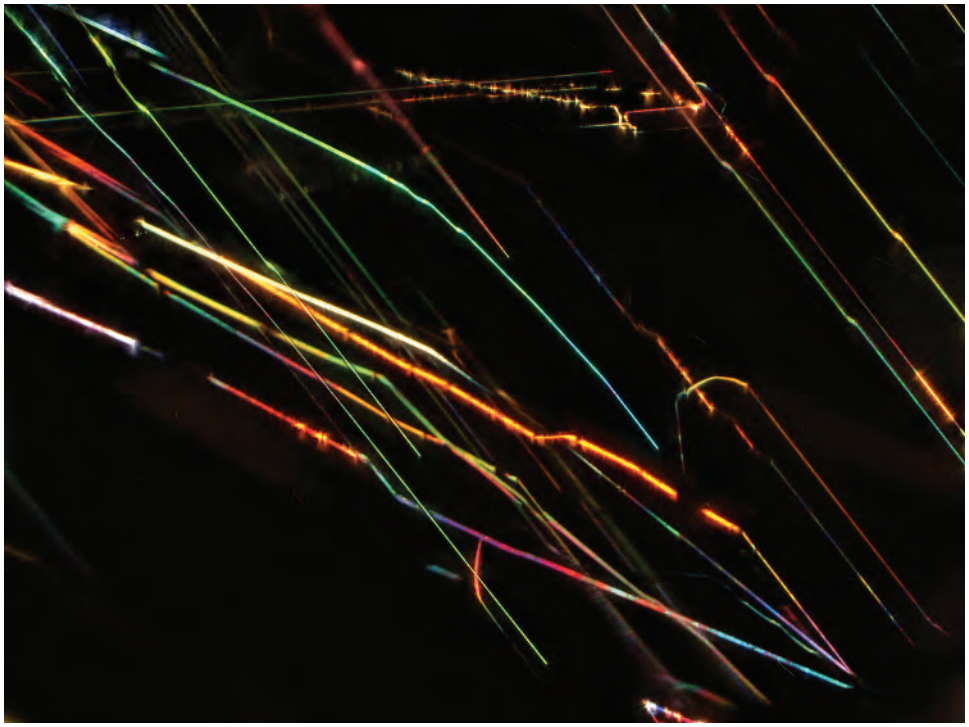

*Figure 7. Thin-film iridescence along crystallographically oriented etch tubes was the source of the colorful phenomenon in this rare musgravite gemstone, viewed using oblique fiber-optic illumination. Field of view 2.47 mm. Photomicrograph by Nathan Renfro.*

*Figure 8. This 38.34 ct phenakite showed a well-defined cat's eye when viewed with point-source illumination. Photo by Kevin Schumacher.*

sentially transparent, it also showed relatively strong chatoyancy (figure 8) in the form of a sharp eye extending across the dome of the cabochon when illuminated from above with a single light source, such as sunlight or a fiber-optic illuminator. This gem was said to be from Sri Lanka; while gem-quality Sri Lankan phenakite is known to contain "needle-like" inclusions, chatoyancy is not specifically mentioned as a phenomenon in major gemological reference books such as Robert Webster's *Gems* or Joel Arem's *Color Encyclopedia of Gemstones.*

Numerous minute acicular tubes and platy voids were clearly seen under 30× magnification using fiber-optic illumination. These inclusions were all aligned parallel to the optic axis, which was oriented in a plane parallel to the cabochon's base and perpendicular to the reflective chatoyant band (figure 9). Under 90× magnification, some of the iridescent platy voids displayed complex multi-component interiors. The various components showed contrasting iridescent colors, which made them stand out from their surroundings. The examination demonstrated that light reflections from the numerous tubes and the iridescent voids were responsible for the pronounced chatoyancy in this phenakite cabochon. Because they were only clearly visible when illuminated from overhead, these inclusions created an interesting balance between transparency and chatoyancy that is rarely seen in gems displaying cat's eyes. Very few phenakites have been examined by GIA, which makes this example of a chatoyant variety a very exciting experience.

It is interesting to note that another cat's-eye phenakite was reported on in *G&G*'s Fall 2009 GNI section. Unlike the transparent, colorless gem reported here, that stone had a light brownish yellow color and was discovered in Madagascar. This author was reminded somewhat of the initial discovery of another gemological rarity, sapphirine, which was completely unknown to gemologists until it was iden-

*Figure 9. Viewed using oblique fiber-optic illumination, some of the iridescent platy voids in the phenakite contained complex multi-phase components consisting of a liquid, gas, and solid daughter crystals. Field of view 0.90 mm. Photomicrograph by John I. Koivula.*

tified within a short period from Australia, Kenya, Thailand, and Sri Lanka. As the world's population grows and we search the earth's surface for gems, more places will be more thoroughly explored and in turn new discoveries will be made.

*John I. Koivula*

### Unusual Pink Sapphire Bead

How to ruin a gem-quality natural untreated tumble-polished sapphire? Fill it with numerous drill holes! At 9.36 ct and measuring 17.25 × 9.13 × 6.21 mm, the purplish pink bead shown in figure 10 had the perfect form to produce a very attractive faceted pear-shaped gem, but that effort seemingly ended in failure. These drill holes, more than 30 of them in all, stood out in high relief because they were at least partially filled with a dark unidentified residue. This leaves the question of why anyone would drill so many holes in a perfectly good sapphire. Closer microscopic examination revealed a possible clue. At the surface of three of the holes were small bright red fragments, identified by Raman analysis as ruby (figure 11). Yet we were unable to determine if the fragments were natural or synthetic, due to their small size. Further analysis with advanced analytical equipment would be required to make this separation. The implication is that if all the drill holes contained a bright red ruby, this would have enhanced the light pink appearance of the bead. Because so many of the ruby fragments were missing, the unsightly drill holes made for a rather unattractive gem bead.

*Nathan Renfro and John I. Koivula*

*Figure 10. This 17.25-mm-long bead contained more than 30 randomly oriented drill holes. Photo by Nathan Renfro.*

### Bicolor Double-Eye Tourmaline

The Summer 2009 *G&G* Lab Notes section (pp. 139–140) described a 5.44 ct tourmaline double cabochon that displayed a sharp, silvery white chatoyant band on one side and a deep golden brownish yellow eye on the reverse side. Microscopic examination revealed that this phenomenal optical effect was due to a combination of pronounced color zoning and growth tubes that were in precise crystallographic alignment.

This same phenomenon was observed in a double cabochon cat's-eye tourmaline cut from rough discovered at the

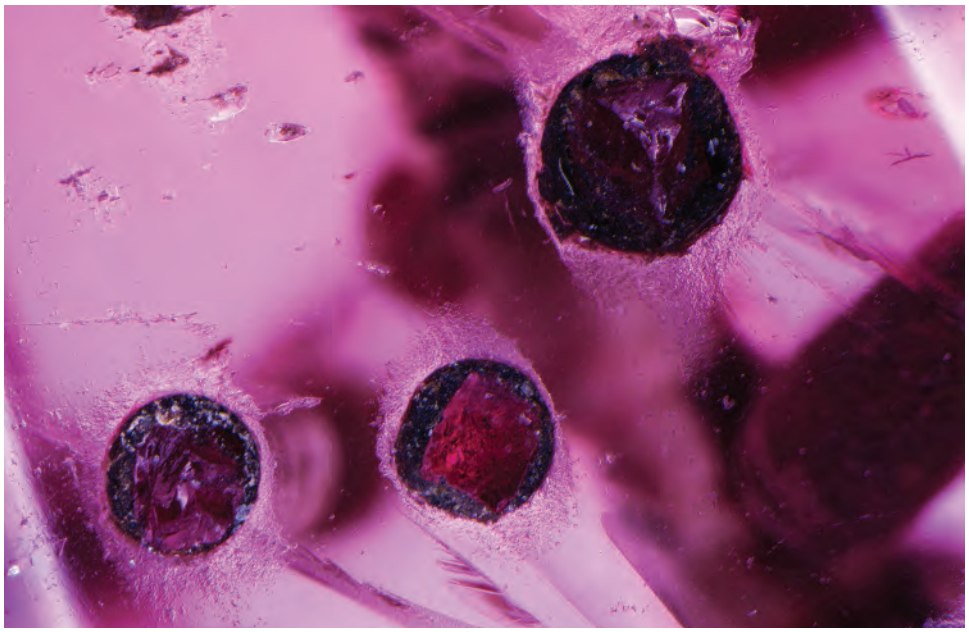

*Figure 11. Three of the drill holes, seen here using diffuse transmitted light and oblique fiber-optic illumination, contained a small ruby fragment identified by Raman analysis. Field of view 4.40 mm. Photomicrograph by Nathan Renfro.*

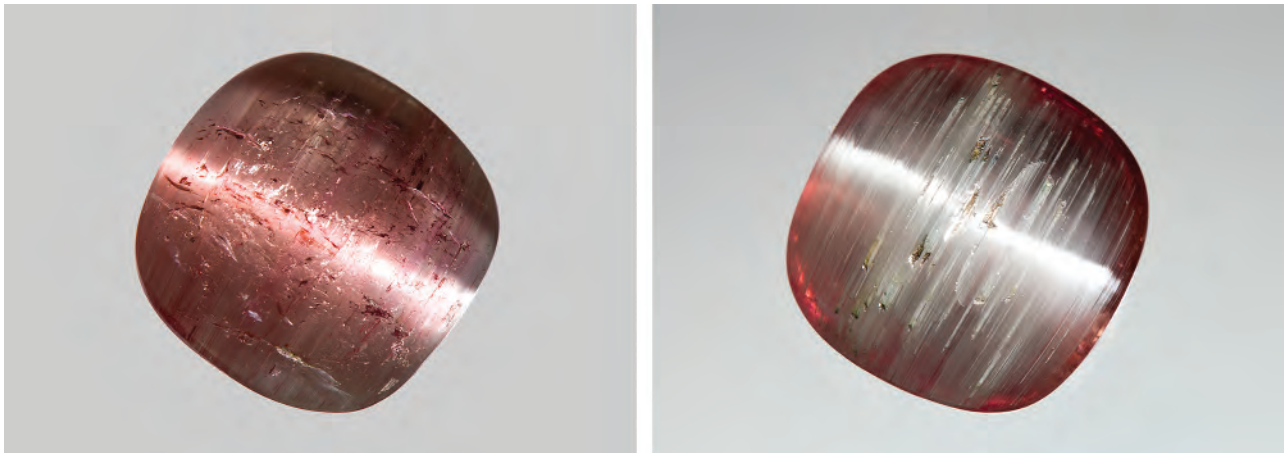

*Figure 12. Fashioned as a double cabochon and weighing 6.39 ct, this bicolor tourmaline from Newry, Maine, displays pink and white chatoyant bands on opposite sides. One side of this tourmaline is pink (left), while the reverse side is colorless (right). Even though the chatoyancy-causing growth tubes are only in the colorless portion, both sides exhibit a sharp cat's eye. Photos by Kevin Schumacher.*

well-known pegmatite complex in Newry, Maine. This cushion-shaped cabochon, weighing 6.39 ct and measuring 11.31 × 11.12 × 6.39 mm, was pink on one side and essentially colorless to white on the opposite side. Consequently, its chatoyant bands had clearly different colors, one pink and the other a silvery white (figure 12).

As expected of a cat's-eye gem, when two incident light sources (fiber-optic wands) were positioned side by side above this tourmaline, two separate eyes became visible. As the gem was rotated under and between the light beams, these eyes appeared to converge, closing to form a single chatoyant band and then opening, like a winking eye. This interactive phenomenon was visible on both sides of the double cabochon.

As with the previously reported example, microscopic examination revealed very strong color zoning, with a pink layer positioned parallel to a zone of near-colorless tourmaline, also known as achroite. The gem was fashioned so that the color layers were divided parallel to the girdle plane. The achroite layer appeared silvery white because of numerous parallel reflective growth tubes uniformly distributed throughout it (figure 13), while no growth tubes

*Figure 13. Growth tubes oriented along the c-axis and present only in the colorless portion are responsible for the chatoyancy in this bicolor tourmaline, observed using fiber-optic illumination. Field of view 3.59 mm. Photomicrograph by Nathan Renfro.*

were present in the transparent pink-colored zone. Reflection of light from these parallel tubes caused the silvery white eye observed on the colorless side of the cabochon. The opposite side owes its pink chatoyancy to reflection from those same tubes inhabiting the near-colorless zone as the light is transmitted back through the pink transparent layer of tourmaline.

This is the second time we have encountered a tourmaline displaying different colors of chatoyancy on opposite sides of a double cabochon. In order to enjoy both eyes, such a stone should be set as a pendant in a simple bezel with a swivel, allowing exposure of either the pink or the silvery white cat's eye as desired.

*John I. Koivula*


ABOUT THE EDITORS

*Nathan Renfro is the analytical manager of the gem identification department and analytical microscopist in the inclusion research department at GIA in Carlsbad, California. Mr. Renfro holds a degree in geology and a Graduate Gemologist diploma (GIA) and is a Fellow of the Gemmological Association of Great Britain (FGA). He has authored and co-authored numerous gemological articles and has particular interests in inclusion identification and lapidary arts.*

*Elise A. Skalwold, an Accredited Senior Gemologist of the American Gemological Association (AGA), is involved in curating and research at her alma mater, Cornell University. A Graduate Gemologist and Diploma Merit graduate of the Gemmological Association of Great Britain, she has written gemological and mineralogy-related articles, as well as the book* The Edward Arthur Metzger Gem Collection. *Her primary interests are inclusions, crystallography, and optical mineralogy.*

*John I. Koivula is the analytical microscopist at GIA and a Fellow of the Royal Microscopical Society. A mineralogist, chemist, and gemologist with more than 40 years of experience, he is a world-renowned inclusion expert and photomicrographer. In addition to hundreds of articles and peer-reviewed scientific papers, Mr. Koivula is author of* The MicroWorld of Diamonds *and co-author of the three-volume* Photoatlas of Inclusions in Gemstones, *which features over 5,000 of his unique photomicrographs.*


## Micro-World

The inner space of gem materials holds surprising and stunning vistas. Visit *G&G*'s photomicrograph gallery, an online exclusive, to view slideshows that delve deeper into the breathtaking world of gem inclusions.

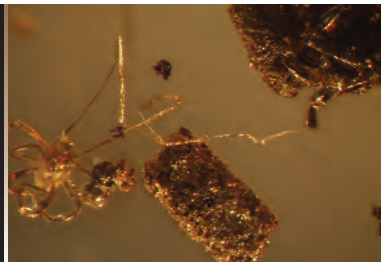

Visit www.gia.edu/gems-gemology/micro-world-gallery, or scan the QR code on the right.

# G&G Gem News International

**Contributing Editors**
Emmanuel Fritsch, *CNRS, Team 6502, Institut des Matériaux Jean Rouxel (IMN), University of Nantes, France* (fritsch@cnrs-imn.fr)
Kenneth Scarratt, *GIA, Bangkok* (ken.scarratt@gia.edu)

## DIAMOND

**Diamond-bearing eclogite xenoliths from the Ardo So Ver dykes.** Specimens of gem diamond crystals in rock matrix are almost never found due to the rigorous processing that occurs during diamond mining. Occasionally, a diamond is found in a sample of the kimberlite host rock that brought it to the surface, but finding a diamond in the rock in which it likely crystallized in the earth's mantle is extremely rare. When pieces of the mantle break off and are transported to the surface in a kimberlite magma, they are called *xenoliths* (meaning "foreign rock," because the mantle rocks are not formed from the kimberlite magma itself).

Recently, five small rock samples containing diamond crystals (figure 1) were sent to GIA Research for examination. The samples were submitted by Charles Carmona (Guild Laboratories, Los Angeles) on behalf of owners Jahn Hohne (Ekapa Mining, Kimberley, South Africa) and Vince Gerardis (an occasional trader and collector of unique diamonds and producer of the television series "Game of Thrones"). The specimens were sourced over 25 years ago from a kimberlite fissure mine located 40 miles (65 km) northwest of Kimberley, South Africa. The So Ver mine is located in a group of narrow kimberlite dykes discovered in the 1940s, known as the Ardo dykes, that intruded into Ventersdorp lavas and overlying Karoo shales (M. Field et al., "Kimberlite-hosted diamond deposits of southern Africa: A review," *Ore Geology Reviews*, Vol. 34, 2008, pp. 33–75).

Mineralogical examination using microscopy and Raman spectroscopy revealed that the rocks were composed primarily of garnet and clinopyroxene and would be classified as eclogite xenoliths (figure 2). In simple terms, eclogites are metamorphic rocks, typically created when basaltic crust from the ocean floor is subducted deep into the earth's mantle where high temperatures and pressures cause chemical reactions that change the basaltic minerals into garnet and clinopyroxene. Eclogites, along with peridotites, are considered the most common mantle host rocks for diamond crystallization. EDXRF chemical analysis of the garnets and clinopyroxenes in these samples showed pyrope mole fractions up to about 49% and jadeite mole fractions up to approximately 31%. These results are consistent with other reported diamond-bearing eclogites (T.F. Fung and S.E. Haggerty, "Petrography and mineral compositions of eclogites from the Koidu Kimberlite Complex, Sierra Leone," *Journal of Geophysical Research*, Vol. 100, 1995, pp. 20451–20473).

*Figure 1. These five diamond-bearing eclogite xenoliths from the Ardo So Ver dykes in South Africa ranged in weight from 2.24 to 12.40 grams, with the largest measuring 2.5 centimeters in length. Photo by Kevin Schumacher.*

*Editors' note: Interested contributors should send information and illustrations to Stuart Overlin at soverlin@gia.edu or GIA, The Robert Mouawad Campus, 5345 Armada Drive, Carlsbad, CA 92008.*

Gems & Gemology, Vol. 51, No. 2, pp. 198–219.

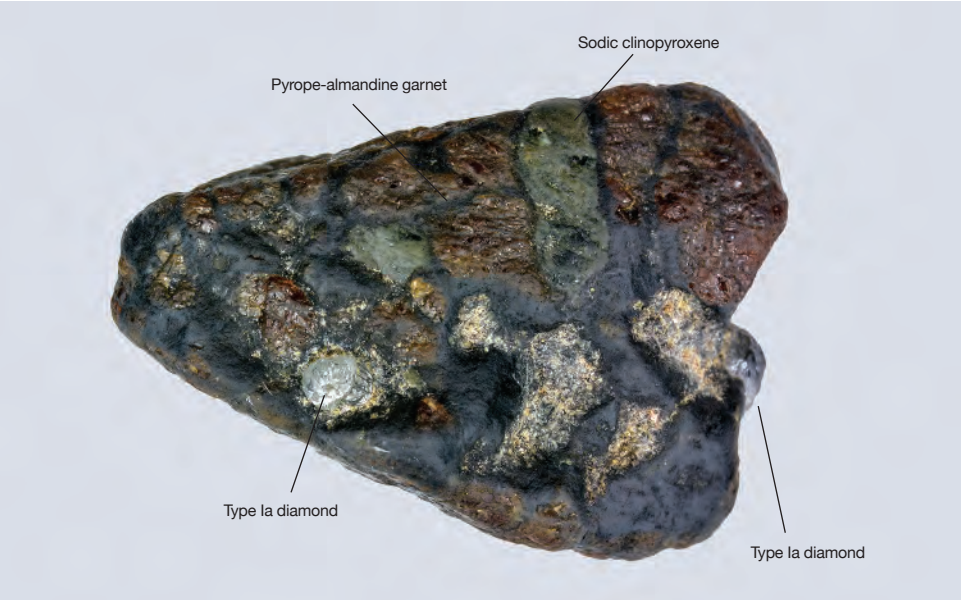


*Figure 2. The diamond-bearing xenoliths were composed of pyrope-almandine garnet and sodic clinopyroxene, classifying them as eclogites. Photo by Robison McMurtry.*

The diamond crystals in the xenoliths ranged from 1.5 to 4.0 mm in length, and were transparent and near-colorless to pale yellow (figure 3). They occurred as octahedral and combination forms with no visible resorption. No inclusions were visible within the crystals under 10× magnification. FTIR analysis (using an FTIR microscope in reflected light mode) revealed that all of the diamonds were type Ia with abundant nitrogen impurities. Three of the seven diamonds analyzed showed nitrogen impurities dominantly as A-aggregates in concentrations ranging from approximately 420 to 800 ppm.

The data provided here, along with additional ongoing work, will hopefully shed more light on the temperature, pressure, and depth in the earth's mantle where the diamonds crystallized.

*Christopher M. Breeding (christopher.breeding@gia.edu)*
*GIA, Carlsbad*

## COLORED STONES AND ORGANIC MATERIALS

**Cat's-eye calcite from Pakistan.** Cat's-eye calcites have been sold at auctions and gem shows for some years, but a gemological description of the material has not been published. Low-quality cat's-eye calcites do exist, such as blue calcites from Mogok, Myanmar, but their chatoyancy is weak. It was very surprising, therefore, to see sharp cha-

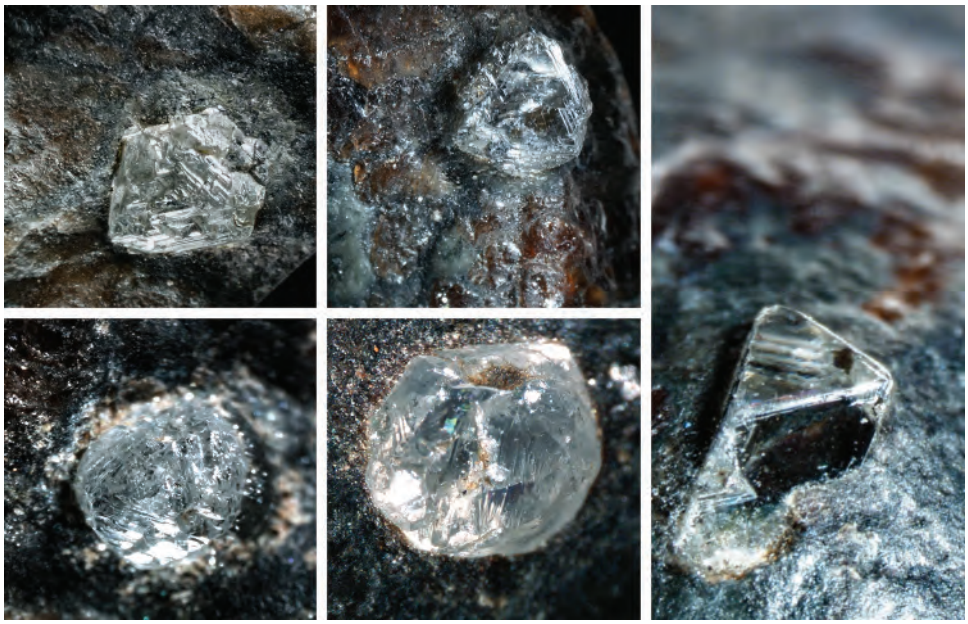

*Figure 3. Seven transparent, near-colorless to pale yellow gem diamonds (five shown in these photos) were observed in the eclogite samples, ranging in length from 1.5 to 4.0 mm. Photos by Christopher M. Breeding.*

*Figure 4. This 57.60 ct calcite from Pakistan shows a cat's-eye. Photo by Jaroslav Hyršl.*

toyancy on the beautiful calcite cabochon in figure 4.

The stone, purchased during the Tucson shows in February 2015, came from the Baluchistan province of Pakistan. It weighed 57.60 ct and measured 25.0 × 24.6 × 12.3 mm. It was light green and translucent, without eye-visible inclusions. The spot RI ranged from 1.48 to 1.66, and when rotated the cabochon showed a strong "blink" typical for carbonates. This is significant because the stone resembled chrysoprase; without the rotation, the measured RI in a given position might also approximate that of chrysoprase. There were no lines in the visible spectrum, the stone was inert under UV light, and its specific gravity was 2.72. Viewed in the polariscope, it remained bright, indicating a doubly refractive aggregate. Strong banding (figure 5) was present in the direction of chatoyancy, but the bands were inclined at about 20° angles. The bands were approximately 0.7 mm thick.

Only at 40× magnification did the cause of the chatoyancy become apparent. Numerous tiny needles perpendicular to the chatoyancy were likely evidence of a columnar to needle-like texture. Other than the chatoyancy, this specimen is similar in appearance to the green and orangy yellow calcites from Pakistan that were described in the Fall 2012 GNI section (pp. 217–218). It is the opinion of both the seller and the author that this calcite is from the same locality.

*Figure 5. Banding in chatoyant calcite from Pakistan, as seen through the bottom of the cabochon. Photo by Jaroslav Hyršl.*

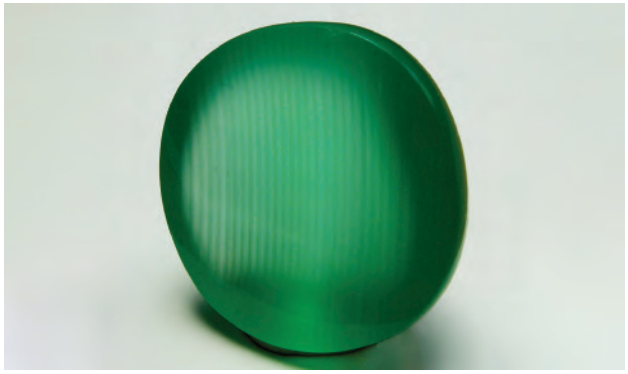

*Figure 6. This emerald from Itabira–Nova Era in Minas Gerais weighs approximately 43 ct (approximately 25.30 × 18.10 × 13.75 mm) making it one of the largest Brazilian cat's-eye emeralds examined by the Gübelin Gem Lab. Photo by Janine Meyer.*

*Jaroslav Hyršl (hyrsl@hotmail.com)*
*Prague*

**Large cat's-eye emerald from Brazil.** Gübelin Gem Laboratories (GGL) in Hong Kong and Lucerne recently had the opportunity to examine a translucent emerald, weighing approximately 43 ct, that exhibited a pronounced and well-centered chatoyancy (figure 6). The stone had a spot RI of 1.57 and a hydrostatic SG of 2.73, and it was inert under long- and short-wave UV radiation. Microscopic observation in reflected and transmitted light presented a series of dense elongated, rectangular, and square multiphase inclusions (figure 7).

The UV-Vis absorption spectra showed the characteristic $Cr^{3+}$- as well as $Fe^{2+}$- and $Fe^{3+}$- related bands. In the FTIR absorption spectra, type I and type II water molecules were observed. An intense band at around 2360 $cm^{-1}$ indicated the presence of $CO_2$, most likely in the multiphase inclusions. Trace-element analysis of the sample with laser ablation–inductively coupled plasma–mass spectrometry (LA-ICP-MS) showed contents consistent with schist- and pegmatite-related emeralds. It also showed lower Li, Cs, and Rb than in emeralds related to highly evolved pegmatites, such as those from Sandawana (Zimbabwe) and Kafubu (Zambia); see J.C. Zwaan et al., "Emeralds from the Fazenda Bonfim region, Rio Grande do Norte, Brazil," Spring 2012 *G&G*, pp. 2–17. The stone's composition was consistent with emeralds from Itabira–Nova Era, Minas Gerais, based on GGL's reference collection and the published literature on the pegmatites of the area (C. Preinfalk et al., "The pegmatites of the Nova Era–Itabira–Ferros pegmatite district and the emerald mineralisation of Capoeirana and Belmont (Minas Gerais, Brazil): geochemistry and Rb-Sr dating," *Journal of South American Sciences*, Vol. 14, No. 8, 2002,

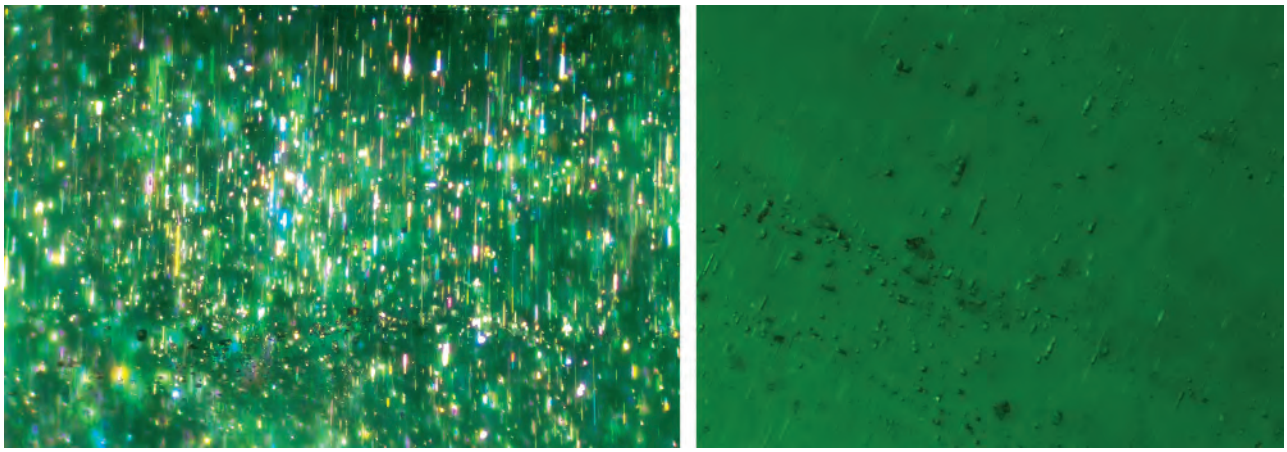

*Figure 7. Multiphase inclusions of different shapes and sizes, seen in reflected light (left) and brightfield illumination (right), gave rise to the cat's-eye effect in the Brazilian emerald. Photomicrographs by Wenxing Xu (left) and Stefanos Karampelas (right). Image width 2 mm (left) and 1.2 mm (right).*

pp. 867–887). This exceptional stone is one of the largest Brazilian cat's-eye emeralds examined by GGL to date.

*Stefanos Karampelas (Stefanos.Karampelas@gubelingemlab.com), Lore Kiefert, and Wenxing Xu*
*Gübelin Gem Lab, Lucerne, Switzerland*

**Nonbead-cultured pearls from *Strombus gigas*.** Among the saltwater porcelaneous (non-nacreous) pearls, those of *Strombus gigas* gastropods are probably the best known among jewelers and collectors because of their vivid to pastel colors ranging from pink to white to brownish. Also known as "pink pearl," "conch pearl," or "Queen conch pearl," this material was used extensively in Art Deco jewelry, and many designers are now incorporating them into modern pieces. Various articles and books have described the extraordinary beauty, use and related traditions, and early attempts at cultivation of pink pearls (see E. Fritsch and E. Misiorowski, "The history and gemology of the queen conch 'pearls'," Winter 1987 *G&G*, pp. 208–231). The typical structure responsible for the sought-after "flame pattern" was detailed extensively a decade ago (S. Kamat et al., "Structural basis for the fracture toughness of the shell of the conch *Strombus gigas*," *Nature*, Vol. 405, No. 6790, 2000, pp. 1036–1040; H. Hänni, "Explaining the flame structure of non-nacreous pearls," *The Australian Gemmologist*, Vol. 24, No. 4, 2010, pp. 85–88). Found in the Caribbean region, where *Strombus gigas* live and are fished for meat, the pearls had no documented cultured counterpart until the work of Hector Acosta-Salmon and Megan Davis at Florida Atlantic University in 2009.

The Laboratoire Français de Gemmologie (LFG) recently had the opportunity to analyze a parcel of eight samples, presented as cultured conch pearls, from a new farm based in Honduras (figure 8). The colors ranged from white and pinkish white to yellowish orange. The shapes varied from oval to baroque, and weights ranged from 0.21 ct (2.7–3.4 × 4.1 mm) to 3.13 ct (6.5–7.6 × 9.3 mm). Their luster was porcelaneous, and the surface was very smooth and homogenous with no defects. Almost all the samples possessed a typical but subtle flame pattern (figure 9).

*Figure 8. These two nonbead-cultured pearls (1.40 and 2.22 ct) from a parcel of eight specimens produced by* Strombus gigas *show a light pink and yellowish orange color with a discreet flame pattern. Photo by Olivier Segura.*

*Figure 9. These six nonbead-cultured pearls from* Strombus gigas *range from 0.21 to 3.13 ct. Inset: Detail of a 0.47 ct pearl, showing a typical thin flame pattern. Photo by Olivier Segura.*

Initial examination revealed no indication of the culturing process, but X-radiography analysis left no doubt about the material's origin. The samples' inner structures revealed a darker central zone, suggesting a less dense material, typical of the graft remainder of the nonbead culture process (figure 10, left). This kind of pattern is not found in the natural conch pearls we have examined in the laboratory (figure 10, right).

According to the farm owners, queen conch pearl culture is undergoing intensive development, and the quality—size, flame pattern, and color—improves with each harvest. While current laboratory techniques are adequate to unambiguously identify nonbead cultured pearls from *Strombus gigas*, the LFG has established a close working relationship with the pearl farm, paying close attention to possible developments in their distinctive inner structures.

*Olivier Segura (o.segura@bjop.fr)*
*Laboratoire Français de Gemmologie (LFG), Paris*
*Emmanuel Fritsch*

**Purple scapolite.** Two brownish purple faceted specimens (figure 11) were submitted for identification at the Gem Testing Laboratory, Jaipur, India. The 2.95 ct mixed cushion measured 9.95 × 8.05 × 5.88 mm, while the 1.58 ct mixed oval measured 9.07 × 7.08 × 4.46 mm. Both were relatively clean to the unaided eye. Based on their color, theywere thought to be spinel, but testing soon proved otherwise. Testing yielded the following gemological properties: optic figure—uniaxial; RI—1.549–1.559; birefringence—0.010; and hydrostatic SG—2.63. The material fluoresced a weak orangy red under short-wave UV and was inert under long-wave UV. An absorption band was observed in the yellow-green region using a desk-model spectroscope. In addition, both samples displayed strong dichroism (figure 12) with deep saturated and pale purple colors along the "o" and "e" rays, respectively; this also influenced their face-up color. Under magnification, growth zones and two-directional cleavage planes intersecting at almost 90° were visible. The cleavage planes also contained some fine dendritic films; additionally, the oval specimen had an unidentified brown crystal.

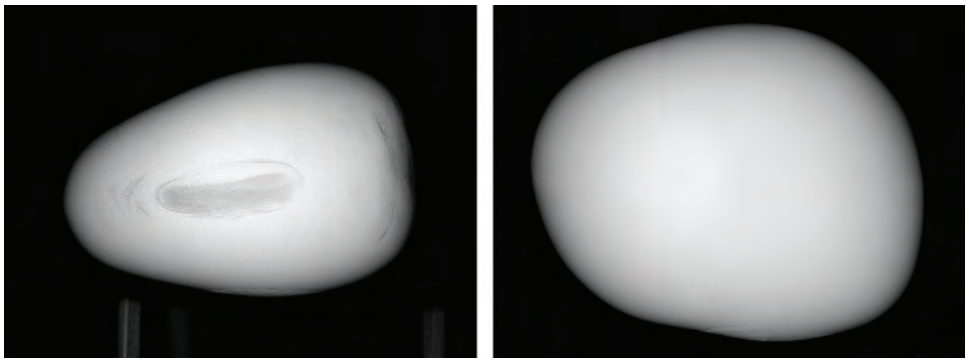

*Figure 10. Left: An X-ray of the pearl seen in the figure 9 inset. It shows clear evidence of a nonbead culturing process. Right: An X-ray of a natural conch pearl. Images by Olivier Segura.*

*Figure 11. These two brownish purple specimens, a 1.58 ct oval and a 2.95 ct cushion, were identified through gemological testing as scapolite. Photo by Gagan Choudhary.*

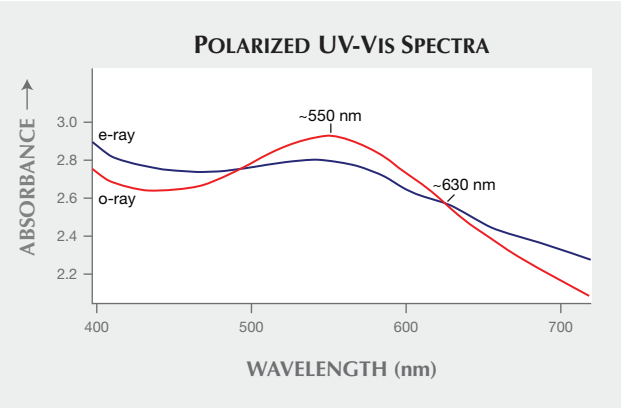


*Figure 13. Polarized UV-Vis spectra of the cushion-cut scapolite (shown here in the cushion) displayed Fe-related absorption at approximately 550 nm, which is responsible for the purple color of these specimens.*

These gemological properties were consistent with scapolite. Raman spectroscopy confirmed this, showing the characteristic peaks for scapolite at approximately 260, 296, 359, 418, 455, 534, 771, 993, and 1093 $cm^{-1}$. The Raman spectra suggested the specimens belonged to the marialite end of the meionite-marialite solid solution series of the scapolite group (see rruff.info); this was supported by their RI and SG values (R. Webster, *Gems: Their Sources, Descriptions and Identification*, 5th ed., rev. by P.G. Read, Butterworth-Heinemann, Oxford, UK). Polarized absorption spectra (figure 13) revealed a broad absorption centered at approximately 550 nm in both specimens. The intensity of this absorption was stronger in the o-ray direction, while a weak hump at about 630 nm was also present in the e-ray direction. Such absorption bands, associated with $Fe^{3+}$ ions and producing purple coloration, have been reported in sugilite (Spring 1995 GNI, pp. 66–67); however, additional $Fe^{3+}$ features at approximately 350–365 and 410–420 nm were absent in both the "e" and "o" rays of those specimens. Qualitative EDXRF analysis revealed the presence of Al, Si, K, Ca, Fe, Br, and Sr. Mn is a common impurity resulting in purple coloration of stones such as kunzite or some sugilites, but it was not detected in these specimens. On the basis of absorption spectra and elemental analysis, the purple color of these scapolites appears to be caused exclusively by an Fe impurity.

Purple scapolite is known from many localities such as Myanmar, Tanzania, and Tajikistan, but the client did not know the source of these stones. Although we have seen many purple to violet scapolites in the past, these specimens were different because of their brown color component, reminiscent of spinel.

*Gagan Choudhary (gagan@gjepcindia.com)*
*Gem Testing Laboratory, Jaipur, India*

## SYNTHETICS AND SIMULANTS

**Synthetic sapphire with diffusion-induced color and star.** The Dubai Central Laboratory recently examined an asteriated blue oval cabochon that weighed 24.58 ct and measured 17.37 × 14.61 × 9.59 mm. The client submitted the sample for an identification report and origin determination.

The cabochon appeared to be completely transparent, evenly colored, and clean. Fiber-optic lighting revealed two sharp, six-rayed white stars with long, straight arms of

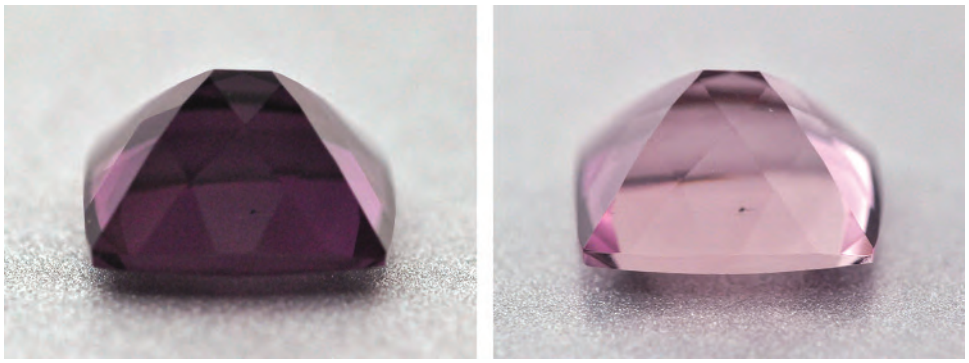

*Figure 12. The scapolite specimens displayed intense dichroism (shown here in the cushion), with a deep saturated purple along the o-ray (left) and pale purple along the e-ray (right). Photos by Gagan Choudhary.*

*Figure 14. This 24.58 ct star cabochon was a colorless synthetic sapphire whose color and star had been induced by diffusion treatment. Photo by Sutas Singbamroong.*

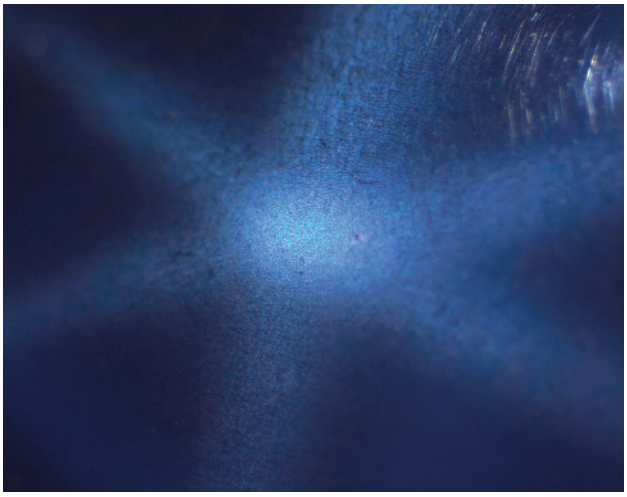

*Figure 16. Very fine oriented needle-like inclusions causing the star were confined to a shallow layer below the surface. Photomicrograph by Sutas Singbamroong, magnified 25×.*

equal length. The stars seemed to float over the dome surface with internal reflection from the base, very similar to those typically seen in synthetic star sapphires (figure 14).

Standard gemological testing established the following properties: spot RI—1.76; pleochroism—distinct light green and bluish violet (viewed parallel to the girdle); hydrostatic SG—3.98; and fluorescence—inert to both long- and short-wave UV radiation. No characteristic absorption spectrum was seen with a desk-model spectroscope; a faint absorption band was observed at about 560 nm. These properties were consistent with sapphire, though the sample did not show the Fe line at 450 nm commonly seen in natural blue sapphire. Observation of the cabochon immersed in water with diffused transmitted light revealed shallow coloration and a colorless circular area of repolishing (figure 15). This suggested that the specimen owed its color to a diffusion process. The melted appearance of the cabochon's base confirmed that it had been subjected to the heat required for diffusion treatment. Microscopic examination showed only a few small melted fingerprint-like inclusions near the surface, and very fine oriented needle-like inclusions confined to a shallow layer below the surface (figure 16). No curved color banding or angular color zoning was present. Higher magnification indicated that the oriented needles were approximately 5–25 microns long. Further examination with immersion in methylene iodide between crossed polarizers, viewing parallel to the optic axis direction, uncovered the distinct Plato lines strongly indicative of Verneuil synthetic origin.

*Figure 15. Immersed in water and viewed with diffused transmitted light, the star cabochon showed shallow coloration with a colorless circular area of repolishing. This feature, along with the melted appearance of the base, indicated that the color and asterism had been produced by a diffusion process. Photo by Sutas Singbamroong.*

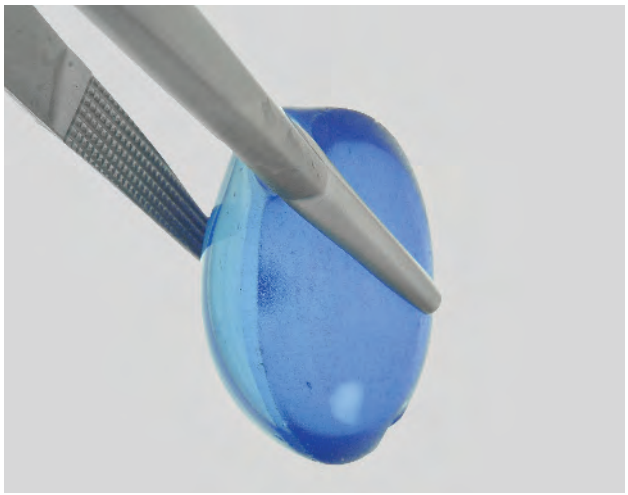

EDXRF chemical analysis revealed traces of Ti, Fe, and V; no Ga, Cr, or other trace elements were detected. Unoriented UV-Vis-NIR absorption spectroscopy showed two broad bands, one centered at about 330 nm due to $Fe^{3+}$ ions, and one with maxima at about 565 nm due to $Fe^{2+}$-$Ti^{4+}$ intervalence charge transfer (figure 17). No $Fe^{3+}$-related sharp bands at approximately 375, 390, and 450 nm were seen.

This combination of properties and features indicated that colorless synthetic sapphire was used as a starting material, and both the color and the asterism were produced by a diffusion process.

*Sutas Singbamroong (sssutas@dm.gov.ae), Nazar Ahmed, and Nahla Al Muhairi*
*Gemstone Unit, Dubai Central Laboratory*
*Dubai, United Arab Emirates*

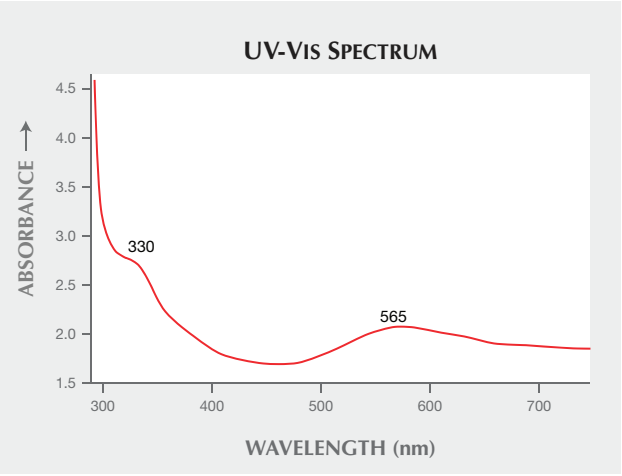


*Figure 17. An unoriented UV-Vis-NIR spectrum of the diffusion-induced star synthetic sapphire exhibited two broad bands centered at about 330 and 565 nm, the latter of which is typically responsible for sapphire color.*

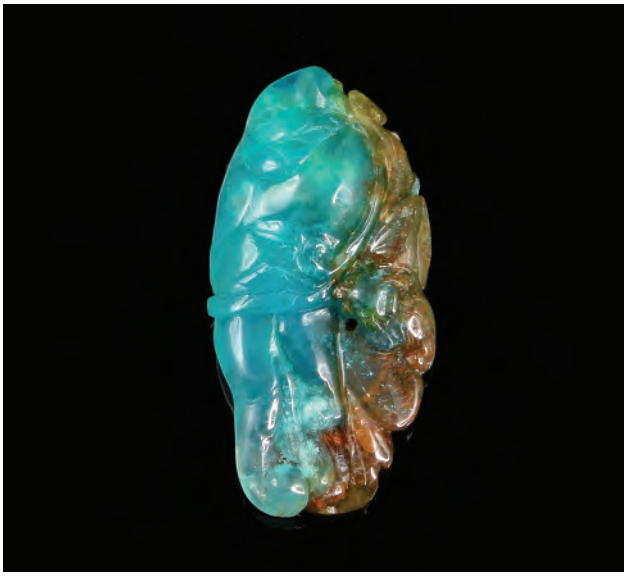

*Figure 18. The eye-catching carving weighing 18.43 ct and measuring 31.7 × 15.7 × 7.6 mm, submitted for identification as blue chalcedony. Photo by Larry Tai-An Lai.*

## TREATMENTS

**Blue chalcedony partially filled with epoxy resin.** Blue chalcedony is one of Taiwan's most famous stones; there, high-quality blue chalcedony is sometimes prized as much as jadeite jade. Compared with production from sources such as the United States, Indonesia, Peru, Mexico, and Chile, chalcedony from DuLan Mountain in Taitung, in southeast Taiwan, reveals fine texture and a saturated blue color. Locals and tourists collect the stone as it symbolizes the national spirit, and its value seems to rise year after year.

Local merchants often sell blue chalcedony under the name "Taiwanese blue sapphire," leading to confusion among consumers who believe they are purchasing sapphire. Imitations and treatments are also of concern in the market, with blue opal the most likely imitation to confuse would-be purchasers at first glance. Dyed quartzite and dyed chalcedony also rank among the more common imitations encountered.

The Lai Tai-An Gem Lab in Taipei recently received for identification an 18.43 ct carving measuring 31.7 × 15.7 × 7.6 mm (figure 18). The client claimed the uneven blue and brown translucent item was blue chalcedony. The spot RI of 1.53, SG of 2.55, and FTIR results were consistent with published values for blue chalcedony. Raman peaks at 120, 196, 461, and 499 $cm^{-1}$ (figure 19) confirmed the identity but displayed additional peaks not related to blue chal-

*Figure 19. Raman peaks at 120, 196, 461, and 499 $cm^{-1}$ matched the pattern expected for blue chalcedony.*

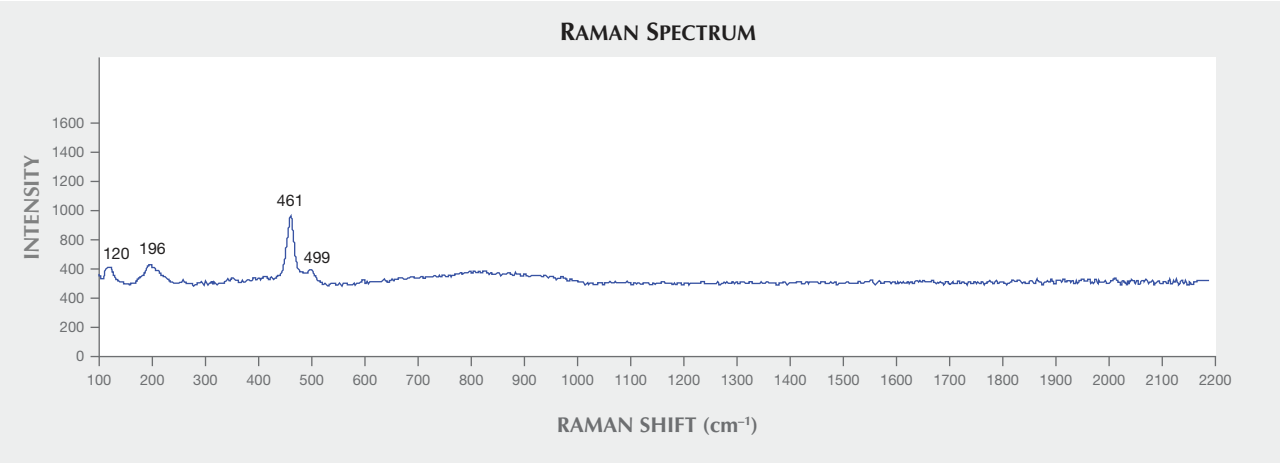

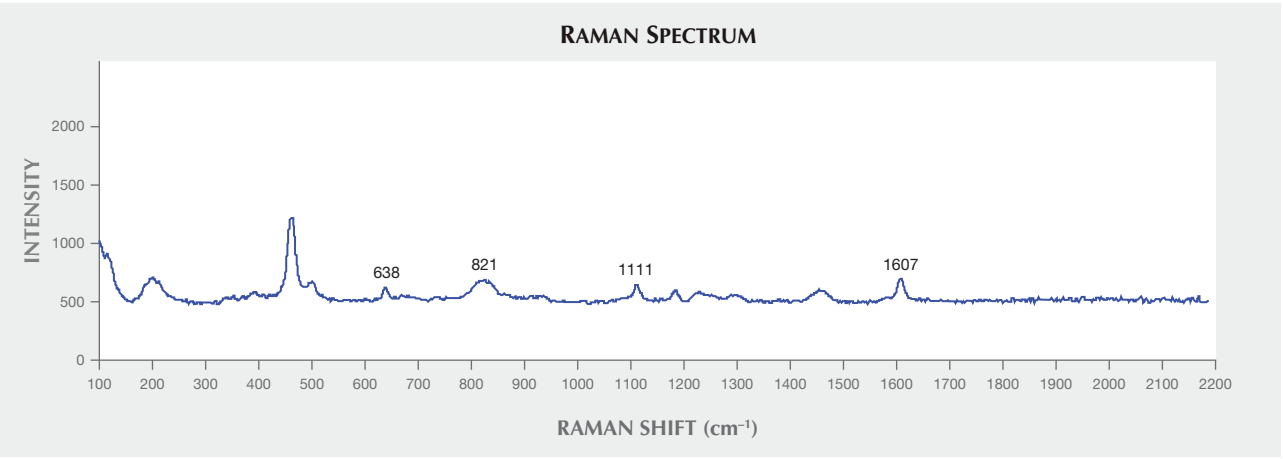


*Figure 20. The blue chalcedony's Raman peaks at 638, 821, 1111, and 1607 $cm^{-1}$ matched those expected for epoxy resin.*

cedony (figure 20). Examination with a gemological microscope at 40× magnification, which was increased in increments up to 60×, revealed a structure consistent with blue chalcedony but also explained the source of the suspicious Raman peaks: numerous clear bubbles of different sizes at the border of the blue- and brown-colored areas, as seen in figures 21 and 22. The evidence pointed to an epoxy resin as the foreign material; a moderate blue reaction under long-wave UV seemed to confirm a partially filled portion on the carving. Additional Raman analysis on the area in question showed peaks at 638, 821, 1111, and 1607 $cm^{-1}$ (again, see figure 20), as expected for epoxy resin.

In our experience, blue chalcedony is seldom treated, and such treatment is usually applied to repair or conceal cavities or fractures. Even when a filling is only partial, as in this example, traders should disclose any treatments to their clients.

*Figure 21. Numerous transparent bubbles of different sizes were visible within a treated portion of the blue chalcedony carving at the border of the blue and brown areas. Photo by Larry Tai-An Lai; inset magnified 60×.*

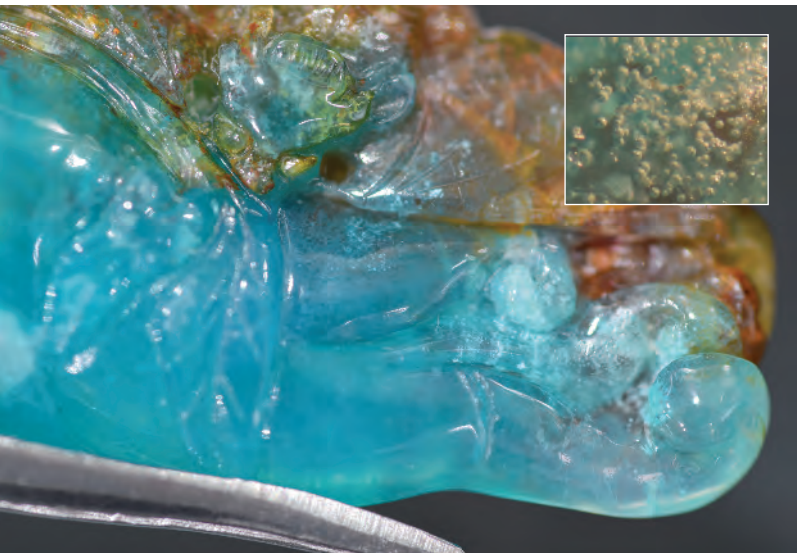

*Larry Tai-An Lai (service@laitaian.com.tw)*
*Lai Tai-An Gem Laboratory, Taipei*

**An unusual filled ruby.** A 12.12 ct corner-cut rectangular red stone (figure 23) was submitted to the Laboratoire Français de Gemmologie (LFG) for analysis. The sample's refractive index, specific gravity, and Raman spectrum confirmed its identity as a ruby. It fluoresced a medium to strong red in long-wave UV radiation, and a weaker red in short-wave UV. Under magnification, it showed fairly dense accumulations of long needles, some of them rather flat and most of them iridescent (figure 24). Many parallel twin lamellae crossed the gem (figure 25). There was no indication of thermal enhancement. The inclusions and chemical composition were consistent with ruby from Myanmar.

*Figure 22. The epoxy resin area as seen through a gemological microscope. Photo by Larry Tai-An Lai; magnified 40×.*

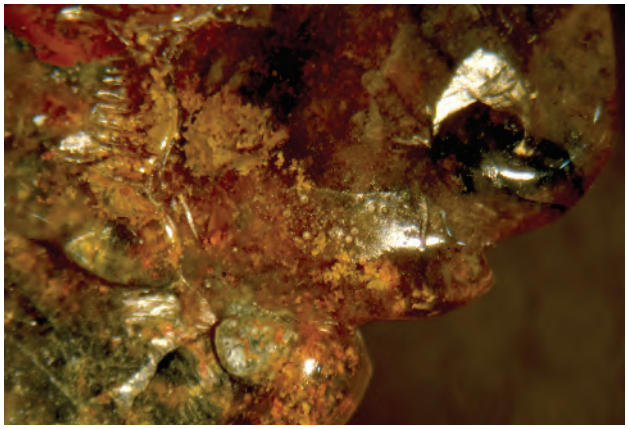

*Figure 23. This 12.12 ct red stone showed features typically associated with a natural ruby. Photo by A. Droux/LFG.*

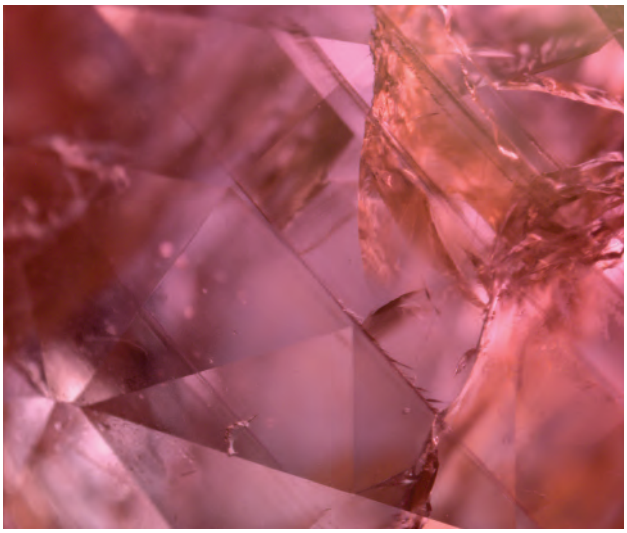

*Figure 25. Contrasted twin lamellae in this ruby are similar to those often observed in material from Myanmar. Photomicrograph by A. Droux/LFG; magnified 60×.*

Many fractures were apparent, with smaller ones following the twin lamellae. Examining the surface of the fissure, it became apparent that some material was present inside the fractures, and in some locations had left a whitish trace in the fracture close to the surface. Deeper within the fractures there were flat bubbles and networks of cracks similar to those seen in drying mud, with a somewhat dendritic aspect.

*Figure 24. Dense accumulations of iridescent needles were visible within the red stone. Photomicrograph by A. Droux/LFG; magnified 50×.*

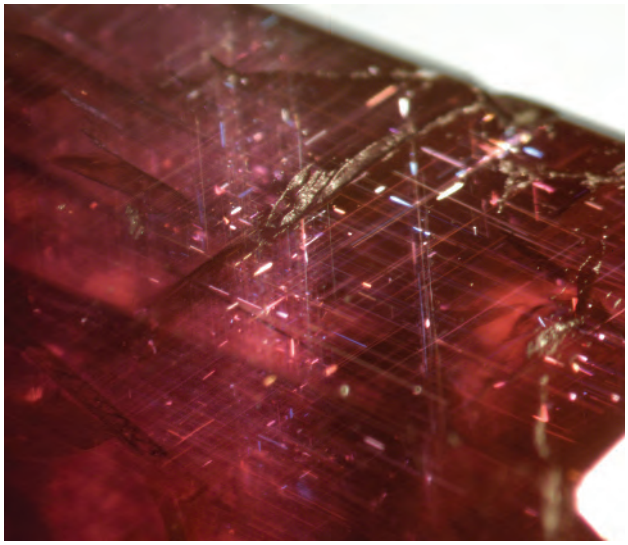

These same patterns were observed with the drying of oil in emerald (H. Hänni, "Gemmology, an oil well in your garden?" *Schweizer Uhren & Schmuck Journal*, No. 3, 1988, pp. 461–464; H. Hänni et al., "How to identify fillings in emeralds using Raman spectroscopy," *Jewellery News Asia*, No. 145, 1996, pp. 154–156). Under the heat of the optical fiber used for observation, some droplets formed at the outcrop of the fissure, indicating that the material was either liquid or had a melting point just above room temperature, suggesting that the filler could be either oil or wax.

Exposure to the ultra-short UV wavelength of the DiamondView revealed the filling material inside the fractures (figure 26). Infrared absorption confirmed the presence of an organic material in the fractures (figure 27). "Oil" peaks at about 2852, 2925, and 2955 $cm^{-1}$ were at positions nearly identical to those observed for oil-impregnated emerald (P. Zecchini and P. Maitrallet, "Que peut apporter la spectrographie infrarouge dans l'étude des émeraudes?" In D. Giard, Ed., *L'émeraude: Connaissances Actuelles et Prospectives*, Association Française de Gemmologie, Paris, 1998, pp. 81–96; M. Johnson et al., "On the identification of various emerald filling substances," Summer 1999 *G&G*, 82–107). The peaks were accompanied by sharp features around 3600–3700 $cm^{-1}$, attributed to kaolinite group minerals (A. Beran and G. Rossman, "OH in naturally occurring corundum," *European Journal of Mineralogy*, Vol. 18, 2006, pp. 441–447). The band at 2463 $cm^{-1}$ was produced by $CO_2$.

On the basis of microscopic observation and infrared spectroscopy, we concluded that the ruby showed moderate indications of clarity enhancement—with oil, in this case. Although glass-filled rubies are common on the market today, oiled corundum is much rarer. This oiled

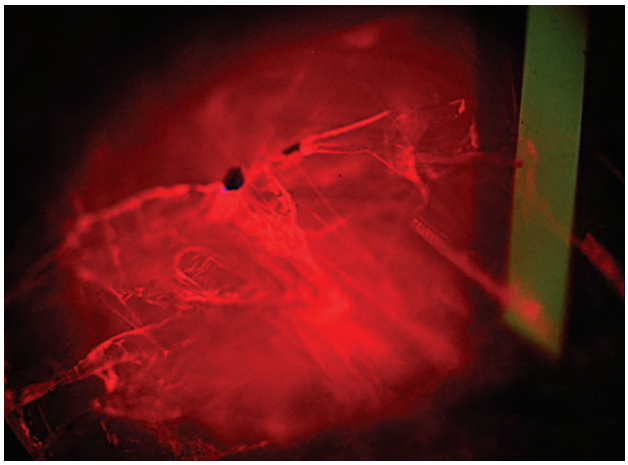

*Figure 26. DiamondView imaging of the ruby showed the filling of fractures. Image by A. Droux/LFG.*

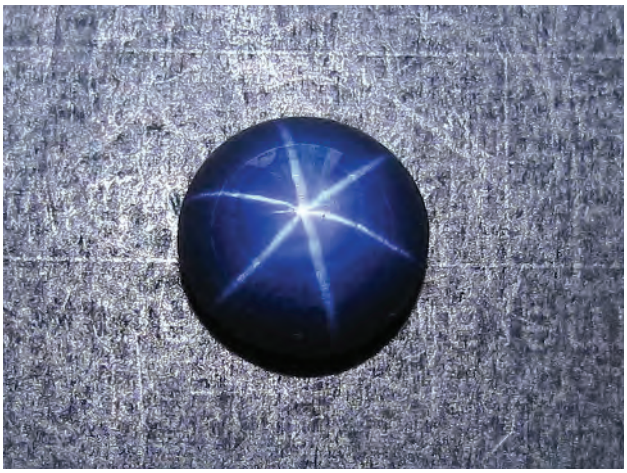

*Figure 28. This 8.975 ct specimen was identified as synthetic star sapphire. Photo by Pragati Verma.*

ruby was also unusual for its size and evidently Burmese origin.

*Alexandre Droux (a.droux@bjop.fr)*
*Laboratoire Français de Gemmologie (LFG), Paris*
*Emmanuel Fritsch*

**Unusual combination of inclusions in synthetic star sapphire.** Recently, an 8.975 ct blue oval cabochon exhibiting asterism (figure 28) was submitted to the Indian Gemological Institute – Gem Testing Laboratory in Delhi for identification. Standard gemological testing revealed a spot RI of 1.76 and hydrostatic SG of 4.00. These properties were consistent with sapphire.

Microscopic examination at 25× magnification showed three-directional "needles" intersecting at 60°/120° angles (figure 29). Under 60× magnification, the three-directional needles appeared as a series of dots. The expected solid rutile needles were not resolved at the magnification used. These three-directional needles were further surrounded by a coarse hexagonal boundary (again, see figure 29) made up of gas bubbles (figure 30, left). The presence of the hexagonal boundary initially led to an impression of natural origin, but the presence of gas bubbles and chalky blue fluorescence under SWUV confirmed a synthetic origin. These three-directional needles (series of dots intersecting at 60°/120° angles) with possibly unresolved rutile needles are responsible for the six-rayed asterism. When the stone was checked in the DiamondView, it showed a dark blue ring around the gas bubbles (figure 30, right). This was the first time this author had seen such a reaction to gas bubbles in a synthetic material in the DiamondView.

*Figure 27. Infrared spectrum of the ruby showing the same absorptions as for the filling of some emeralds.*

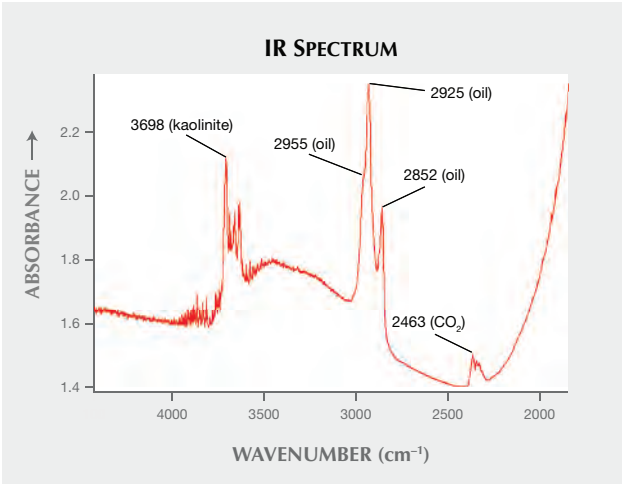


*Figure 29. Three-directional needles intersecting at 60°/120° angles. Also notice the coarse hexagonal boundary created by the gas bubbles surrounding the three-directional needles. Photomicrograph by Meenakshi Chauhan; field of view 11.30 mm.*

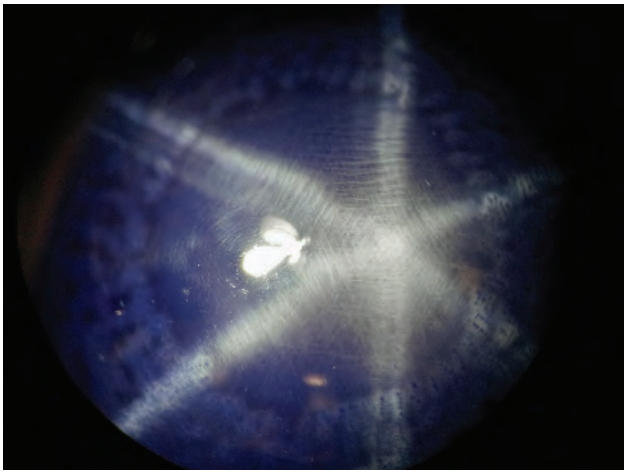

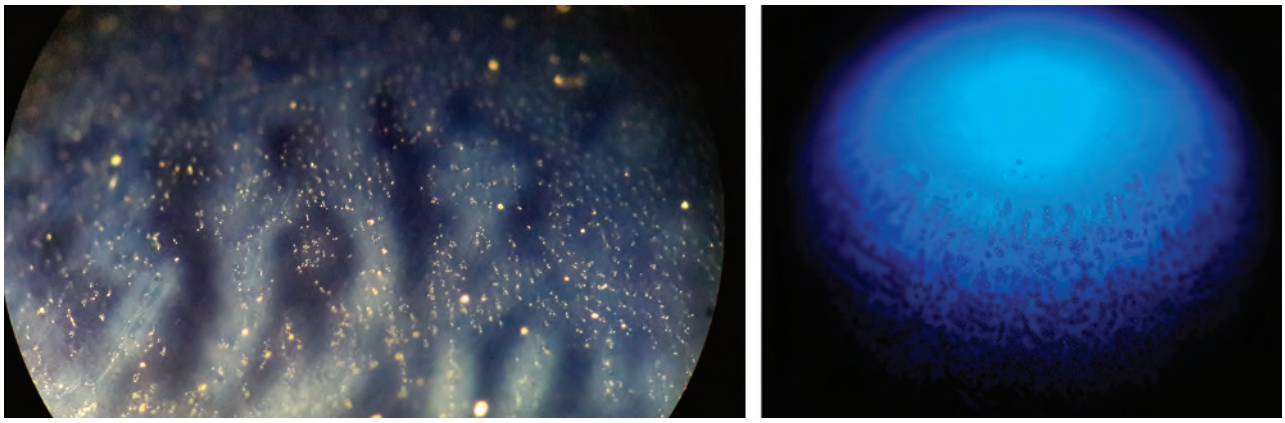

*Figure 30. Left: Gas bubbles appearing as whitish dots under 50× magnification. Right: DiamondView imaging of the gas bubbles. Notice the dark blue areas visible around the gas bubbles, which were inert to UV. This may indicate compositional variation where the whitish and dark areas are visible in the left-hand image. Photomicrograph and DiamondView image by Pragati Verma.*

The three-directional intersecting needles that give rise to asterism in synthetic sapphire are a by-product of the titanium oxide added in the feed material for crystal growth. As mentioned above, the three-directional needles observed here were actually resolved microscopically as a series of dots, and the expected rutile needles were not observed. After growth, the boule was likely reheated, causing the previously disseminated titanium oxide to precipitate out as needles of rutile (R. Webster, *Gems: Their Sources, Descriptions and Identification*, 5th ed., rev. by P.G. Read, Butterworth-Heinemann, Oxford, UK).

When the sample was viewed in transmitted light, it appeared transparent in the center but translucent from the sides, resembling an eye (figure 31). No gas bubbles were visible in the center of the cabochon, but there were increasingly higher concentrations of gas bubbles toward the edges. Under SWUV, this material showed chalky blue fluorescence confined to the central transparent part. Such hexagonal patterns were previously reported in synthetic sapphire in *G&G* (Summer 2007 GNI, pp. 177–178). While observing any stone, one must not consider a single inclusion or characteristic, such as the hexagonal boundary observed here, as an indicator of natural or synthetic origin. There must be a thorough examination of all inclusions and properties (in this case, gas bubbles and chalky blue fluorescence under SWUV) to conclude the origin of a material.

*Figure 31. Under fiber-optic light, the material showed an eye-like pattern, with a pink and transparent center and blue and translucent sides. Also notice the hexagonal boundary made from the gas bubbles. Photomicrograph by Pragati Verma; field of view 22.94 mm.*

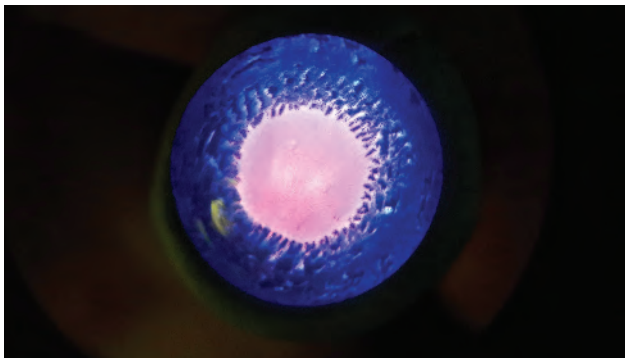

*Pragati Verma (igi@gjepcindia.com)*
*Indian Gemological Institute – Gem Testing Laboratory, Delhi*

## MORE FROM TUCSON 2015

**Diamond slices.** Gem and mineral slices were very popular at this year's Tucson shows, with opaque, translucent, clear, included, rough-edged, and finely shaped slices found in every color and price point. Materials such as fossilized coral, rutilated quartz, lacy agates, labradorite, chalcedony, watermelon tourmaline, sapphire, and diamond were on display. A wide variety of sizes were available as well, with pieces measuring several centimeters in diameter finding their way into dramatic necklaces, while some high-end jewelry and collector pieces used extremely thin and small gem slices.

Notably, the third-place winner in the bridal category of the 2015 AGTA Spectrum Awards was a pair of platinum and diamond earrings designed by Michael Endlich, featuring three pairs of diamond slices in addition to several pavé-set diamonds (figure 32). Endlich finds this gem material unusual, exciting, and subtle. Most of his clients have never seen these slices and are fascinated once they

*Figure 32. These AGTA Spectrum Award–winning earrings, designed by Michael Endlich, incorporate three matched pairs of diamond slices totaling 7.07 carats into a platinum setting. Photo courtesy of Michael Endlich.*

realize they are looking at diamonds. He goes through thousands of slices to select those he will incorporate into pieces. He particularly likes slices with patterns, such as concentric squares. This material is relatively new to the marketplace, and he first came upon it six years ago. Even though more diamond dealers offer them today, few slices have the distinct patterns Endlich looks for.

At the GJX show, Punya Malpani (Dynamic International, Hong Kong) discussed the diamond slice market with us and shared some particularly eye-catching and rare examples. He noted that the price of these goods has gone up approximately 20× in the past decade, as jewelry designers continue to go beyond traditional faceted gem shapes. There is also a strong collectors' market for this material,

*Figure 33. The three-rayed "trapiche" pattern is found in less than 0.1% of diamond slices, and rarely is it so distinct. The collection of nine slices, including these four samples, took years to assemble. Photo by Jennifer Stone-Sundberg, courtesy of Dynamic International.*

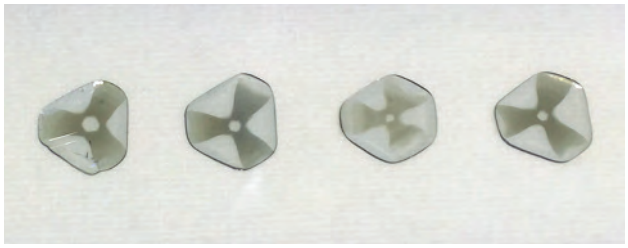

*Figure 34. These two large colorless diamond slices from the same piece of rough show dramatic patterning. Photo by Duncan Pay, courtesy of Dynamic International.*

as the unique nature of each piece adds to its appeal. In fact, there are very few larger slices of diamond in the marketplace, because the outer "skin" from the rough material was generally discarded before this niche market was identified. Unlike faceted diamonds, inclusions increase the value of slices, especially if they are unusual, striking, and highlight growth patterns.

Diamond slices today are mainly cut by laser and can vary widely in diameter and thickness, though diameters greater than one centimeter are difficult to come by, as rough in that size is much rarer. Many slices are slightly faceted to add some sparkle to the finished piece. Most of the diamond slices maintain the rough outline, as this can add to the appeal, but some are shaped into fanciful and matched sizes such as the "snowflakes" Malpani showed us.

Three-rayed "trapiche" diamond slices are among the most scarce and striking, as they contain a recognizable radiation-symbol pattern (figure 33). These are only found about once in a couple of thousand slices, and even then it is rare to find distinct coloring. The collection shown in the photo took years to assemble.

Malpani's most prized slices are the matched pair of large colorless diamond slices with dramatic white patterning (figure 34). These two pieces, separated from a skin cut of a large piece of rough, date back about 20 years. This is unusual, as such slices were not retained in the past.

It appears that the use of gem slices in jewelry has penetrated the high-end market. Since diamond is clearly a prominent material capitalizing on this gem "cut" with natural appeal, we can expect this trend to continue.

*Jennifer Stone-Sundberg*
*(jennifer@crystal-solutions.net)*
*Portland, Oregon*

**Large Namibian demantoid garnet.** At the GJX show, Stefan Reif (Tsuen Wan, N.T., Hong Kong), showed us an 11.63

ct round brilliant demantoid garnet. It was an exceptional stone of intense vibrant green with a touch of blue (figure 35, second from the left). According to Reif, the original rough weighed approximately 46 ct—about 9 grams—making the yield a little over 25%. This is an exceptionally large gem for Namibia's Green Dragon mine, where the bulk of production is suitable for small calibrated gems.

Namibian demantoid was first discovered in the 1990s (Fall 1997 GNI, pp. 222–223). The current production came from an open-pit, hard rock mine with an annual production between 5,000 and 10,000 carats. According to Reif, the local geology includes marble, pegmatite, and rhyolite. The distribution of demantoid pockets within these rocks is irregular and difficult to predict. Beside the geological challenges, water is scarce, and temperature extremes range from freezing at night to baking desert heat in the daytime.

The Green Dragon mine is renowned for its production of well-proportioned rough. This material is suitable for cutting smaller gems into 2–3 mm sizes in a range of colors from slightly bluish green (top color) through "lemongrass" green to greenish yellows and reddish browns. These are used for precision-cut calibrated and melee-sized goods placed as accent stones in high-end jewelry. Most of the cutting is done in Thailand, and the yield is approximately 10% due to the desire for well-proportioned cut gems. Besides precision-cut demantoid and andradite garnet in calibrated sizes, Reif also cuts to higher tolerances for the watch industry, producing 3 × 2 mm tapered baguettes for watch bezels.

Even in these small sizes, well-cut gems display high luster and very distinct fire, making them an excellent visual alternative to diamond. Rough suitable for gems of 6.0 mm (about 1 ct) is much rarer, but material for larger gems does come up once in a while.

*Figure 35. This selection of andradite garnet from Namibia's Green Dragon mine includes an 11.63 ct demantoid round brilliant, an unusually large stone for this source. Photo by Robert Weldon/GIA, courtesy of Green Dragon mine.*

*Duncan Pay (dpay@gia.edu)*
*GIA, Carlsbad*

**Green nephrite jade attracts buyers in Tucson.** The Jade West Group, a leading nephrite jade company in North America for the past 30 years, drew many buyers at their 2015 GJX booth. Prized in Chinese culture for over 5,000 years, nephrite regained its momentum in the domestic Chinese market after the 2008 Beijing Olympics, when it

*Figure 36. This photo shows half of the Polar Pride jade boulder discovered at the Polar jade mine in British Columbia. The original boulder weighed 18 tons. Courtesy of Jade West Group.*

*Figure 37. This strand of 41 nephrite beads is comprised of material from the Polar mine. Photo by Robert Weldon, courtesy of Jade West Group.*

was used in the gold, silver, and bronze medals. At the same time, the Chinese government launched a campaign promoting the significance of nephrite jade in the country's history. This reignited the love of nephrite among the Chinese people, and the increasing demand and price drove a new Canadian jade rush in northern British Columbia (BC).

A tectonic belt running from Alaska through BC to Mexico favored the formation of nephrite. Tectonic and lithological contacts are the predominant ore body controls. BC has more than 50 known nephrite deposits, distributed mainly along tectonic inclusions of country rocks, dikes, and mafic rock layers within serpentinites, or along the contact between serpentinite and the wall rocks. This formation is very similar to other green nephrite occurrences all over the world. Nephrite is found both *in situ* and as boulders; the Polar Pride boulder, found in BC's Polar mine, is a well-known example of the latter (figure 36).

Nephrite boulders are the products of erosion from the last ice age. They are usually drilled or sawed to test the quality, and only the good-quality material is transported for sale. While some of today's nephrite is from boulders, primary deposits supply the bulk of BC's production. This is partially due to the lack of high-quality boulders; however, the growing demand and price for nephrite also make it profitable to mine the primary deposits.

According to Kirk Makepeace, president of Jade West Group, the price of jewelry-grade jade from BC (figure 37) experienced at least a tenfold increase from a decade ago. Before 2008, top-quality nephrite from BC sold for about $20 a kilo; equivalent stones now range from $200 to $2,000 a kilo.

The annual production of BC nephrite jade is about 400 tons. Most of the output comes from four active mines; together, they produce about three-quarters of the world's high-quality green nephrite. Of these four, Jade West operates the Polar, Ogden, and Kutcho jade mines. Jade West also deals with material from Wyoming and Siberia. Over the last 10 years, approximately 90% of the company's BC production was exported to mainland China; the remaining 10% was sent to Taiwan, Vietnam, and Thailand.

*Figure 38. This Canadian jade fish hook pendant features a piece of nephrite from the Kutcho mine. This is one of the styles Jade West has customized for the North American market. Photo by Robert Weldon/GIA, courtesy of Jade West Group.*

Jade West sends almost all of its rough nephrite to Guangdong for carving and jewelry manufacturing, with designs customized for different markets (figure 38). In addition to traditional carvings and jewelry, there is demand from Southeast Asian countries for giant Buddha statues and from Western countries for home decor. This demand leads Mr. Makepeace to be very optimistic about the future of BC nephrite.

*Tao Hsu (thsu@gia.edu)*
*GIA, Carlsbad*

**Baroque pearls.** Several vendors at this year's Tucson gem shows, including AGTA and GJX, carried baroque pearls in an assortment of colors, sizes, and qualities. A common request from buyers was for pairs in larger sizes. The increased availability of less-expensive, quickly produced freshwater baroque cultured pearls from China in a wide range of sizes has had a noticeable impact on the market, as more designers are experimenting with them and more consumers are seeking them out. At the same time, sizable high-quality baroque pearls from the Philippines and Australia, particularly golden pearls, are becoming harder to

*Figure 39. This hummingbird brooch features a 20.0 mm silver pink baroque pearl. It is surrounded by 319 diamonds (2.54 carats total), with a single 0.03 ct ruby eye mounted in 18K white gold. Photo by Robert Weldon/GIA, courtesy of Ron Greenidge and Emiko Pearls International.*

find, as noted by AGTA exhibitor Ron Greenidge (Emiko Pearls International, Bellevue, Washington).

Emiko Pearls, founded in 1980, specializes in large and unusual classic and baroque pearls of gem and near-gem quality, namely South Sea, Tahitian, and "keshi" cultured pearls in golden, silver blue, gray, and pink hues. Greenidge showed us several examples of handmade jewelry that maximized the potential of exceptional baroque cultured pearls, particularly "jumbo" baroques in the 20–22 mm range. In response to market conditions, Emiko has transitioned over the past decade from offering loose pearls to almost exclusively producing finished goods.

*Figure 40. The whimsical design of this octopus brooch accentuates the 17.3 mm gray baroque Tahitian cultured pearl set in black-plated 18K gold. Also featured are 374 black diamonds totaling 3.78 carats, 26 yellow diamonds totaling 0.33 carats, and 169 white diamonds totaling 1.64 carats. Photo by Robert Weldon/GIA, courtesy of Ron Greenidge and Emiko Pearls International.*

*Figure 41. This brooch depicting four swallows contains two golden "keshi" cultured pearls from the Philippines and two silver blue Australian South Sea keshi, ranging from 9 to 11 mm. They are surrounded by 211 yellow diamonds totaling 1.70 carats, 170 white diamonds totaling 1.23 carats, and eight ruby eyes totaling 0.28 carats, all set in white and yellow 18K gold. Photo by Robert Weldon/GIA, courtesy of Ron Greenidge and Emiko Pearls International.*

Greenidge's love of jewelry, paired with the increasing scarcity of high-quality larger pearls, has led the company to make one-of-a-kind pieces that showcase the uniqueness of individual pearls. Instead of finding pearls to place into existing jewelry, the firm designs jewelry around the pearl. The results are exquisite with whimsical and natural qualities, as seen in their hummingbird and octopus brooches (figures 39 and 40). Each piece is hand-welded from 18K gold, with diamonds and other precious stones added. The pieces, which take several months to create, are sought by clients in Asia and Europe (particularly China, Thailand, and Italy). High-end stores with one or two locations are the primary buyers, as Emiko does not mass-produce any of its designs. The swallow pin in figure 41, complete with forked tails, uses multiple keshi cultured pearls in two tones with matching diamond and gold colors.

As the consumption of pearls, including large baroque cultured material, increases with greater availability of lower-priced goods, expect to see other suppliers of high-quality pearls strive to differentiate themselves as Emiko has done.

*Jennifer Stone-Sundberg*


*Figure 42. The Namya mining area is about 300 km north of Mogok. Namya, Mogok, and Mong Hsu together form a "ruby triangle" in northern Myanmar, as these three locations have produced high-quality ruby. Adapted from R. Hughes,* Ruby & Sapphire: A Collector's Guide*, 2014, Gem and Jewelry Institute of Thailand, Bangkok, p. 132.*

**Crimson Prince ruby from Namya.** Mogok, Myanmar is considered the source of the finest rubies on Earth. In 2000, an exciting new ruby discovery was made in Namya, located in the Kachin state approximately 300 km north of Mogok and east of the jade mine at Hpakant (figure 42). While known mostly for its vibrant pink and red spinels, Namya also produces fine rubies, typically of medium saturation. Due to the remarkably similar geology of the two deposits, it is often impossible to separate Mogok rubies from Namya material.

In the spring of 2014, a rough stone with strong red color and unusually fine clarity weighing approximately 1.2 grams was discovered in Namya. The stone was entrusted to a skilled and experienced ruby cutter, who finished it as a 3.32 ct roundish cushion measuring 7.99 mm in diameter (figure 43). The color, clarity, and cutting are so unusual for a ruby that on initial casual observation, most experts have mistaken it for a spinel.

*Figure 43. The 3.32 ct Crimson Prince ruby was cut from a 1.2 gram rough. Both the color and the clarity make this stone extremely rare. Photo by Robert Weldon/GIA, courtesy of Jeffery Bergman.*

In December 2014, Richard Hughes of Lotus Gemology examined the stone, commenting on its "pigeon's blood" color. Additionally, he remarked that its clarity was "extraordinary," mentioning that only "a light dusting of silk is evenly distributed across the stone" and noting that it was "obvious that the lapidary took great care in its fashioning, befitting a gem of such high value…."

This exceptional ruby deserved a befitting name. Several ideas were put forward; calling it a "King" seemed grandiose, and it was too vividly saturated to be a

*Figure 44. Excavators and a washing plant on Gem Mountain process gravel for sapphire recovery. Photo by Warren Boyd.*

*Figure 45. A trench on Gem Mountain showing the sapphire-rich colluvium on the hilltops between the previously worked gulches. Photo by Keith Barron.*

"Princess." In March 2015, the Crimson Prince ruby found a fitting new home at a prestigious *haute joaillerie* on Place Vendôme in Paris.

*Jeffery Bergman (jeffery@primagem.com)*
*PrimaGem, Bangkok*

**Update on Rock Creek Sapphire deposit.** Recently, Montana-based Potentate Mining LLC secured approximately 3,000 acres of sapphire-bearing ground covering the famous Rock Creek district, including the Gem Mountain mine near Philipsburg, Montana. Since the discovery of these sapphire deposits in the 1890s, this is the first time that one company has consolidated such a large land position, encompassing the old alluvial sites as well as the area on the hills in between these old workings (figure 44). Potentate has assembled a team of highly experienced placer miners, geologists, mining engineers, and heavy equipment operators to recover and process the sapphires from this mine.

The Rock Creek deposits occur in debris flow, colluvium, and secondary alluvial deposits (figure 45). Although the bedrock for these deposits has not yet been defined, Potentate plans further geological mapping and geophysical surveys in the near future to uncover these sources.

To date, the rough sapphires recovered from the bulk sampling pits range in size from 0.25 ct to over 20 ct. Approximately 15% of this rough occurs naturally in marketable colors, including pink, orange, orange-pink, lavender, golden yellow, blue-green and green, and fine blue (figure 46). A substantial percentage of the remaining rough responds very well to heat treatment technologies that improve clarity and turn greenish and grayish rough to desirable colors such as blue, orange, yellow, pink, and parti-color.

The high-grade concentration of the sapphires recovered from the various test pits, and the substantial inferred rough sapphire resource on Gem Mountain, indicate that Potentate would be able to provide a long-term, consistent supply of sapphire rough to the global market (figure 47).

*Figure 46. A selected assortment of unheated rough sapphires from the Rock Creek deposit, ranging from 0.50 to 17 ct. Photo by Warren Boyd.*

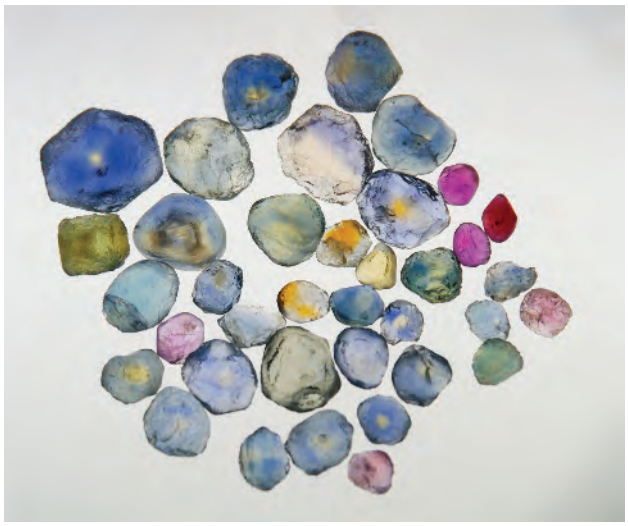

*Figure 47. A selection of natural and heat-treated Rock Creek sapphire ranging from 0.50 to 4.70 ct. Photo by Jeff Scovil.*

*Figure 48. A unique parti-color Brazilian tourmaline necklace with a total weight of 961 carats. Photo by Duncan Pay/GIA, courtesy of Atlas Gemstones, Inc.*

Potentate would be the only large-volume source for the Rock Creek sapphires. The company is developing a marketing strategy that would provide sustainable supply chain guarantees to their clients. These clients, including wholesale gemstone cutters, polishers, and fine jewelry retailers, would in turn be able to provide guarantees of origin and the presence (or absence) of any heat treatment to their consumers.

*Warren Boyd (warren@potentatemining.com)*
*Keith Barron*
*Potentate Mining, LLC*
*Philipsburg, Montana*

**Unique tourmaline necklace.** At the AGTA show, Anna Jankowiak (Atlas Gemstones Inc., Toronto) showed us a unique 961 ct parti-color tourmaline necklace and clasp (figure 48). This piece, which Ms. Jankowiak said she purchased in India, was reportedly cut from a single large, slender Brazilian tourmaline crystal reportedly mined within the last three years. The cutter tried to salvage as much of the material as possible by slicing down the crystal's length. This produced large flattened sections with rounded edges that showed alternating green and pink color zoning down their lengths. The zoning was strong, neat, and "tight." This was in contrast to many of the parti-color tourmaline crystal slices we saw at the show, which were sliced perpendicular to their lengths to show the typical concentric "watermelon" zoning.

*Duncan Pay*

## CONFERENCE REPORTS

**Maine pegmatite workshop.** The 2015 Maine pegmatite workshop took place at the Poland mining camp, May 29–June 6. As readers know, many important colored gemstones including tourmaline, beryl, topaz, garnet, quartz, and spodumene are mined worldwide from pegmatites, and these rocks are the source for most fine gem crystals. Maine pegmatites have been mined for many decades (some back as far as the 1820s) and are renowned for their fine tourmaline, beryl, and quartz crystals. The workshop's website is at pegworkshop.com.

The workshop is conducted by Dr. William "Skip" Simmons, Dr. Karen Webber, and Alexander Falster—all formerly of the University of New Orleans—and Ray Sprague, a local pegmatite miner. Simmons, Weber, and Falster were the core of the university's mineralogy, petrology, and pegmatology ("MP$^2$") research group. Following the closure of the university's mineralogy department, they relocated to the new Maine Mineral and Gem Museum in Bethel (www.mainemineralgemmuseum.org).

The workshop has taken place annually since 2001. The 2015 workshop had a total of 26 attendees, including six undergraduate mineralogy students from University of New Orleans, one postgraduate mineralogy student from the University of the Basque Country (Bilbao, Spain), a well-known mineral dealer, a variety of mineral collectors, and interested members of the public.

The workshop is structured with morning presentations and lectures, followed by excursions to mines and quarries in the afternoon. Given the breadth of participants (rockhounds from mineral clubs, undergraduate and graduate geology students, mineral dealers, gemologists, and PhD-level researchers), the content varied from introductory to quite complex—and sometimes contentious— topics, such as pegmatite genesis (fractional crystallization from granite vs. anatexis) and crystallization time. In particular, the relationship of pegmatites to tectonic settings was well explored, as was the current consensus on cooling time and the formation of large crystals. Nonetheless, the presenters did an excellent job and encouraged plenty of debate. Some of the best questions came from the mineral collectors in the group, many of whom have visited these quarries repeatedly.

The selection of field excursions (figures 49 and 50) varies from year to year and is dependent on which mines are available or being worked at the time. This year's destinations included the following quarries: Western Mount Apatite, Tamminen, Waisanen, Bennett, Orchard, Havey, Mount Mica, and Emmons. Around noon each day, participants would caravan in a stream of cars to the "quarry du jour." The workshop organizers enjoy excellent relationships with local mine owners, dependent on the good conduct of the attendees.

At each quarry, Simmons or Falster explained pegmatite mineralogy and miners Frank Perham or Ray Sprague outlined current or past mining history at the site. The remainder of the time could be spent mineral collecting, which was a focus for a good portion of the group. Those interested in more depth could talk with members of the MP$^2$ research group about the exposures, or with Per-

*Figure 49. Workshop attendees at the Havey Quarry, which has produced some of the finest Maine elbaite tourmalines. The mine was originally opened in 1902 and worked for feldspar. This view shows the Havey pegmatite body, with three pockets visible. Photo by Duncan Pay/GIA.*

ham and Sprague about the practice of mining pegmatites. Indeed, this is the workshop's strong suit: The theory from the morning presentations is applied to real rocks in the afternoon.

Besides the quarries, workshop attendees also visited the new Maine Mineral and Gem Museum in Bethel. There they could see the progress of the exhibits and view the $MP^2$ research group's laboratory in the basement, which includes an electron microprobe, scanning electron microscope, X-ray diffraction equipment, and other advanced instrumentation.

Following an evening lecture on pegmatite mineralogy complemented by numerous hand specimens, the opening session kicked off with a general introduction to pegmatites, the earth's chemistry, and phase equilibria. Throughout the week, the presentations delivered by Simmons, Webber, and Falster built on the basics to cover the relationship of granites to pegmatites, magmatic differen-

*Figure 50. Colorful mineralogy at the Havey quarry. Pink and green tourmaline, clevelandite, lepidolite, and "salmon"-colored feldspar all indicate the presence of a nearby pocket. Photo by Duncan Pay/GIA.*

tiation, pegmatite classification, magma genesis, and the influence of tectonic setting. Some of the more complex topics covered included crystallization dynamics, such as the influence of volatiles and fluxes (water, lithium, fluorine, boron, and phosphorous), pegmatite textures, aplites ("line rocks"), pocket formation and indicators, and regional and internal zonation of pegmatites.

Besides these instructional sessions, workshop attendees were also treated to a variety of other presentations, including:

**Myles Fetch** (Maine Mineral and Gem Museum, Bethel) described the garnet line in Oxford County pegmatites. He explained that the garnet line marks the lower edge of the pegmatite's productive zone. It might swell upward close to a pocket, serving as an important indicator.

**Dr. Encar Roda-Robles** (University of the Basque Country and a member of the MP[2] pegmatite research group) presented on pegmatites from the Iberian Massif and the central Maine belt, covering the differentiation of granitic melts vs. anatexis. Dr. Roda-Robles also delivered a talk on tourmaline, mica, and garnet as sensitive indicators of pegmatite evolution in the Berry-Havey pegmatite. This last talk was very relevant, as the afternoon's field trip was to this quarry.

**Idoia Garante-Olave** (University of the Basque Country) delivered a presentation on mineralogy and geochemistry of micas from the Tres Arroyos pegmatite field in Badajoz, Spain.

**Frank Perham**, a noted Maine pegmatite miner, reminisced on the remarkable Newry tourmaline discovery, which produced an estimated $30 million worth of gem and specimen-grade tourmaline crystals in 1972. Perham also delivered a talk on Maine feldspar mining.

**Dr. Skip Simmons** presented previous work on the chemistry and a calculation of volume, by mineral, for the Mt. Mica pegmatite. The volume of tourmaline was estimated at >1%.

**Jim Nizamoff** (a mineralogist with Omya AG and former University of New Orleans research associate) and mineral collector **Don Dallaire** discussed the pegmatite mineralogy of the Conway and Osceola granites from the White Mountains of New Hampshire.

**Ray Sprague** (pegmatite workshop organizer and miner) presented on the mineralogy of specimens from the Emmons pegmatite in preparation for the all-day visit to that quarry.

*Duncan Pay*

**2015 Sinkankas Symposium.** The thirteenth annual Sinkankas Symposium was held April 18 at GIA headquarters in Carlsbad, California. Co-hosted by the Gemological Society of San Diego, GIA, and Pala International, the event drew a capacity crowd eager to learn about opal.

After welcoming remarks from organizer **Roger Merk**, the morning presentations began with an overview by **Dr. Eloïse Gaillou** (Paris School of Mines) on geology, color, and microstructure. **Andrew Cody** (Cody Opal, Melbourne) chronicled the Australian opal market before delving into fossilized specimens. **Dr. Raquel Alonso-Perez** (Mineralogical and Geological Museum, Harvard University, Cambridge, Massachusetts) spoke on the history of the museum and shared photos and data of specimens from its collection. Photographer **Jack Hobart** showed superb images from his extensive database of Mexican opals. **Bill Larson** (Pala International, Fallbrook, California) described his personal collection of Mexican, Australian, Ethiopian, and Brazilian opals, many of which were on display throughout the campus.

The afternoon sessions began with a presentation by **Alan Hart** (Natural History Museum, London) on the museum's opal collection. Noted lapidary **Meg Berry** (Megagem, Fallbrook, California) described various techniques for cutting and carving. Buying guide author **Renée Newman** (International Jewelry Publications, Los Angeles) discussed the jewelry uses of matrix and common opal. **Helen Serras-Herman** (Gem Art Center, Rio Rico, Arizona) followed with additional insight on the many varieties of common opal. **Robert Weldon** (GIA, Carlsbad) discussed the challenges of photographing opal's shifting flashes of color, as well as the instruments and post-production techniques best suited to the task. **Nathan Renfro** (GIA, Carlsbad) looked at the gem's internal features and the wide range of mineral inclusions that create vibrant, colorful scenes. **Dr. George Rossman** (Caltech, Pasadena, California) examined causes of color and offered closing remarks.

Sapphire will be the theme of the 2016 symposium. For more information on the event or to purchase the proceedings volume, visit www.sinkankassymposium.net.

*Stuart Overlin (soverlin@gia.edu)*
*GIA, Carlsbad*

## ERRATA

1. In the Spring 2015 announcement of the Dr. Edward J. Gübelin Most Valuable Article Award winners (p. 31), the first-place article, "Sri Lanka: Expedition to the Island of Jewels," should have been listed as a Fall 2014 rather than Summer 2014 article.
2. In the Spring 2015 Gem News International entry "Fine tsavorite and spinel" (p. 74), the company "Tsavorite USA" should have been listed as "Bridges Tsavorite."
3. Also in the Spring 2015 issue, we published an update on Brazilian copper-bearing tourmaline seen at this year's Tucson gem shows (GNI, pp. 71–72). It now appears that the gemstones represented to GIA as production from the Mineração Terra Branca (MTB) Brazil Paraíba mine in Rio Grande do Norte—and photographed for the entry—were mined instead at the Parazul Mineração mine in neighboring

Paraíba province, in the area where the gem was originally discovered. As soon as this came to our attention, we withdrew the story from the GIA website.

Reports in the Brazilian and international media circulated during May and June 2015 about an ongoing federal investigation into both mines. Several principals from each mine are in custody at the time of writing as part of the operation into alleged laundering of gems from a mining operation lacking the necessary permits (Parazul), through one with the required permissions (MTB). Reports indicate that the investigation commenced in 2009, and continued through the 2015 Tucson show with the cooperation of the U.S. Federal Bureau of Investigation (FBI).

We wish to note that neither the original discoverer of Paraíba tourmaline, Heitor Dimas Barbosa, nor his son Sergio, are part of any investigation or implicated in this affair in any way.

4. Finally, we would like to post a correction to L.T.-T. Huong et al.'s article "A preliminary study on the separation of natural and synthetic emeralds using vibrational spectroscopy" (Winter 2014 *G&G*). In figure 3 (p. 289), the vertical axis legend should read "$SiO_2$ wt.%." Similarly, in table 1 (p. 291), both silicon and alkalis (Li, Na, K, Rb, and Cs) should be expressed as oxides rather than elements.

In the Materials and Methods section, the authors mentioned different measurement techniques for Si (electron microprobe) and the alkalis (laser ablation–inductively coupled plasma–mass spectrometry, or LA-ICP-MS). As a result, one original measurement was in parts per million (ppm, either parts per million atoms—ppma—or parts per million by weight—ppmw) for the alkalis (LA-ICP-MS) and the other was in wt.% for $SiO_2$ (electron microprobe). This indicates that a conversion between ppm and wt.% was made but not mentioned in the paper. Our technical editor noted that the wt.% values reported for alkalis in the paper (0.330 to 1.872), which correspond to 670 to 18,720 ppm, were in line with the published literature.

The article's lead author, Dr. Le Thi-Thu Huong, confirmed that all the alkali values published in the paper were converted from ppm to wt.%. We thank Dr. Karl Schmetzer for bringing this to our attention.